MUTAGENIC ANALYSIS OF RESIDUES CRITICAL FOR TOXICITY IN DOMAIN II OF THE *Bacillus thuringiensis* Cry4Ba TOXIN

TIPPARAT TUNTITIPPAWAN

A THESIS SUBMITTED IN PARTIAL FULFILLMENT
OF THE REQUIREMENTS FOR
THE DEGREE OF DOCTOR OF PHILOSOPHY
(MOLECULAR GENETICS AND GENETIC ENGINEERING)
FACULTY OF GRADUATE STUDIES
MAHIDOL UNIVERSITY
2004

ISBN 974-04-5510-7
COPYRIGHT OF MAHIDOL UNIVERSITY

Copyright by Mahidol University

Thesis
Entitled

MUTAGENIC ANALYSIS OF RESIDUES CRITICAL FOR TOXICITY IN DOMAIN II OF THE *Bacillus thuringiensis* Cry4Ba TOXIN

.....
Miss Tipparat Tuntitippawan
Candidate

.....
Assoc. Prof. Chanan Angsuthanasombat, Ph.D.
Major-Advisor

.....
Asst. Prof. Gerd Katzenmeier, Ph.D.
Co-Advisor

.....
Ms. Panadda Boonserm, Ph.D.
Co-Advisor

.....
Prof. Emeritus Sakol Panyim, Ph.D.
Co-Advisor

.....
Asst. Prof. Chartchai Krittanai, Ph.D.
Co-Advisor

.....
Assoc. Prof. Rassmidara Hoonsawat, Ph.D.
Dean
Faculty of Graduate Studies

.....
Asst. Prof. Varaporn Akkarapatumwong, Ph.D.
Chair
Doctor of Philosophy Programme in
Molecular Genetics and Genetic Engineering
Institute of Molecular Biology and Genetics

Copyright by Mahidol University

Thesis
Entitled

MUTAGENIC ANALYSIS OF RESIDUES CRITICAL FOR TOXICITY IN DOMAIN II OF THE *Bacillus thuringiensis* Cry4Ba TOXIN

was submitted to the Faculty of Graduate Studies, Mahidol University
for the degree of Doctor of Philosophy (Molecular Genetics and Genetic Engineering)
on
December 8, 2004

.....
Miss Tipparat Tuntitippawan
Candidate

.....
Assoc. Prof. Chanan Angsuthanasombat, Ph.D.
Chair

.....
Asst. Prof. Chartchai Krittanai, Ph.D.
Member

.....
Asst. Prof. Boonhiang Promdonkoy, Ph.D.
Member

.....
Asst. Prof. Gerd Katzenmeier, Ph.D.
Member

.....
Asst. Prof. Kusol Pootanakit, Ph.D.
Member

.....
Prof. Emeritus Sakol Panyim, Ph.D.
Member

.....
Ms. Panadda Boonserm, Ph.D.
Member

.....
Assoc. Prof. Rassmidara Hoonsawat, Ph.D.
Dean
Faculty of Graduate Studies
Mahidol University

.....
Asst. Prof. Chartchai Krittanai, Ph.D.
Acting Director
Institute of Molecular Biology and Genetics
Mahidol University

Copyright by Mahidol University

ACKNOWLEDGEMENT

The successs of this thesis can be attributed to the extensive support and assistance from my advisor, Dr. Chanan Angsuthanasombat and my co-advisors, Dr. Sakol Panyim, Dr. Gerd Katzenmeier, Dr. Chartchai Krittanai and Dr. Panadda Boonserm.

My sincere appreciation is expressed to Dr. Urai Chaisri, Department of Tropical Pathology, Faculty of Tropical Medicine, Mahidol University and Dr. Kusol Pootanakit for helpful advice and technical support in immunocytochemical method.

My appreciation is extended to Ms. Chaweewan Shimwai for preparing eggs of *Aedes aegypti* mosquitoes to use in Mosquito-larvicidal activity assay.

I would like to thank Dr. Pongsopee Attasart, Ms. Somsri Sakdee and staffs in autoclave department for technical support.

I would like to thank all staffs in computer department for helpful advice in computer program.

Special thanks are extended to all members in Institute of Molecular Biology and Genetics, Mahidol University for their help, kindness and friendship.

The financial support in this work comes from PhD scholarship of Ministry of Science and Technology.

Finally, I would like to express my deepest appreciation to my parent, my grandmother, my aunt, my brother and all members in my family for their love and encouragement throughout my study life.

Tipparat Tuntitippawan

Copyright by Mahidol University

MUTAGENIC ANALYSIS OF RESIDUES CRITICAL FOR TOXICITY IN DOMAIN II OF THE *Bacillus thuringiensis* Cry4Ba TOXIN

TIPPARAT TUNTITIPPAWAN 4537404 MBMG/D

Ph.D. (MOLECULAR GENETICS AND GENETIC ENGINEERING)

THESIS ADVISOR : CHANAN ANGSUTHANASOMBAT, Ph.D., PANADDA BOONSERM, Ph.D., CHARTCHAI KRITTANAI, Ph.D., GERD KATZENMEIER, Ph.D., SAKOL PANYIM, Ph.D.

ABSTRACT

Loop residues in domain II of *Bacillus thuringiensis* Cry δ-endotoxins have been demonstrated to be involved in insecticidal specificity. In this study, selected residues in loops β6-β7 ($SSPS_{390}$), β8-β9 (S_{410}, N_{411}, T_{413}, T_{415}, E_{417} and G_{418}) and β10-β11 ($DYNS_{457}$) in domain II of the Cry4Ba mosquito-larvicidal protein were changed individually to alanine via PCR-based site-directed mutagenesis. All mutant toxins were highly expressed in *Escherichia coli* as 130-kDa protoxins at levels comparable to the wild type. Only *E. coli* cells expressing the P389A, S410A, E417A, Y455A or N456A mutants reduced larvicidal activity against *Aedes aegypti* mosquito larvae. The toxic involvement of S_{410}, E_{417}, Y_{455} and N_{456} was confirmed by a more adverse effect on toxicity observed for the two double mutants (S410A/E417A and Y455A/N456A). Furthermore, alanine substitutions of residues that stabilise the β2-β3 and β4-β5 hairpins via Swiss-Pdb (T_{319} and R_{323} in β2 and Y_{408} in β8) revealed that only the Y408A mutant showed a drastic reduction in larvicidal activity. Further replacement of Y_{408} with phenylalanine still retained larvicidal activity as the wild-type level, while replacements with valine, tryptophan, aspartate, glutamate and cysteine drastically decreased larvicidal activity. Structural analysis suggested that the aromatic side chain of Y_{408} interacts with that of F_{326} in β2 implying its functional significance. Using immunocytochemical staining with a specific monoclonal antibody, the larvicidal inactive Y408D mutant reduced binding activity on apical microvilli of *A. aegypti* posterior midgut cells compared with the wild-type toxin, suggesting that Y_{408} is involved in receptor binding. Based on all the results, it is proposed that P_{389} in the β6-β7 loop, S_{410} and E_{417} in the β8-β9 loop, and Y_{455} and N_{456} in the β10-β11 loop are involved in Cry4Ba toxicity. In addition, Y_{408} in β8 that possibly stabilises functional conformation of β2-β3 and β4-β5 hairpins is conceivably important for receptor binding of the Cry4Ba toxin.

KEY WORDS : MUTAGENIC ANALYSIS/ LOOP RESIDUE/ β-HAIRPIN STABILISING RESIDUE/ *Bacillus thuringiensis*/ CRY TOXIN/ RECEPTOR BINDING/ MOSQUITO-LARVICIDAL ACTIVITY

163 P. ISBN 974-04-5510-7

Copyright by Mahidol University

การเปลี่ยนแปลงยีนเพื่อศึกษากรดอะมิโนที่เกี่ยวข้องกับความเป็นพิษซึ่งอยู่ในส่วนที่ 2 ของโปรตีนชนิด Cry4Ba จากแบคทีเรีย *Bacillus thuringiensis* (MUTAGENIC ANALYSIS OF RESIDUES CRITICAL FOR TOXICITY IN DOMAIN II OF THE *Bacillus thuringiensis* Cry4Ba TOXIN)

ทิพย์รัตน์ ตันติทิพย์วรรณ 4537404 MBMG/D

ปร.ด. (อณูพันธุศาสตร์และพันธุวิศวกรรมศาสตร์)

คณะกรรมการควบคุมวิทยานิพนธ์ : ชนันท์ อังศุธนสมบัติ Ph.D., ปนัดดา บุญเสริม Ph.D., ชาติชาย กฤตนัย Ph.D., GERD KATZENMEIER Ph.D., สกล พันธุ์ยิ้ม Ph.D.

บทคัดย่อ

การศึกษาก่อนหน้านี้พบว่ากรดอะมิโนบริเวณส่วนเชื่อมต่อระหว่างเบต้า (β) ซึ่งอยู่ในส่วนที่ 2 ของโปรตีน Cry หลายชนิดจากแบคทีเรีย *Bacillus thuringiensis* มีส่วนเกี่ยวข้องกับความเป็นพิษต่อแมลงที่จำเพาะเจาะจง ในการศึกษานี้ กรดอะมิโนในส่วนเชื่อมต่อระหว่าง β6-β7 ($SSPS_{390}$) β8-β9 (S_{410} N_{411} T_{413} T_{415} E_{417} และ G_{418}) และ β10-β11 ($DYNS_{457}$) ซึ่งอยู่ในส่วนที่ 2 ของโปรตีนฆ่าลูกน้ำยุงชนิด Cry4Ba ได้ถูกแทนที่ทีละตำแหน่งด้วย alanine โดยอาศัยการเปลี่ยนแปลงยีนด้วยเทคนิค PCR ซึ่งพบว่าโปรตีนกลายพันธุ์ทั้งหมดซึ่งมีขนาด 130 kDa ได้ถูกสร้างในแบคทีเรีย *Escherichia coli* ที่ระดับปริมาณใกล้เคียงกับ wild type และเมื่อทดสอบความเป็นพิษต่อลูกน้ำยุงลาย (*Aedes aegypti*) พบว่า เฉพาะ *E. coli* ที่สร้างโปรตีนกลายพันธุ์ชนิด P389A S410A E417A Y455A หรือ N456A เท่านั้นที่ออกฤทธิ์ฆ่าลูกน้ำยุงลดลง ซึ่งความสำคัญต่อการฆ่าลูกน้ำของตำแหน่ง S_{410} E_{417} Y_{455} และ N_{456} ได้ถูกยืนยัน โดยการแทนที่ทีละสองตำแหน่งของกรดอะมิโนเหล่านั้น (S410A/E417A และ Y455A/N456A) และพบว่า โปรตีนกลายพันธุ์ทั้ง 2 ชนิด สูญเสียความเป็นพิษมากยิ่งขึ้น นอกจากนี้ได้ศึกษาโดยการแทนที่ด้วย alanine ของกรดอะมิโนที่ทำนายโดยโปรแกรม Swiss-Pdb ว่าทำหน้าที่รักษาเสถียรภาพของโครงสร้างแบบ β-hairpin ระหว่าง β2-β3 และ β4-β5 (T_{319} R_{323} ใน β2 และ Y_{408} ใน β8) ซึ่งพบว่าโปรตีนกลายพันธุ์ชนิด Y408A แสดงความสามารถในการฆ่าลูกน้ำลดลงอย่างชัดเจน เมื่อได้ศึกษาเพิ่มเติมพบว่าการแทนที่ Y_{408} ด้วย phenylalanine ยังคงแสดงความสามารถในการฆ่าลูกน้ำได้เท่ากับ wild type แต่เมื่อแทนที่ด้วย valine tryptophan aspartate glutamate หรือ cysteine พบว่าโปรตีนกลายพันธุ์เหล่านี้แสดงความเป็นพิษลดลงอย่างชัดเจน จากการวิเคราะห์โครงสร้างจึงได้เสนอว่า โครงสร้าง aromatic ในส่วน side chain ของ Y_{408} ซึ่งมีแนวโน้มที่จะมีปฏิสัมพันธ์กับโครงสร้าง aromatic ของ F_{326} ใน β2 นั้นอาจแสดงให้เห็นถึงความสำคัญต่อความเป็นพิษของโปรตีน Cry4Ba นอกจากนี้เมื่อใช้วิธี immunocytochemistry โดยอาศัย monoclonal antibody ที่จำเพาะ พบว่าโปรตีนกลายพันธุ์ชนิด Y408D ซึ่งไม่สามารถฆ่าลูกน้ำได้นั้นสามารถจับกับส่วนบนสุดของเซลบุผิวในส่วนท้ายของกระเพาะลูกน้ำยุงลายลดลงเมื่อเปรียบเทียบกับโปรตีน wild type ซึ่งแสดงว่า Y_{408} น่าจะเกี่ยวข้องกับการจับกับ receptor โดยสรุปจากผลการศึกษาทั้งหมดนี้จึงเสนอว่า P_{389} ในส่วนที่เชื่อมต่อระหว่าง β6-β7 S_{410} และ E_{417} ในส่วนที่เชื่อมต่อระหว่าง β8-β9 Y_{455} และ N_{456} ในส่วนที่เชื่อมต่อระหว่าง β10-β11 นั้นเกี่ยวข้องกับความเป็นพิษของโปรตีน Cry4Ba นอกจากนี้ Y_{408} ใน β8 ซึ่งน่าจะทำหน้าที่รักษาเสถียรภาพของโครงสร้างแบบ β-hairpin ระหว่าง β2-β3 และ β4-β5 ให้เหมาะสมต่อการจับกับ receptor นั้นมีความสำคัญต่อการจับกับ receptor ของโปรตีน Cry4Ba

163 หน้า. ISBN 974-04-5510-7

Copyright by Mahidol University

CONTENTS

		Page
ACKNOWLEDGEMENT		iii
ABSTRACT		iv
LIST OF TABLES		x
LIST OF FIGURES		xi
LIST OF ABBREVIATIONS		xv
PREFACE		xviii
CHAPTER		
I	INTRODUCTION	1
	1.1 Insect control	1
	1.2 *Bt* insecticidal proteins	1
	1.2.1 Classification of *Bt* insecticidal proteins	3
	1.2.2 Mechanism of action of Cry toxins	3
	1.2.3 Cry toxin structures	3
	1.2.4 Solubilisation of Cry toxin inclusions	9
	1.2.5 Proteolytic activation of Cry toxins	9
	1.2.6 Receptor binding of Cry toxins	11
	1.2.6.1 Cry binding proteins	11
	1.2.6.2 Functionality of Cry binding proteins in larvicidal activity	12
	1.2.6.3 Identification of Cry binding regions of receptors	13
	1.2.6.4 Identification of receptor-binding regions of Cry toxins	16
	1.2.6.5 The involvement of receptor binding in insecticide resistance	18
	1.2.6.6 *In vitro* receptor binding studies of Cry toxins	18
	1.2.7 Pore formation of Cry toxins	23

Copyright by Mahidol University

CONTENTS (CONT.)

		Page
II	OBJECTIVES	27
III	MATERIALS	29
	3.1 Chemicals	29
	3.2 Enzymes	30
	3.3 Growth media	31
	3.4 Bacterial strain	31
	3.5 Oligonucleotide primers	32
	3.5.1 Site-directed mutagenesis	32
	3.5.2 DNA sequencing	34
	3.6 Recombinant plasmid	34
	3.7 Antibodies	34
IV	METHODS	36
	4.1 Preparation of plasmid DNA template using the CTAB method	36
	4.2 *In vitro* site-directed mutagenesis	37
	4.2.1 Setting up and cycling the PCR reactions	37
	4.2.2 Digesting the PCR products with *Dpn* I	39
	4.2.3 Transforming the *Dpn* I-digested PCR products into *E. coli* cells	39
	4.2.3.1 Preparation of competent cells using $MgCl_2$-$CaCl_2$ method	39
	4.2.3.2 Transforming the *Dpn* I-digested PCR products into competent cells	40
	4.3 Small-scale extraction of plasmid DNA by alkaline lysis method	40
	4.4 Restriction endonuclease digestion of plasmid DNA	40
	4.5 Agarose gel electrophoresis	41
	4.6 Automated DNA sequencing	41
	4.7 Preparation of target proteins from *E. coli* cell lysates	42
	4.8 SDS-polyacrylamide gel electrophoresis (SDS-PAGE)	42

Copyright by Mahidol University

CONTENTS (CONT.)

		Page
	4.9 Mosquito-larvicidal activity assay	43
	4.10 Partial purification of protoxin inclusions	43
	4.11 Determination of protein concentration	44
	4.12 Solubilisation and proteolytic activation of protoxin inclusions	44
	4.13 FPLC purification of the activated toxins	44
	4.14 *In vitro* receptor binding assay using immunocytochemical method	45
V	RESULT I: INVOLVEMENT IN TOXICITY OF β6-β7, β8-β9 AND β10-β11 LOOP RESIDUES	47
	5.1 Constructions of β6-β7, β8-β9 and β10-β11 loop mutants	47
	5.2 Screening of the loop mutant plasmids	47
	5.3 Protoxin expression of the β6-β7, β8-β9 and β10-β11 loop mutants	48
	5.4 Mosquito-larvicidal activity of the β6-β7, β8-β9 and β10-β11 loop mutants	48
	5.5 Constructions and screening of S410A/E417A and Y455A/N456A mutants	71
	5.6 Protoxin expression of the S410A/E417A and Y455A/N456A mutants	71
	5.7 Mosquito-larvicidal activity of the S410A/E417A and Y455A/ N456A mutants	71
	5.8 Solubilisation and proteolytic activation of the S410A/E417A and Y455A/N456A mutant inclusions	72
VI	RESULT II: INVOLVEMENT IN TOXICITY OF RESIDUES STABILISING β2-β3 AND β4-β5 HAIRPINS	80
	6.1 Constructions and screening of T319A, R323A and Y408A mutants	80

Copyright by Mahidol University

CONTENTS (CONT.)

		Page
	6.2 Protoxin expression of T319A, R323A and Y408A mutants	88
	6.3 Mosquito-larvicidal activity of T319A, R323A and Y408A mutants	88
	6.4 Constructions of Y408F, Y408W, Y408D, Y408E and Y408C mutants	91
	6.5 Protoxin expression of Y408V, Y408F, Y408W, Y408D, Y408E and Y408C mutants	102
	6.6 Larvicidal activity of Y408V, Y408F, Y408W, Y408D, Y408E and Y408C mutants	102
	6.7 Solubilisation and proteolytic activation of the Y408A, Y408V, Y408F, Y408W, Y408D, Y408E and Y408C mutants	102
	6.8 Binding activity of the Y408D mutant toxin	114
VII	DISCUSSION	118
	7.1 Involvement of β6-β7, β8-β9 and β10-β11 loop residues in toxicity	118
	7.2 Involvement in toxicity of residues stabilising β2-β3 and β4-β5 hairpins	124
VIII	CONCLUSIONS	127
REFERENCES		130
APPENDIX		151
BIOGRAPHY		163

Copyright by Mahidol University

LIST OF TABLES

Table		Page
1	The revised nomenclature of *Bt* insecticidal proteins	5
2	Molecular masses, insecticidal activities and crystal shapes of *Bt* insecticidal proteins	6
3	Restriction endonucleases with their recognition sites and optimal conditions	31
4	Cycling parameter for the site-directed mutagenesis method	39
5	Formulation for SDS-polyacrylamide gel	43

Copyright by Mahidol University

LIST OF FIGURES

Figure		Page
1	Electron micrograph of *Bacillus thuringiensis* subsp. *israelensis* during sporulation	2
2	The tertiary structures of Cry3Aa (6), Cry1Aa (7), Cry3Bb1 (8), Cry2Aa (9) and Cry4Ba (10) toxins	7
3	Domain II of Cry3Aa (6), Cry1Aa (7) and Cry4Ba (10) toxins	8
4	Bt-R_1 structural model based on the domain organisation of the cadherin superfamily	15
5	The midgut of *Aedes aegypti* fourth-instar larva under light microscope	20
6	Electron micrograph of an epithelial cell in gastric caeca of *Aedes aegypti* fourth-instar larva	21
7	Electron micrographs of an epithelial cell in anterior midgut (A, B) and posterior midgut (C) of *Aedes aegypti* fourth-instar larva	22
8	The umbrella model for insertion of *Bt* toxins into the insect plasma membrane based on the Cry3Aa structure	26
9	Domain II of the Cry4Ba toxin	28
10	Physical map of plasmid pMU388	35
11	Overview of the Quick Change site-directed mutagenesis method	38
12	Amplification of the β6-β7 and β8-β9 loop mutant plasmids	50
13	*Dpn* I digestion of the PCR products of the β6-β7 and β8-β9 loop mutant plasmids	51
14	Amplification and *Dpn* I digestion of the p4B-D454A and p4B-N456A mutant plasmids	52
15	Amplification and *Dpn* I digestion of the p4B-S457A mutant plasmid	53
16	Restriction endonuclease and DNA sequence analysis of p4B-S387A	54
17	Restriction endonuclease and DNA sequence analysis of p4B-S388A	55

Copyright by Mahidol University

LIST OF FIGURES (CONT.)

Figure		Page
18	Restriction endonuclease and DNA sequence analysis of p4B-P389A	56
19	Restriction endonuclease and DNA sequence analysis of p4B-S390A	57
20	Restriction endonuclease and DNA sequence analysis of p4B-S410A	58
21	Restriction endonuclease and DNA sequence analysis of p4B-N411A	59
22	Restriction endonuclease and DNA sequence analysis of p4B-T413A	60
23	Restriction endonuclease and DNA sequence analysis of p4B-T415A	61
24	Restriction endonuclease and DNA sequence analysis of p4B-E417A	62
25	Restriction endonuclease and DNA sequence analysis of p4B-G418A	63
26	Restriction endonuclease and DNA sequence analysis of p4B-D454A	64
27	Restriction endonuclease and DNA sequence analysis of p4B-Y455A	65
28	Restriction endonuclease and DNA sequence analysis of p4B-N456A	66
29	Restriction endonuclease and DNA sequence analysis of p4B-S457A	67
30	Expression of the β6-β7 and β10-β11 loop mutant protoxins	68
31	Expression of the β8-β9 loop mutant protoxins	69
32	Mosquito-larvicidal activity of *E. coli* cells expressing β6-β7, β8-β9 and β10-β11 loop mutants	70
33	Amplification and *Dpn* I digestion of the double mutant plasmids; p4B-S410A/E417A and p4B-Y455A/N456A	73
34	Restriction endonuclease and DNA sequence analysis of p4B-S410A/E417A	74
35	Restriction endonuclease and DNA sequence analysis of p4B-Y455A/N456A	75
36	Expression of the S410A/E417A and Y455A/N456A mutant protoxins	76
37	Expression of S410A/E417A and Y455A/N456A mutant inclusions	77
38	Solubility of the Cry4Ba wild type and its double mutant (S410A/E417A and Y455A/N456A) inclusions	78

Copyright by Mahidol University

LIST OF FIGURES (CONT.)

Figure		Page
39	Proteolytic processing of the Cry4Ba wild type and its double mutant (S410A/E417A and Y455A/N456A) protoxins	79
40	β2-β3 and β4-β5 hairpins in domain II of the Cry4Ba toxin	81
41	Hydrogen bonding networks at T_{319}, R_{323} and T_{328} in β2 of Cry4Ba	82
42	β-sheets 1 and 2 in domain II of the Cry4Ba toxin	83
43	Amplification and *Dpn* I digestion of the p4B-T319A, p4B-R323A and p4B-Y408A mutant plasmids	84
44	Restriction endonuclease and DNA sequence analysis of p4B-T319A	85
45	Restriction endonuclease and DNA sequence analysis of p4B-R323A	86
46	Restriction endonuclease and DNA sequence analysis of p4B-Y408A	87
47	Expression of the T319A, R323A and Y408A mutant protoxins	89
48	Mosquito-larvicidal activity of *E. coli* cells expressing T319A, R323A or Y408A mutants	90
49	Predicted hydrogen bonding at position 408 of Cry4Ba	93
50	Amplification and *Dpn* I digestion of the p4B-Y408W, p4B-Y408D, p4B-Y408E and p4B-Y408C mutant plasmids	94
51	Amplification and *Dpn* I digestion of the p4B-Y408F mutant plasmid	95
52	Restriction endonuclease and DNA sequence analysis of p4B-Y408W	96
53	Restriction endonuclease and DNA sequence analysis of p4B-Y408D	97
54	Restriction endonuclease and DNA sequence analysis of p4B-Y408E	98
55	Restriction endonuclease and DNA sequence analysis of p4B-Y408C	99
56	Restriction endonuclease and DNA sequence analysis of p4B-Y408F	100
57	DNA sequence analysis of Y408V mutant	101
58	Expression of the Y408V, Y408F, Y408W, Y408D, Y408E and Y408C mutant protoxins	103
59	Mosquito-larvicidal activity of *E. coli* cells expressing Y408V, Y408F, Y408W, Y408D, Y408E or Y408C mutants	104
60	Expression of Y408A mutant inclusion	105

Copyright by Mahidol University

LIST OF FIGURES (CONT.)

Figure		Page
61	Expression of Y408D, Y408E and Y408C mutant inclusions	106
62	Expression of Y408W, Y408V and Y408F mutant inclusions	107
63	Solubility of Cry4Ba wild type and Y408A mutant inclusions	108
64	Solubility of the Cry4Ba wild type and its mutant (Y408D, Y408E and Y408C) inclusions	109
65	Solubility of the Cry4Ba wild type and its mutant (Y408W, Y408V and Y408F) inclusions	110
66	Proteolytic processing of Cry4Ba wild type and Y408A mutant protoxins	111
67	Proteolytic processing of the Cry4Ba wild type and its mutant (Y408D, Y408E and Y408C) protoxins	112
68	Proteolytic processing of the Cry4Ba wild type and its mutant (Y408W, Y408V and Y408F) protoxins	113
69	Purification of the activated Cry4Ba and its Y408D mutant toxins	115
70	Immunocytochemical staining of the Y408D mutant toxin detected with undiluted monoclonal antibody	116
71	Immunocytochemical staining of the Y408D mutant toxin detected with 1:20 dilution of monoclonal antibody	117
72	Sequence alignment of parts of different Cry toxin-domain II	119
73	Domain II of the Cry4Ba toxin	122
74	β2-β3 and β8-β9 hairpins in domain II of the Cry4Ba toxin	123
75	β-sheets 1 and 2 in domain II of the Cry4Ba toxin and its Y408F mutant	125

Copyright by Mahidol University

LIST OF ABBREVIATIONS

Å	Angstrom
BBMV	Brush border membrane vesicle
bp	Base pair
Bs	*Bacillus sphericus*
BSA	Bovine serum albumin
Bt	*Bacillus thuringiensis*
°C	Degree Celsius
ca.	Approximately
cm	Centimeter
Cry	Crystal protein
CTAB	Cetyl trimethyl ammonium bromide
Cyt	Cytolytic protein
DAB	3,3′-diaminobenzidine
DNA	Deoxyribonucleic acid
dNTP	dATP, dCTP, dGTP, dTTP
DTT	Dithiothreitol
E. coli	*Escherichia coli*
EDTA	Ethylene diamine tetraacetic acid
et al.	and others
g	gram
hr	hour
IPTG	Isopropyl-β-D-thiogalactopyranoside
kb	Kilobase pair
kDa	Kilodalton
LB	Luria-Bertani media
µg	Microgram
µl	Microliter

Copyright by Mahidol University

LIST OF ABBREVIATIONS (CONT.)

µm	Micrometer
µM	Micromolar
M	Molar
mA	Milliampere
mg	Milligram
min	Minute
ml	Milliliter
mM	Millimolar
N	Normal (concentration)
ng	Nanogram
nm	Nanometer
OD	Optical density
PC	Phosphatidylcholine
PCR	Polymerase chain reaction
psi	Pounds per square inch
RNA	Ribonucleic acid
RNase	Ribonuclease
rpm	Revolutions per minute
SDS	Sodium dodecyl sulphate
SDS-PAGE	Sodium dodecyl sulphate polyacrylamide gel electrophoresis
sec	second
subsp.	subspecies
TEMED	N, N, N´, N´-tetramethylenediamine
TPCK	Tosyl-phenylalanine chloromethyl ketone
Tris	Tri(hydroxymethyl)-aminoethane
U	Unit
V	Volt
v/v	volume/volume

Copyright by Mahidol University

LIST OF ABBREVIATIONS (CONT.)

w/v	weight/volume
w/w	weight/weight

Copyright by Mahidol University

PREFACE

The work described in this thesis was carried out in Laboratory of Molecular Biophysics, Institute of Molecular Biology and Genetics, Mahidol University. *In vitro* receptor binding study based on immunocytochemical method was performed in collaboration with Dr. Urai Chaisri at Department of Tropical Pathology, Faculty of Tropical Medicine, Mahidol University. I certify that this work has not been submitted to any other universities.

Some sections of this work have been published as given in the lists below:

1. Tuntitippawan T, Boonserm P, Katzenmeier G, Panyim S, Angsuthanasombat C (2003) Role in Toxicity of Loop Residues in Domain II of the *Bacillus thuringiensis* Cry4Ba Toxin. Abstract in 1st *Bacillus thuringiensis* Meeting, Institute of Molecular Biology and Genetics, Mahidol University, Nakornprathom.
2. Tuntitippawan T, Boonserm P, Katzenmeier G, Angsuthanasombat C (2004) Targeted Mutagenesis of Loop Residues in the Receptor-Binding Domain of the *Bacillus thuringiensis* Cry4Ba Toxin Affects Larvicidal Activity. FEMS Microbiol Lett (in press).

Tipparat Tuntitippawan

Copyright by Mahidol University

CHAPTER I
INTRODUCTION

1.1 Insect control

Chemical insecticides have been used to control important agricultural insect pests and mosquito vectors of human diseases such as *Anopheles* (malaria vector), *Culex* (filariasis vector) and *Aedes* (dengue vector). However, because of their environmental impact on non-target organisms especially on human by contaminating in food and water as well as the development of insecticide resistance in target populations, biological agents become a first choice to control insect (1). A number of insecticidal products based on *Bacillus thuringiensis* (*Bt*) and *Bacillus sphericus* (*Bs*) have been developed as biological insecticides for the past 30 years. Four commercial products, based on *Bt* subsp. *israelensis* (*Bti*), VectorBac®, Teknar®, Bactimos® and Acrobe® are available to control mosquitoes and blackflies in many countries (1). In addition, a product based on *Bs*, VectoLex® has been used recently for the control of mosquito vectors of filariasis and viral diseases (1).

1.2 *Bt* insecticidal proteins

During sporulation, *Bt,* a rod-shaped Gram-positive soil bacterium, produces cytoplasmic parasporal inclusions which consist of one or more insecticidal proteins (δ-endotoxins) of different molecular masses and shapes. *Bti* (Figure 1, (2)) produces at least four larvicidal proteins: Cry4Aa (125 kDa), Cry4Ba (135 kDa), Cry11Aa (68 kDa) and Cyt1Aa (28 kDa) that are specifically toxic to *Aedes*, *Anopheles* and *Culex* mosquito vectors with various degrees.

Copyright by Mahidol University

Figure 1: Electron micrograph of *Bacillus thuringiensis* subsp. *israelensis* during sporulation (2)

A transmitted electron micrograph of *Bacillus thuringiensis* subsp. *israelensis* during sporulation stage. Arrowheads indicate cytoplasmic parasporal inclusions.

Copyright by Mahidol University

1.2.1 Classification of *Bt* insecticidal proteins

In the past, *Bt* insecticidal proteins were classified into at least five classes based on their deduced amino acid sequence homology and insecticidal activities (3). To organise the many new cloned sequences, the classification of *Bt* insecticidal proteins has been revised based only on amino acid sequence identity (4). Under this, each toxin is assigned a new name by changing Roman numerals of class name to Arabic numerals, as shown in Table 1. There are a few exceptions in nomemclature of some toxins: CryIG becomes Cry9Aa, CryIIIC becomes Cry7Aa, CryIIID becomes Cry3Ca, CryIVC becomes Cry10Aa, CryIVD becomes Cry11Aa, CytA becomes Cyt1Aa, CytB becomes Cyt2Aa. The current nomemclature is available at http://www.biols.susx.ac.uk/home/Neil_Crickmore/Bt/index.html. Table 2 represents molecular masses, crystal shapes and insect specificities of certain Cry and Cyt toxins (5).

1.2.2 Mechanism of action of Cry toxins

The informative mechanism of Cry toxins to kill insect larvae is still being investigated (5). Generally, it has been believed that Cry toxins are synthesised as insoluble inactive protoxins which require solubilisation and proteolytic activation in the insect larval midgut after ingestion to form active toxins. After activation, the active toxins bind to specific receptors located on the surface of midgut epithelial cells and then insert into the plasma membrane of the midgut epithelial cells to create transmembrane leakage pores, causing swelling and death of cells.

1.2.3 Cry toxin structures

The previously solved tertiary structures (Figure 2) of five Cry toxins, Cry3Aa (6), Cry1Aa (7), Cry3Bb1 (8), Cry2Aa (9) and Cry4Ba (10) suggest that all the activated Cry toxins are a globular molecule of three distinct domains with a high degree of overall structural similarity. Domain I which is composed of seven α-helices has been shown to play a critical role in membrane insertion and pore formation (11-16). Domain II consisted of three anti-parallel β-sheets, each ending with surface-exposed loops which are the most varible parts among the five Cry toxin structures. Surface-exposed loops of the Cry3Aa and Cry3Bb1 toxins look very similar (85% amino acid sequence identity, Figure 2). Mutagenic studies have been shown that the

Copyright by Mahidol University

certain surface-exposed loops (β2-β3 and/or β6-β7 and/or β10-β11 loops) of Cry3Aa and Cry1Aa, and the two surface-exposed loops (β2-β3 and β4-β5 loops) of Cry4Ba at molecular apex (Figure 3) participate in receptor binding (17-21). Domain III, a sandwich of two anti-parallel β-sheets, is believed to play a crucial role in structural stability (6), ion channel activity (22; 23) and receptor binding (24-29).

Copyright by Mahidol University

Table 1: The revised nomenclature of *Bt* insecticidal proteins

Revised name	Original name
Cry1Aa	CryIA(a)
Cry1Ab	CryIA(b)
Cry1Ac	CryIA(c)
Cry1Ad	CryIA(d)
Cry1Ae	CryIA(e)
Cry1Af	
Cry1Ag	
Cry1Ba	CryIB
Cry1Bb	ET5
Cry1Bc	PEG5
Cry1Bd	CryIE
Cry1Be	
Cry1Ca	CryIC
Cry1Cb	CryIC(b)
Cry1Da	CryID
Cry1Db	PrtB
Cry1Ea	CryIE
Cry1Eb	CryIE(b)
Cry1Fa	CryIF
Cry1Fb	PrtD
Cry1Ga	PrtA
Cry1Gb	CryH2
Cry1Ha	PrtC
Cry1Hb	
Cry1Ia	CryV
Cry1Ib	CryV
Cry1Ic	
Cry1Id	
Cry1Ie	
Cry1Ja	ET4
Cry1Jb	ET1
Cry1Jc	
Cry1Ka	
Cry2Aa	CryIIA
Cry2Ab	CryIIB
Cry2Ac	CryIIC
Cry2Ad	
Cry3Aa	CryIIIA
Cry3Ba	CryIIIB
Cry3Bb	CryIIIBb
Cry3Ca	CryIIID
Cry4Aa	CryIVA
Cry4Ba	CryIVB
Cry5Aa	CryVA(a)
Cry5Ab	CryVA(b)
Cry5Ac	

Revised name	Original name
Cry5Ba	
Cry6Aa	CryVIA
Cry6Ba	CryVIB
Cry7Aa	CryIIIC
Cry7Ab	CryIIICb
Cry8Aa	CryIIIE
Cry8Ba	CryIIIG
Cry8Ca	CryIIIF
Cry9Aa	CryIG
Cry9Ba	CryIX
Cry9Ca	CryIH
Cry9Da	
Cry10Aa	CryIVC
Cry11Aa	CryIVD
Cry11Ba	Jeg80
Cry11Bb	
Cry12Aa	CryVB
Cry13Aa	CryVC
Cry14Aa	CryVD
Cry15Aa	34kDa
Cry16Aa	cbm71
Cry17Aa	cbm72
Cry18Aa	CryBPI
Cry18Ba	
Cry18Ca	
Cry19Aa	Jeg65
Cry19Ba	
Cry20Aa	
Cry21Aa	
Cry22Aa	
Cry23Aa	
Cry24Aa	Jeg72
Cry25Aa	Jeg74
Cry26Aa	
Cry27Aa	
Cry28Aa	
Cry29Aa	
Cry30Aa	
Cry31Aa	
Cyt1Aa	CytA
Cyt1Ab	CytM
Cyt1Ba	
Cyt2Aa	CytB
Cyt2Ba	CytB
Cyt2Bb	

Copyright by Mahidol University

Table 2: Molecular masses, insecticidal activities and crystal shapes of *Bt* insecticidal proteins (5)

Class	Approximate molecular mass (kDa)	Insecticidal activity[a]	Crystal shape
Cry1	130-140	Lepidoptera	Bipyramid
Cry2	70	Lepidoptera/ Diptera	Cuboid
Cry3	70	Coleoptera	Rhomboid
Cry4	130	Diptera	Bipyramid
Cry10Aa, Cry11Aa	70	Diptera	Bar
Cyt1Aa	27	Diptera/ Cytolytic activity *in vitro*	Amorphous

[a]Lepidoptera, Coleoptera and Diptera are the insect orders of moths and butterflies, beetles, and mosquitoes and blackflies, respectively.

Copyright by Mahidol University

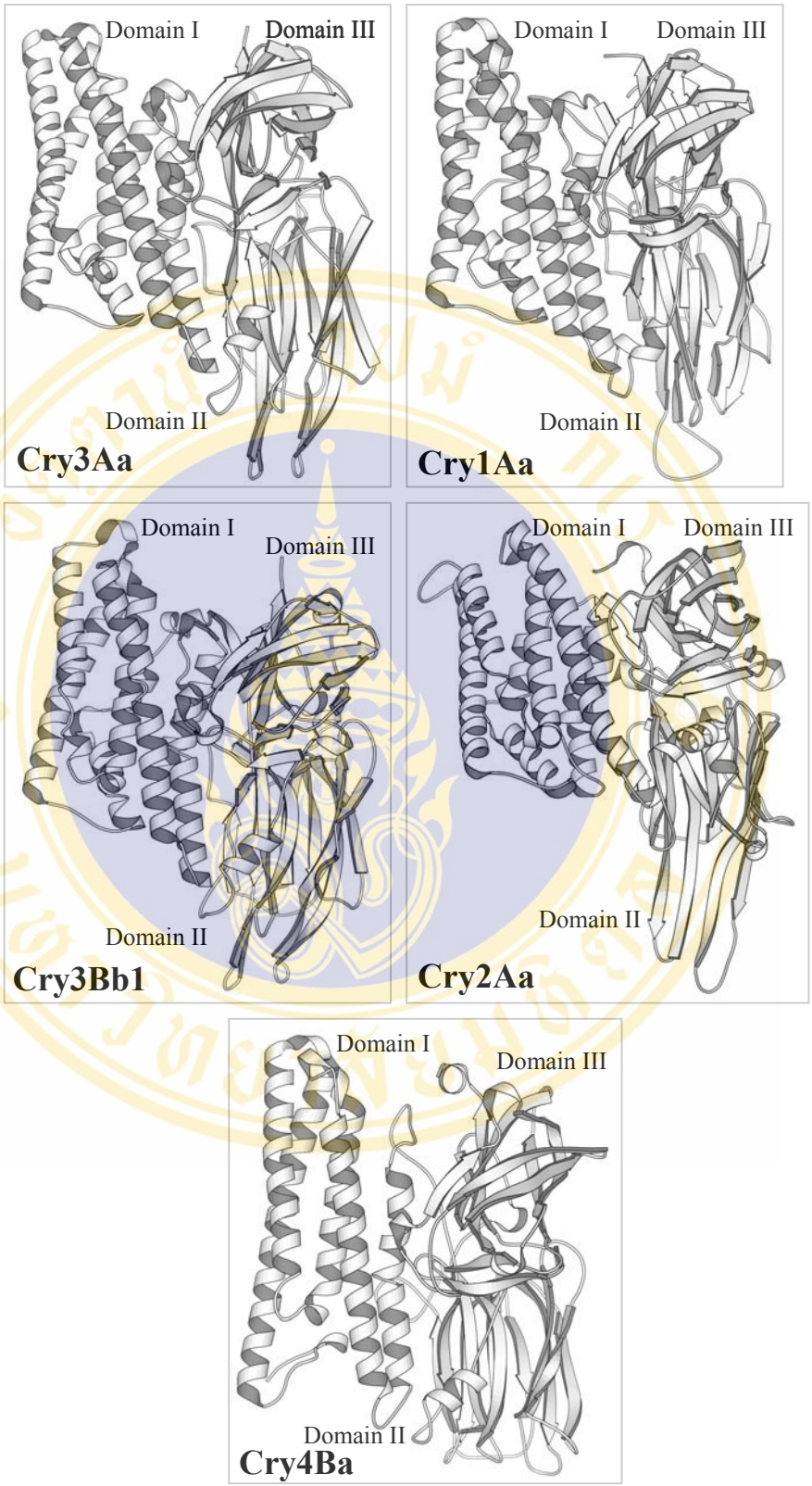

Figure 2: The tertiary structures of Cry3Aa (6), Cry1Aa (7), Cry3Bb1 (8), Cry2Aa (9) and Cry4Ba (10) toxins

The figure shows ribbon representation of the Cry3Aa, Cry1Aa, Cry3Bb1, Cry2Aa and Cry4Ba toxins illustrating domain organisation.

Copyright by Mahidol University

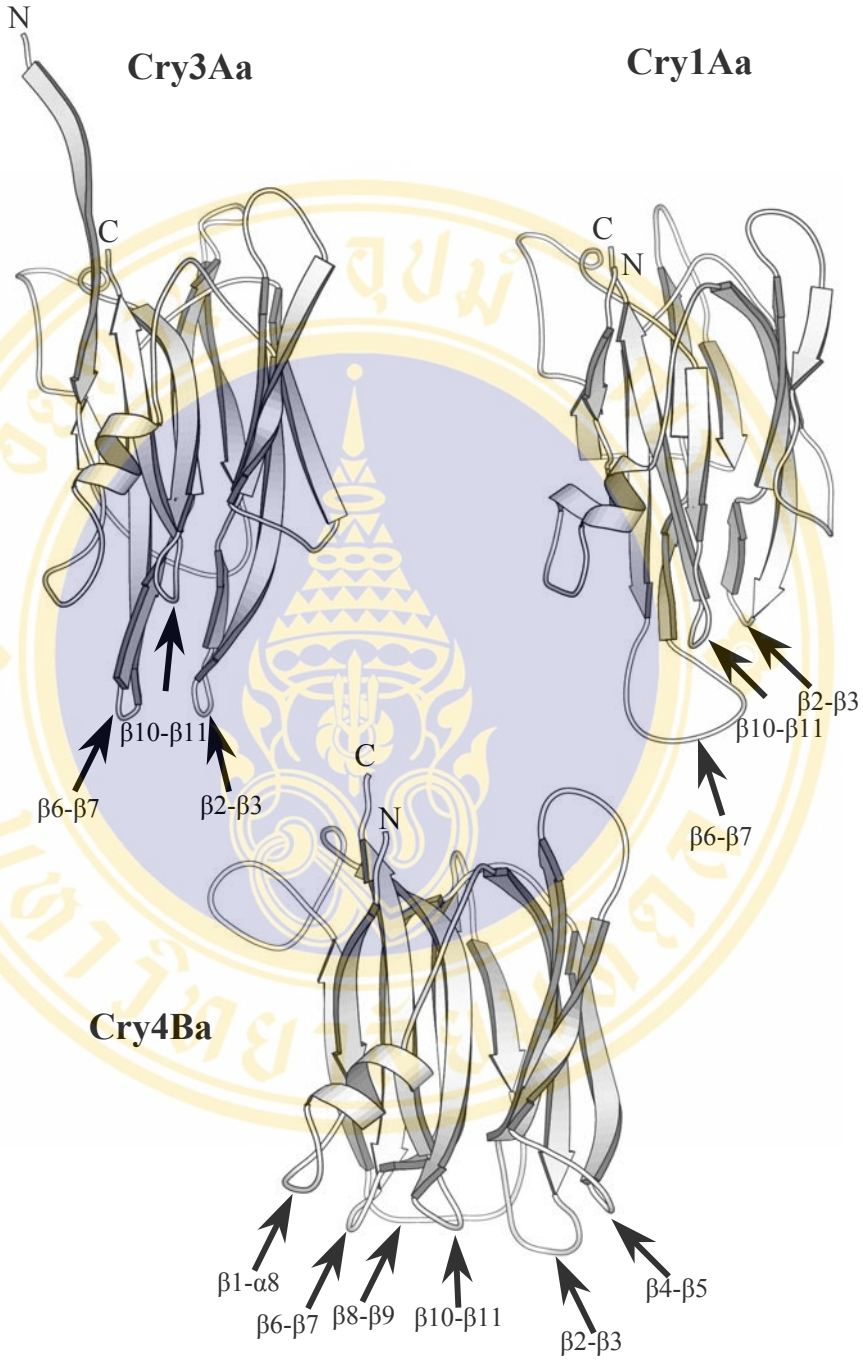

Figure 3: Domain II of Cry3Aa (6), Cry1Aa (7) and Cry4Ba (10) toxins

Arrows indicate the surface-exposed loops at molecular apex of Cry3Aa, Cry1Aa and Cry4Ba toxins. The amino and carboxyl termini are marked.

Copyright by Mahidol University

1.2.4 Solubilisation of Cry toxin inclusions

Most Cry protoxin inclusions are solubilised in alkaline pH and reducing conditions in the insect larval midgut (5). The solubility was shown to correlate directly with toxicity (30; 31). A reduction in the solubility was shown to be a potential mechanism of insecticide resistance (32). Interchain disulphide bonds were proposed to be involved in the insolubility (33). Cysteine residues that are located in the first few amino acids at the N-terminus and in the C-terminal half were found to be not involved in larvicidal activity (34). The regions were also suggested to be removed after proteolytic activation (3). However, it has been proposed that four salt bridges linking between polypeptide chains are involved in solubility of Cry3Aa (6).

1.2.5 Proteolytic activation of Cry toxins

Based on molecular mass (Mr), Cry toxins are divided into two groups: protoxins of approximately 130 kDa such as Cry1A, Cry4Aa and Cry4Ba, and protoxins of approximately 70 kDa such as Cry2Aa, Cry3Aa and Cry11Aa. After proteolytic activation, approximately 25-30 amino acids of the N-terminus and the C-terminal half of the large Cry protoxins are removed, leaving an active toxin of around 65 kDa (35-40) while the smaller Cry protoxins are cleaved only at the N-terminus where approximately 50 residues are removed, resulting in an active toxin of around 65 kDa (41; 42). The role of C-terminal half of the 130-kDa Cry1Ca toxin has been proposed to be involved in the formation of crystalline inclusions but not involved in toxicity (43). The importance of removal of the N-terminal peptide has been suggested to be important for activation of several Cry toxins, e.g. Cry1Ab and Cry1Ca (44-46). Presence of this peptide of Cry1Ca was demonstrated to prevent the proper interaction with a specific receptor on target cell membrane (46). Recently, it was also shown that the presence of the N-terminal peptide of Cry1Ac prevented pore formation in *Manduca sexta* brush border membrane vesicles (BBMVs) *in vitro*, reduced insecticidal activity *in vivo* and affected binding by changing binding pattern (47).

Intramolecular cleavage has been found for many Cry toxins. The toxins are cleaved in domain I: Cry1Ab (48), Cry2Aa (49), Cry3Aa (41), Cry4Aa (38), Cry4Ba (39; 40) and Cry9Aa (50), and cleaved in domain II: Cry11Aa (42), Cry1Ac (51) and Cry1Aa (52). The Cry4Aa protoxin was processed by *Culex pipiens* midgut proteases

Copyright by Mahidol University

into two fragments of 20 and 45 kDa through the cleavage between α5 and α6 (38). Processing of the Cry11Aa toxin in domain II generated fragments between 30 and 40 kDa by *C. quinqasfasciatus* midgut proteases (42). Treatment of the Cry1Ab protoxin with *M. sexta* midgut juice resulted in removal of α1 and α2a in domain I producing a 58-kDa protein, and further cleavage in domain II giving two fragments of 30 kDa (53). The removal of α1 was suggested to be important for Cry1Ab activation while generation of 30-kDa fragments was suggested to be involved in the toxin degradation pathway (53). The Cry4Ba protoxin which is treated with gut extract from *Aedes aegypti* mosquito larvae produced two main cleavage products of 46-47 kDa and 16-18 kDa, occuring from cleavage at arginine-203 in the loop between α5 and α6 (40). The activation was shown to be important for *in vitro* toxicity against mosquito cell lines (39). Alanine substitution of the arginine-203 prevented proteolytic cleavage at this position and showed a significant decrease in toxicity *in vitro* but an increase in larvicidal activity (40). Another proteolytic cleavage site was introduced into the loop linking α3 and α4 of the Cry4Ba toxin using PCR-based site-directed mutagenesis. The result showed that the mutant apparently reduced larvicidal activity against *A. aegypti* larvae (54).

Insect midgut proteases have been studied using their specific substrates and inhibitors. The midguts of lepidopteran and dipteran insect larvae contain mainly serine proteases (55-57), especially trypsin-like proteases (36; 39; 40; 55; 58). In contrast, cysteine and aspartic proteases are the major proteases in coleopteran insect larvae (57).

Involvement of proteolytic processing in insecticide resistance to certain Cry toxins has been investigated. The lack of major gut proteases resulted in insecticide resistance in *Plodia interpunctella* larvae to Cry toxins from *Bt* subsp. *entomocidus* HD198 (59). Processing of the Cry1Ac protoxin with proteases from a resistant strain of *Heliothis virescens* larvae was more slowly than with enzymes from a susceptible strain (60). However, it was recently shown that the difference in susceptibility to the Cry1Ab toxin of resistant and susceptible *Plutella xylostella* larvae was not due to their midgut proteolytic activity since proteolytic patterns of the Cry1Ab toxin in the two populations were similar (36).

Copyright by Mahidol University

Proteolytic activation of Cry3Aa and Cry1Ab after receptor binding was shown to facilitate the formation of tetrameric prepore structure, leading to the formation of a lytic pore in target membrane (61; 62). This also was observed in other bacterial pore-forming toxins (63-65). A functional prepore oligomer in membrane was observed after proteolytic cleavage of aerolysin following receptor binding (65).

1.2.6 Receptor binding of Cry toxins

1.2.6.1 Cry binding proteins

Aminopeptidase N (APN) and cadherin-like proteins (Bt-R_1 and Bt-R_{175}) from the larval midguts of lepidopteran insects have been identified as Cry1A binding proteins. In *Lymantria dispar*, Bt-R_{270}, a high molecular mass anionic protein, was identified as a Cry1A binding protein in addition to APN and cadherin-like proteins (66). The 120-kDa *L. dispar* APN was identified as a binding protein of the Cry1Ac toxin (29; 67; 68). Using surface plasmon resonance (SPR) technique, the binding between Cry1Ac and its receptor was shown to be a 1:1 stoichiometry and almost completely inhibited by preincubation with *N*-acetylgalactosamine (GalNAc) (68). Recently, the binding region of the Cry1Ac toxin to the APN was identified in domain II loop residues and domain III (29). A sequential binding model was therefore proposed: the domain III firstly binds to GalNAc on the APN with fast association and dissociation kinetics, and domain II loop residues then bind to the APN with slower kinetic, but tighter affinity (29).

In *M. sexta*, a 210-kDa Bt-R_1 and a 120-kDa APN were suggested as binding proteins of both Cry1Aa and Cry1Ab toxins (69), while only the 120-kDa APN was identified as a Cry1Ac binding protein (70-73). A 106-kDa APN in *M. sexta* was also identified as a binding protein of Cry1Ab (73) and Cry1Ca (74). Using SPR technique, the Cry1Ac toxin was shown to bind to two sites on the *M. sexta* APN with 2:1 toxin-receptor stoichiometries (75) and the binding was specifically inhibited by GalNAc but not by *N*-acetylglucosamine (GlcNAc) (71; 75). Domain III of the Cry1Ac toxin was shown to bind to GalNAc on the APN (25; 27; 28; 76; 77) through residues in a region on and adjacent to β16 in domain III (N_{506}, Q_{509}, R_{511} and Y_{513}) (25; 28; 76; 77). In contrast, this binding region in domain III was not found in Cry1Aa and Cry1Ab, and the binding of these two toxins to the APN was not inhibited by preincubation

Copyright by Mahidol University

with GalNAc (75), suggesting that Cry1Aa and Cry1Ab bind to the APN with different mechanism from Cry1Ac.

In *Bombyx mori*, Bt-R_{175} was shown to bind to the Cry1Aa toxin (78; 79). The Bt-R_{175} was reported to have three alleles, Bt-R_{175}a, b and c, which have 1, 6 and 5 amino acid replacement, respectively. Four and three of the replacement in Bt-R_{175}b and c, respectively, were located in the published Cry1Aa binding region of Bt-R_{175} (80). All the three alleles transiently expressed in COS7 mammalian cells bound to the Cry1Aa toxin with similar affinity (81). A 120-kDa APN from *B. mori* was also identified as a binding protein of the Cry1Aa toxin (79; 82-84).

In *H. virescens*, a 170-kDa APN is a binding protein for the Cry1Ac toxin (85-87). The Cry1Ac toxin was shown to bind to two sites on the APN with 2:1 toxin-receptor stoichiometries (85).

In *Spodoptera litura*, a 108-kDa APN expressed on the surface of *S. frugiperda* (Sf21) insect cells using baculovirus expression system was recognised by the active Cry1Ca toxin but not by the non-active Cry1Ac toxin (88). In *S. littoralis*, 40- and 110-kDa proteins were found to interact with the Cry1Ca toxin (89).

For dipteran larvae, a protein ranging from 18 to 30 kDa was identified from *C. pipiens* BBMVs as Cry4Aa binding proteins (90). In addition, proteins of 65 and 62 kDa from brush border membranes of *A. aegypti* larvae showed a binding affinity to Cry4Ba and Cry11Aa (91).

1.2.6.2 Functionality of Cry binding proteins in larvicidal activity

In some cases, it was found that Cry toxins could bind to BBMVs of insusceptible insects (92). Therefore, it is important to investigate the functionality of Cry binding proteins in induction of the event after receptor binding including pore formation in the target membranes. It was shown that the Cry1Aa toxin caused morphological change of Sf9 insect cells expressing *B. mori* Bt-R_{175} (78). The Cry1Ab toxin was also shown to induce cytotoxicity in COS7 mammalian cells expressing *M. sexta* Bt-R_1 (93). Recently, HEK293 mammalian cells expressing *B. mori* Bt-R_{175}b were demonstrated to swell and die in the presence of the Cry1Aa toxin (81).

M. sexta APN reconstituted in planar lipid bilayers was shown to mediate irreversible Cry1Ac binding (94). In addition, *M. sexta* APN in phosphatidylcholine

Copyright by Mahidol University

(PC) liposomes could catalyse Cry1Ac-induced pore formation in the liposomes (72). *M. sexta* APN fused into planar lipid bilayers was able to allow the Cry1Ac and Cry1Ca toxins, but not the Cry1Ba toxin to form ion channels (95). *M. sexta* APN in PC vesicles promoted Cry1Ac-induced $^{86}Rb^{+}$ release from the membrane vesicles (96).

In vivo receptor functionality assay was also performed by expressing *M. sexta* APN in both midgut and mesodermal tissues of Cry1Ac insusceptible *Drosophila melanogaster* larvae (dipteran insect larvae) using the GAL4 enhancer trap technique (97; 98). The result showed that the transgenic *Drosophila* larvae became susceptible to the Cry1Ac toxin (99).

1.2.6.3 Identification of Cry binding regions of receptors

In *B. mori*, a region of 64 residues (135-198) in APN (83) and a region between residues 1245-1391 of Bt-R_{175} (78) were identified as Cry1Aa binding regions. Recently, two amino acid regions in *B. mori* Bt-R_{175} (IIDTNNK$_{880}$ and LDETTN$_{1301}$) were shown to be involved in binding to the Cry1A toxin (100).

In *M. sexta*, an eight-amino acid region of Bt-R_1 (HITDTNNK$_{876}$) was suggested to bind to domain II β6-β7 loop of the Cry1A toxin (69). However, based on hydropathic profile comparison of residues in the β6-β7 loop with the residues in the Cry1A binding region of Bt-R_1 (HITDTNNK$_{876}$), it was shown that the NITIHITDTNN$_{875}$ region is more possible to be the binding partner of the loop in the Cry1A toxin (69). The involvement of the NITIHITDTNN$_{875}$ region of Bt-R_1 in toxin binding was confirmed by showing that the binding of the Cry1Ab toxin to the residues 831-900 of Bt-R_1 containing the NITIHITDTNN$_{875}$ region and to scFv73 antibody acting as Bt-R_1 could promote the formation of a 250-kDa tetrameric prepore structure (61; 101). Binding of the Cry1Ab toxin to the scFv73 antibody also caused the formation of functional ionic pores *in vitro* (61). It was also shown that *M. sexta* larvae fed with the Cry1Ab toxin mixed with the residues 831-900 region of Bt-R_1 greatly reduced larvicidal activity of the Cry1Ab toxin (101). Another group has suggested that a 66-amino acid region from residues 1296-1362, EC11 of the Bt-R_1 ectodomain (see Figure 4), is as a second Cry1A binding site in Bt-R_1 based on the binding of the ^{125}I-labelled Cry1A toxin to truncated Bt-R_1 peptides (93). In addition, feeding *M. sexta* larvae with the mixture of Cry1Ab and the toxin binding region

Copyright by Mahidol University

containing the 66-amino acid region was found to cause an inhibition of insecticidal activity (93). Binding of the Cry1Ab toxin to the Bt-R_1 containing the 66-amino acid region was also shown to facilitate the formation of 250-kDa prepore oligomer (101). The 66-amino acid region involving in the Cry1A toxin binding was narrowed to a region of 12 amino acids, $IPLPASILTVTV_{1342}$, using synthetic peptides of this region in competing the binding of Cry1Ab to Bt-R_1 (101). The 12-amino acid region was also shown to bind to β1-α8 loop of the Cry1Ab toxin (101).

Copyright by Mahidol University

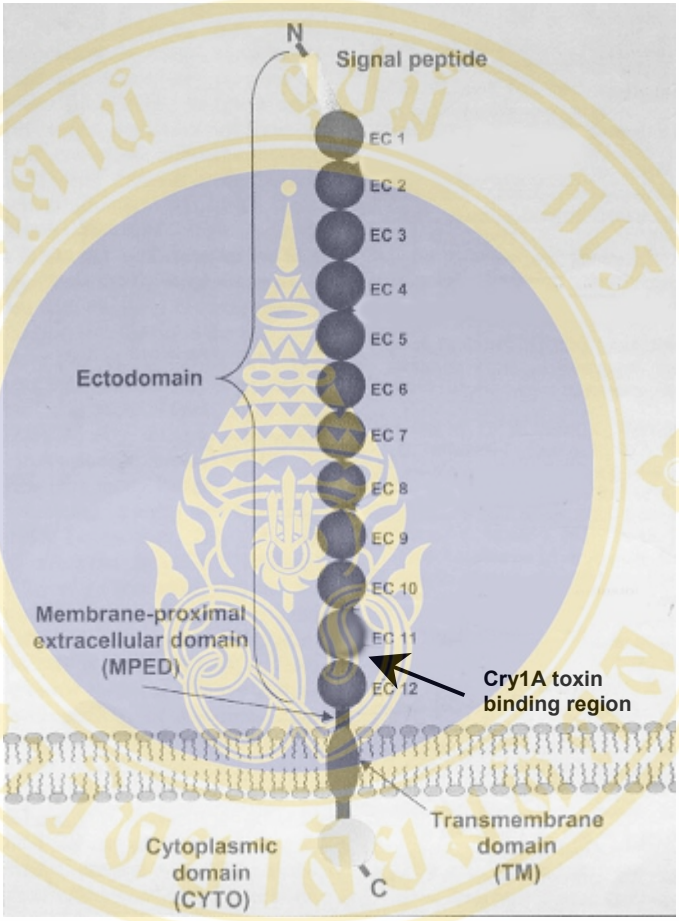

Figure 4: Bt-R_1 structural model based on the domain organisation of the cadherin superfamily (93)

The Bt-R_1 is consisted of four domains: ectodomain (EC), membrane-proximal extracellular domain (MPED), transmembrane domain (TM) and cytoplasmic domain (CYTO). The EC domain is composed of EC1 through EC12. The Cry1A toxin binding region is located in EC11, which is close to MPED.

Copyright by Mahidol University

1.2.6.4 Identification of receptor-binding regions of Cry toxins

It has been shown that swapping residues 330-450 of Cry1Ac with the corresponding segment of Cry1Aa which is highly active to *B. mori* resulted in a hybrid Cry1Ac toxin with high toxicity against *B. mori* (102) and high binding activity toward *B. mori* BBMVs (103). Segment swapping between these two toxins also demonstrated that residues 335-450 and 335-615 in domain II of Cry1Ac are involved in *Trichoplusia ni* activity and *H. virescens* activity, respectively (104). Independent segment-swapping studies on the same toxins have indicated that only Cry1Ac segment of residues 429-447 is responsible for *M. sexta* activity while segments 332-428 (domain II), 429-447 (domain II) and 448-722 (domain II-III) affected *H. virescens* activity (105).

Domain III swapping studies have suggested that domain III involves in receptor binding (24; 27). The Cry1Aa-Cry1Ac hybrid toxin which has domain III from Cry1Ac revealed strong binding to purified *L. dispar* APN and 120-kDa *L. dispar* BBMV protein (24). In contrast, the hybrid with Cry1Aa domain III failed to bind to the APN, but bound to a 210-kDa protein (24). Recently, the Cry1Ac-Cry1Ca hybrid toxin containing Cry1Ac domain III was shown to bind specifically to *M. sexta* APN and the binding was inhibited by GalNAc (27). In some cases, domain III swapping could result in new hybrid toxins with higher toxicity than that of its parental toxins (26; 104; 106; 107). Combination of Cry1Ca domain III with domain I and domain II of various Cry1 toxins showed that all the Cry1 hybrid toxins increased activity against *S. exigue*, suggesting that domain III of Cry1Ca is an important determinant of insect specificity (108).

A number of surface-exposed loops (β2-β3, β6-β7 and β10-β11 loops) which are located at the molecular apex in domain II of certain Cry toxins (see Figure 3) have been studied for the importance of their residues in receptor binding using site-directed mutagenesis and *in vitro* binding study based on the interaction of BBMVs isolated from susceptible insect larval midguts with radioactive-labelled toxins. Deletion of residues 365-371 in the β6-β7 loop of Cry1Aa was found to disturb toxin binding to *B. mori* BBMVs (18) while deletion of the β10-β11 loop residues $AAGA_{443}$ resulted in reduction of binding to *B. mori* and *M. sexta* BBMVs (19). However, mutations in the β2-β3 loop showed no effect on binding of Cry1Aa to *B. mori* BBMVs (20). The

Copyright by Mahidol University

Cry1Ab and Cry1Ac toxins that show a high degree of structural similarity and amino acid sequence identity with the Cry1Aa toxin, the β6-β7 and β10-β11 loops also have been suggested being involved in receptor binding. Mutation of N_{372} in the β6-β7 loop of Cry1Ab was shown to affect toxin binding to *L. dispar* BBMVs (109). In addition, alanine substitutions of residues RRP_{370}, G_{374} and I_{375} in the same loop were found to disturb the binding to *H. virescens* BBMVs (110). Alanine substitutions of RRP_{370} residues were also shown to affect Cry1Ab binding to *M. sexta* BBMVs (110). It was also found that alanine substitutions of β10-β11 loop residues (G_{439} and F_{440}) of Cry1Ab showed an adversed effect on binding to *M. sexta* and *H. virescens* BBMVs (19). Mutations of R_{386} and R_{369} in the β6-β7 loop were shown to affect the binding of Cry1Ac to *M. sexta* (111; 112) and *L. dispar* BBMVs (112) while mutation of Y_{367} in the same loop affected the toxin binding to *M. sexta* BBMVs (111). Mutation of G_{439} in the β10-β11 loop of Cry1Ac was also found to affect the binding to *M. sexta* BBMVs (111). In the Cry1Ca toxin, mutations of residues in β6-β7 and β10-β11 loops showed a decrease in binding to *S. littoralis* and *A. aegypti* BBMVs with exception of R_{437} mutants (113). It was also found that mutational analysis of residues in β2-β3 and β6-β7 loops of the Cry1Ca toxin showed their involvement in insect specificity for *A. aegypti* larvae and a Sf9 cell line (114). In the Cry3Aa toxin, alanine replacements of residues in β2-β3 and β10-β11 loops showed effect on binding to *Tenebrio molitor* BBMVs while no effect on the binding was found with alanine substitutions of β6-β7 loop residues (17). Importance of residues in the β1-α8 loop for receptor binding also was examined in Cry1Ac. Alanine substitutions of R_{281} and R_{289} of Cry1Ac showed an adversed effect on binding to *L. dispar and M. sexta* APNs (115). However, in the Cry2Aa toxin, residues at core β sheet (an 800 $Å^2$ hydrophobic region surrounded by three loops, β4-β5, β5-β6 and β7-β8 which are also a part of the putative binding site) were suggested to be responsible for receptor binding (9).

The specific amino acid residues in the outer sheet of Cry1Ac domain III, especially the residues on or around β16 (a putative sugar-binding pocket) have been extensively studied the involvement in binding to GalNAc on *L. dispar* and *M. sexta* APNs. Individual alanine substitutions of Q_{509}, R_{511}, and Y_{513} in domain III affected binding to *M. sexta* APN (76) and BBMVs (25; 76; 77). In another group, mutations of N_{506}, Q_{509} and Y_{513} in domain III were also shown to affect binding to *M. sexta* APN

Copyright by Mahidol University

and BBMVs, and to affect a rate of pore formation in *M. sexta* BBMVs (28). Mutations of residues Q_{509}, R_{511}, and Y_{513} also affected *L. dispar* BBMV binding (25; 77).

1.2.6.5 The involvement of receptor binding in insecticide resistance

Understanding of the receptor-binding mechanism would help to overcome an insecticide resistance problem since loss or mutation of Cry binding proteins on surface of midgut epithelial cells has been shown to be involved in development of Cry toxin resistance (116-120). Recently, studies of the binding and pore forming ability of Cry1Aa, Cry1Ab, Cry1Ac and Cry1Fa using BBMVs prepared from sensitive and resistant strains of *H. virescens* suggested that a dramatic reduction of toxin binding is responsible for the increased resistance and cross-resistance to the Cry toxins observed in the resistant strain. This observation also showed a correlation with altered glycosylation of specific BBMV proteins (121).

1.2.6.6 *In vitro* receptor binding studies of Cry toxins

Numerous *in vitro* receptor-binding studies have been carried out using BBMVs, purified receptors fused in artificial membranes and expression of receptors on the surface of insect cell lines. Interactions are detected by many developed techniques such as detection of Cry toxin-labelled radioactive, immunocytochemistry, detection of biotinylated Cry toxins with streptavidin conjugated with enzyme and SPR assays.

Immunocytochemical method has been used to detect binding of Cry toxins on insect larval midguts exclusively dissected from mosquito larvae. Figure 5 shows a midgut of *A. aegypti* fourth-instar larva under light microscope (122) which consists of four parts: cardia (not shown), gastric caeca, anterior midgut and posterior midgut. The pH of gastric caeca, anterior midgut and posterior midgut is mildly alkaline (pH less than or about 8), highly alkaline (pH about or more than 9.2) and mildly alkaline (pH about 8), respectively. The midgut epithelial cells of the four parts (Figure 5A) form a single layer containing an apical brush border and an uneven basal border. The apical brush border protrudes into the ectoperitrophic space which is seperated from the midgut contents by the peritrophic membrane. The basal border is bounded by a basal lamina.

Copyright by Mahidol University

The epithelial cells of anterior midgut are smaller than the posterior midgut (Figure 5A) and show no apical brush border, thus the luminal margin is smoth (Figure 5C). In contrast, the apical brush border of posterior midgut is 5-7 mm long on the tall columnar cells, which extend further into the lumen than the cuboidal cells, so the luminal margin is uneven (Figure 5D). Similarly, epithelial cells in gastric caeca show an extensive brush border (not clear in Figure 5B).

The midgut of *A. aegypti* fourth-instar larva under electron microscope (122) shows that the gastric caeca looks similar to that of *C. pipiens* larva (123; 124) and the epithelial cells in gastric caeca contain two cell types: one with long, thin microvilli that do not contain mitochondria and another cell type containing long, thick microvilli that contain mitochondria (Figure 6). The apical microvilli of anterior midgut are very short and broad (approximately 1 μm long and 0.4 μm wide) (Figures 7A and 7B). In contrast, the posterior midgut cells have numerous, long, thin apical microvilli (> 10 μm long and 0.2 μm wide) (Figure 7C). Each microvillus is a distinct structure with no connection to adjacent microvilli and no branches along its entire length (Figure 7C, inset).

Immunocytochemical studies of *Bti* toxins have been reported. Cry4Aa, Cry4Ba, Cry11Aa and Cyt1Aa were detected on the apical brush border of midgut cells from *Anopheles gambiae* larvae in gastric caecae and posterior midgut while Cyt1Aa was also detected with a less extent on microvilli of anterior midgut cells (125). The immunocytochemical staining of the midgut section of *C. pipiens* larvae showed that the Cry4Aa toxin bound to the microvilli of the epithelial cells of posterior midgut and gastric caecae *in vitro* and the binding was almost abolished in the presence of excess unlabelled Cry4Aa, suggesting that the binding of Cry4Aa to the microvilli was specific (126). Immunocytochemical method was also used to investigate binding of Cry1Aa, Cry1Ab, Cry1Ac and Cry1Ea to susceptible and resistant *Plutella xylostella* to analyse mechanism of insecticide resistance in the insect pest (127). Binding to *M. sexta* and *Trichoplusia ni* larval midgut tissue sections *in vitro* revealed that the Cry1Ab domain II-III fragment bound along the microvilli of the midgut epithelial cells, suggesting that this fragment still retains binding property without domain I (128). It was shown that Cry1Ca and Cry4Aa bound to the microvilli of epithelial cells of *C. pipiens* in immunocytochemical staining of the larval midgut sections (129).

Copyright by Mahidol University

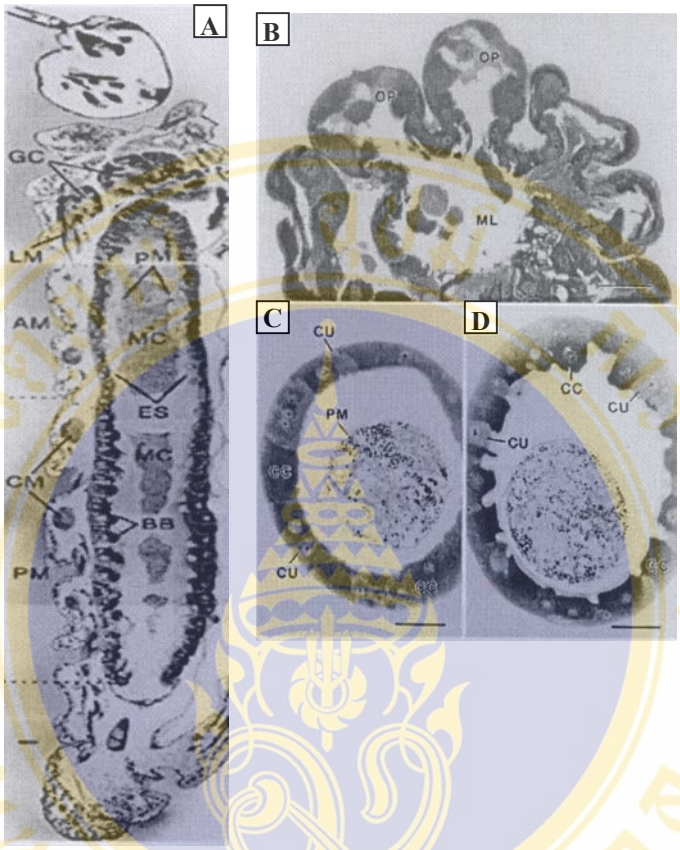

Figure 5: The midgut of *Aedes aegypti* fourth-instar larva under light microscope (122)

A: longitudinal section of a fourth-instar *A. aegypti* larva showing the alimentary canal at low magnification. GC: gastric caeca, AM: anterior midgut, PM: posterior midgut between dash lines, MC: midgut contents, PM: peritrophic membrane, ES: ectoperitrophic space, BB: brush border, CM: circular muscles and LM: longitudinal muscle. Scale bar, 50 μm.

B, C and D: cross sections of the gastric caeca, the anterior midgut and the posterior midgut, respectively. CU, CC and PM are cuboidal cells, columnar cells and peritrophic membrane, respectively. Scale bars, 20 μm.

Copyright by Mahidol University

Figure 6: Electron micrograph of an epithelial cell in gastric caeca of *Aedes aegypti* fourth-instar larva (122)

The figure shows an ion-transporting cell in gastric caeca. Mitochondria are seen in the apical region of this ion-transporting cell. Scale bar, 2 μm. The inset is a high-magnification, longitudinal view of microvilli containing mitochondria. Scale bar,100 nm.

Copyright by Mahidol University

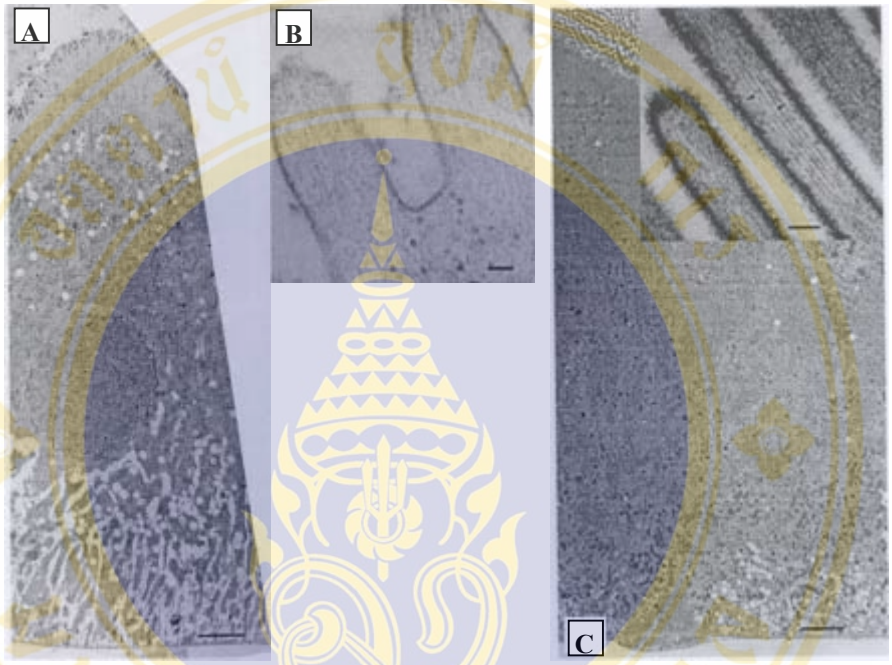

Figure 7: Electron micrographs of an epithelial cell in anterior midgut (A, B) and posterior midgut (C) of *Aedes aegypti* fourth-instar larva (122)

A: cross section showing short, broad apical microvilli (top) and mitochondria at the basal side (scale bar, 7 μm). B: a high-magnification view of the apical region of the cell showing two short microvilli (scale bar, 100 nm). C: low-magnificant cross section showing extensive, long, thin microvilli with wave-like besides perfectly straight and mitochondria at both apical and basal sides (scale bar, 5 μm) and the inset: a high-magnification view of the apical microvilli showing a fuzzy glycocalax coated on its outer side (scale bar, 100 nm).

Copyright by Mahidol University

1.2.7 Pore formation of Cry toxins

It has been proposed that after receptor binding, a monomeric activated Cry toxin forms a tetramer (prepore structure) before insertion into the membrane and subsequently pore formation (61; 62; 130; 131; 132; 133). Confirming this proposal, a tetrameric structure of the Cry1Aa toxin was demonstrated in synthetic lipid membrane (130). A stable oligomeric structure of Cry1Ab and Cry1Ac was found in BBMVs of susceptible insects (61; 131; 132), and this oligomeric structure resulted in formation of lytic pores (61). The regions involved in oligomerisation of Cry1Ab and Cry1Ac were identified in α4 and α5 and in loop between α2 and α3 (131; 132). The binding of Cry1Ab and Cry3Aa to their receptors resulted in proteolytic cleavage of helix 1 of the two toxins and a formation of a 250-kDa tetrameric prepore structure of which hydrophobic surfaces were exposed (61; 62). Formation of an oligomeric structure was also found in a pore-forming toxin from *Staphylococcus aureus* (134). Recently, using tryptophan spectroscopy studies and black lipid bilayer analysis, oligomeric structure of the Cry1Ab toxin was shown to be the membrane-insertion intermediate (133).

Two alternative models for mechanism of pore formation have been suggested: (i) the penknife model (135) which involves the filpout of α5 and α6 into the membrane like a penknife opening, and (ii) the umbrella model as shown in Figure 8 (5), which involves the insertion of α4 and α5, while the remaining helices opening on the surface of the membrane like the ribs of umbrella. Experimental data support the umbrella model which α4 and α5 insert into the membrane as a helical hairpin. Using a spectrofluorometric approach (14), a synthetic α5 peptide was shown to self-assemble in a membrane-bound state and caused a leakage of vascular content. α7, on the other hand, tended to lie on the surface of the membrane. Disulphide bridges were introduced into the pore-forming region of the Cry1Aa toxin to restrict the flexibility of helix movement within domain I and it was found that α4 and α5 are the most likely to partition into the lipid bilayer membrane and line the ion channel pore (15). Subsequently, synthetic peptides of α4 and α5 were shown to co-assemble in a lipid membrane and the other helices, with exception of α1, were located on surface of the membrane (16). By monitoring cysteine accessibility in the Cry1Aa toxin-induced channels, charged residues in α4 were suggested to play a direct role in regulating ion

Copyright by Mahidol University

flow, thus α4 was suggested to face to the pore lumen in planar lipid bilayers (136). Helical bundles of domain I seperated from the whole toxins of Cry1Ac and Cry3B2 could form ionic pores in planar lipid bilayer but the ionic conductance was not similar to that of the whole toxins (137; 138).

The structure of domain I suggests that the length of α1 and α2 (less than 14 amino acids) is not enough to span a 35-Å thick membrane bilayer while the other five α-helices, containing 22-36 amino acids in length, are long enough to span the membrane. In addition, α5 is relatively hydrophobic, surrounded by the other six amphipathic helices.

Mutagenic studies of α-helices in domain I have been extensively conducted. Mutations of some α5 residues of Cry1Ac (139) and of cysteine residues in the same α-helix of Cry1Ab (140) caused a complete loss of toxicity. Mutations of α4 residues resulted in a loss of irreversible binding and toxicity of Cry1Ab (13). Also, single proline substitutions in α4 of Cry4Ba showed a high loss of toxicity while the substitutions in α3 showed no effect on toxicity (141). Recently, individual changes of charged residues with exception of those involved in intramolecular salt bridges in α3 of Cry1Aa with either a neutral or an oppositely charged amino acid resulted in most mutants with a pore-forming ability similar to that of wild type, confirming that α3 is not directly involved in determining properties of the pore (142). Mutations that were introduced in α6 of Cry1Ac also showed no significant loss of toxicity (143).

However, there were two reports showing a contrast observation with the umbrella model and the previous studies that suggested α7 interacting with the membrane surface but not directly participating in membrane insertion and pore formation. Replacement of an amino acid region ($TVLDIVALF_{247}$, a conserved hydrophobic motif in Cry toxins) on the C-terminus of α7 of Cry1Ac with a corresponding region of the diptheria toxin suggested that this region is involved in pore formation and toxicity (144). In another report, individual alanine substitutions of all residues in α7 of Cry1Ab suggested certain residues being involved in toxicity and ion channel activity (145).

Domain III has also been suggested to be involved in ion channel function. The first and fourth arginines in a four-arginine region in a conserved β17 strand (the fourth conserved block in the five conserved blocks among Cry toxin family) have

Copyright by Mahidol University

been suggested to have a possible role in ion channel function of Cry1Aa (22; 23; 146). Recently, mutations in the Cry1Ac toxin of all the four arginines suggested that they are involved in maintaining both the structural stability of the wild type toxin and the full functionality of the pore formation (147).

Pore-forming activity assays have been performed using membranes containing receptor (brush border membrane from susceptible larval midgut, an insect cell line, and planar lipid bilayer or liposome containing receptor) and membranes without receptor (liposome or planar lipid bilayer). In most cases, Cry toxins caused inefficient pores and higher concentration of the toxins was required to cause the pores when the membranes without receptor were used (7; 148-151). In contrast, using the membranes containing receptor, the pore formation occurred at lower concentration of the toxins and showed higher efficient pores (152; 153).

Atomic force microscopy was carried out to measure the pore structure of Cry1Aa (130). The result clearly showed that the structure is composed of four subunits surrounding a 1.5-nm diameter central depression. Recently, using non-electrolyte exclusion technique and polyethylene glycol of various molecular weights, the radius of pore formed by the Cry1Ca toxin was estimated between 1.0 and 1.3 nm in planar lipid bilayers by estimating the radius of the smallest polyethylene glycol that was excluded from the pore (151).

Copyright by Mahidol University

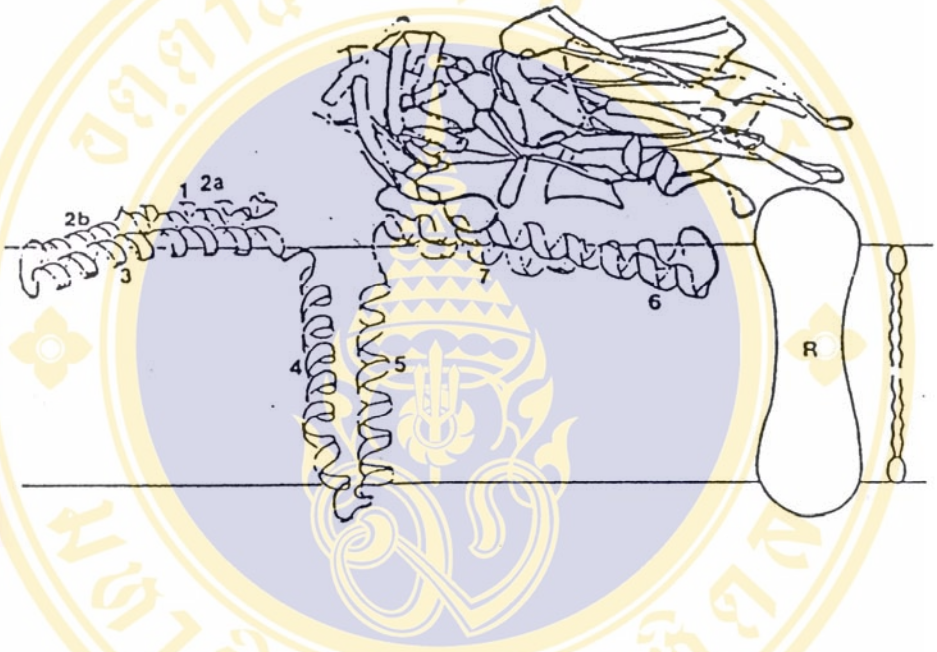

Figure 8: The umbrella model for insertion of *Bt* toxins into the insect plasma membrane based on the Cry3Aa structure (5)

The model shows that α4 and α5 drop down into the plasma membrane as a helical hairpin, and the other helices flat out on the membrane surface: their hydrophobic surfaces face toward the membrane.

Copyright by Mahidol University

CHAPTER II
OBJECTIVES

Certain surface-exposed loops (β2-β3 and/or β6-β7 and/or β10-β11 loops) at the molecular apex of domain II of Cry3Aa and Cry1Aa (Figure 3) have been suggested to play an important role in receptor binding. Based on the crystal structure of the mosquito-specific Cry4Ba toxin (10, Figures 3 and 9), six surface-exposed loops (β1-α 8, β2-β3, β4-β5, β6-β7, β8-β9 and β10-β11 loops) are located at the molecular apex of domain II. This suggests that residues in all the six surface-exposed loops may play a role in receptor binding. Previously, alanine substitutions of β2-β3 and β4-β5 loop residues revealed that only the Y332A and F364A mutants in β2-β3 and β4-β5 loops, respectively almostly lost their toxicity against *A. aegypti* mosquito larvae (21). It was suggested that an aromatic structure of tyrosine-332 and phenylalanine-364 (Figure 9) plays a critical role in larvicidal activity.

In this study, it was aimed to identify a critical residue in β6-β7, β8-β9 and β10-β 11 loops of the Cry4Ba domain II by changing individually to alanine. Their importance for toxicity was investigated against *A. aegypti* larvae.

Copyright by Mahidol University

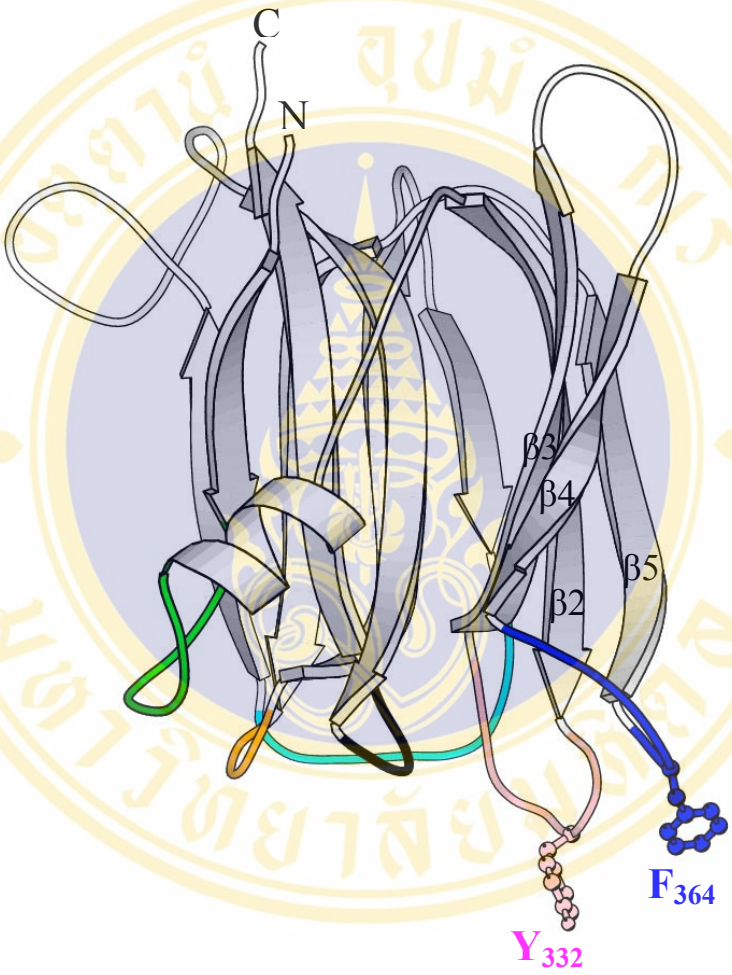

Figure 9: Domain II of the Cry4Ba toxin

The figure shows ribbon representation of the Cry4Ba-domain II generated by MolScript v2.1.2 based on the crystal structure of Cry4Ba (10), illustrating six surface-exposed loops at the molecular apex. The two critical residues (Y_{332} and F_{364} in β2-β3 and β4-β5 loops, respectively) are shown. The β2-β3, β4-β5, β6-β7, β8-β9, β10-β11 and β1-α8 loops are shaded by pink, blue, orange, cyan, black and green colours, respectively.

Copyright by Mahidol University

CHAPTER III
MATERIALS

3.1 Chemicals

ABI PRISM® BigDye™ Terminator Cycle Sequencing Ready Reaction Kits	Applied Biosystems
Acrylamide	Sigma
Ammonium persulfate	Sigma
Ampicillin	Sigma
Bovine serum albumin (2 mg/ml, no. 23209) used as a standard protein in protein concentration assay	Promega
Bradford protein assay reagent (Cat. no. 500-0006)	BIORAD
Cetyl trimethyl ammonium bromide (CTAB, $C_{19}H_{42}NBr$, FW: 364.5, Code H5882)	Sigma
Chloroform	Merck
Deoxynucleotide triphosphates	Pharmacia Biotech
3,3´-diaminobenzidine (DAB)	Vector, USA
Dithiothreitol (DTT, $C_4H_{10}O_2S_2$, MW: 154.25)	Merck
Ethanol	Merck
Glacial acetic acid	Merck
Glycerol	Merck
Isopropyl-β-D-thiogalactopyranoside (IPTG, $C_9H_{18}O_5S$, MW: 238.31)	Sigma
Lamda-*Bst*E II digested DNA marker (50 µg/ml)	BioLabs
Lamda-*Hin*d III digested DNA marker (50 µg/ml)	GIBCO BRL
Methanol	Merck
N,N´-methylene bis acrylamide	Sigma
pRB322-*Msp* I digested DNA marker (1000 µg/ml)	BioLabs
QIAprep Spin Miniprep Kit	QIAGEN

Copyright by Mahidol University

SDS-PAGE molecular mass standards (Broad range)	BIORAD
Sodium carbonate (Na_2CO_3, MW: 105.99, Cat. no. 71351)	Fluka
TEMED	BIORAD
Triton X-100	Sigma

3.2 Enzymes

Lysozyme (EC 3.2.1.17, L-6876)	Sigma
Ribonuclease A (RNase A, EC 3.1.27.5)	Sigma
Cloned *Pfu* DNA polymerase	Promega
Trypsin Type XIII (TPCK treated)	Sigma
Restriction endonucleases (Table 3)	Promega, BioLabs
Streptavidin conjugated with horseradish peroxidase (product number: 21126, ImmunoPure® streptavidin, horseradish peroxidase conjugated)	Pierce biotechnology, Inc.

Copyright by Mahidol University

Table 3: Restriction endonucleases with their recognition sites and optimal conditions

Enzyme	Recognition site	Buffer	Incubation temperature (°C)
Dpn I (Promega)	$G^{me}A\downarrow TC$	-	37
*Sau*3A I (Promega)	↓GATC	B	37
Cla I (Promega)	AT↓CGAT	C	37
*Bst*B I (BioLabs)	TT↓CGAA	NEBuffer 4	65
Sac I (Promega)	GAGCT↓C	J	37
*Bst*E II (Promega)	G↓GTNACC	D	60
Kpn I (Promega)	GGTAC↓C	J	37
Pst I (Promega)	CTGCA↓G	H	37
*Hin*d III (Promega)	A↓AGCTT	E	37
*Bst*N I (BioLabs)	CC↓(A/T)GG	NEBuffer 2	60
Acc I (Promega)	GT↓(A/C)(T/G)AC	G	37
*Eco*R I (Promega)	G↓AATTC	H	37
Dde I (Promega)	C↓TNAG	D	37

3.3 Growth media

Luria-Bertani (LB) broth: 0.5% yeast extract, 0.5% NaCl, 1% peptone

Luria-Bertani (LB) agar: 0.5% yeast extract, 0.5% NaCl, 1% peptone, 1.5% agar

3.4 Bacterial strain

Escherichia coli JM109 [*rec*A1 *sup*E44 *end*A1 *hsd*R17 *gyr*A96 *rel*A1 *thi*Δ(*lac-pro*AB) F′ (*tra* D36 *pro*AB^+ *lac*I^q l*acZ*ΔM15)], previously described by Yanisch-Perron et al. (154), was employed as a host cell for the expression of the Cry4Ba protoxin and its mutants.

Copyright by Mahidol University

3.5 Oligonucleotide primers

3.5.1 Site-directed mutagenesis

The oligonucleotide primers as shown below were designed as two complementary oligonucleotides containing the desired mutations according to the published *cry4Ba* gene sequence (155) and purchased from GENESET, Singapore. The complete sequence of the *cry4Ba* gene is shown in the appendix. The recognition sites introduced for restriction enzyme analysis are underlined. Bold letters represent the mutated nucleotide residues. f and r represent forward and reversed primers, respectively. The E417A primers were used to construct the S410A/E417A mutant.

Complementary primers for constructing β6-β7 loop mutants

S387A-f_*Bst*B I: 5′ -CACAGATACT**GC**CTCCCC**TTCGAA**TCGAGTTAC- 3′

S387A-r_*Bst*B I: 5′ -CTCGA**TTCGAA**GGGGAG**GC**AGTATCTGTGATAG- 3′

S388A-f_*Bst*B I: 5′ -GATACTAGC**G**CCCC**TTCGAA**TCGAGTTAC- 3′

S388A-r_*Bst*B I: 5′ -CTCGA**TTCGAA**GGGG**C**GCTAGTATCTGTG- 3′

P389A-f_*Sac* I: 5′ -CACAGATAC**GAGCTC**C**G**CCTCTAATCGAG- 3′

P389A-r_*Sac* I: 5′ -CGATTAGAGG**C**G**GAGCTC**GTATCTGTGATAG- 3′

S390A-f_*Bst*E II: 5′ -GCTCCCCC**G**CTAATA**G**G**GTTACC**AAAATGGATTTC- 3′

S390A-r_*Bst*E II: 5′ -CCATTTT**GGTAACC**C**T**ATTAG**C**GGGGGAGCTAG- 3′

Complementary primers for constructing β8-β9 loop mutants

S410A-f_*Kpn* I: 5′ -GAT**GGTACC**CTTGCCTCTTATAAT**G**CAAATATAACACC- 3′

S410A-r_*Kpn* I: 5′ -GTTATATTTG**C**ATTATAAGAGGCAAG**GGTACC**ATCAATTTTG- 3′

N411A-f_*Kpn* I: 5′ -GAT**GGTACC**CTTGCCTCTTATAATTCA**GC**TATAACACC- 3′

N411A-r_*Kpn* I: 5′ -GGTGTTATA**GC**TGAATTATAAGAGGCAAG**GGTACC**ATCAATTTTG- 3′

T413A-f_*Bst*B I: 5′ -CTTATAA**TTCGAA**TATA**G**CACCAACTCC- 3′

T413A-r_*Bst*B I: 5′ -GAGTTGGTG**C**TATA**TTCGAA**TTATAAGAG- 3′

T415A-f_*Bst*B I: 5′ -CTTATAA**TTCGAA**TATAACACCA**G**CTCCTGAAGG- 3′

T415A-r_*Bst*B I: 5′ -CTTCAGGAG**C**TGGTGTTATA**TTCGAA**TTATAAGAG- 3′

Copyright by Mahidol University

E417A-f_*Pst* I: 5′ -CAACTCCTG**C**AGGTTTAAGGACCAC- 3′
E417A-r_*Pst* I: 5′ -GTCCTTAAACCT**G**CAGGAGTTGGTG- 3′

G418A-f_*Hin*d III: 5′ -CAACTCCTGAAG**C**TTAAGGACCAC- 3′
G418A-r_*Hin*d III: 5′ -GTCCTTAA**G**CTTCAGGAGTTGGTG- 3′

Complementary primers for constructing β10-β11 loop mutants

D454A-f_*Sau*3A I: 5′ -CTGATGT**G**ATC**C**G**C**G**C**TATAACAGTAACAG- 3′
D454A-r_*Sau*3A I: 5′ -CTGTTATA**C**G**C**G**A**TC**C**ACATCAGTTTTTATATAG- 3′

Y455A-f_*Cla* I: 5′ -GATGTTATCGAT**G**C**G**AACAGTAACAG- 3′
Y455A-r_*Cla* I: 5′ -GTTACTGTT**C**G**C**ATC**G**ATAACATCAG- 3′

N456A-f_*Cla* I: 5′ -GATGTTATCGATTAT**G**CCAGTAACAGG- 3′
N456A-r_*Cla* I: 5′ -CTGTTACTG**G**CATAATC**G**ATAACATCAG- 3′

S457A-f_*Cla* I: 5′ -GATGTTATCGATTATAAC**G**CTAACAGGGTTTC- 3′
S457A-r_*Cla* I: 5′ -CCCTGTTA**G**CGTTATAATC**G**ATAACATCAG- 3′

Complementary primers for constructing Y455A/N456A mutant

Y455A/N456A-f: 5′ -GATGTTAT**A**GAT**G**C**G**GCCAGTAACAGGG- 3′
Y455A/N456A-r: 5′ -CCCTGTTACTGGC**C**G**C**ATC**T**ATAACATC- 3′

Complementary primers for constructing mutants in β-strand

T319A-f_*Bst*N I: 5′ -CATTTATTC**G**C**C**TGGCTAAAGAGAG- 3′
T319A-r_*Bst*N I: 5′ -CTTTAGCCA**G**G**C**GAATAAATGAACATC- 3′

R323A-f_*Acc* I: 5′ -GGCTAAAG**G**CAGTAGA**C**TTCTGGACCAATAC- 3′
R323A-r_*Acc* I: 5′ -GTCCAGAA**G**TCTACT**G**CCTTTAGCCAAGTG- 3′

Y408A-f_*Eco*R I: 5′ -CTTGCCTCT**G**C**G**AATTCAAATATAAC- 3′
Y408A-r_*Eco*R I: 5′ -TATTTGAATT**C**G**C**AGAGGCAAGAGTA- 3′

Y408W-f_*Eco*R I: 5′ -GCCTCTT**G**G**G**AATTCAAATATAAC- 3′
Y408W-r_*Eco*R I: 5′ -ATTTGAATT**C**C**C**AAGAGGCAAGAG- 3′

Copyright by Mahidol University

Y408D-f_*Dde* I: 5′ -GCCTC**AG**ATAATTCAAATATAAC- 3′
Y408D-r_*Dde* I: 5′ -ATTTGAATTAT**CT**GAGGCAAGAG- 3′

Y408E-f_*Eco*R I: 5′ -GCCTCT**G**A**G**AATTCAAATATAAC- 3′
Y408E-r_*Eco*R I: 5′ -ATTTGAATT**C**T**C**AGAGGCAAGAG- 3′

Y408C-f_*Kpn* I: 5′ -GGTAC**C**CTTGCCTCTT**G**TAATTCAAATATA- 3′
Y408C-r_*Kpn* I: 5′ -TTTGAATTA**C**AAGAGGCAAG**G**GTACCATC- 3′

Y408F-f_*Kpn* I: 5′ -GGTAC**C**CTTGCCTCTT**T**TAATTCAAATATA- 3′
Y408F-r_*Kpn* I: 5′ -TTTGAATTA**A**AAGAGGCAAG**G**GTACCATC- 3′

3.5.2 DNA sequencing

The primer for doing sequencing of S387A, S388A, P389A, S390A, S410A, N411A, T413A, T415A, E417A, G418A, D454A, Y455A, N456A, S457A, S410A/E417A, Y455A/N456A, Y408A, Y408W, Y408D, Y408E, Y408C and Y408F mutants:

H370A-f: 5′ -CAAATCTTACT**GC**TCA**G**ATTCAAC- 3′

The primer for sequencing of T319A and R323A mutants:

S387A-r: 5′ -CTCGATT**C**GAA**G**GGGGAG**GC**AGTATCTGTGATAG- 3′

3.6 Recombinant plasmid

pMU388 (156, Figure 10): The recombinant plasmid containing the *cry4Ba* protoxin gene encoding the 130-kDa protoxin was employed as the template for site-directed mutagenesis.

3.7 Antibodies

Mouse monoclonal antibody, 2F(1H2), that specifically recognises the Cry4Ba-domain III was provided by Dr. Watchara Kasinrerk, Faculty of Associated Medical Sciences, Chiang Mai University.

Rabbit anti mouse IgGs conjugated with biotin was purchased from Pierce biotechnology, Inc., product number: 31813 (ImmunoPure® Rabbit Anti-Mouse IgG, Fc Fragment Specific, Biotin Conjugated).

Copyright by Mahidol University

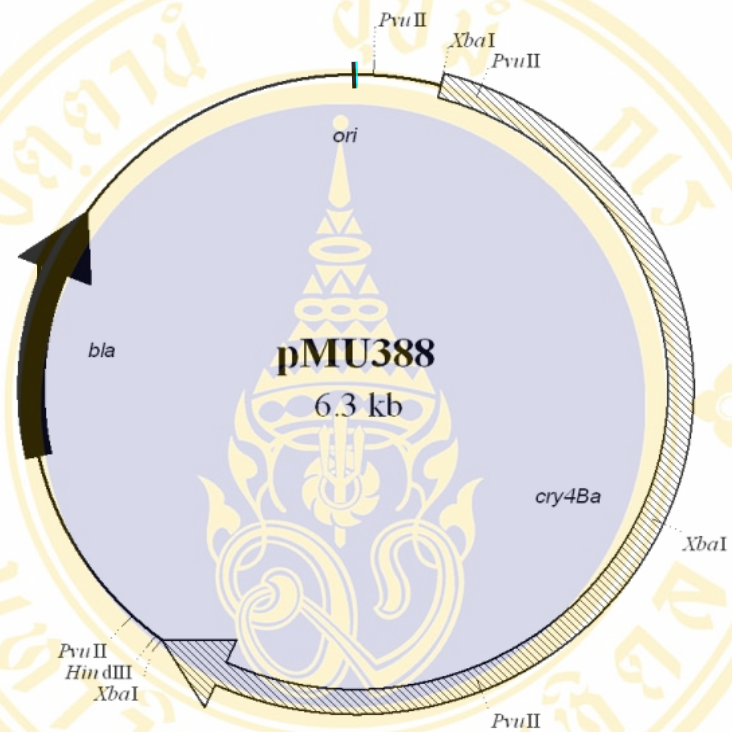

Figure 10: Physical map of plasmid pMU388

The figure shows the recombinant pMU388 plasmid containing the 130-kDa *cry4Ba* toxin gene (cross-hatch arrow). Ampicillin resistant gene (*bla*) and origin of replication (*ori*) in the pUC12 vector (thin line) are indicated. For clarity, not all restriction sites are shown.

Copyright by Mahidol University

CHAPTER IV
METHODS

4.1 Preparation of plasmid DNA template using the CTAB method (157)

A single colony of *E. coli* was inoculated in 3 ml LB broth containing 100 µg/ml ampicillin and incubated at 37 °C with 250 rpm shaking for 16-20 hr. Cell pellets were harvested in 1.5 ml microcentrifuge tube by centrifugation at 10,000 rpm for 1 min and then resuspended in 200 µl STET buffer (8% sucrose, 5% Triton X-100, 50 mM EDTA, 50 mM Tris-HCl, pH 8.0). The cell mixture was added with 10 µl of freshly prepared lysozyme solution (10 mg/ml) and incubated at room temperature for 20 min. Then, the mixture was boiled for exactly 30 sec and immediately centrifuged at 10,000 rpm for 15 min at room temperature. The pellet (chromosomal DNA) was removed with steriled toothpick. Plasmid DNA and residual low molecular weight RNA were recovered from the supernatant by adding 20 µl of 5% CTAB. The content was inverted 5-6 times, left at room temperature for 20 min and centrifuged at 12,000 rpm for 5 min at room temperature. The pellet was resuspended in 300 µl of 1.2 M NaCl by vigorously vortexing and 10 µl of 10 mg/ml RNase A was added to the suspension. The mixture was inverted and incubated at 37 °C for 30 min. The protein was removed by adding equal volume of chloroform and the mixture was inverted vigorously and centrifuged at 12,000 rpm for 5 min at room temperature. The clear aqueous phase was transferred to a new tube. The DNA pellets were precipitated with 2 volumes of absolute ethanol at -20 °C for 15 min and centrifuged at 12,000 rpm for 2 min at room temperature. The final DNA pellets were washed in 70% ethanol, dried and resuspended in 20 µl steriled double distilled water.

Copyright by Mahidol University

4.2 *In vitro* site-directed mutagenesis

The basic procedure based on Stratagene's Quick Change™ Site-directed mutagenesis Kit (Figure 11) utilises a supercoiled, double-stranded DNA (dsDNA) plasmid containing an insert of the gene of interest and two synthetic oligonucleotide primers containing the desired mutation. The oligonucleotide primers, each complementary to opposite strands of the plasmid, extend during temperature cycling by *Pfu* DNA polymerase which replicates both plasmid strands with high fidelity and without displacing the mutant primers. A plasmid containing the desired mutation and nicks is generated and treated with *Dpn* I to digest the parental DNA template and to select for mutation-containing synthesised DNA. This endonuclease is specific for methylated and hemimethylated DNA (5′-G^{me}A↓TC-3′). DNA isolated from almost all *E. coli* strains is dam methylated and therefore susceptible to *Dpn* I digestion. The nicked plasmid DNA containing the desired mutation is then transformed into *E. coli* cells.

4.2.1 Setting up and cycling the PCR reactions

The PCR reaction was prepared in a 0.25 ml PCR tube containing 50 µl of a reaction mixture (1x reaction buffer, 50 µM of each dNTP, 180 ng of each mutagenic primer, 20 ng of DNA templete prepared by the CTAB method and steriled double distilled water to a final volume of 50 µl). Then the mixture was added with 1 µl of 3 U/µl *Pfu* DNA polymerase. Each PCR reaction was cycled by using the cycling parameter outlined in Table 4 under the control of a Gene Amp System 2400 of Perkin Elmer Cetus. Following temperature cycling, each 15 µl PCR product was analysed on 1% agarose gel.

Copyright by Mahidol University

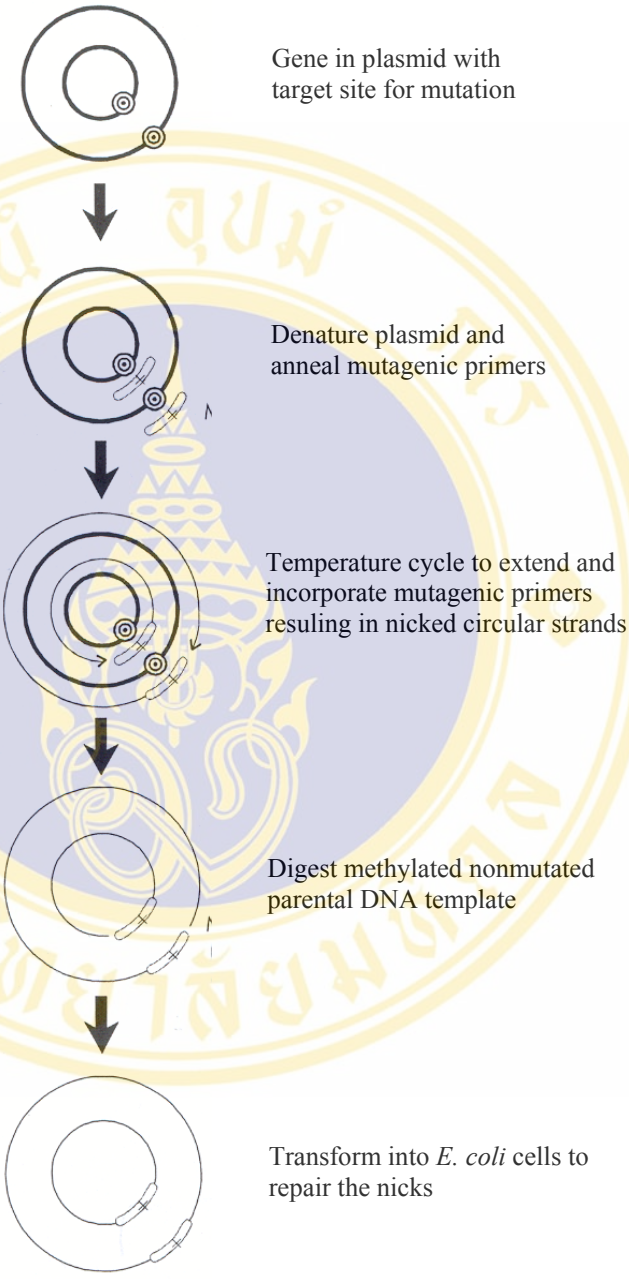

Figure 11: Overview of the Quick Change site-directed mutagenesis method
(redrawn from Stratagene's Quick Change™ Kit)

Copyright by Mahidol University

Table 4: Cycling parameter for the site-directed mutagenesis method

Segment	Cycle	Temperature	Time
1	1	95 °C	1 min
2	25	95 °C	30 sec
		40 °C	1.30 min
		68 °C	13 min
3	1	68 °C	7 min

4.2.2 Digesting the PCR products with *Dpn* I

Each PCR product was added with 1 µl of *Dpn* I restriction enzyme, mixed gently and thoroughly, and incubated at 37 °C for at least 2 hr. *Dpn* I will digest the parental supercoiled dsDNA. Then, the 15 µl *Dpn* I-digested PCR products were analysed on 1% agarose gel.

4.2.3 Transforming the *Dpn* I-digested PCR products into *E. coli* cells

4.2.3.1 Preparation of competent cells using $MgCl_2$-$CaCl_2$ method

A single colony of *E. coli* JM109 was inoculated into 3 ml of LB broth and incubated at 37 °C with 250 rpm shaking for 16-20 hr. The culture was diluted 1:100 into new LB broth and incubated at 37 °C until the OD_{600} was 0.3-0.5. The culture was chilled on ice for 30 min prior to pipetting the 40 ml aliquots of the culture into 50 ml steriled polypropylene tubes. The cells were pelleted by centrifugation at 3,000 rpm for 10 min at 4 °C and the cell pellets were resuspended in 10 ml of ice-cold 0.1 M $MgCl_2$ and placed on ice for 30 min. After centrifugation of the resuspended cells at 3,000 rpm for 10 min at 4 °C, the pellets were resuspended in 10 ml of ice-cold 0.1 M $CaCl_2$ and left on ice for 30 min. After centrifugating the resuspended cells at 3,000 rpm for 10 min at 4 °C, the pellets were resuspended in 1 ml of ice-cold 0.1 M $CaCl_2$ and left on ice for 1 hr to establish competency. Glycerol was added into the cell suspension to give a final concentration of 20% (v/v) and 300 µl aliquots were kept at -80 °C until required.

Copyright by Mahidol University

4.2.3.2 Transforming the *Dpn* I-digested PCR products into competent cells

A 300 µl aliquot of *E. coli* competent cells was mixed with 2 µl of *Dpn* I-digested PCR product and immediately placed on ice for 30 min. The cells were incubated at 42 °C for 90 sec and placed on ice for additional 5 min. The transformed cells were mixed with 900 µl of LB broth and incubated at 37 °C for 1 hr with shaking at 250 rpm. Finally, the 600 µl transformed culture was spreaded on a LB agar plate containing 100 µg/ml ampicillin and incubated at 37 °C for 16 hr.

4.3 Small-scale extraction of plasmid DNA by alkaline lysis method (158)

A single colony of *E. coli* transformants was grown for 16-20 hr in 3 ml LB broth containing 100 µg/ml ampicillin at 37 °C with shaking at 250 rpm. Cell pellets were harvested in 1.5 ml microcentrifuge tube by centrifugation at 10,000 rpm for 1 min and then resuspended in 100 µl of TEG (50 mM glucose, 25 mM Tris-HCl, 10 mM EDTA, pH 8.0, 0.1 mg/ml RNase A). The mixture was added with 200 µl of freshly prepared lysis solution (0.2 N NaOH, 1% SDS) and then gently inverted. After the lysate was neutralised by adding 150 µl of 3M sodium acetate, pH 4.8 to precipitate chromosomal DNA, it was centrifuged at 10,000 rpm for 10 min. Plasmid DNA was recovered from the supernatant by adding 2 volumes of absolute ethanol. The content was mixed by inversion and placed at -80 °C for 5 min. Then, the plasmid DNA pellets were obtained by centrifugation at 10,000 rpm for 10 min and washed with 500 µl of 70% ethanol. After centrifuged at 10,000 rpm for 5 min, the recovered pellets were dried at room temperature for 20 min and dissolved in 40 µl steriled double distilled water.

4.4 Restriction endonuclease digestion of plasmid DNA

The plasmids isolated from selected clones were analysed by restriction endonuclease digestion. The different types of desired mutations were analysed by using different restriction enzymes. The digestion reaction was performed in 20 µl of a mixture containing 1:10 dilution of reaction buffer for each restriction enzyme (Table 3 in Materials), 1:100 dilution of 10 µg/µl acetylated BSA for all enzymes from Promega or 1:100 dilution of 100 µg/ml BSA for *Bst*N I enzyme from BioLabs, 10 U of restriction endonuclease, 200-500 ng of plasmid DNA and steriled double distilled

Copyright by Mahidol University

water to a final volume of 20 µl. The reaction was gently and thoroughly mixed and spun down for 1 min. The reaction was incubated at the recommended temperature (Table 3 in Materials) for at least 2 hr to achieve complete digestion. The resulting DNA digestion patterns were analysed by agarose gel eletrophoresis.

4.5 Agarose gel electrophoresis

Analysis of DNA fragments was performed by submarine agarose gel electrophoresis. Seperation of the different DNA fragments depends on the molecular size of the DNA, gel concentration and conformation of the DNA. The appropriate gel concentration is dependent on the molecular weight of DNA to be analysed. The gel was prepared by completely dissolving the gel powder upon heating in TBE buffer (89 mM Tris-HCl, 89 mM boric acid, 25 mM EDTA, pH 8.0).

DNA samples were analysed by mixing with 1/3 volume of loading dye (0.1% bromophenol blue, 40% ficoll and 5 mM EDTA) and loading into wells of the gel submerged in TBE buffer. Electrophoresis was performed at constant voltage of 120 V. The gel was stained with ethidium bromide (2 µg/ml) for 10 min and destained with a large volume of distilled water. DNA patterns were visualised and photographed with the Geldoc® system from BIORAD.

4.6 Automated DNA sequencing

To confirm the resulting mutations, the ABI PRISM® BigDye™Terminator Cycle Sequencing Ready Reaction Kit was used to prepare samples for sequence analysis on the ABI Prism 377 DNA Sequencer. Principles of this kit are based on fluorescent-labelled terminator cycle sequencing.

The sequencing reaction was performed in 20 µl of a mixture containing 4 µl of Terminator Premix, 2 µl of sequencing buffer, 500 ng of plasmid DNA template prepared by using QIAprep Spin Miniprep Kit, 360 ng of primer for doing sequencing (Material 3.5.2) and steriled double distilled water to a final volume of 20 µl. The reaction mixture was carried out in an automated thermal cycler (Perkin Elmer Cetus Model 2400) with the following conditions:

96 °C 1 min for 1 cycle

96 °C 10 sec, 50 °C 5 sec, 60 °C 4 min for 25 cycles

Copyright by Mahidol University

After completion of the PCR cycles, the PCR product was recovered by the method of ethanol/sodium acetate precipitation in manual of the ABI PRISM® BigDye™ Terminator Cycle Sequencing Ready Reaction Kit. The dye-labelled PCR product was analysed on the ABI Prism 377 DNA Sequencer.

4.7 Preparation of target proteins from *E. coli* cell lysates (159)

A single colony of *E. coli* JM109 containing the desired mutant plasmid was inoculated in 3 ml LB broth containing 100 µg/ml ampicillin and incubated for 16-20 hr at 37 °C with 250 rpm shaking. The culture was inoculated 1% in new LB broth containing 100 µg/ml ampicillin and grown at 37 °C with 250 rpm shaking until the OD_{600} was 0.3-0.5. Subsequently, the culture was induced with IPTG at a final concentration of 1 mM for 4 hr. The cultured cells, 10^8 cells (1 OD_{600}) were collected by centrifugation at 10,000 rpm for 1 min at room temperature. The protoxin expression level of the cells was analysed on 10% SDS-polyacrylamide gel electrophoresis.

4.8 SDS-polyacrylamide gel electrophoresis (SDS-PAGE)

The protein samples were prepared by mixing with 4x sample buffer (4% SDS, 4 mM EDTA, 40% glycerol, 1.45 mM bromophenol blue, 100 mM DTT, 200 mM Tris-HCl, pH 7.5). The sample mixtures were placed in a heat box at 95 °C for 10 min and subsequently centrifuged at 10,000 rpm for 10 min. The supernatants were loaded on each well of SDS-polyacrylamide gel. The SDS-polyacrylamide gel was prepared according to the formulation in Table 5 and tools for electrophoresis were Mini-Protein II electrophoresis set (BIORAD). The electrophoresis was runned in Tri-glycine buffer (192 mM glycine, 0.1% SDS, 25 mM Tris-HCl, pH 8.3) at the constant current of 50 mA. The protein patterns were visualised by incubating with staining solution (0.1% Coomassie Brilliant Blue R250, 50% methanol, 10% glacial acetic acid) for 1 hr at room temperature with shaking and destaining solution (10% methanol, 10% glacial acetic acid) for 5 hr at room temperature with shaking. Finally, the gel was taken photograph using the Geldoc® system from BIORAD and kept in box containing distilled water.

Copyright by Mahidol University

Table 5: Formulation for SDS-polyacrylamide gel

Solution	Stacking gel 6% (6 ml)	Separating gel (20 ml) 10%	15%
30% acrylamide stock solution[a] (ml)	1.2	6.6	10
1.5 M Tris-HCl, pH 8.8 (ml)	-	5	5
0.5 M Tris-HCl, pH 6.8 (ml)	1.5	-	-
Distilled water (ml)	3.2	8	4.7
10% SDS (µl)	60	200	200
10% ammonium persulfate (µl)	40	100	100
TEMED (µl)	20	20	20

[a]30% acrylamide stock solution: 29.7% (w/v) acrylamide, 0.3% (w/v) N,N´-methylene bis acrylamide

4.9 Mosquito-larvicidal activity assay

Larvicidal activity assay was performed in a 48-well microtiter plate (11.3 mm well diameter, Costar). Each well contained 1 ml of distilled water, ten 2-day old *Aedes aegypti* larvae and 10^8 *E. coli* JM109 cells expressing mutant protoxin. A total of 100 larvae were used per each *E. coli* clone. % Mortality was recorded after 24-hr incubation at room temperature (25 °C). *E. coli* JM109 cells expressing mutant protoxin were prepared according to Method 4.7. The 2-day old mosquito larvae were prepared by hatching about 600 larvae from the eggs in a plastic tray (22×30×10 cm) containing about 3 litres of tap water and 3 rat diet pellets. The rearing tray was incubated at room temperature (25 °C) for 2 days.

4.10 Partial purification of protoxin inclusions (160)

A single colony of *E. coli* JM109 containing the desired mutant plasmid was inoculated in 3 ml LB broth containing 100 µg/ml ampicillin and incubated for 16-20 hr at 37 °C with 250 rpm shaking. 1% inoculation of the culture in a new LB broth containing 100 µg/ml ampicillin was grown at 37 °C with 250 rpm shaking until the

Copyright by Mahidol University

OD_{600} was 0.3-0.5. After induction with IPTG at the final concentration of 1 mM for 4 hr at 37 °C with 250 rpm shaking, the cells were harvested by centrifugation at 7,000 rpm for 7 min at 4 °C. The cell pellet was resuspended in ice-cold distilled water. The cell suspension was lysed by using a French Pressure cell at 1,200 psi. The protoxin inclusions were sedimented by centrifugation at 10,000 rpm for 10 min at 4 °C and washed 3 times with ice-cold distilled water and stored at -30 °C. The protoxin inclusion patterns were analysed on 10% SDS-PAGE (Method 4.8).

4.11 Determination of protein concentration

Protein concentration was determined using Bradford protein assay reagent based on the principle of Bradford (161) and bovine serum albumin to construct a standard curve. The reaction mixtures were measured the absorbance at 595 nm using Hitachi U-2000 spectrophotometer.

4.12 Solubilisation and proteolytic activation of protoxin inclusions (39)

Partially purified inclusions were solubilised in 50 mM Na_2CO_3, pH 9.0 at the final concentration of 1 mg/ml at 37 °C for 1.30 hr. Any insoluble protoxin inclusions were removed by centrifugation at 10,000 rpm for 10 min. The extent of solubility was analysed on 10% SDS-PAGE. The soluble protoxins were incubated with trypsin at the ratio of 1:20 (w/w, enzyme/protein) at 37 °C for 12-16 hr. The trypsin digestion patterns were analysed on 15% SDS-PAGE (Method 4.8).

4.13 FPLC purification of the activated toxins

The activated toxin was purified by using ÄKTA purified liquid chromatography system (Amersham Pharmacia Biotech Inc. NJ, USA) linked to a Superdex-200 HR 10/30 column containing 20% ethanol as preservative (Amersham code number: 17-1088-01), based on the principle of gel filtration. Before injection of the activated toxin sample, the column was washed at the flow rate of 0.4 ml/min with 2 column volumes (50 ml) of MilliQ water that was passed through a 0.45 μm filter, and equilibrated at the same flow rate and volume of 50 mM Na_2CO_3, pH 9.0 prepared in filtrated MilliQ water. During the equilibrating step, the activated toxin sample was centrifuged at 12,000 rpm 10 min and the supernatant was taken to a new tube.

Copyright by Mahidol University

Finishing the equilibrating step, the sample was injected into the column and collected as 1-ml fraction at the flow rate of 0.4 ml/min with the 50 mM Na_2CO_3, pH 9.0 as eluting buffer. The fractions were placed on ice, measured protein concentration (Method 4.11) and analysed on 15% SDS-PAGE (Method 4.8).

4.14 *In vitro* receptor binding assay using immunocytochemical method

A. aegypti larval sections were prepared by Dr. Urai Chaisri, Department of Tropical Pathology, Faculty of Tropical Medicine, Mahidol University using the paraffin technique. 5-day old larvae were placed into plastic dish containing ice-cold fixative solution (4% paraformaldehyde, 5% sucrose, PBS-150 mM NaCl, 8.56 mM Na_2HPO_4, 1.42 mM $NaH_2PO_4.H_2O$, pH 7.4) and their heads were cut out. The fixative solution containing the dissected larvae was incubated at 4 ºC for 4-5 hr. After that, the fixative solution was replaced with fixative solution containing 10% sucrose. The fixed larvae were dehydrated in a serial of ethanol baths and cleared in xylene bath. Then, the larvae were infiltrated in three paraffin baths at 65 ºC under evacuation to absolutely remove the clearing solution. The infiltrated larvae were placed in mold and the melted paraffin was filled. The mold was moved to the cooling place. Until the paraffin solidified, the larvae were sectioned into 10-µm slices and attached on mounting glass coated with 3-aminopropyltriethoxysilane.

The slide containing the sectioned larvae was incubated in air bath for 1 hr at 60 º C. The section was then deparaffinated in two baths containing xylene and then in two baths containing absolute ethanol for 2 min in each bath. The section was hydrated in a series of ethanol baths and soaked in tap water for 5 min. To block the endogenous peroxidase, the section was incubated with PBS, pH 7.4 containing 5% H_2O_2 for 30 min at room temperature. The section was covered with normal rabbit serum at dilution 1:200 for 45 min at room temperature in humidified chamber to block non-specific protein binding.

In immunocytochemical detection, the larval sections were incubated with 300 µl of 12.5 ng/µl purified toxin for 45 min at room temperature in humidified chamber. 50 mM Na_2CO_3, pH 9.0 alone that was used as eluting buffer in the toxin purification step was used as a negative control. The sections were washed 3 times with 0.1% Triton X-100 in PBS, pH 7.4 for 5 min each time. The sections were then incubated with 300 µl

Copyright by Mahidol University

of the primary antibodies (mouse-anti Cry4Ba-domain III monoclonal antibody, 2F (1H2)) undiluted or diluted in PBS, pH 7.4 at 1:20 at room temperature in humidified chamber for 45 min. The sections were washed 3 times again with 0.1% Triton X-100 in PBS, pH 7.4 for 5 min each time. Then the sections were incubated with 300 µl of the secondary antibody (rabbit-anti mouse IgGs conjugated with biotin) diluted in PBS, pH 7.4 at 1:2,000 or 1:8,000 for 45 min at room temperature in humidified chamber. The sections were washed 3 times in 0.1% Triton X-100 in PBS, pH 7.4 for 5 min each time. Then, the sections were incubated with 300 µl of 5 µg/ml streptavidin conjugated with horseradish peroxidase diluted with PBS, pH 7.4 at room temperature for 45 min in humidified chamber. The sections were washed 3 times with 0.1% Triton X-100 in PBS, pH 7.4 for 5 min each time followed by 2 times with PBS, pH 7.4 for 5 min each time. The binding of toxin on the larval sections was detected as dark brown color after the addition of 3,3′-diaminobenzidine (Vector, USA) for 2 min and the reaction was stopped with distilled water. Finally, the sections were mounted with permount solution and viewed under 400x magnification of light microscope.

Copyright by Mahidol University

CHAPTER V
RESULT I: INVOLVEMENT IN TOXICITY OF β6-β7, β8-β9 AND β10-β11 LOOP RESIDUES

5.1 Constructions of β6-β7, β8-β9 and β10-β11 loop mutants

Fourteen loop mutants were initially constructed by single mutations of all residues in the β6-β7 loop ($SSPS_{390}$) and the β10-β11 loop ($DYNS_{457}$) and selected residues in the β8-β9 loop (S_{410}, N_{411}, T_{413}, T_{415}, E_{417} and G_{418}) in domain II of the Cry4Ba toxin (Figures 3 and 9) via PCR-based mutagenesis as described in Method 4.2. The plasmid pMU388 containing the *cry4Ba* gene (Material 3.6) was used as template and the oligonucleotides (Material 3.5.1) were used as mutagenic primers to substitute these residues individually with alanine in order to investigate an effect on toxicity.

After temperature cycling, 15 µl of the PCR-amplified products were analysed on agarose gel electrophoresis as shown in Figures 12, 14A and 15A. As can be seen that all the PCR products appeared to contain a major band of 6.3-kb nicked plasmid. In order to eliminate the nonmutated parental DNA template, the PCR products were digested with *Dpn* I endonuclease and 15 µl of *Dpn* I-digested PCR products were analysed on agarose gel electrophoresis. It was found that the bands of 6.3-kb plasmids still appeared (Figures 13, 14B and 15B).

5.2 Screening of the loop mutant plasmids

2 µl of each *Dpn* I-digested PCR product was then transformed into *E. coli* JM109 cells (Method 4.2.3). Ten to twenty ampicillin resistant colonies were randomly selected and screened for the desired loop mutant plasmids by restriction endonuclease digestion in comparison with the wild type plasmid.

For the β6-β7 loop mutant plasmids, p4B-S387A and p4B-S388A were digested with *Bst*B I while p4B-P389A and p4B-S390A were digested with *Sac* I and *Bst*E II, respectively. The results of one clone of each mutant are shown in Figures 16A-19A.

Copyright by Mahidol University

For the β8-β9 loop mutant plasmids, p4B-S410A and p4B-N411A were digested with *Kpn* I, p4B-T413A and p4B-T415A were cut with *Bst*B I, and p4B-E417A and p4B-G418A were cut with *Pst* I and *Hin*d III, respectively. The resulting restriction patterns of the desired loop mutant plasmids are shown in Figures 20A-25A.

For the β10-β11 loop mutant plasmids, p4B-D454A was digested with *Sau*3A I, while p4B-Y455A, p4B-N456A and p4B-S457A were digested with *Cla* I, as the results shown in Figures 26A-29A.

The tentative mutant clones that showed correct restriction patterns were further verified of their mutated regions by automated DNA sequencing (Method 4.6). The DNA sequencing results revealed that all of the mutant clones showed nucleotide changes at the desired positions (Figures 16B-29B). The verified mutant clones were then used as a candidate for protoxin expression in *E. coli* JM109 cells and for toxicity assay against *A. aegypti* mosquito larvae.

5.3 Protoxin expression of the β6-β7, β8-β9 and β10-β11 loop mutants

All the verified mutant plasmids, p4B-S387A, p4B-S388A, p4B-P389A, p4B-S390A, p4B-S410A, p4B-N411A, p4B-T413A, p4B-T415A, p4B-E417A, p4B-G418A, p4B-D454A, p4B-Y455A, p4B-N456A and p4B-S457A were expressed in *E. coli* JM109 cells with 1 mM IPTG induction at 37 °C for 4 hr. Crude extracts from about 10^7 culture cells (0.1 OD_{600}) were analysed for protoxin expression levels on 10% SDS-PAGE (Method 4.7) in comparison with the crude extract from cells expressing the Cry4Ba wild type. As shown in Figures 30 and 31, all the loop mutant clones expressed a 130-kDa protoxin with yields similar to the wild type. The results were based on three independent experiments.

5.4 Mosquito-larvicidal activity of the β6-β7, β8-β9 and β10-β11 loop mutants

When *E. coli* cells expressing the Cry4Ba wild type or mutant protoxins were tested for toxicity against *A. aegypti* mosquito larvae (Method 4.9), the P389A, S410A, E417A, Y455A and N456A mutants showed a reduction in larvicidal activity to about 65%. On the other hand, nine other mutants, S387A, S388A, S390A, N411A, T413A, T415A, G418A, D454A and S457A still retained about 90% larvicidal activity similar to the wild type (Figure 32). These results suggest that P_{389} in the β6-β7 loop,

Copyright by Mahidol University

S_{410} and E_{417} in the β8-β9 loop, and Y_{455} and N_{456} in the β10-β11 loop play a role in larvicidal activity of the Cry4Ba toxin.

Copyright by Mahidol University

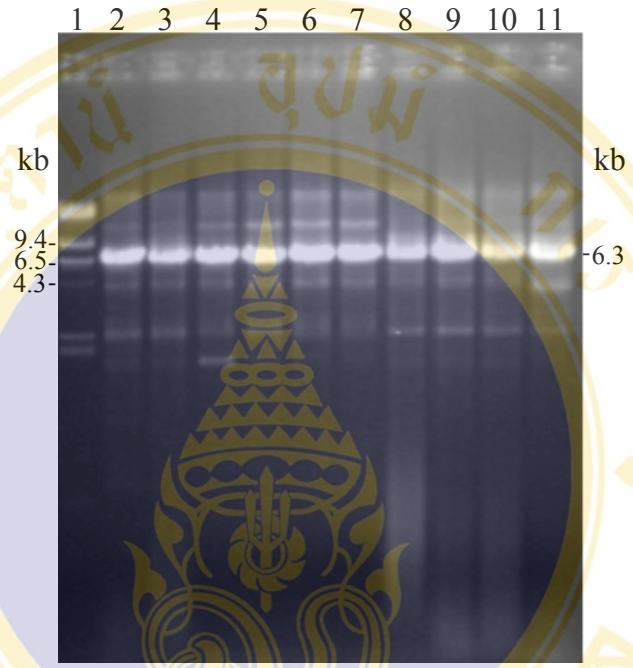

Figure 12: Amplification of the β6-β7 and β8-β9 loop mutant plasmids

The figure shows 1% agarose gel electrophoresis (ethidium bromide stained) of the resulting PCR products.

Lane 1:	*Hin*d III-digested λ DNA markers
Lanes 2-5:	the PCR products of the tentative β6-β7 loop mutant plasmids; p4B-S387A, p4B-S388A, p4B-P389A and p4B-S390A, respectively
Lanes 6-11:	the PCR products of the tentative β8-β9 loop mutant plasmids; p4B-S410A, p4B-N411A, p4B-T413A, p4B-T415A, p4B-E417A and p4B-G418A, respectively

Copyright by Mahidol University

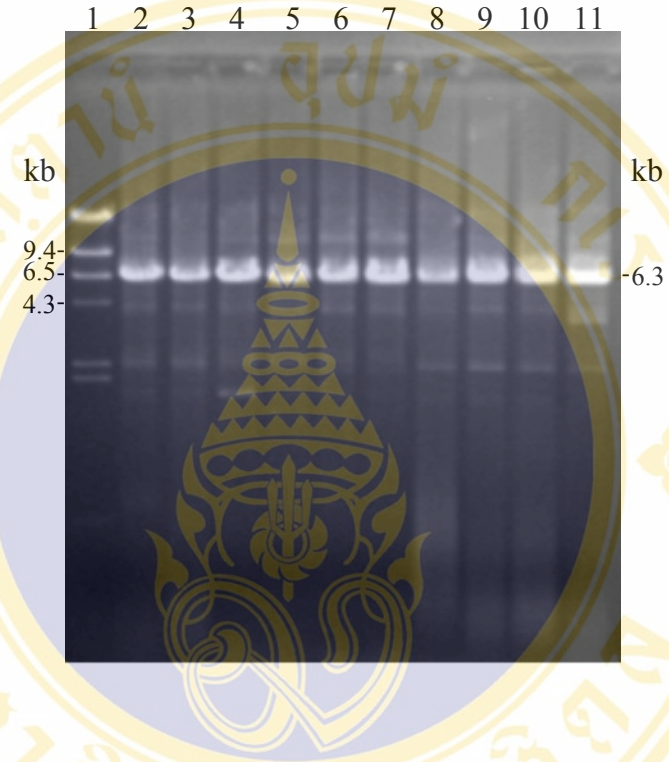

Figure 13: *Dpn* I digestion of the PCR products of the β6-β7 and β8-β9 loop mutant plasmids

The figure shows 1% agarose gel electrophoresis (ethidium bromide stained) of *Dpn* I digestion of the PCR products.

Lane 1: *Hin*d III-digested λ DNA markers
Lanes 2-5: the *Dpn* I-digested PCR products of the tentative β6-β7 loop mutant plasmids; p4B-S387A, p4B-S388A, p4B-P389A and p4B-S390A, respectively
Lanes 6-11: the *Dpn* I-digested PCR products of the tentative β8-β9 loop mutant plasmids; p4B-S410A, p4B-N411A, p4B-T413A, p4B-T415A, p4B-E417A and p4B-G418A, respectively

Copyright by Mahidol University

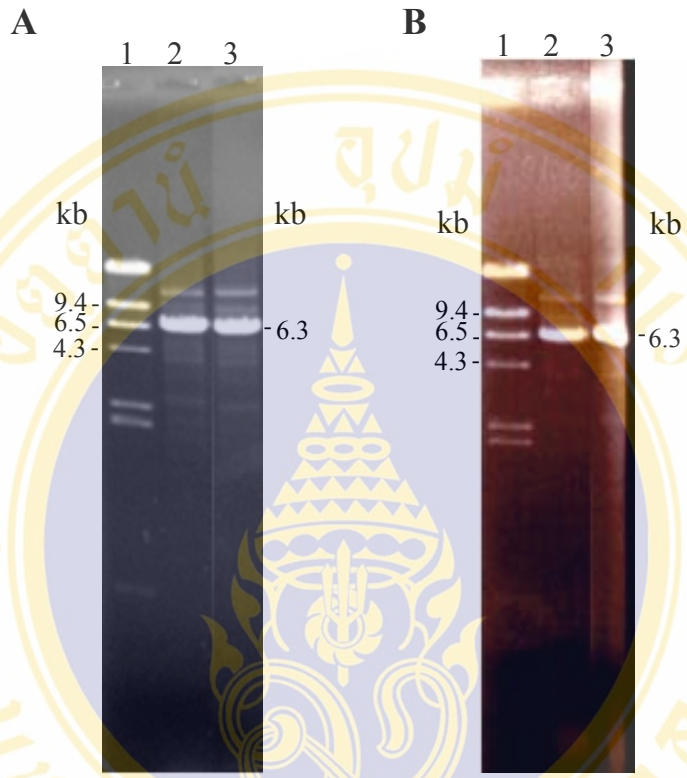

Figure 14: Amplification and *Dpn* I digestion of the p4B-D454A and p4B-N456A mutant plasmids

The figure shows 1% agarose gel electrophoresis (ethidium bromide stained) of the resulting PCR products (panel A) and their *Dpn* I digestion products (panel B).

Lane 1: *Hin*d III-digested λ DNA markers
Lanes 2 & 3: the PCR products of the tentative mutant plasmids; p4B-D454A and p4B-N456A, respectively

Copyright by Mahidol University

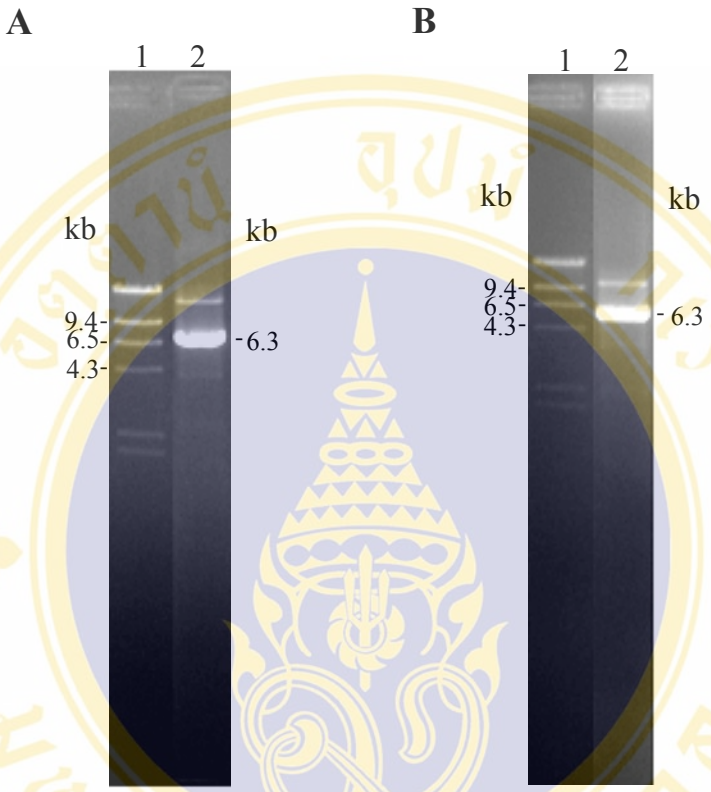

Figure 15: Amplification and *Dpn* I digestion of the p4B-S457A mutant plasmid

The figure shows 1% agarose gel electrophoresis (ethidium bromide stained) of the resulting PCR product (panel A) and its *Dpn* I digestion product (panel B).

Lane 1: *Hin*d III-digested λ DNA markers
Lane 2: the PCR product of the tentative mutant plasmid-p4B-S457A

Copyright by Mahidol University

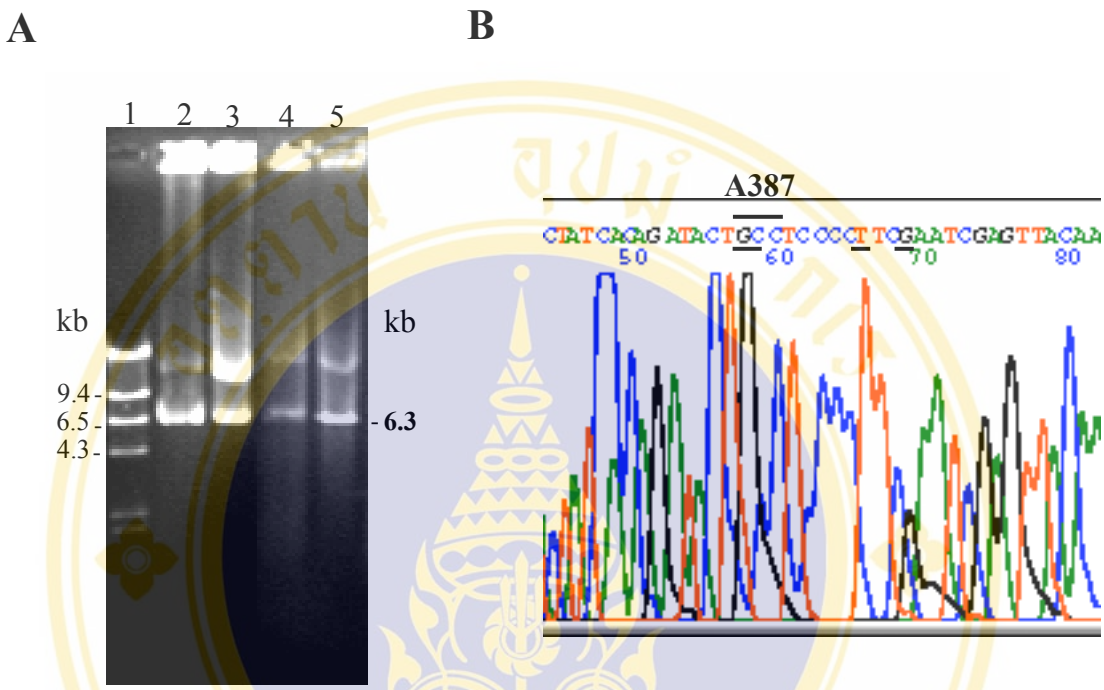

Figure 16: Restriction endonuclease and DNA sequence analysis of p4B-S387A

A: 1% agarose gel electrophoresis (ethidium bromide stained) of *Bst*B I digestion pattern of the mutant plasmid. The 6.3-kb mutant specific DNA band is indicated with the bold label.

Lane 1:	*Hin*d III-digested λ DNA markers
Lanes 2 & 3:	the undigested and *Bst*B I-digested wild type plasmid (pMU388), respectively
Lanes 4 & 5:	the undigested and *Bst*B I-digested mutant plasmid (p4B-S387A), respectively

B: Part of DNA sequencing chromatogram of p4B-S387A. The nucleotide sequence of the coding strand for the mutant plasmid is shown. The substituted bases and amino acid are indicated. Reaction conditions are described in Method 4.6.

Copyright by Mahidol University

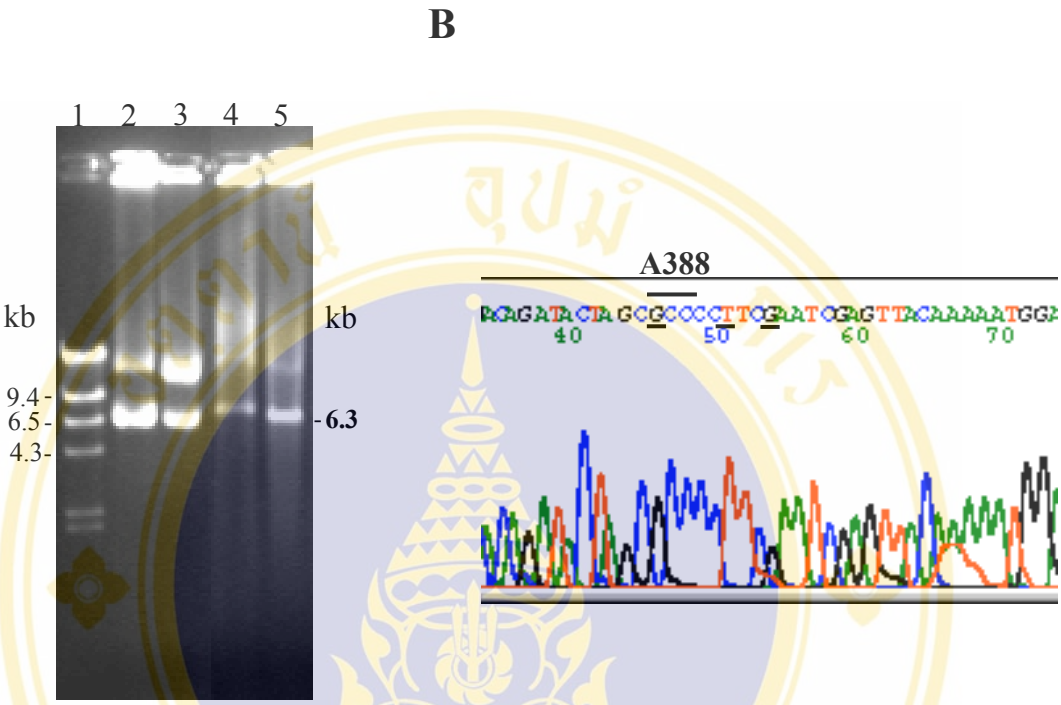

Figure 17: Restriction endonuclease and DNA sequence analysis of p4B-S388A

A: 1% agarose gel electrophoresis (ethidium bromide stained) of *Bst*B I digestion pattern of the mutant plasmid. The 6.3-kb mutant specific DNA band is indicated with the bold label.

Lane 1:	*Hin*d III-digested λ DNA markers
Lanes 2 & 3:	the undigested and *Bst*B I-digested wild type plasmid (pMU388), respectively
Lanes 4 & 5:	the undigested and *Bst*B I-digested mutant plasmid (p4B-S388A), respectively

B: Part of DNA sequencing chromatogram of p4B-S388A. The nucleotide sequence of the coding strand for the mutant plasmid is shown. The substituted bases and amino acid are indicated. Reaction conditions are described in Method 4.6.

Copyright by Mahidol University

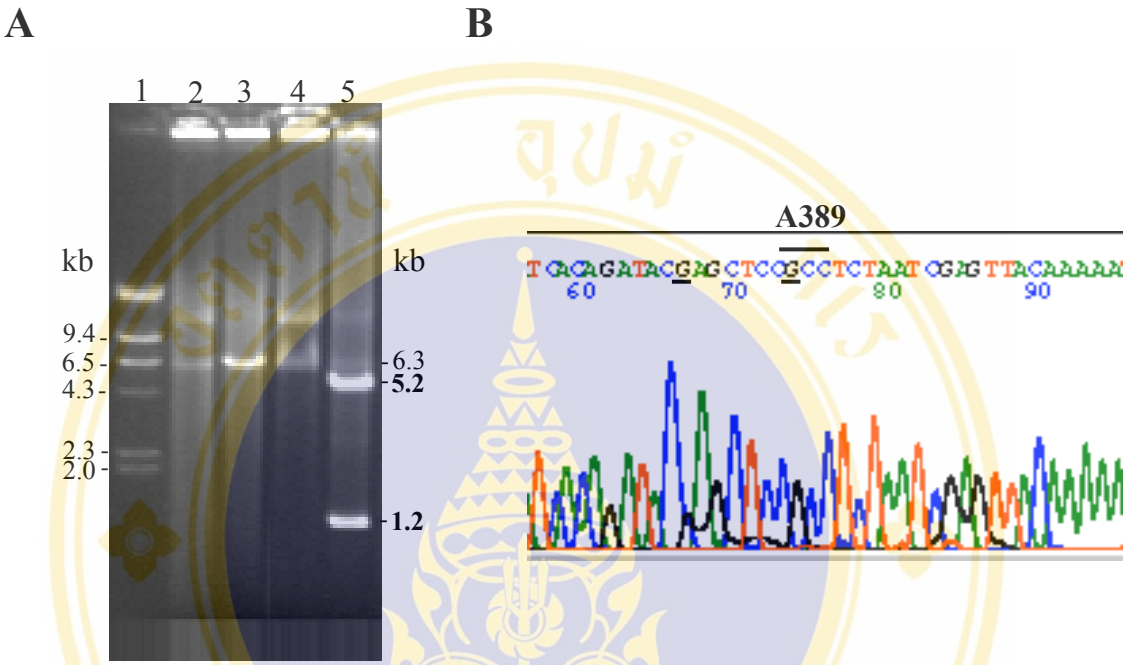

Figure 18: Restriction endonuclease and DNA sequence analysis of p4B-P389A

A: 1% agarose gel electrophoresis (ethidium bromide stained) of *Sac* I digestion pattern of the mutant plasmid. The 5.2- and 1.2-kb mutant specific DNA bands are indicated with the bold labels.

Lane 1:	*Hin*d III-digested λ DNA markers
Lanes 2 & 3:	the undigested and *Sac* I-digested wild type plasmid (pMU388), respectively
Lanes 4 & 5:	the undigested and *Sac* I-digested mutant plasmid (p4B-P389A), respectively

B: Part of DNA sequencing chromatogram of p4B-P389A. The nucleotide sequence of the coding strand for the mutant plasmid is shown. The substituted bases and amino acid are indicated. Reaction conditions are described in Method 4.6.

Copyright by Mahidol University

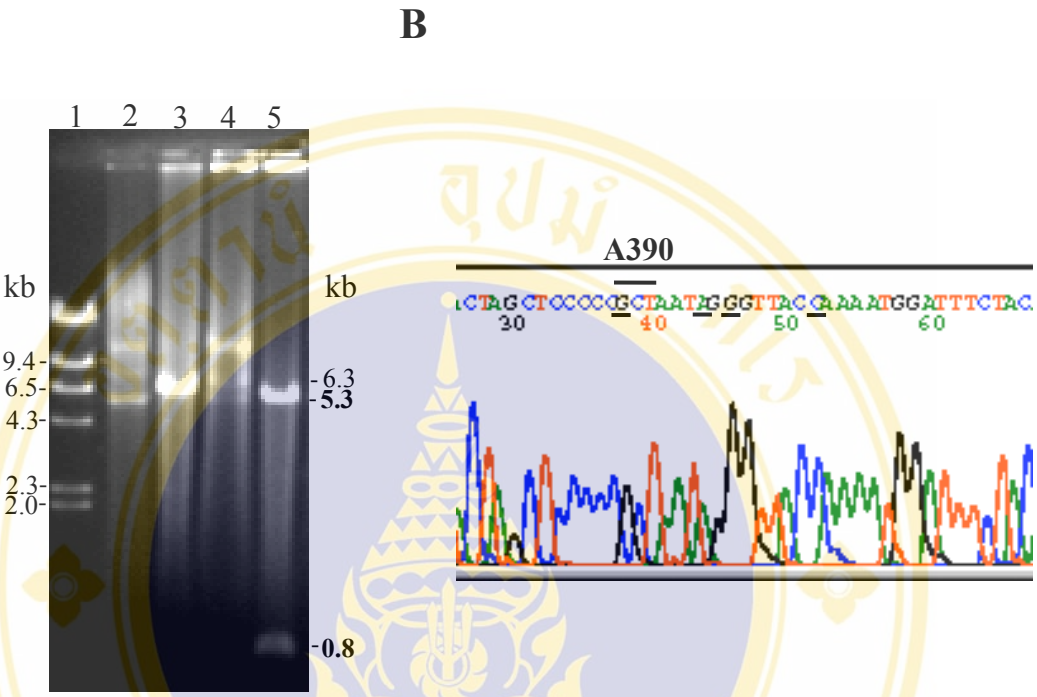

Figure 19: Restriction endonuclease and DNA sequence analysis of p4B-S390A

A: 1% agarose gel electrophoresis (ethidium bromide stained) of *Bst*E II digestion pattern of the mutant plasmid. The 5.3- and 0.8-kb mutant specific DNA bands are indicated with the bold labels.

Lane 1:	*Hin*d III-digested λ DNA markers
Lanes 2 & 3:	the undigested and *Bst*E II-digested wild type plasmid (pMU388), respectively
Lanes 4 & 5:	the undigested and *Bst*E II-digested mutant plasmid (p4B-S390A), respectively

B: Part of DNA sequencing chromatogram of p4B-S390A. The nucleotide sequence of the coding strand for the mutant plasmid is shown. The substituted bases and amino acid are indicated. Reaction conditions are described in Method 4.6.

Copyright by Mahidol University

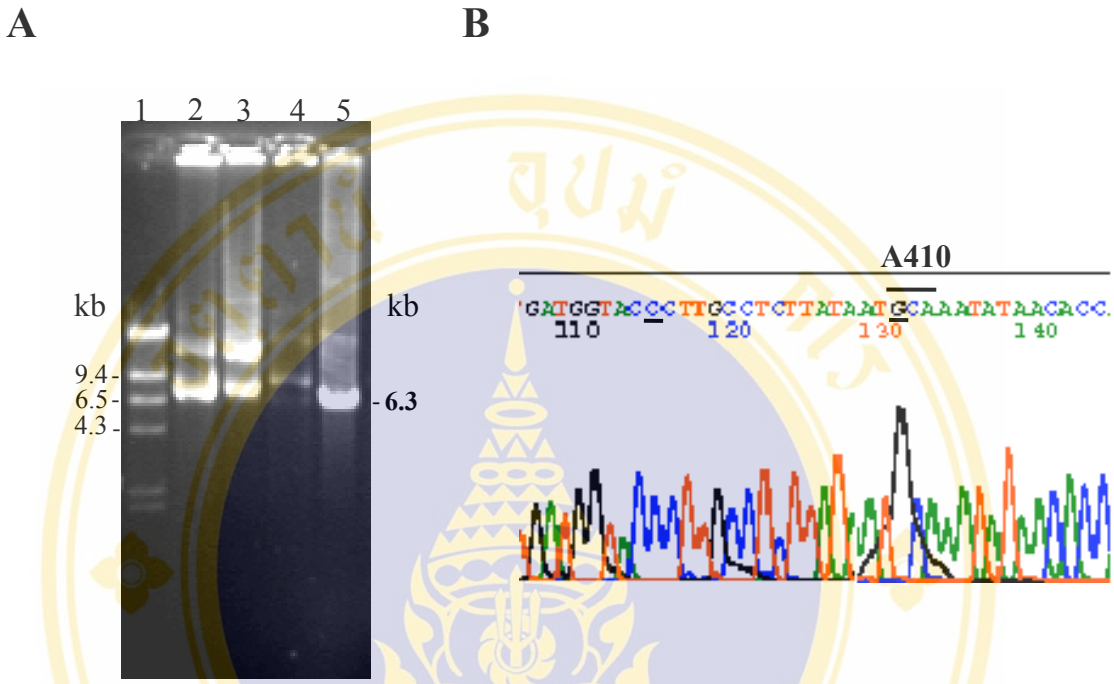

Figure 20: Restriction endonuclease and DNA sequence analysis of p4B-S410A

A: 1% agarose gel electrophoresis (ethidium bromide stained) of *Kpn* I digestion pattern of the mutant plasmid. The 6.3-kb mutant specific DNA band is indicated with the bold label.

Lane 1:	*Hin*d III-digested λ DNA markers
Lanes 2 & 3:	the undigested and *Kpn* I-digested wild type plasmid (pMU388), respectively
Lanes 4 & 5:	the undigested and *Kpn* I-digested mutant plasmid (p4B-S410A), respectively

B: Part of DNA sequencing chromatogram of p4B-S410A. The nucleotide sequence of the coding strand for the mutant plasmid is shown. The substituted bases and amino acid are indicated. Reaction conditions are described in Method 4.6.

Copyright by Mahidol University

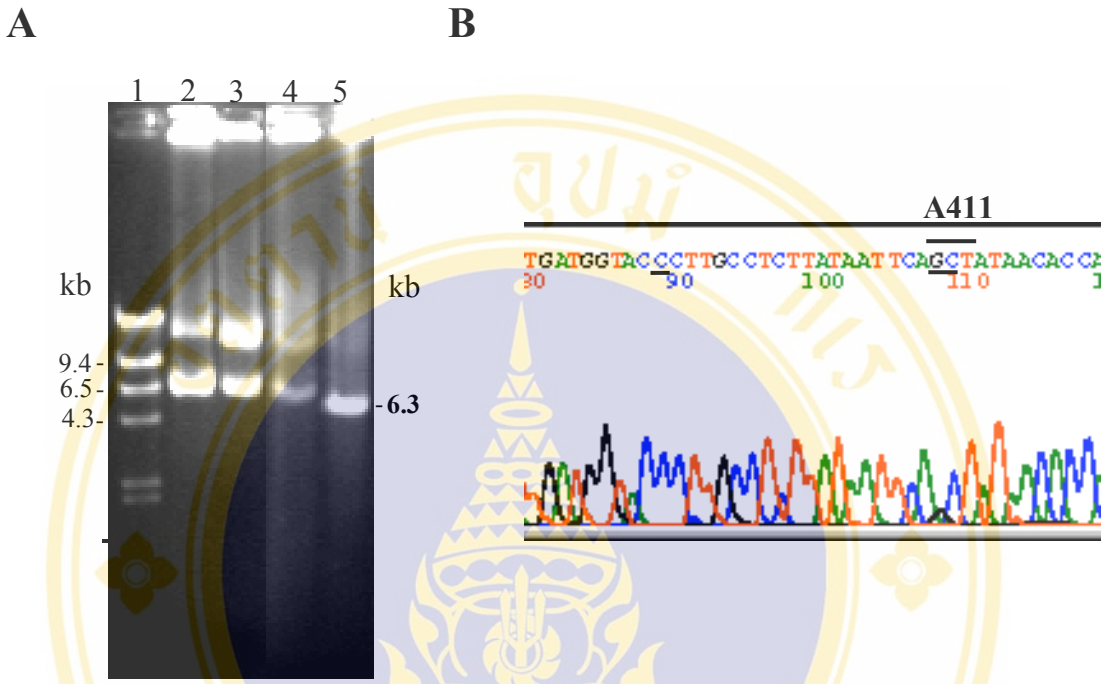

Figure 21: Restriction endonuclease and DNA sequence analysis of p4B-N411A

A: 1% agarose gel electrophoresis (ethidium bromide stained) of *Kpn* I digestion pattern of the mutant plasmid. The 6.3-kb mutant specific DNA band is indicated with the bold label.

Lane 1:	*Hin*d III-digested λ DNA markers
Lanes 2 & 3:	the undigested and *Kpn* I-digested wild type plasmid (pMU388), respectively
Lanes 4 & 5:	the undigested and *Kpn* I-digested mutant plasmid (p4B-N411A), respectively

B: Part of DNA sequencing chromatogram of p4B-N411A The nucleotide sequence of the coding strand for the mutant plasmid is shown. The substituted bases and amino acid are indicated. Reaction conditions are described in Method 4.6.

Copyright by Mahidol University

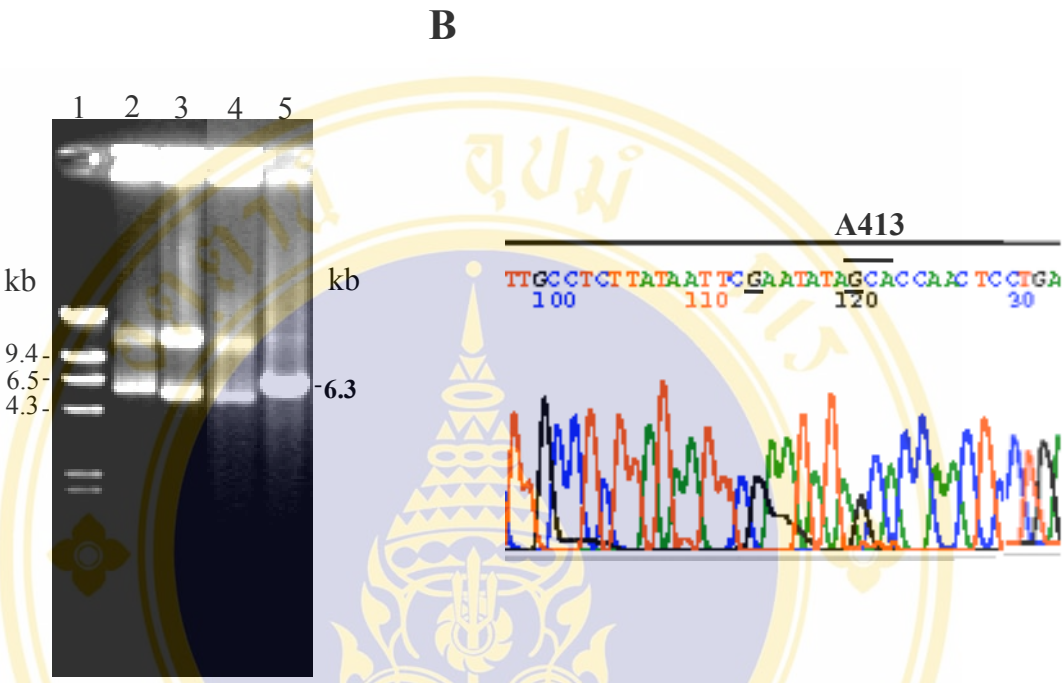

Figure 22: Restriction endonuclease and DNA sequence analysis of p4B-T413A

A: 1% agarose gel electrophoresis (ethidium bromide stained) of *Bst*B I digestion pattern of the mutant plasmid. The 6.3-kb mutant specific DNA band is indicated with the bold label.

Lane 1:	*Hin*d III-digested λ DNA markers
Lanes 2 & 3:	the undigested and *Bst*B I-digested wild type plasmid (pMU388), respectively
Lanes 4 & 5:	the undigested and *Bst*B I-digested mutant plasmid (p4B-T413A), respectively

B: Part of DNA sequencing chromatogram of p4B-T413A. The nucleotide sequence of the coding strand for the mutant plasmid is shown. The substituted bases and amino acid are indicated. Reaction conditions are described in Method 4.6.

Copyright by Mahidol University

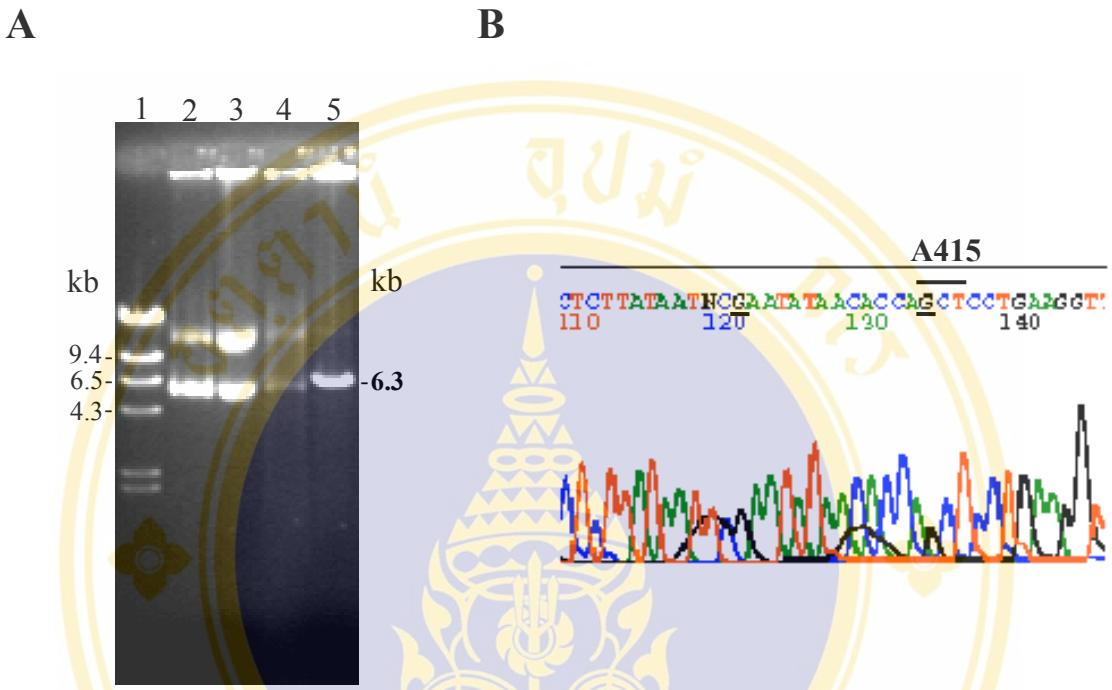

Figure 23: Restriction endonuclease and DNA sequence analysis of p4B-T415A

A: 1% agarose gel electrophoresis (ethidium bromide stained) of *Bst*B I digestion pattern of the mutant plasmid. The 6.3-kb mutant specific DNA band is indicated with the bold label.

Lane 1:	*Hin*d III-digested λ DNA markers
Lanes 2 & 3:	the undigested and *Bst*B I-digested wild type plasmid (pMU388), respectively
Lanes 4 & 5:	the undigested and *Bst*B I-digested mutant plasmid (p4B-T415A), respectively

B: Part of DNA sequencing chromatogram of p4B-T415A. The nucleotide sequence of the coding strand for the mutant plasmid is shown. The substituted bases and amino acid are indicated. Reaction conditions are described in Method 4.6.

Copyright by Mahidol University

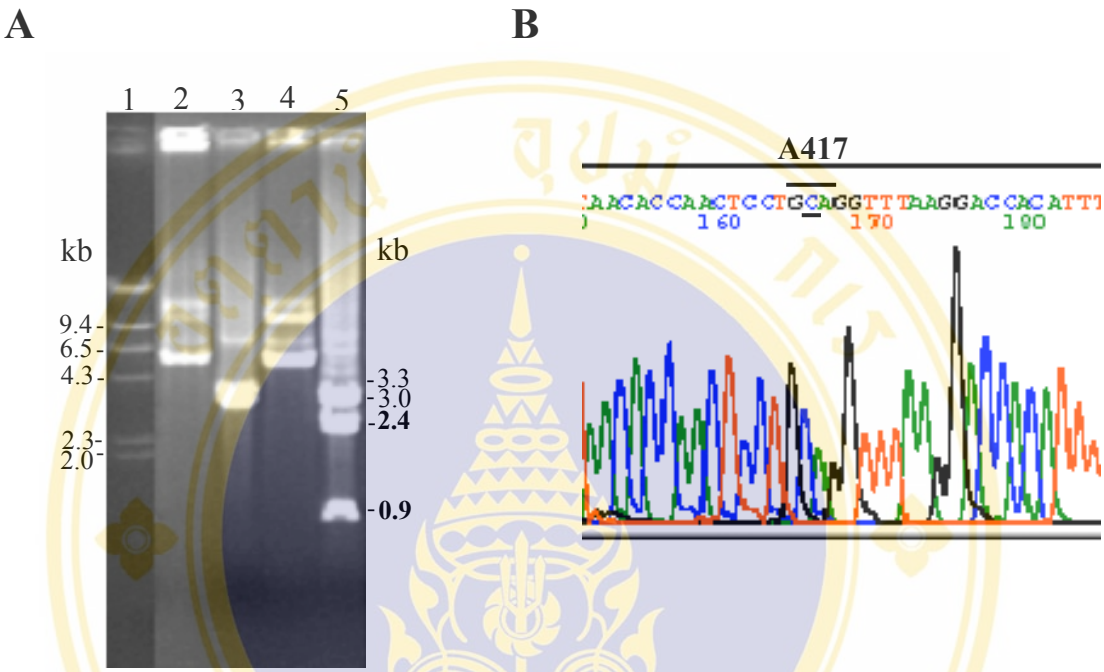

Figure 24: Restriction endonuclease and DNA sequence analysis of p4B-E417A

A: 1% agarose gel electrophoresis (ethidium bromide stained) of *Pst* I digestion pattern of the mutant plasmid. The 2.4- and 0.9-kb mutant specific DNA bands are indicated with the bold labels.

Lane 1:	*Hin*d III-digested λ DNA markers
Lanes 2 & 3:	the undigested and *Pst* I-digested wild type plasmid (pMU388), respectively
Lanes 4 & 5:	the undigested and *Pst* I-digested mutant plasmid (p4B-E417A), respectively

B: Part of DNA sequencing chromatogram of p4B-E417A. The nucleotide sequence of the coding strand for the mutant plasmid is shown. The substituted base and amino acid are indicated. Reaction conditions are described in Method 4.6.

Copyright by Mahidol University

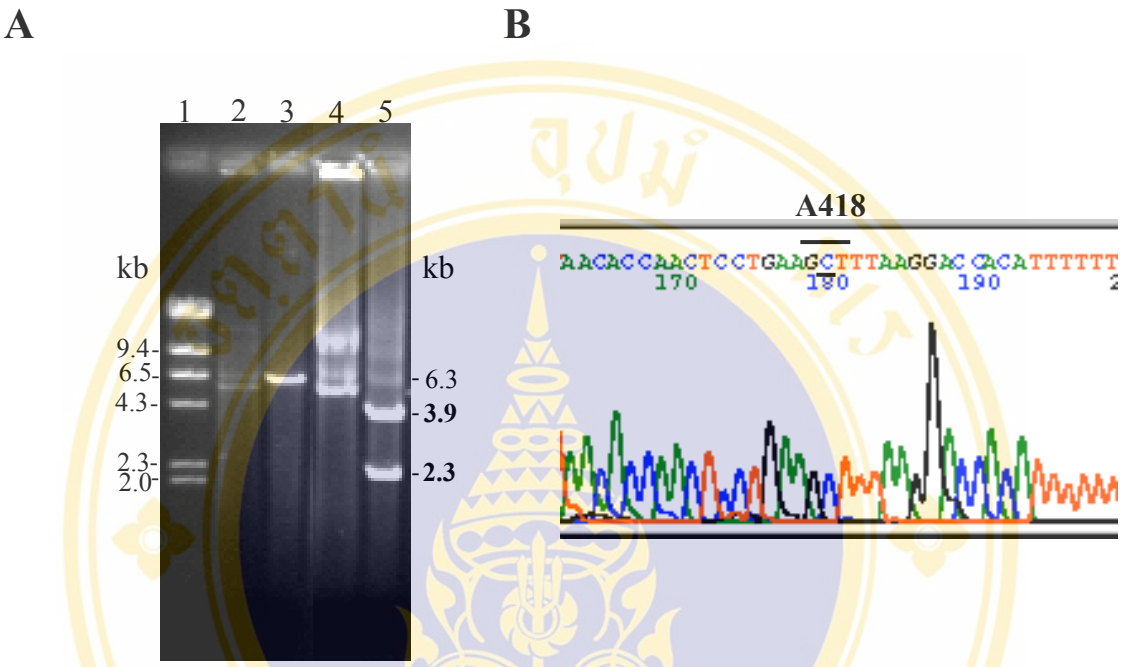

Figure 25: Restriction endonuclease and DNA sequence analysis of p4B-G418A

A: 1% agarose gel electrophoresis (ethidium bromide stained) of *Hin*d III digestion pattern of the mutant plasmid. The 3.9- and 2.3-kb mutant specific DNA bands are indicated with the bold labels.

Lane 1:	*Hin*d III-digested λ DNA markers
Lanes 2 & 3:	the undigested and *Hin*d III-digested wild type plasmid (pMU388), respectively
Lanes 4 & 5:	the undigested and *Hin*d III-digested mutant plasmid (p4B-G418A), respectively

B: Part of DNA sequencing chromatogram of p4B-G418A. The nucleotide sequence of the coding strand for the mutant plasmid is shown. The substituted base and amino acid are indicated. Reaction conditions are described in Method 4.6.

Copyright by Mahidol University

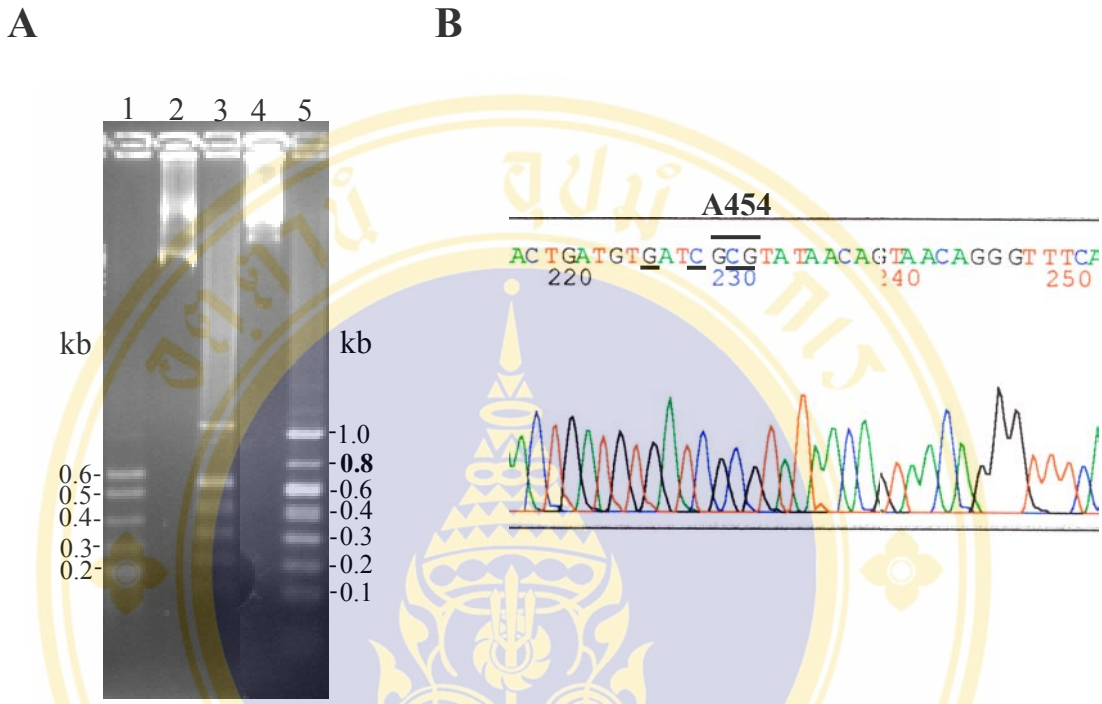

Figure 26: Restriction endonuclease and DNA sequence analysis of p4B-D454A

A: 2% agarose gel electrophoresis (ethidium bromide stained) of *Sau*3A I digestion pattern of the mutant plasmid. The 0.8-kb mutant specific DNA band is indicated with the bold label.

Lane 1:	*Msp* I-digested pBR322 DNA markers
Lanes 2 & 3:	the undigested and *Sau*3A I-digested mutant plasmid (p4B-D454A), respectively
Lanes 4 & 5:	the undigested and *Sau*3A I-digested wild type plasmid (pMU388), respectively

B: Part of DNA sequencing chromatogram of p4B-D454A. The nucleotide sequence of the coding strand for the mutant plasmid is shown. The substituted bases and amino acid are indicated. Reaction conditions are described in Method 4.6.

Copyright by Mahidol University

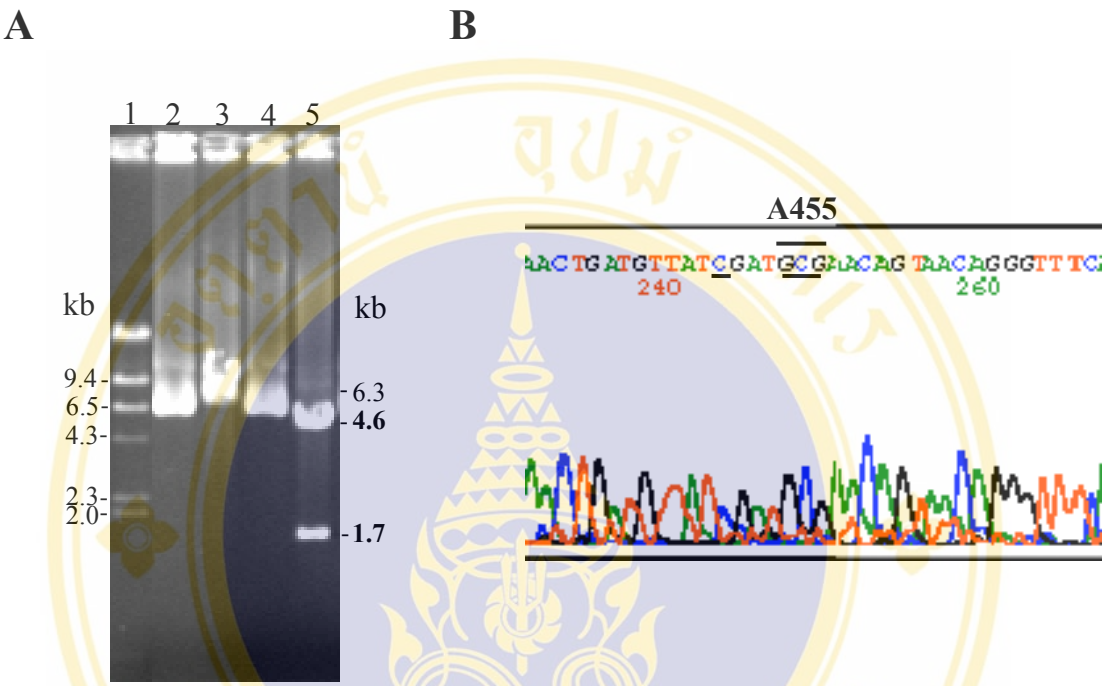

Figure 27: Restriction endonuclease and DNA sequence analysis of p4B-Y455A

A: 1% agarose gel electrophoresis (ethidium bromide stained) of *Cla* I digestion pattern of the mutant plasmid. The 4.6- and 1.7-kb mutant specific DNA bands are indicated with the bold labels.

Lane 1:	*Hin*d III-digested λ DNA markers
Lanes 2 & 3:	the undigested and *Cla* I-digested wild type plasmid (pMU388), respectively
Lanes 4 & 5:	the undigested and *Cla* I-digested mutant plasmid (p4B-Y455A), respectively

B: Part of DNA sequencing chromatogram of p4B-Y455A. The nucleotide sequence of the coding strand for the mutant plasmid is shown. The substituted bases and amino acid are indicated. Reaction conditions are described in Method 4.6.

Copyright by Mahidol University

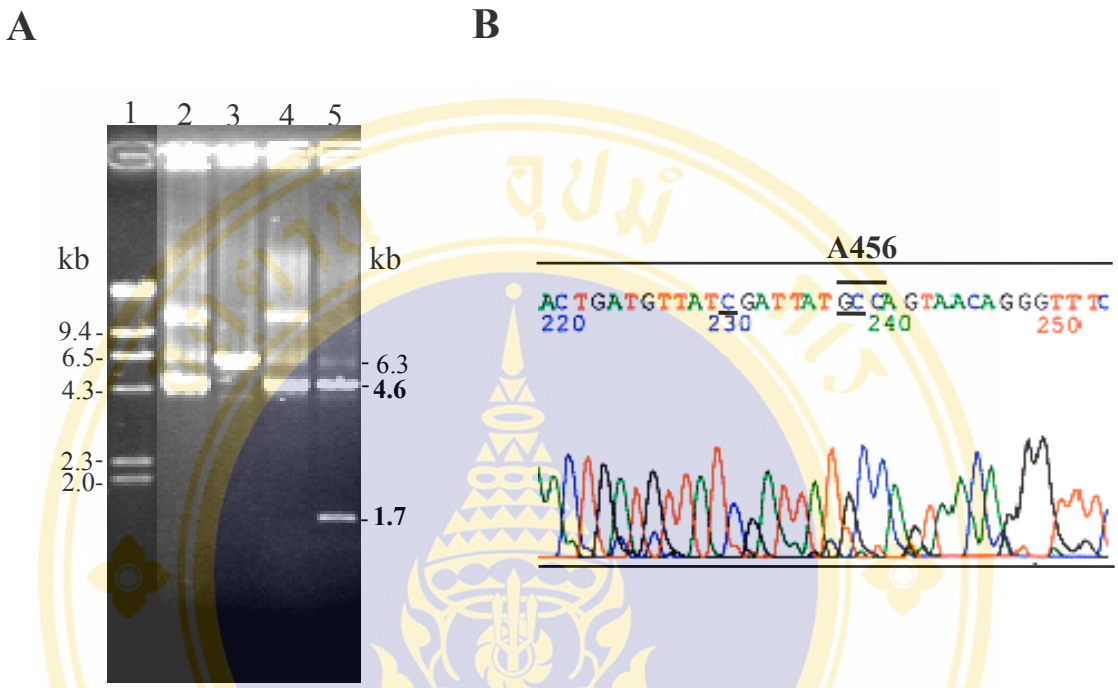

Figure 28: Restriction endonuclease and DNA sequence analysis of p4B-N456A

A: 1% agarose gel electrophoresis (ethidium bromide stained) of *Cla* I digestion pattern of the mutant plasmid. The 4.6- and 1.7-kb mutant specific DNA bands are indicated with the bold labels.

Lane 1:	*Hin*d III-digested λ DNA markers
Lanes 2 & 3:	the undigested and *Cla* I-digested wild type plasmid (pMU388), respectively
Lanes 4 & 5:	the undigested and *Cla* I-digested mutant plasmid (p4B-N456A), respectively

B: Part of DNA sequencing chromatogram of p4B-N456A. The nucleotide sequence of the coding strand for the mutant plasmid is shown. The substituted bases and amino acid are indicated. Reaction conditions are described in Method 4.6.

Copyright by Mahidol University

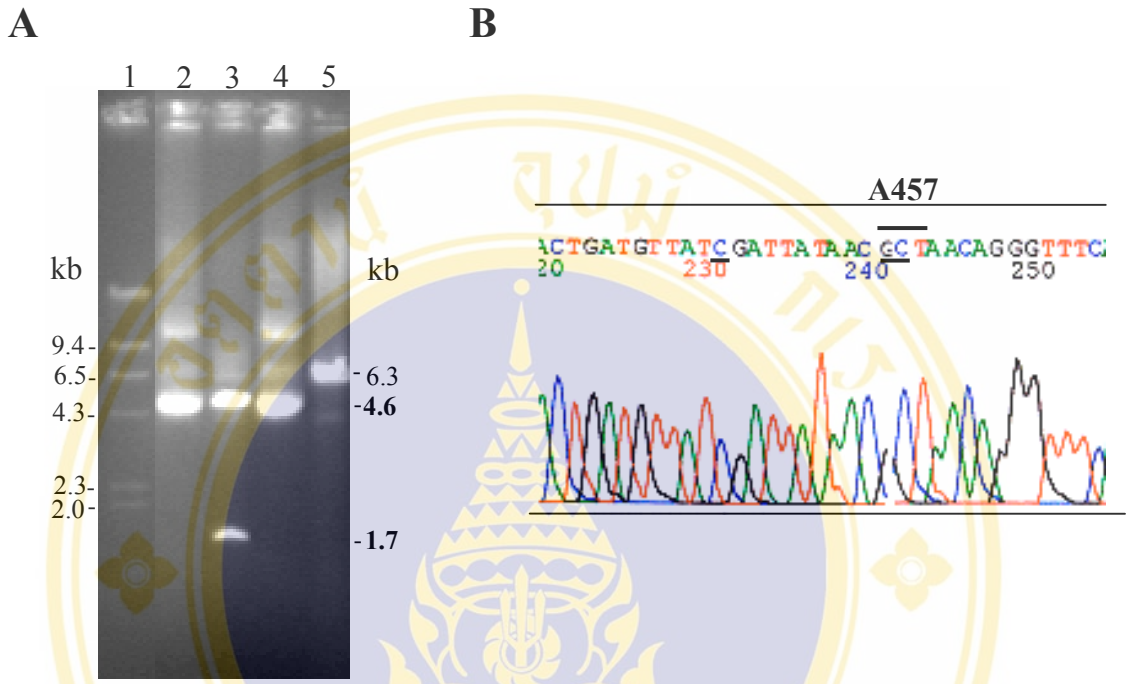

Figure 29: Restriction endonuclease and DNA sequence analysis of p4B-S457A

A: 1% agarose gel electrophoresis (ethidium bromide stained) of *Cla* I digestion pattern of the mutant plasmid. The 4.6- and 1.7-kb mutant specific DNA bands are indicated with the bold labels.

Lane 1:	*Hin*d III-digested λ DNA markers
Lanes 2 & 3:	the undigested and *Cla* I-digested mutant plasmid (p4B-S457A), respectively
Lanes 4 & 5:	the undigested and *Cla* I-digested wild type plasmid (pMU388), respectively

B: Part of DNA sequencing chromatogram of p4B-S457A. The nucleotide sequence of the coding strand for the mutant plasmid is shown. The substituted bases and amino acid are indicated. Reaction conditions are described in Method 4.6.

Copyright by Mahidol University

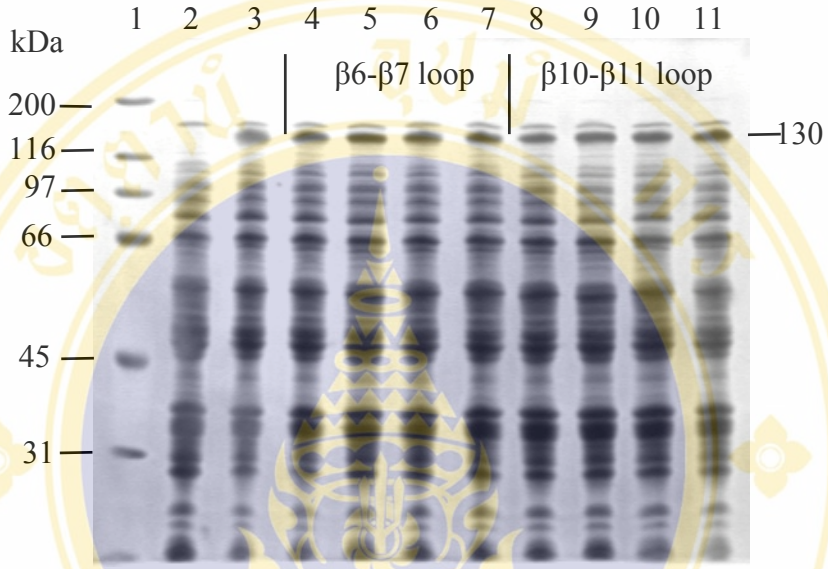

Figure 30: Expression of the β6-β7 and β10-β11 loop mutant protoxins

The figure shows Coomassie brilliant blue-stained 10% SDS-PAGE comparing expression levels of the Cry4Ba wild type and the β6-β7 and β10-β11 loop mutant protoxins from *E. coli* clones (0.1 OD_{600} ~ 10^7 cells).

Lane 1:	standard protein marker
Lanes 2 & 3:	crude lysates of *E. coli* cells containing pUC12 alone (negative control) and pMU388 (the Cry4Ba wild type), respectively
Lanes 4-7:	crude lysates of *E. coli* cells containing β6-β7 loop mutant plasmids; p4B-S387A, p4B-S388A, p4B-P389A and p4B-S390A, respectively
Lanes 8-11:	crude lysates of *E. coli* cells containing β10-β11 loop mutant plasmids; p4B-D454A, p4B-Y455A, p4B-N456A and p4B-S457A, respectively

Copyright by Mahidol University

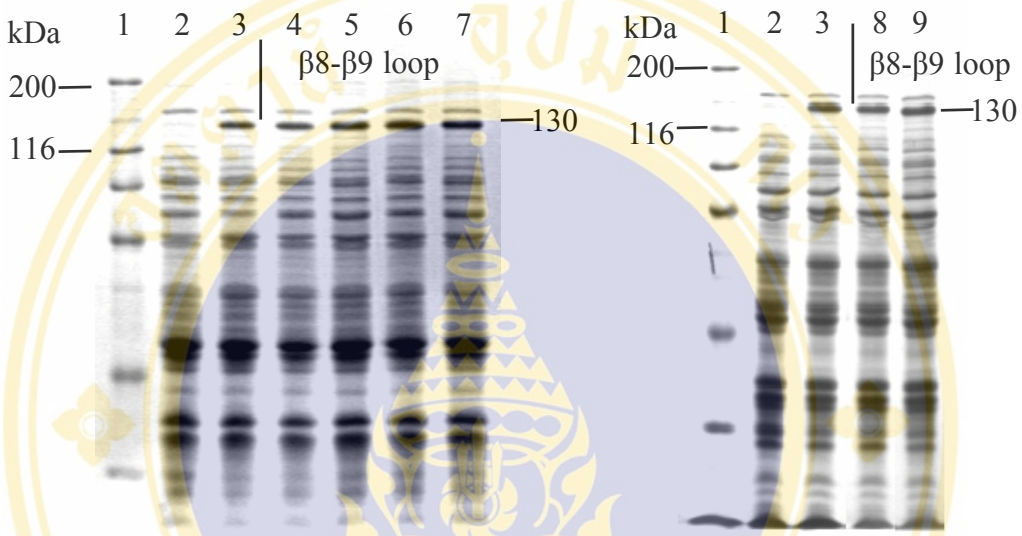

Figure 31: Expression of the β8-β9 loop mutant protoxins

The figure shows Coomassie brilliant blue-stained 10% SDS-PAGE comparing the expression levels of the Cry4Ba wild type and the β8-β9 loop mutant protoxins from *E. coli* clones (0.1 OD_{600} ~ 10^7 cells).

Lane 1:	standard protein marker
Lanes 2 & 3:	crude lysates of *E. coli* cells containing pUC12 alone (negative control) and pMU388 (the Cry4Ba wild type), respectively
Lanes 4-9:	crude lysates of *E. coli* cells containing mutant plasmids; p4B-N411A, p4B-T413A, p4B-T415A, p4B-G418A, p4B-S410A and p4B-E417A, respectively

Copyright by Mahidol University

Toxin	% Mortality																	
	S387A	S388A	P389A	S390A	S410A	N411A	T413A	T415A	E417A	G418A	D454A	Y455A	N456A	S457A	S410A/E417A	Y455A/N456A	Cry4Ba	pUC12
mean	86.0	91.3	67.3	91.3	65.7	89.0	86.0	90.0	66.0	90.0	88.3	69.0	64.7	88.3	20.3	16.7	90.7	0.0
SEM	2.1	1.8	1.3	1.3	2.3	1.5	2.1	1.2	1.7	1.7	1.8	1.7	1.5	0.9	1.5	6.0	0.3	0.0

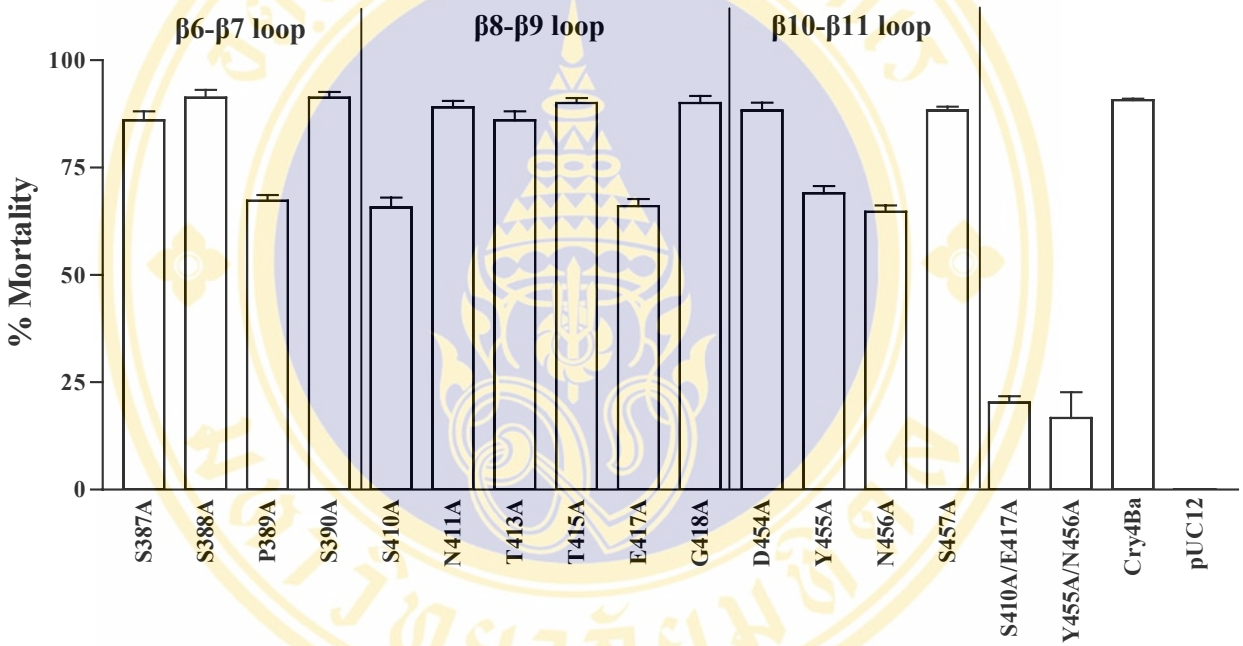

Figure 32: Mosquito-larvicidal activity of *E. coli* cells expressing β6-β7, β8-β9 and β10-β11 loop mutants

The figure shows comparison of larvicidal activity of *E. coli* cells expressing the Cry4Ba wild type and its β6-β7, β8-β9 and β10-β11 loop mutants against *A. aegypti* larvae. *E. coli* cells containing plasmid pUC12 alone were used as negative control. Data in the table and bar represent mean of % mortality from three independent assays ± SEM (standard error of mean).

Copyright by Mahidol University

5.5 Constructions and screening of S410A/E417A and Y455A/N456A mutants

In order to confirm the involvement in toxicity of S_{410} and E_{417} in the β8-β9 loop, and Y_{455} and N_{456} in the β10-β11 loop, two double mutants, S410A/E417A and Y455A/N456A were further constructed. The S410A and N456A mutant plasmids were used as templates for constructing the S410A/E417A and Y455A/N456A mutants, respectively. The PCR-amplified products analysed on agarose gel electrophoresis revealed that the two PCR products contained 6.3-kb plasmid bands (Figure 33A) which still remained after digestion with *Dpn* I endonuclease (Figure 33B).

After the *Dpn* I-digested PCR products were transformed into *E. coli* cells, ten ampicillin resistant colonies were randomly selected for screening the presence of mutant plasmids, p4B-S410A/E417A and p4B-Y455A/N456A by digesting with *Pst* I and *Cla* I, respectively. One clearly correct digestion pattern clone (Figures 34A and 35A) was revealed to contain the mutated DNA sequences by doing DNA sequencing (Figures 34B and 35B). The two candidate clones were selected to further investigate for protoxin expression and toxicity against *A. aegypti* mosquito larvae.

5.6 Protoxin expression of the S410A/E417A and Y455A/N456A mutants

After induction with IPTG, SDS-PAGE analysis of crude extracts from each mutant clone revealed that the 130-kDa protoxins of both double mutants, S410A/E417A and Y455A/N456A were highly expressed at the wild type levels while the protoxin band was not found in the crude extract of *E. coli* cells containing plasmid alone (pUC12) (Figure 36).

5.7 Mosquito-larvicidal activity of the S410A/E417A and Y455A/N456A mutants

For larvicidal activity, *E. coli* cells expressing S410A/E417A and Y455A/N456A mutant protoxins showed a decrease in larvicidal activity of Cry4Ba wild-type toxin against *A. aegypti* larvae to about 20% (Figure 32).

Copyright by Mahidol University

5.8 Solubilisation and proteolytic activation of the S410A/E417A and Y455A/ N456A mutant inclusions

The *E. coli* cells that express the Cry4Ba wild type protoxin or the two double mutant protoxins (S410A/E417A and Y455A/N456A) were lysed with French Pressure cells at 1,200 psi (Method 4.10) prior to SDS-PAGE analysis. It was found that the 130-kDa protoxins of the two mutants were produced as inclusion bodies which could be sedimented from cell lysates as similar to the wild type (Figure 37).

The two double mutants (S410A/E417A and Y455A/N456A) were also examined for the effect on solubilisation and proteolytic activation (Method 4.12). To compare the solubility of the two double mutant inclusions with the wild type inclusion, the protoxin inclusions were solubilised in 50 mM Na_2CO_3 (pH 9.0) for 1.30 hr at 37 °C. As shown in Figure 38, the two mutant inclusions could be solublised in the carbonate buffer at the levels similar to the wild type, giving about 70% solubility. After the two solubilised mutant protoxins were treated with trypsin at a ratio of 1:20 (enzyme:protoxin, w/w) at 37 °C for 13 hr, both mutants gave the same trypsin digestion patterns of 47 and 20 kDa similar to the wild type as analysed on 15% SDS-PAGE (Figure 39).

Copyright by Mahidol University

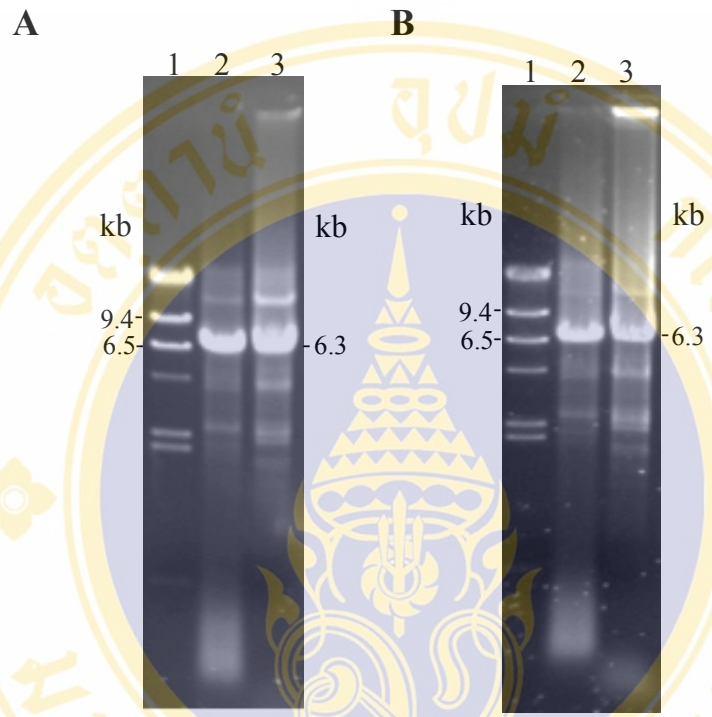

Figure 33: Amplification and *Dpn* I digestion of the double mutant plasmids; p4B-S410A/E417A and p4B-Y455A/N456A

The figure shows 1% agarose gel electrophoresis (ethidium bromide stained) of the resulting PCR products (panel A) and their *Dpn* I digestion products (panel B).

Lane 1:	*Hin*d III-digested λ DNA markers
Lanes 2 & 3:	the PCR products of the tentative mutant plasmids; p4B-Y455A/N456A and p4B-S410A/E417A, respectively

Copyright by Mahidol University

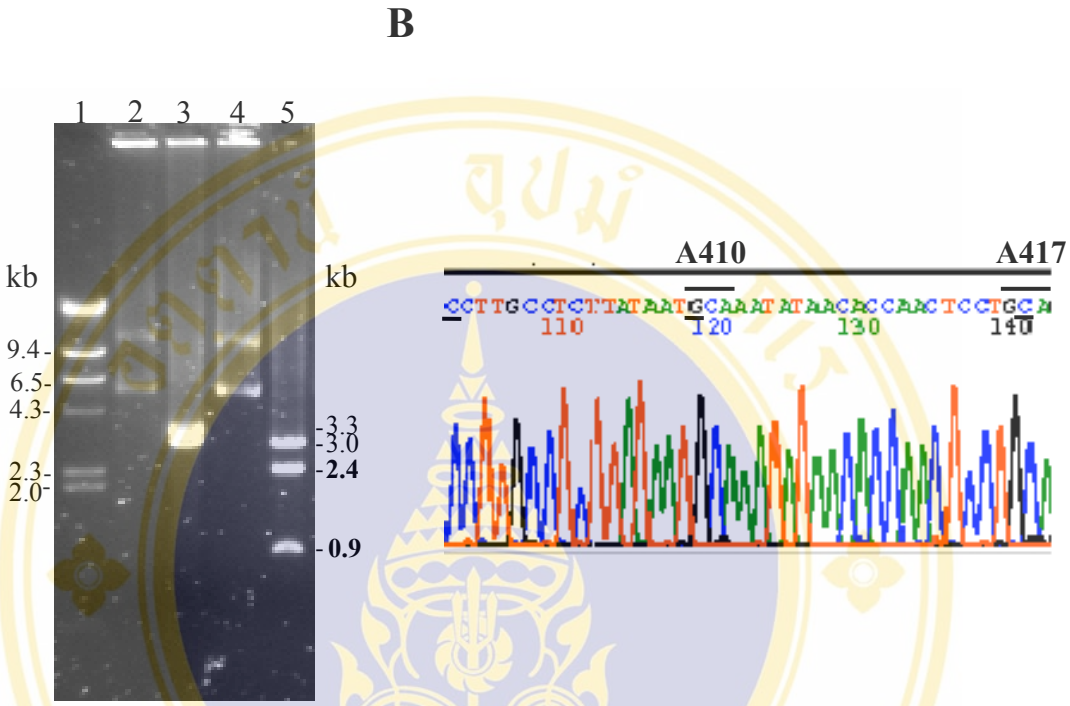

Figure 34: Restriction endonuclease and DNA sequence analysis of p4B-S410A/E417A

A: 1% agarose gel electrophoresis (ethidium bromide stained) of *Pst* I digestion pattern of the mutant plasmid. The 2.4- and 0.9-kb mutant specific DNA bands are indicated with the bold labels.

Lane 1:	*Hin*d III-digested λ DNA markers
Lanes 2 & 3:	the undigested and *Pst* I-digested wild type plasmid (pMU388), respectively
Lanes 4 & 5:	the undigested and *Pst* I-digested double mutant plasmid (p4B-S410A/E417A), respectively

B: Part of DNA sequencing chromatogram of p4B-S410A/E417A. The nucleotide sequence of the coding strand for the mutant plasmid is shown. The substituted bases and amino acid are indicated. Reaction conditions are described in Method 4.6.

Copyright by Mahidol University

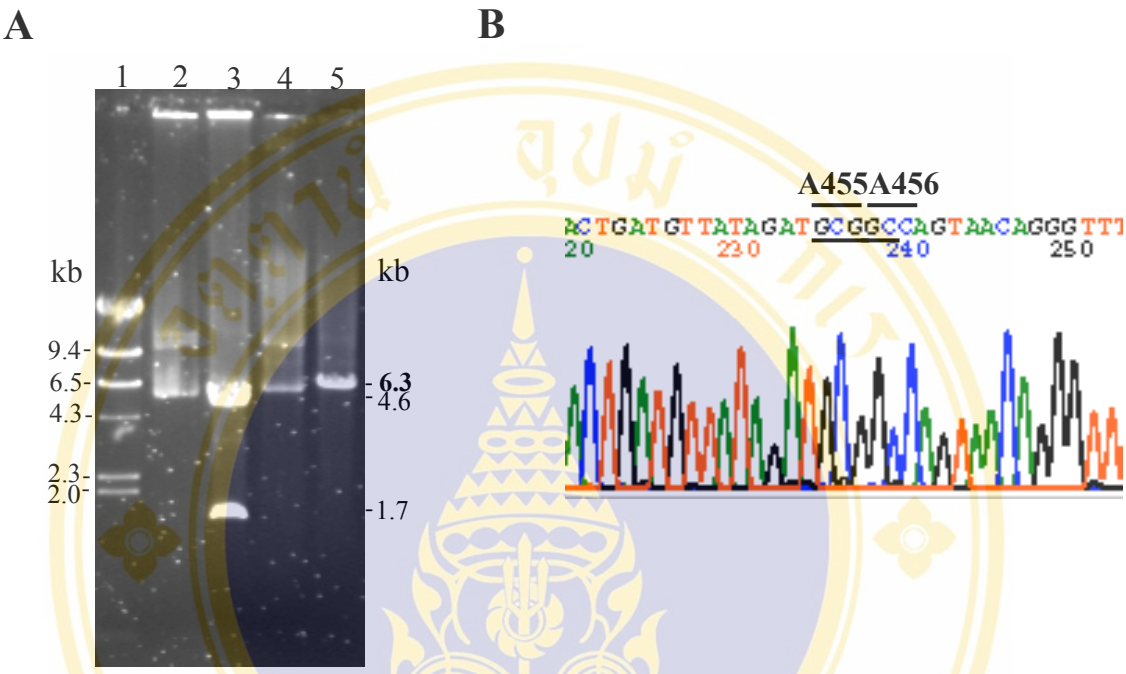

Figure 35: Restriction endonuclease and DNA sequence analysis of p4B-Y455A/N456A

A: 1% agarose gel electrophoresis (ethidium bromide stained) of *Cla* I digestion pattern of the mutant plasmid. The 6.3-kb mutant specific DNA band is indicated with the bold label.

Lane 1:	*Hin*d III-digested λ DNA markers
Lanes 2 & 3:	the undigested and *Cla* I-digested mutant template plasmid (p4B-N456A), respectively
Lanes 4 & 5:	the undigested and *Cla* I-digested double mutant plasmid (p4B-Y455A/N456A), respectively

B: Part of DNA sequencing chromatogram of p4B-Y455A/N456A. The nucleotide sequence of the coding strand for the mutant plasmid is shown. The substituted bases and amino acid are indicated. Reaction conditions are described in Method 4.6.

Copyright by Mahidol University

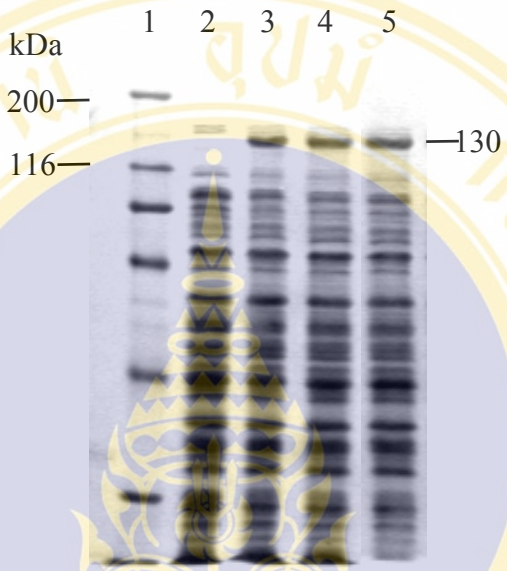

Figure 36: Expression of the S410A/E417A and Y455A/N456A mutant protoxins

The figure shows Coomassie brilliant blue-stained 10% SDS-PAGE comparing expression levels of the Cry4Ba wild type and the S410A/E417A and Y455A/N456A mutant protoxins from *E. coli* clones (0.1 OD_{600} ~ 10^7 cells).

Lane 1:	standard protein marker
Lanes 2 & 3:	crude lysates of *E. coli* cells containing pUC12 alone (negative control) and pMU388 (the Cry4Ba wild type), respectively
Lanes 4 & 5:	crude lysates of *E. coli* cells containing the double mutant plasmids; p4B-S410A/E417A and p4B-Y455A/N456A, respectively

Copyright by Mahidol University

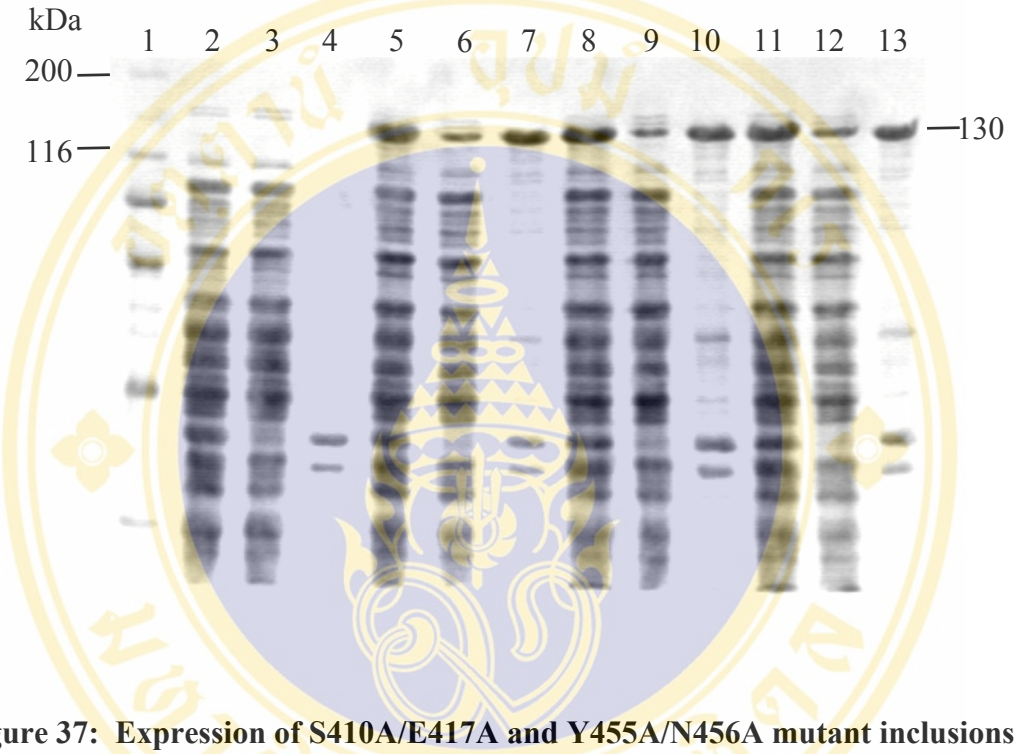

Figure 37: Expression of S410A/E417A and Y455A/N456A mutant inclusions

The figure shows Coomassie brilliant blue-stained 10% SDS-PAGE comparing the inclusion levels of *E. coli* clones (0.1 OD_{600} ~ 10^7 cells) expressing Cry4Ba wild type and its mutants, S410A/E417A and Y455A/N456A.

Lane 1:	standard protein marker
Lanes 2-4:	crude lysate, supernatant and sedimented fractions of *E. coli* clone containing pUC12 alone (negative control), respectively
Lanes 5-7:	crude lysate, supernatant and sedimented fractions of *E. coli* clone containing pMU388 (the Cry4Ba wild type), respectively
Lanes 8-10:	crude lysate, supernatant and sedimented fractions of *E. coli* clone containing the mutant plasmid-p4B-S410A/E417A, respectively
Lanes 11-13:	crude lysate, supernatant and sedimented fractions of *E. coli* clone containing the mutant plasmid-p4B-Y455A/N456A, respectively

Copyright by Mahidol University

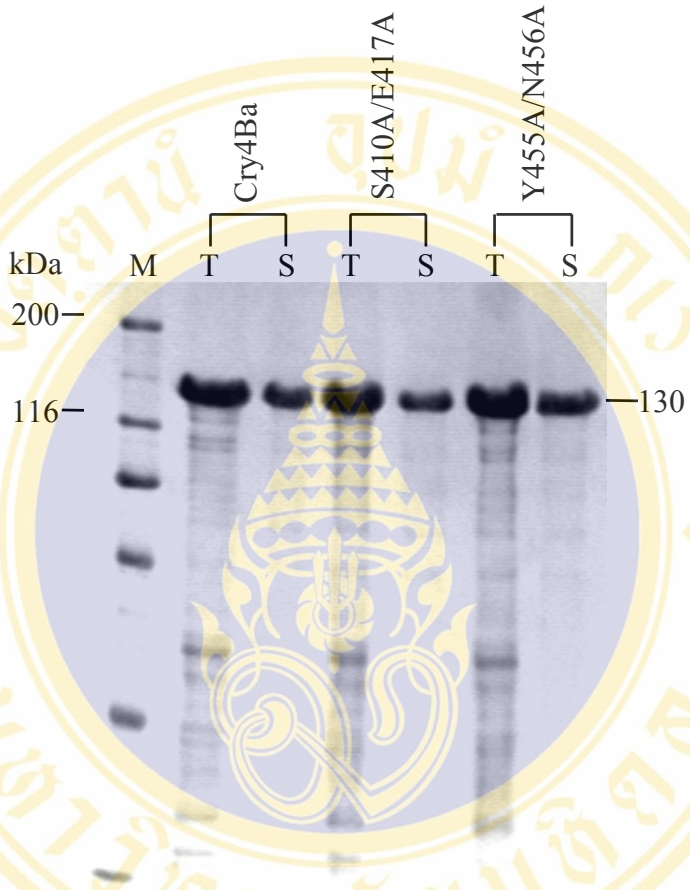

Figure 38: Solubility of the Cry4Ba wild type and its double mutant (S410A/E417A and Y455A/N456A) inclusions

The figure shows Coomassie brilliant blue-stained 10% SDS-PAGE comparing the solubility of the wild type and its double mutant inclusions in 50 mM Na_2CO_3 (pH 9.0). T and S represent total and solubilised fractions, respectively. M represents standard protein markers.

Copyright by Mahidol University

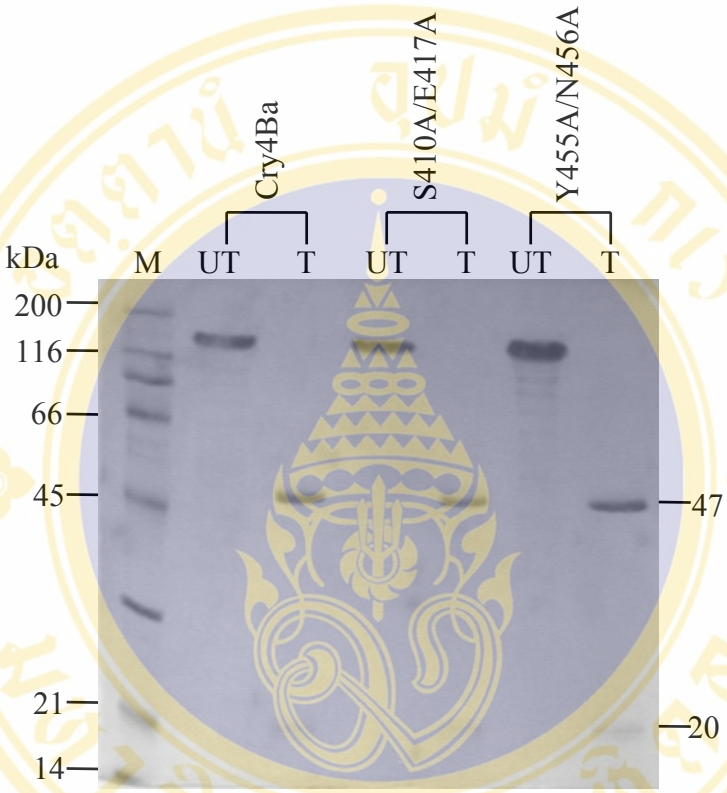

Figure 39: Proteolytic processing of the Cry4Ba wild type and its double mutant (S410A/E417A and Y455A/N456A) protoxins

The figure shows Coomassie brilliant blue-stained 15% SDS-PAGE comparing trypsin digestion of the wild type and its double mutant protoxins solubilised in 50 mM Na_2CO_3 (pH 9.0). UT and T represent untreated and treated protoxins with trypsin, respectively. M represents standard protein markers.

Copyright by Mahidol University

CHAPTER VI
RESULT II: INVOLVEMENT IN TOXICITY OF RESIDUES STABILISING β2-β3 AND β4-β5 HAIRPINS

Previously, it has been shown that hydrogen bonding between T_{328} and T_{369} that are located in β2 and β5, respectively (Figure 40) plays a critical role in Cry4Ba activity by stabilising an optimal conformation of β2-β3 and β4-β5 hairpins (21).

In this study, a Swiss-PdbViewer 3.7 programme was used to further screen for side chain-side chain hydrogen bonding between residues in β2, β3, β4 and β5 with the other residues. As shown in Figure 41, T_{319}, R_{323} and T_{328} in β2 were found to be involved in three complex networks of hydrogen bonding with other residues. Interestingly, T_{328} is involved in two inter β-strand hydrogen bonds forming with Y_{408} in β8 and with T_{369} in β5. Hydrogen boding between T_{328} and Y_{408} is an inter β-sheet interaction between β sheets 1 and 2 (Figure 42).

Therefore, T_{319} and R_{323} in β2 and Y_{408} in β8 were selected for investigating an involvement in toxicity.

6.1 Constructions and screening of T319A, R323A and Y408A mutants

Three more mutants were constructed using pMU388 as a template together with the mutagenic oligonucleotide primers shown in Material 3.5.1. As shown in Figure 43A, 6.3-kb PCR products of the mutant plasmids, p4B-T319A, p4B-R323A and p4B-Y408A, were clearly detected. In addition, the PCR products still contained the 6.3-kb bands after being treated with *Dpn* I (Figure 43B). The *Dpn* I-cut PCR products were then transformed into *E. coli*. Seven to ten ampicillin resistant transformants were selected for screening the clones containing p4B-T319A, p4B-R323A and p4B-Y408A by digesting with *Bst*N I, *Acc* I and *Eco*R I, respectively. The tentative mutant clones that revealed the correct digestion patterns (Figures 44A-46A) were further verified for the correct mutagenic sequences by DNA sequencing as the results shown in Figures 44B-46B.

Copyright by Mahidol University

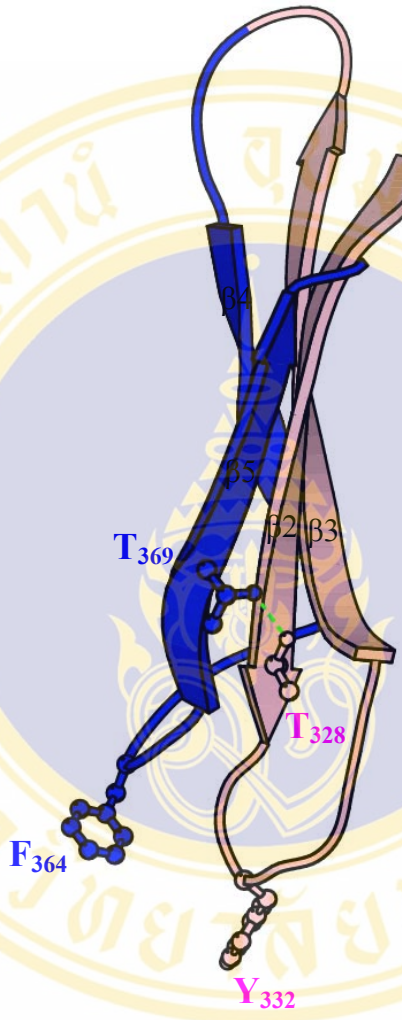

Figure 40: β2-β3 and β4-β5 hairpins in domain II of the Cry4Ba toxin

The figure shows ribbon representation of a part of the Cry4Ba-domain II generated by MolScript v2.1.2 based on the crystal structure of Cry4Ba (10), illustrating β2-β3 and β4-β5 hairpins as shaded with pink and blue colours, respectively. The critical hydrogen bond between T_{328} in β2 and T_{369} in β5 (a green-colour dash line) and the two critical residues, Y_{332} and F_{364} in β2-β3 and β4-β5 loops, respectively, are indicated.

Copyright by Mahidol University

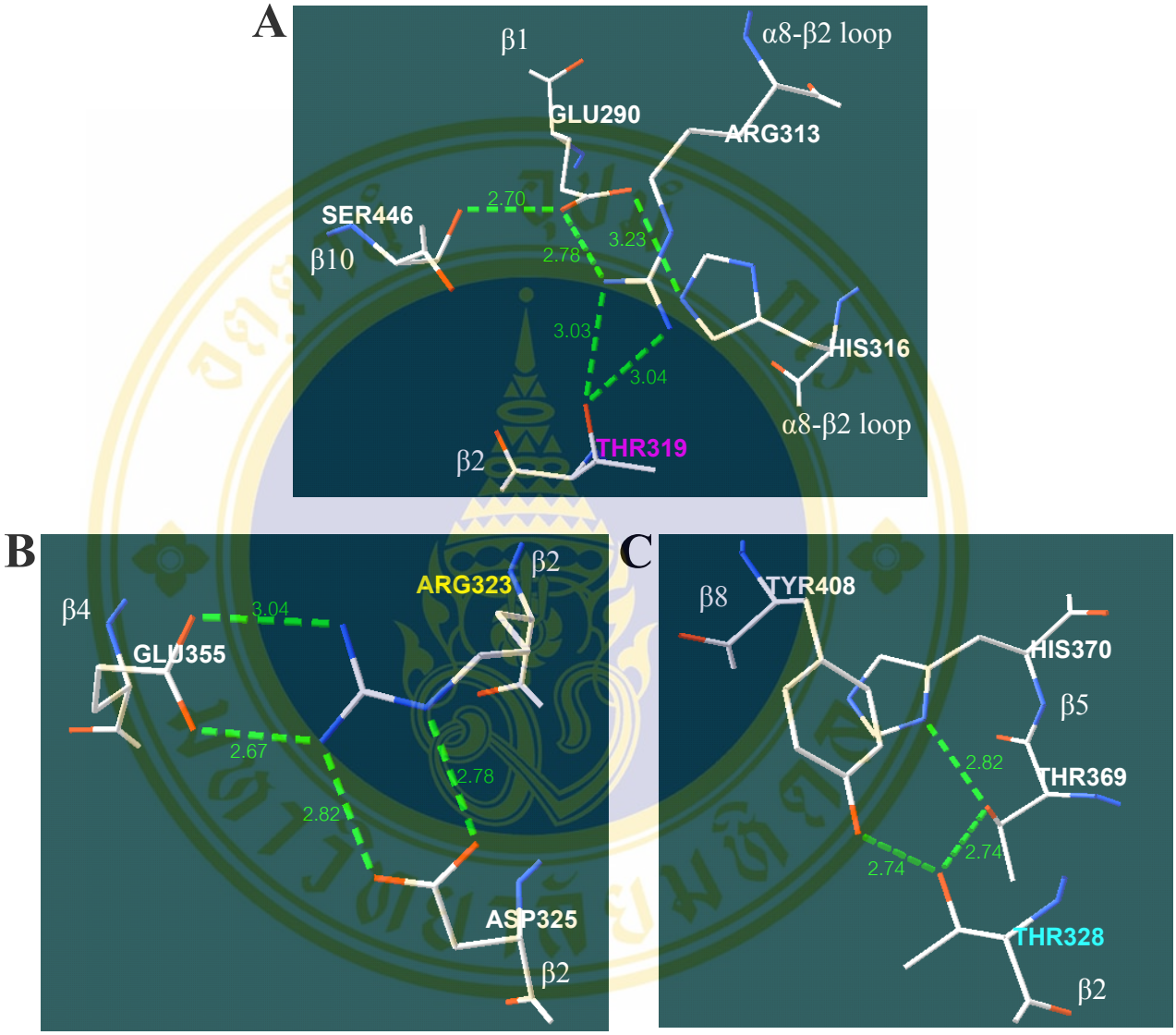

Figure 41: Hydrogen bonding networks at T_{319}, R_{323} and T_{328} in β2 of Cry4Ba

The figure shows residues in the three hydrogen bonding networks at T_{319} (A), R_{323} (B) and T_{328} (C) analysed by Swiss-PdbViewer 3.7 based on the Cry4Ba crystal structure (10). Hydrogen bonds are represented with green-colour dash lines and their bond lengths are in Å. The location of each residue in domain II is indicated. Red- and blue-colour sticks represent oxygen and nitrogen atoms, respectively.

Copyright by Mahidol University

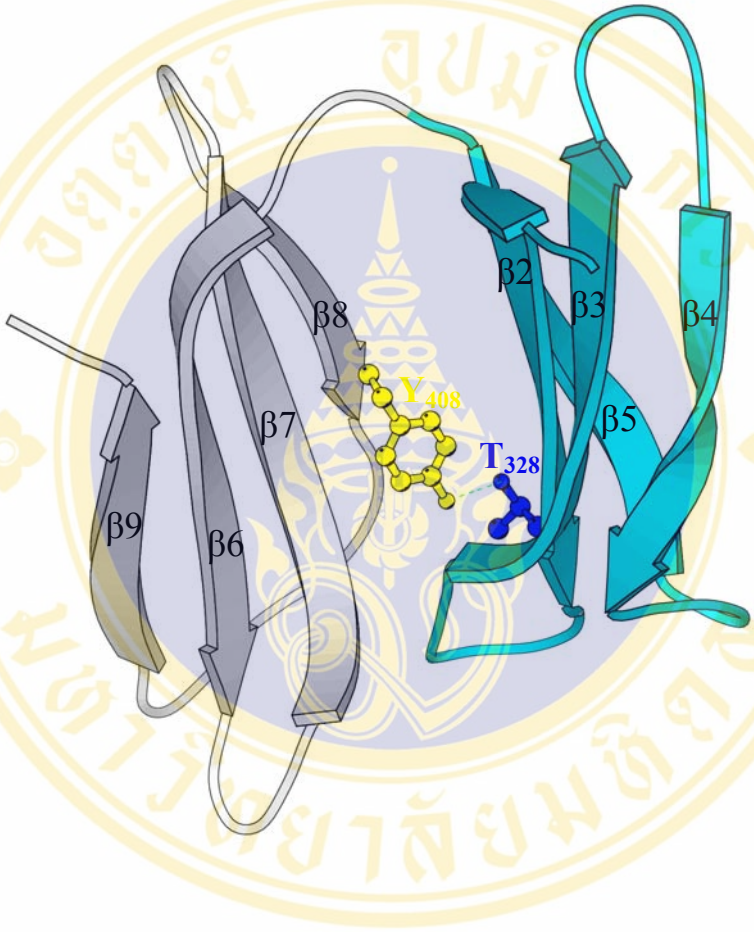

Figure 42: β-sheets 1 and 2 in domain II of the Cry4Ba toxin

The figure shows a part of domain II of Cry4Ba generated by MolScript v2.1.2 based on the crystal structure of Cry4Ba (10), illustrating β-sheets 1 and 2 as shaded with cyan and grey colours, respectively. An inter β-sheet hydrogen bond forming between Y_{408} in β8 and T_{328} in β2 is illustrated with a green-colour dash line.

Copyright by Mahidol University

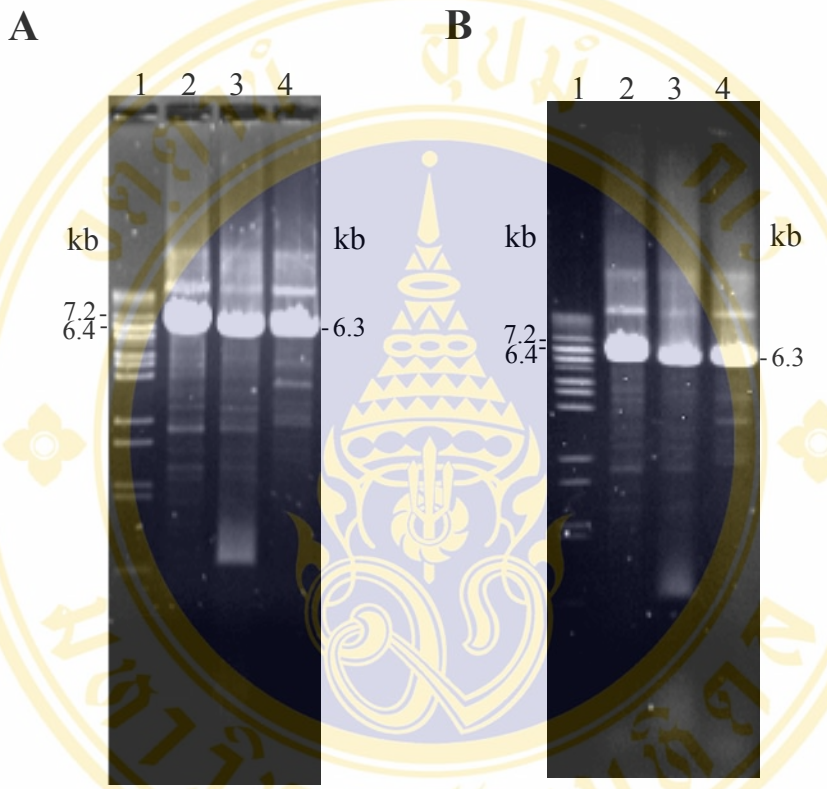

Figure 43: Amplification and *Dpn* I digestion of the p4B-T319A, p4B-R323A and p4B-Y408A mutant plasmids

The figure shows 1% agarose gel electrophoresis (ethidium bromide stained) of the resulting PCR products (panel A) and their *Dpn* I digestion products (panel B).

Lane 1: *Bst*E II-digested λ DNA markers
Lanes 2-4: the PCR products of the tentative mutant plasmids; p4B-T319A, p4B-R323A and p4B-Y408A, respectively

Copyright by Mahidol University

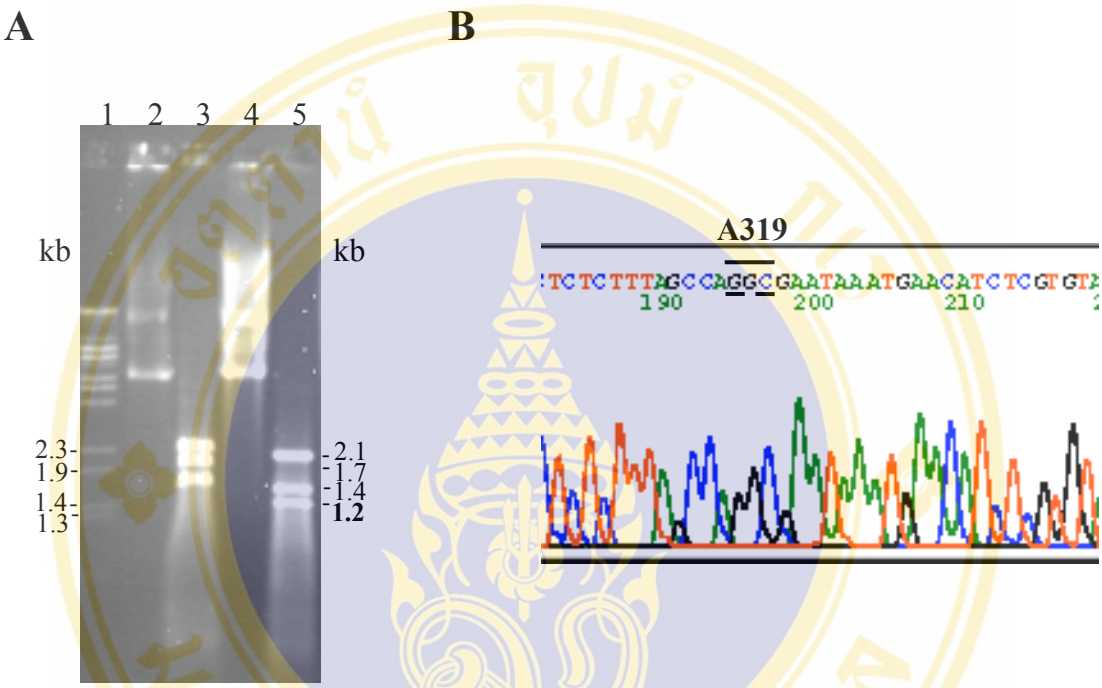

Figure 44: Restriction endonuclease and DNA sequence analysis of p4B-T319A

A: 1% agarose gel electrophoresis (ethidium bromide stained) of *Bst*N I digestion pattern of the mutant plasmid. The 1.2-kb mutant specific DNA band is indicated with the bold label.

Lane 1:	*Bst*E II-digested λ DNA markers
Lanes 2 & 3:	the undigested and *Bst*N I-digested wild type plasmid (pMU388), respectively
Lanes 4 & 5:	the undigested and *Bst*N I-digested mutant plasmid (p4B-T319A), respectively

B: Part of DNA sequencing chromatogram of p4B-T319A. The nucleotide sequence of the non-coding strand for the mutant plasmid is shown. The substituted bases and amino acid are indicated. Reaction conditions are described in Method 4.6.

Copyright by Mahidol University

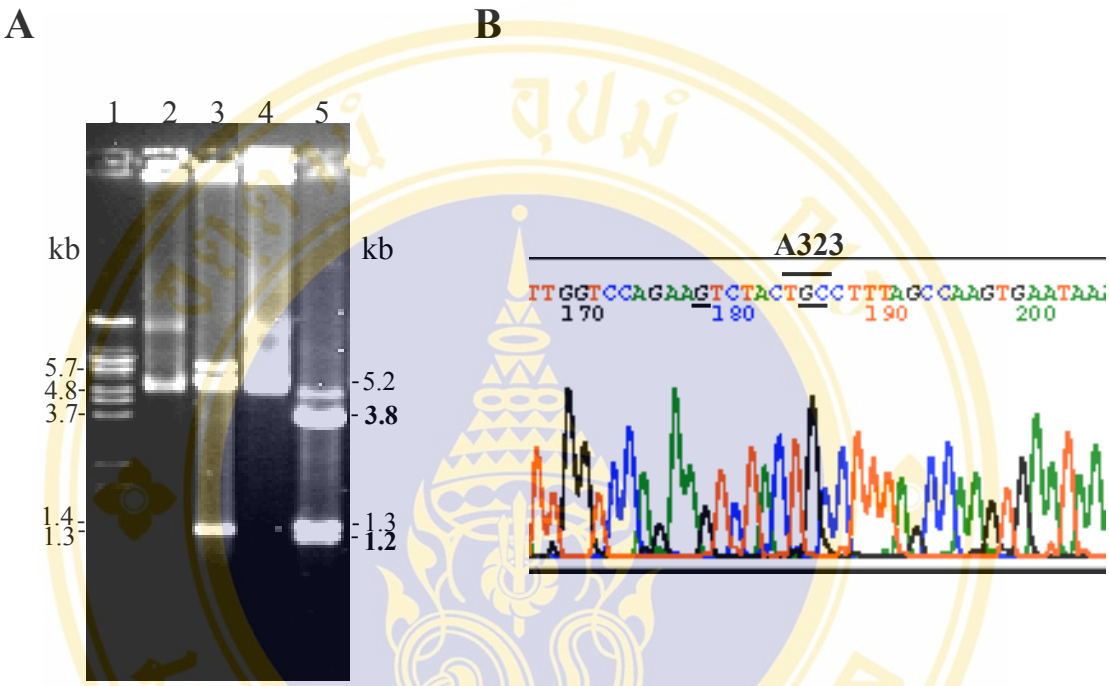

Figure 45: Restriction endonuclease and DNA sequence analysis of p4B-R323A

A: 1% agarose gel electrophoresis (ethidium bromide stained) of *Acc* I digestion pattern of the mutant plasmid. The 3.8- and 1.2-kb mutant specific DNA bands are indicated with the bold labels.

Lane 1:	*Bst*E II-digested λ DNA markers
Lanes 2 & 3:	the undigested and *Acc* I-digested wild type plasmid (pMU388), respectively
Lanes 4 & 5:	the undigested and *Acc* I-digested mutant plasmid (p4B-R323A), respectively

B: Part of DNA sequencing chromatogram of p4B-R323A. The nucleotide sequence of the non-coding strand for the mutant plasmid is shown. The substituted bases and amino acid are indicated. Reaction conditions are described in Method 4.6.

Copyright by Mahidol University

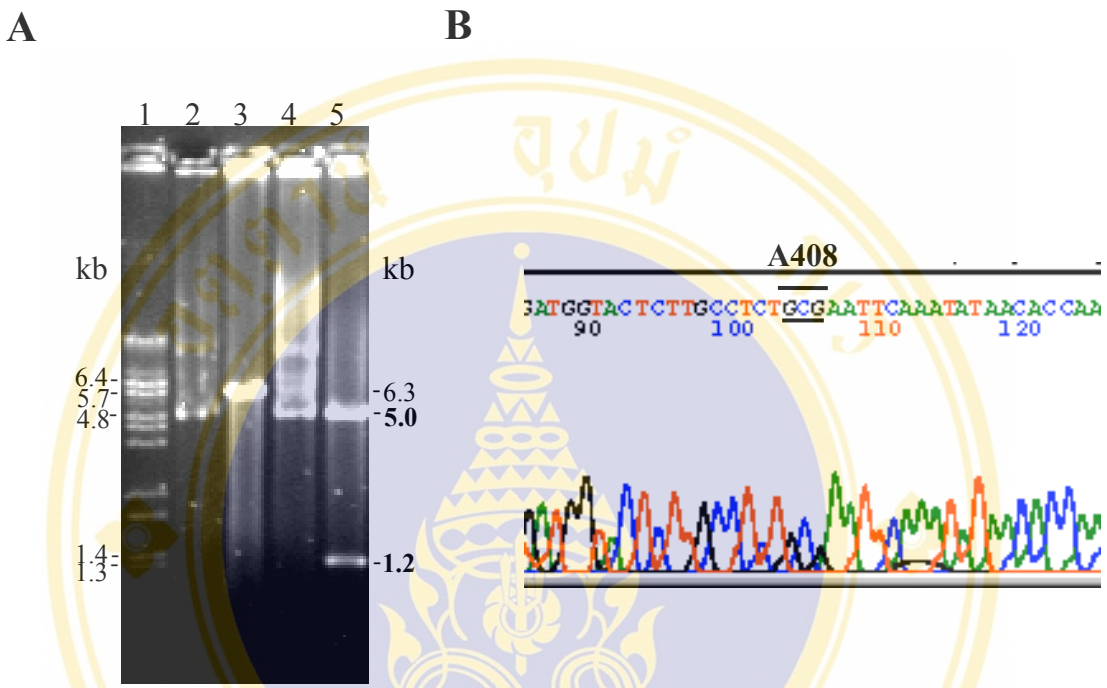

Figure 46: Restriction endonuclease and DNA sequence analysis of p4B-Y408A

A: 1% agarose gel electrophoresis (ethidium bromide stained) of *Eco*R I digestion pattern of the mutant plasmid. The 5.0- and 1.2-kb mutant specific DNA bands are indicated with the bold labels.

Lane 1:	*Bst*E II-digested λ DNA markers
Lanes 2 & 3:	the undigested and *Eco*R I-digested wild type plasmid (pMU388), respectively
Lanes 4 & 5:	the undigested and *Eco*R I-digested mutant plasmid (p4B-Y408A), respectively

B: Part of DNA sequencing chromatogram of p4B-Y408A. The nucleotide sequence of the coding strand for the mutant plasmid is shown. The substituted bases and amino acid are indicated. Reaction conditions are described in Method 4.6.

Copyright by Mahidol University

6.2 Protoxin expression of T319A, R323A and Y408A mutants

Expression in *E. coli* cells of all three mutants was induced with IPTG and the protoxin expression levels were analysed on 10% SDS-PAGE as shown in Figure 47. The levels of the expected band of the 130-kDa protoxin from cell lysates containing plasmids p4B-T319A, p4B-R323A and p4B-Y408A were found to be similar to that of the wild type.

6.3 Mosquito-larvicidal activity of T319A, R323A and Y408A mutants

E. coli cells expressing T319A, R323A or Y408A mutants were examined for larvicidal activity and the results (Figure 48) showed that only the Y408A mutant showed a reduction of larvicidal activity to about 40% whereas the two other mutants showed the same larvicldal activity as the wild type at about 90%.

Copyright by Mahidol University

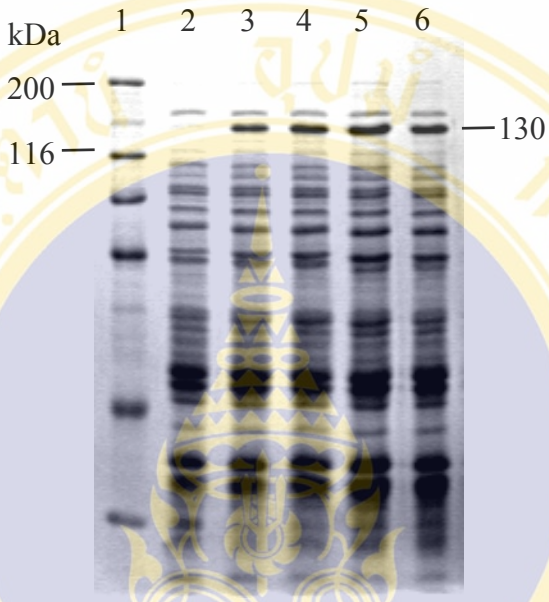

Figure 47: Expression of the T319A, R323A and Y408A mutant protoxins

The figure shows Coomassie brilliant blue-stained 10% SDS-PAGE comparing expression levels of the Cry4Ba wild type and the T319A, R323A and Y408A mutant protoxins from *E. coli* clones (0.1 OD_{600} ~ 10^7 cells).

Lane 1:	standard protein marker
Lanes 2 & 3:	crude lysates of *E. coli* cells containing pUC12 alone (negative control) and pMU388 (the Cry4Ba wild type), respectively
Lanes 4-6:	crude lysates of *E. coli* cells containing the mutant plasmids; p4B-T319A, p4B-R323A and p4B-Y408A, respectively

Copyright by Mahidol University

Toxin	% Mortality				
	T319A	R323A	Y408A	Cry4Ba	pUC12
mean	89.3	88.0	39.7	88.0	0.3
SEM	4.4	4.0	2.4	3.8	0.6

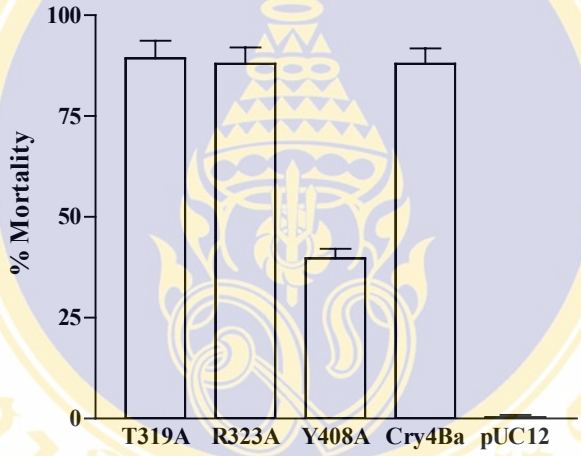

Figure 48: Mosquito-larvicidal activity of *E. coli* cells expressing T319A, R323A or Y408A mutants

The figure shows comparison of larvicidal activity of *E. coli* cells expressing the Cry4Ba wild type and its mutants (T319A, R323A and Y408A) against *A. aegypti* larvae. *E. coli* cells containing plasmid pUC12 alone were used as negative control. Data in the table and bar represent mean of % mortality from three independent assays ± SEM (standard error of mean).

Copyright by Mahidol University

6.4 Constructions of Y408F, Y408W, Y408D, Y408E and Y408C mutants

In order to confirm the importance in toxicity of the hydrogen bonding between Y_{408} in β8 and T_{328} in β2, Y_{408} was further substituted with phenylalanine, tryptophan, aspartate, glutamate and cysteine based on Swiss-PdbViewer 3.7. Swiss-PdbViewer 3.7 was used to screen for replacement of hydrogen bonding at Y_{408} (Figure 49). It was found that Y_{408} formed two main chain-main chain hydrogen bonding with M_{396} in β7 and formed one side chain-side chain hydrogen bonding with T_{328} in β2. When replacing Y_{408} with most amino acids including phenylalanine and tryptophan, there was no hydrogen bonding between side chains at this position. However, replacing with aspartate, serine, threonine or cysteine, one hydrogen bond was formed between the side chain of these amino acids with the main chain of the other residues. These include serine, threonine and cysteine forming a hydrogen bond with M_{396} in β7 while aspartate forming a hydrogen bond with N_{409} in β8. Also, when replacing Y_{408} with glutamate, two side chain-side chain hydrogen bonds with H_{370} in β5 and two hydrogen bonds between side chain of the glutamate with main chain of N_{409} were formed. The two hydrogen bonds of glutamate (one side chain-side chain hydrogen bond with H_{370} in β5 and one side chain-main chain hydrogen bond with N_{409}) are the same hydrogen bonds formed by glutamine. However, no side chain-side chain hydrogen bonding was found with T_{328} in β2 when replacing the Y_{408} with any amino acids.

Y_{408} was further changed to phenylalanine, tryptophan, aspartate, glutamate and cysteine by PCR-based site-directed mutagenesis. Similar to the previous results, a 6.3-kb band of the mutant plasmids was suscessfully PCR amplified (Figures 50A and 51A) and all the PCR-amplified mutant plasmids were insusceptible to *Dpn* I digestion (Figures 50B and 51B). After transformation of the *Dpn* I-cut PCR products into *E. coli* cells, ten ampicillin resistant transformants were selected for analysis of the mutant plasmids using restriction endonuclease digestion. p4B-Y408W and p4B-Y408E were digested with *Eco*R I, while p4B-Y408D was digested with *Dde* I. In addition, p4B-Y408C and p4B-Y408F were digested with *Kpn* I. One clone that revealed the correct restriction endonuclease digested pattern (Figures 52A-56A) was confirmed by DNA sequencing as results shown in Figures 52B-56B. Fortunately, one clone obtained from the Y408D mutant transformant showed the mutated region of

Copyright by Mahidol University

Y408V (see Figure 57), which was then used as a candidate clone of the Y408V mutant for further characterisation. Analysis by Swiss-Pdb also revealed that when replacing Y_{408} with valine, no hydrogen bonding between side chains was found (Figure 49).

Copyright by Mahidol University

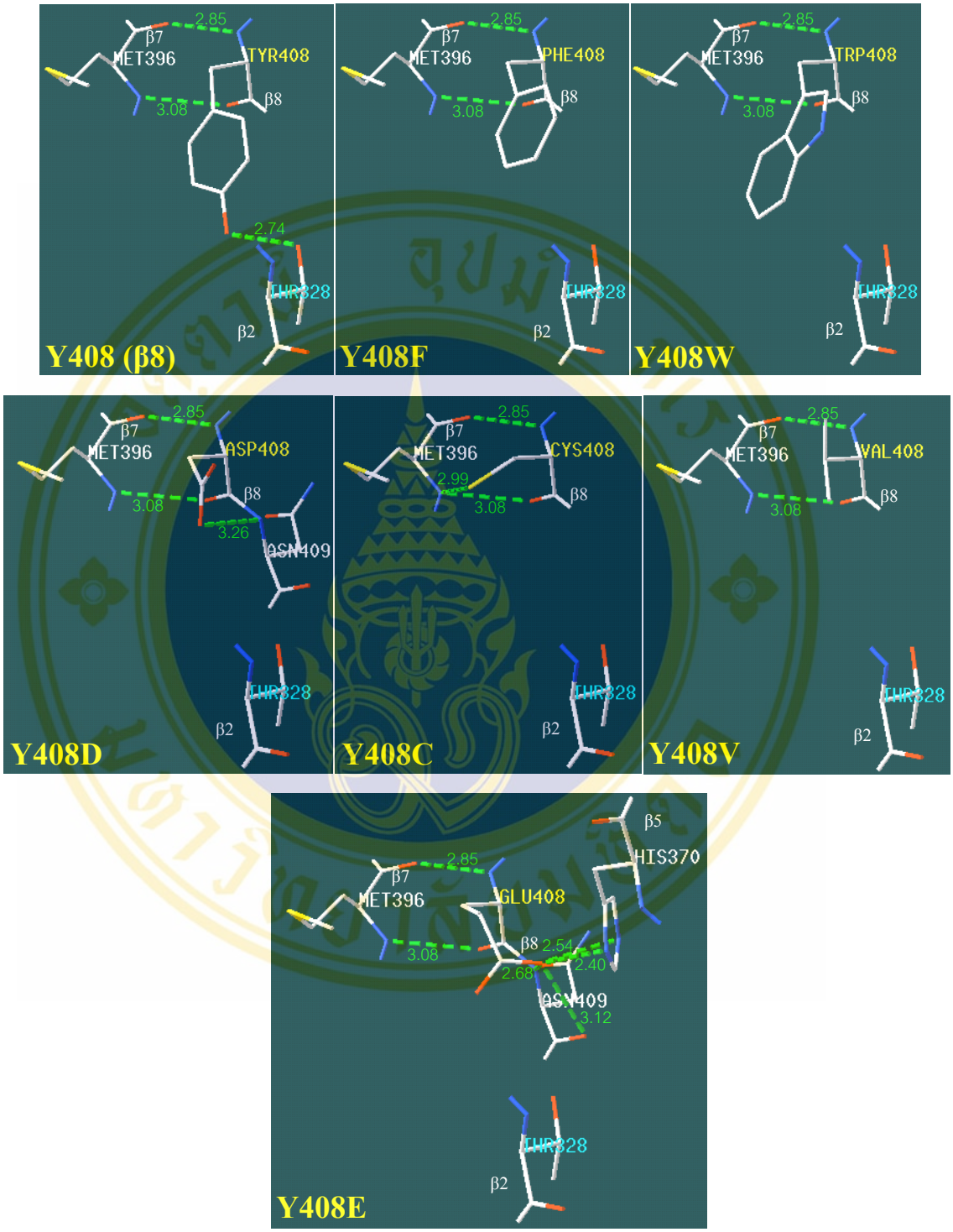

Figure 49: Predicted hydrogen bonding at position 408 of Cry4Ba

This figure shows predicted hydrogen bonding at position 408 when tyrosine replaced with phenylalanine, tryptophan, aspartate, glutamate, cysteine and valine analysed by Swiss-PdbViewer 3.7 based on the Cry4Ba crystal structure (10). Green-colour dash lines represent hydrogen bonds and their bond lengths are in Å. Red-, blue- and yellow-colour sticks illustrate oxygen, nitrogen and sulfur atoms, respectively.

Copyright by Mahidol University

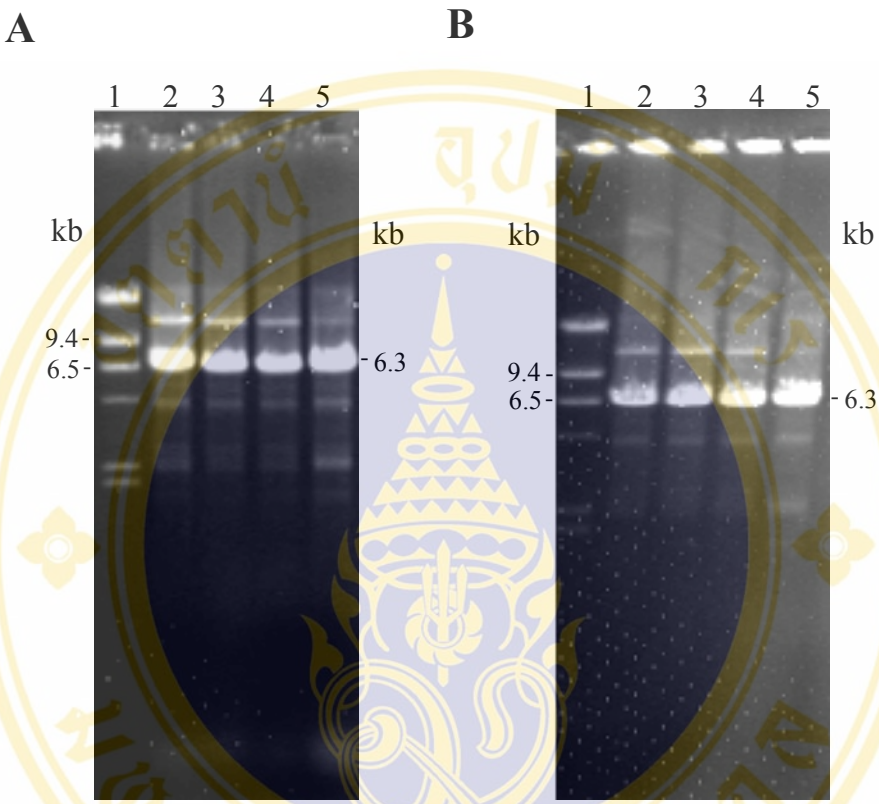

Figure 50: Amplification and *Dpn* I digestion of the p4B-Y408W, p4B-Y408D, p4B-Y408E and p4B-Y408C mutant plasmids

The figure shows 1% agarose gel electrophoresis (ethidium bromide stained) of the resulting PCR products (panel A) and their *Dpn* I digestion products (panel B).

Lane 1: *Hin*d III-digested λ DNA markers
Lanes 2-5: the PCR products of the tentative mutant plasmids; p4B-Y408W, p4B-Y408D, p4B-Y408E and p4B-Y408C, respectively

Copyright by Mahidol University

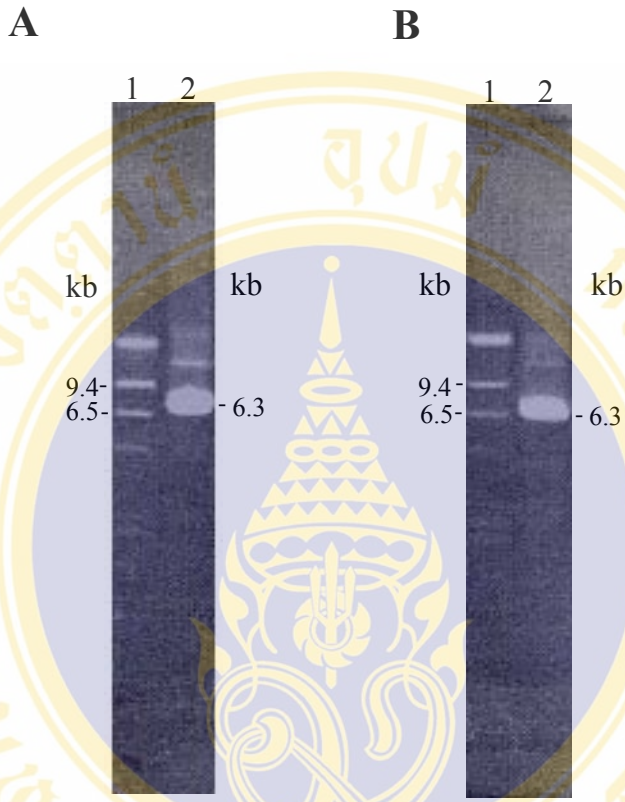

Figure 51: Amplification and *Dpn* I digestion of the p4B-Y408F mutant plasmid

The figure shows 1% agarose gel electrophoresis (ethidium bromide stained) of the resulting PCR product (panel A) and its *Dpn* I digestion product (panel B).

Lane 1: *Hin*d III-digested λ DNA markers
Lane 2: the PCR product of the tentative mutant plasmids-p4B-Y408F

Copyright by Mahidol University

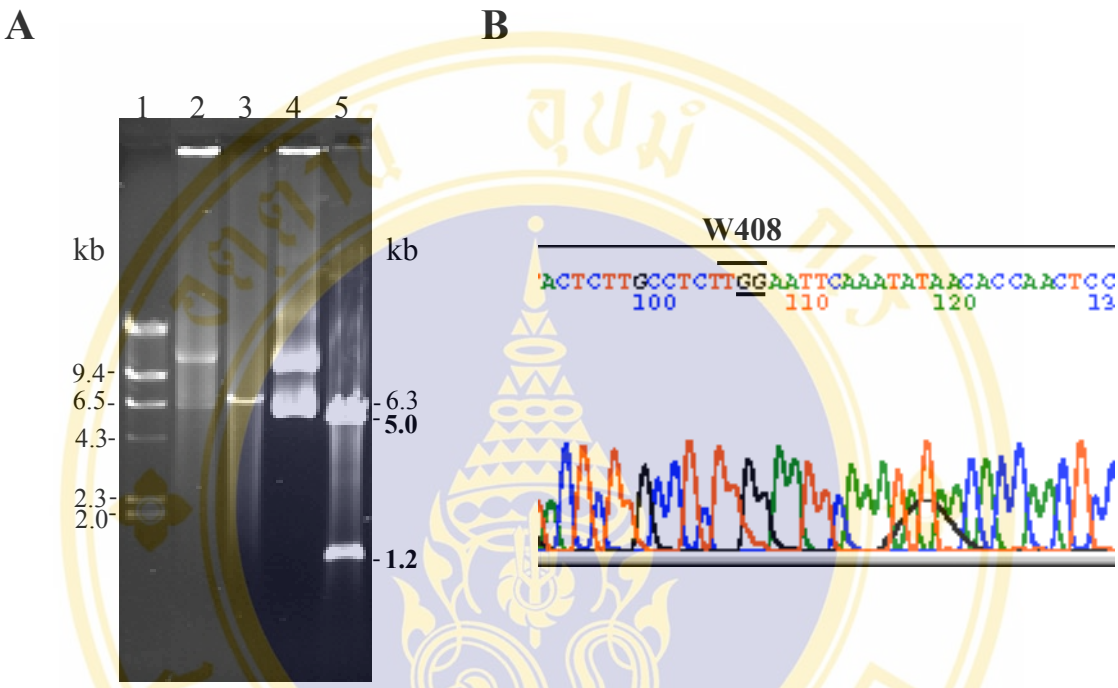

Figure 52: Restriction endonuclease and DNA sequence analysis of p4B-Y408W

A: 1% agarose gel electrophoresis (ethidium bromide stained) of *Eco*R I digestion pattern of the mutant plasmid. The 5.0- and 1.2-kb mutant specific DNA bands are indicated with the bold labels.

Lane 1:	*Hin*d III-digested λ DNA markers
Lanes 2 & 3:	the undigested and *Eco*R I-digested wild type plasmid (pMU388), respectively
Lanes 4 & 5:	the undigested and *Eco*R I-digested mutant plasmid (p4B-Y408W), respectively

B: Part of DNA sequencing chromatogram of p4B-Y408W. The nucleotide sequence of the coding strand for the mutant plasmid is shown. The substituted bases and amino acid are indicated. Reaction conditions are described in Method 4.6.

Copyright by Mahidol University

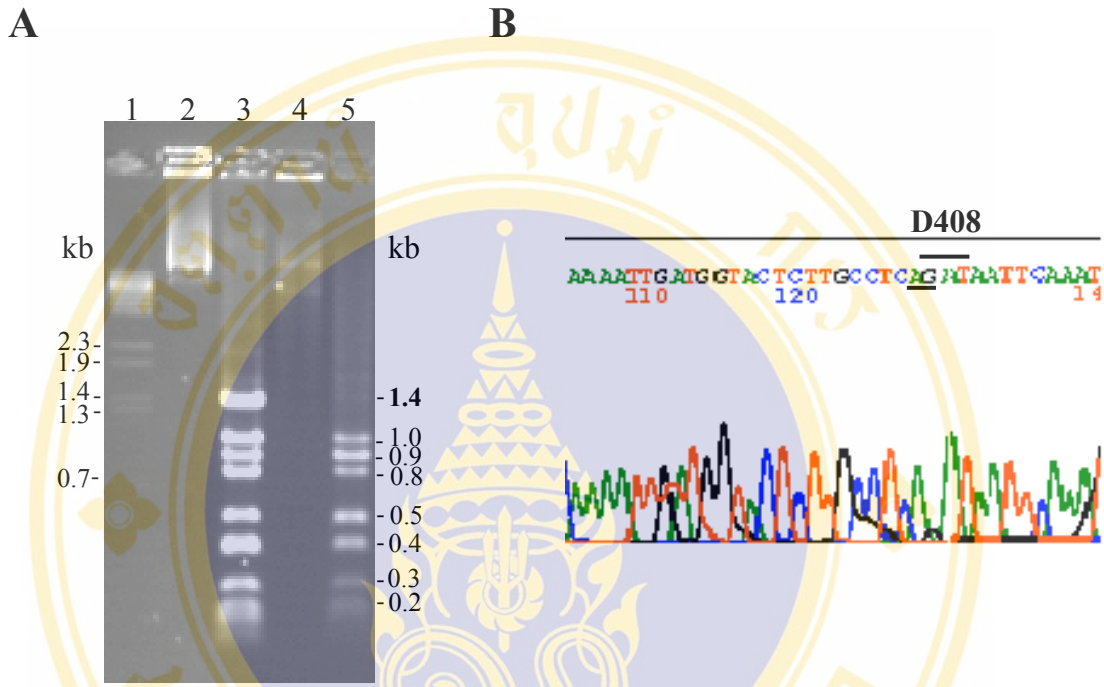

Figure 53: Restriction endonuclease and DNA sequence analysis of p4B-Y408D

A: 2% agarose gel electrophoresis (ethidium bromide stained) of *Dde* I digestion pattern of the mutant plasmid. The 1.4-kb wild-type specific DNA band is indicated with the bold label.

Lane 1:	*Bst*E II-digested λ DNA markers
Lanes 2 & 3:	the undigested and *Dde* I-digested wild type plasmid (pMU388), respectively
Lanes 4 & 5:	the undigested and *Dde* I-digested mutant plasmid (p4B-Y408D), respectively

B: Part of DNA sequencing chromatogram of p4B-Y408D. The nucleotide sequence of the coding strand for the mutant plasmid is shown. The substituted bases and amino acid are indicated. Reaction conditions are described in Method 4.6.

Copyright by Mahidol University

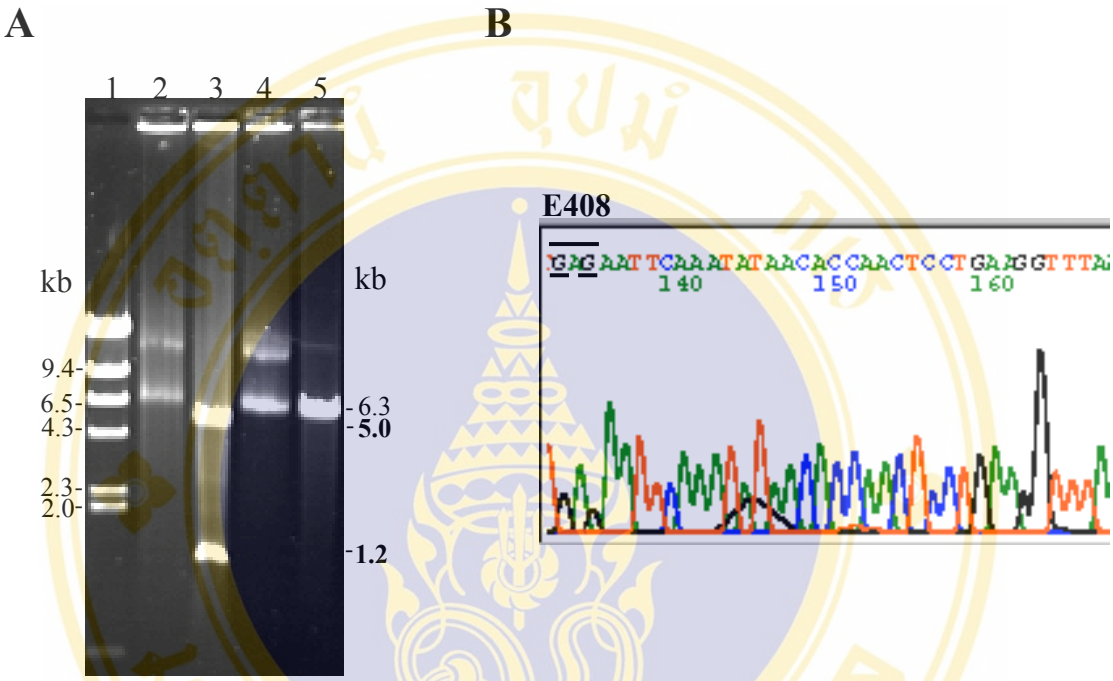

Figure 54: Restriction endonuclease and DNA sequence analysis of p4B-Y408E

A: 1% agarose gel electrophoresis (ethidium bromide stained) of *Eco*R I digestion pattern of the mutant plasmid. The 5.0- and 1.2-kb mutant specific DNA bands are indicated with the bold labels.

Lane 1:	*Hin*d III-digested λ DNA markers
Lanes 2 & 3:	the undigested and *Eco*R I-digested mutant plasmid (p4B-Y408E), respectively
Lanes 4 & 5:	the undigested and *Eco*R I-digested wild type plasmid (pMU388), respectively

B: Part of DNA sequencing chromatogram of p4B-Y408E. The nucleotide sequence of the coding strand for the mutant plasmid is shown. The substituted bases and amino acid are indicated. Reaction conditions are described in Method 4.6.

Copyright by Mahidol University

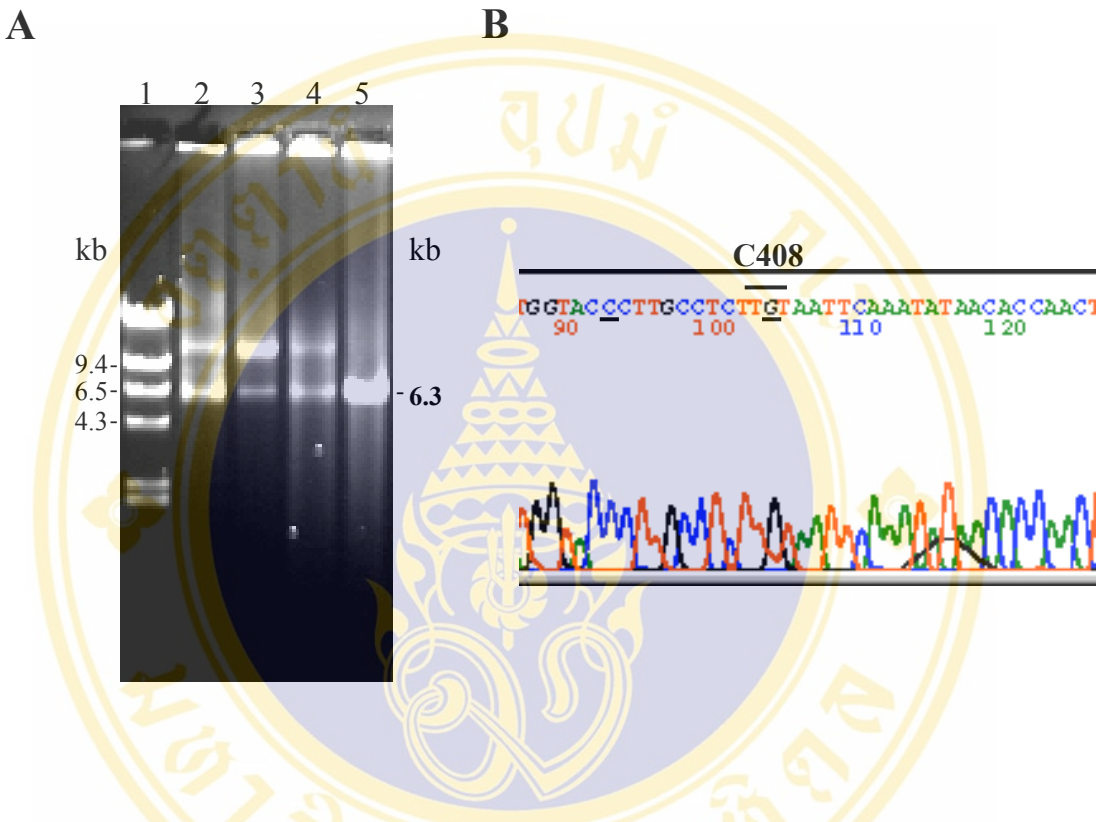

Figure 55: Restriction endonuclease and DNA sequence analysis of p4B-Y408C

A: 1% agarose gel electrophoresis (ethidium bromide stained) of *Kpn* I digestion pattern of the mutant plasmid. The 6.3-kb mutant specific DNA band is indicated with the bold label.

Lane 1:	*Hin*d III-digested λ DNA markers
Lanes 2 & 3:	the undigested and *Kpn* I-digested wild type plasmid (pMU388), respectively
Lanes 4 & 5:	the undigested and *Kpn* I-digested mutant plasmid (p4B-Y408C), respectively

B: Part of DNA sequencing chromatogram of p4B-Y408C. The nucleotide sequence of the coding strand for the mutant plasmid is shown. The substituted bases and amino acid are indicated. Reaction conditions are described in Method 4.6.

Copyright by Mahidol University

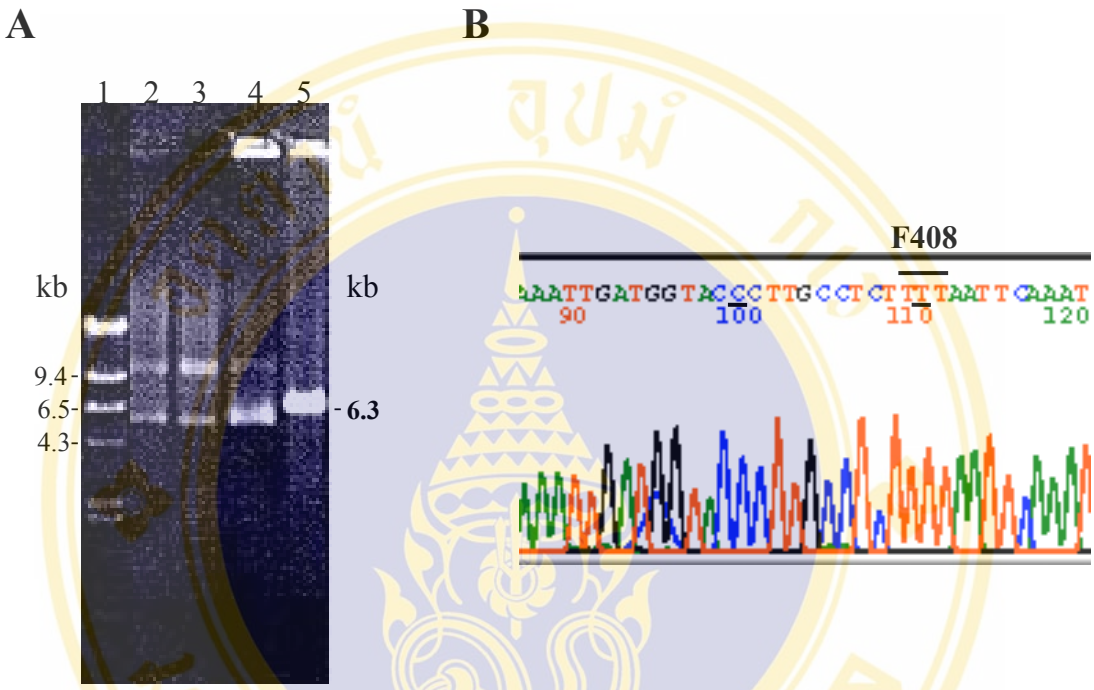

Figure 56: Restriction endonuclease and DNA sequence analysis of p4B-Y408F

A: 1% agarose gel electrophoresis (ethidium bromide stained) of *Kpn* I digestion pattern of the mutant plasmid. The 6.3-kb mutant specific DNA band is indicated with the bold label.

Lane 1:	*Hin*d III-digested λ DNA markers
Lanes 2 & 3:	the undigested and *Kpn* I-digested wild type plasmid (pMU388), respectively
Lanes 4 & 5:	the undigested and *Kpn* I-digested mutant plasmid (p4B-Y408F), respectively

B: Part of DNA sequencing chromatogram of p4B-Y408F. The nucleotide sequence of the coding strand for the mutant plasmid is shown. The substituted bases and amino acid are indicated. Reaction conditions are described in Method 4.6.

Copyright by Mahidol University

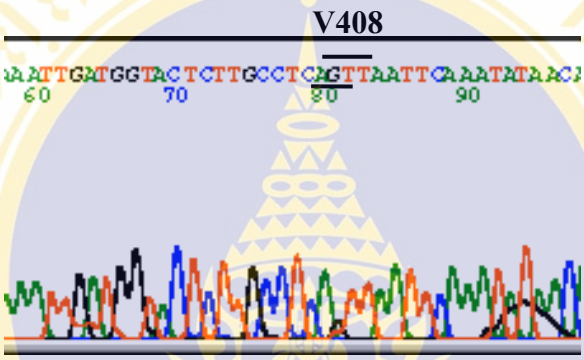

Figure 57: DNA sequence analysis of Y408V mutant

The figure shows part of DNA sequencing chromatogram of Y408V. The nucleotide sequence of the coding strand for the mutant is shown. The substituted bases and amino acid are indicated. Reaction conditions are described in Method 4.6.

Copyright by Mahidol University

6.5 Protoxin expression of Y408V, Y408F, Y408W, Y408D, Y408E and Y408C mutants

Upon IPTG induction, all the six mutants (Y408V, Y408F, Y408W, Y408D, Y408E and Y408C) were highly expressed and their expression levels analysed on 10% SDS-PAGE showed the same intensity of the 130-kDa protoxin bands as that of the wild type (Figure 58).

6.6 Larvicidal activity of Y408V, Y408F, Y408W, Y408D, Y408E and Y408C mutants

Investigating for toxicity against *A. aegypti* mosquito larvae, only *E. coli* cells expressing the Y408F mutant still exhibited about 90% larvicidal activity as the wild type. However, the Y408V, Y408W, Y408D, Y408E and Y408C mutants reduced larvicidal activity to about 50%, 9%, 2%, 2% and 14%, respectively (Figure 59).

6.7 Solubilisation and proteolytic activation of the Y408A, Y408V, Y408F, Y408W, Y408D, Y408E and Y408C mutants

After breaking with French Pressure cells at 1,200 psi and analysed on 10% SDS-PAGE (Figures 60-62), the 130-kDa protoxins from the *E. coli* cells expressing the seven mutants (Y408A, Y408V, Y408F, Y408W, Y408D, Y408E and Y408C) or wild type protoxins were found in sedimented fractions at the same levels.

When the seven mutant inclusions were solubilised in 50 mM Na_2CO_3 (pH 9.0) for 1.30 hr at 37 °C, the mutants showed the same solubility as the wild type (Figures 63-65). After cutting with trypsin at a ratio of 1:20 (enzyme:protoxin, w/w) for 13 hr at 37 °C, the 130-kDa solubilised mutant protoxins showed the same proteolytic activating patterns of 47 and 20 kDa as similar to the wild type on 15% SDS-PAGE (Figures 66-68).

Copyright by Mahidol University

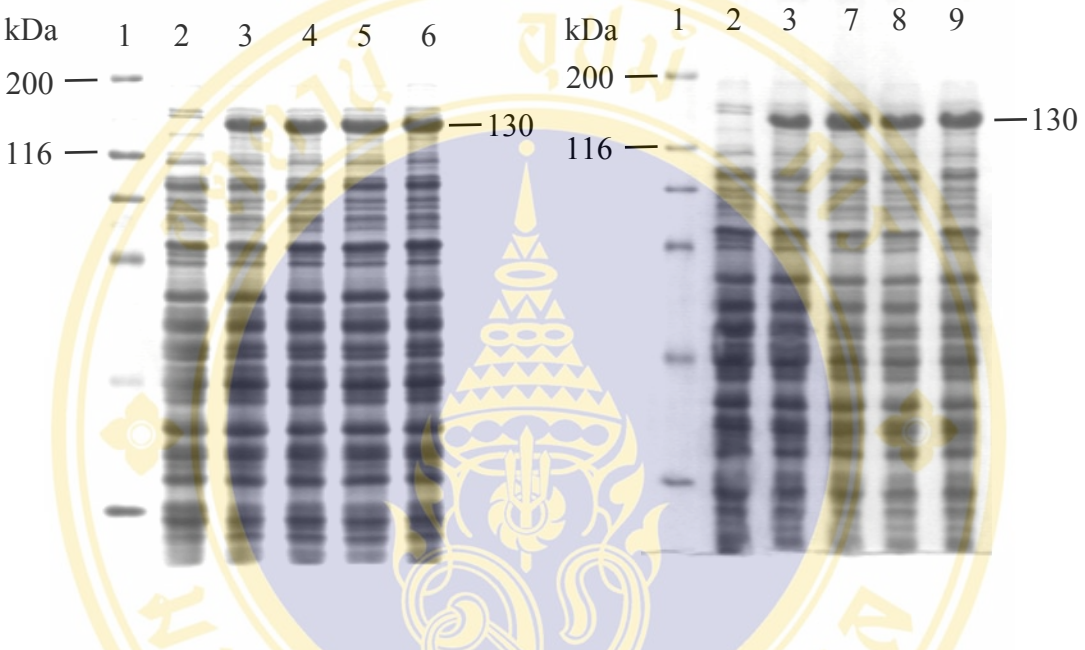

Figure 58: Expression of the Y408V, Y408F, Y408W, Y408D, Y408E and Y408C mutant protoxins

The figure shows Coomassie brilliant blue-stained 10% SDS-PAGE comparing expression levels of the Cry4Ba wild type and the Y408V, Y408F, Y408W, Y408D, Y408E and Y408C mutant protoxins from *E. coli* clones (0.1 OD_{600} ~ 10^7 cells).

Lane 1:	standard protein marker
Lanes 2 & 3:	crude lysates of *E. coli* cells containing pUC12 alone (negative control) and pMU388 (the Cry4Ba wild type), respectively
Lanes 4-9:	crude lysates of *E. coli* cells containing the mutant plasmids; p4B-Y408V, p4B-Y408F, p4B-Y408W, p4B-Y408D, p4B-Y408E and p4B-Y408C, respectively

Copyright by Mahidol University

Toxin	% Mortality							
	Y408V	Y408F	Y408W	Y408D	Y408E	Y408C	Cry4Ba	pUC12
mean	50.3	89.0	8.7	2.3	1.7	13.7	95.7	2.0
SEM	3.7	2.6	0.7	0.7	0.3	2.6	2.4	0.6

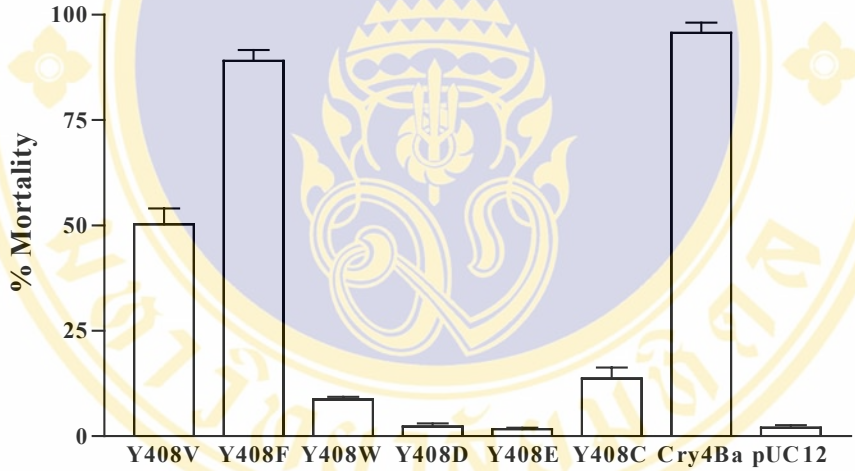

Figure 59: Mosquito-larvicidal activity of *E. coli* cells expressing Y408V, Y408F, Y408W, Y408D, Y408E or Y408C mutants

The figure shows comparison of larvicidal activity of *E. coli* cells expressing the Cry4Ba wild type and its mutants (Y408V, Y408F, Y408W, Y408D, Y408E and Y408C) against *A. aegypti* larvae. *E. coli* cells containing plasmid pUC12 alone were used as negative control. Data in the table and bar represent mean of % mortality from three independent assays ± SEM (standard error of mean).

Copyright by Mahidol University

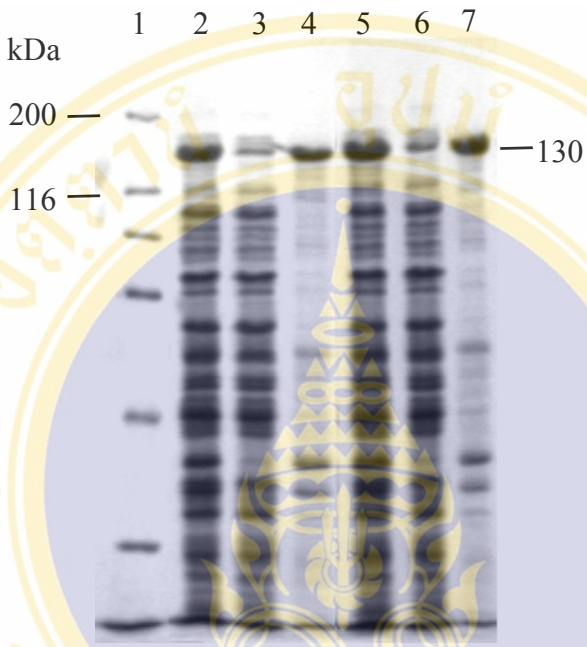

Figure 60: Expression of Y408A mutant inclusion

The figure shows Coomassie brilliant blue-stained 10% SDS-PAGE comparing the inclusion levels of *E. coli* clones (0.1 OD_{600} ~ 10^7 cells) expressing Cry4Ba wild type and Y408A mutant.

Lane 1:	standard protein marker
Lanes 2-4:	crude lysate, supernatant and sedimented fractions of *E. coli* clone containing pMU388 (the Cry4Ba wild type), respectively
Lanes 5-7:	crude lysate, supernatant and sedimented fractions of *E. coli* clone containing the mutant plasmid-p4B-Y408A, respectively

Copyright by Mahidol University

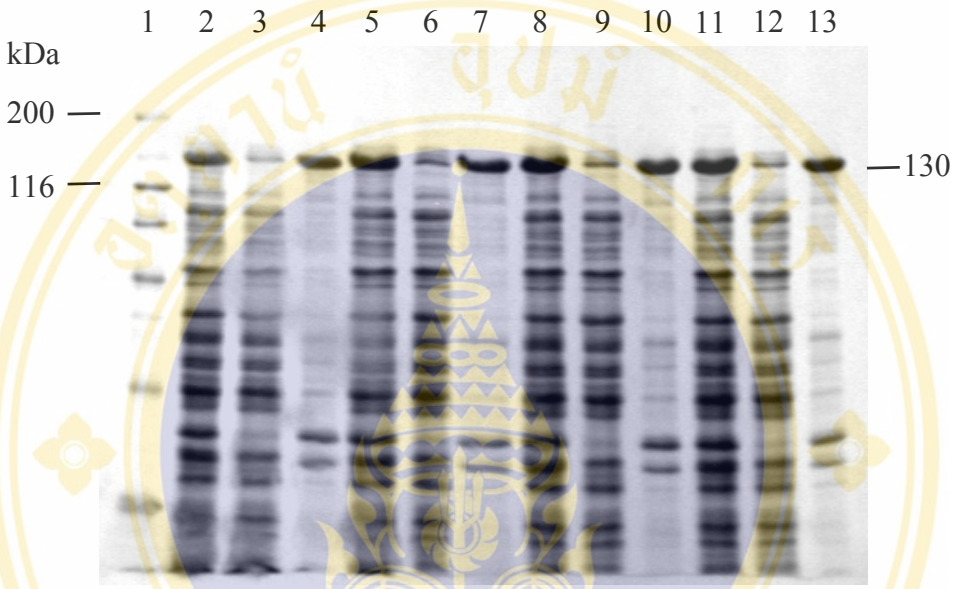

Figure 61: Expression of Y408D, Y408E and Y408C mutant inclusions

The figure shows Coomassie brilliant blue-stained 10% SDS-PAGE comparing the inclusion levels of *E. coli* clones (0.1 OD_{600} ~ 10^7 cells) expressing Cry4Ba wild type and its mutants, Y408D, Y408E and Y408C.

Lane 1:	standard protein marker
Lanes 2-4:	crude lysate, supernatant and sedimented fractions of *E. coli* clone containing pMU388 (the Cry4Ba wild type), respectively
Lanes 5-7:	crude lysate, supernatant and sedimented fractions of *E. coli* clone containing the mutant plasmid-p4B-Y408D, respectively
Lanes 8-10:	crude lysate, supernatant and sedimented fractions of *E. coli* clone containing the mutant plasmid-p4B-Y408E, respectively
Lanes 11-13:	crude lysate, supernatant and sedimented fractions of *E. coli* clone containing the mutant plasmid-p4B-Y408C, respectively

Copyright by Mahidol University

Figure 62: Expression of Y408W, Y408V and Y408F mutant inclusions

The figure shows Coomassie brilliant blue-stained 10% SDS-PAGE comparing the inclusion levels of *E. coli* clones (0.1 OD_{600} ~ 10^7 cells) expressing Cry4Ba wild type and its mutants, Y408W, Y408V and Y408F.

Lane 1:	standard protein marker
Lanes 2-4:	crude lysate, supernatant and sedimented fractions of *E. coli* clone containing pMU388 (the Cry4Ba wild type), respectively
Lanes 5-7:	crude lysate, supernatant and sedimented fractions of *E. coli* clone containing the mutant plasmid-p4B-Y408W, respectively
Lanes 8-10:	crude lysate, supernatant and sedimented fractions of *E. coli* clone containing the mutant plasmid-p4B-Y408V, respectively
Lanes 11-13:	crude lysate, supernatant and sedimented fractions of *E. coli* clone containing the mutant plasmid-p4B-Y408F, respectively

Copyright by Mahidol University

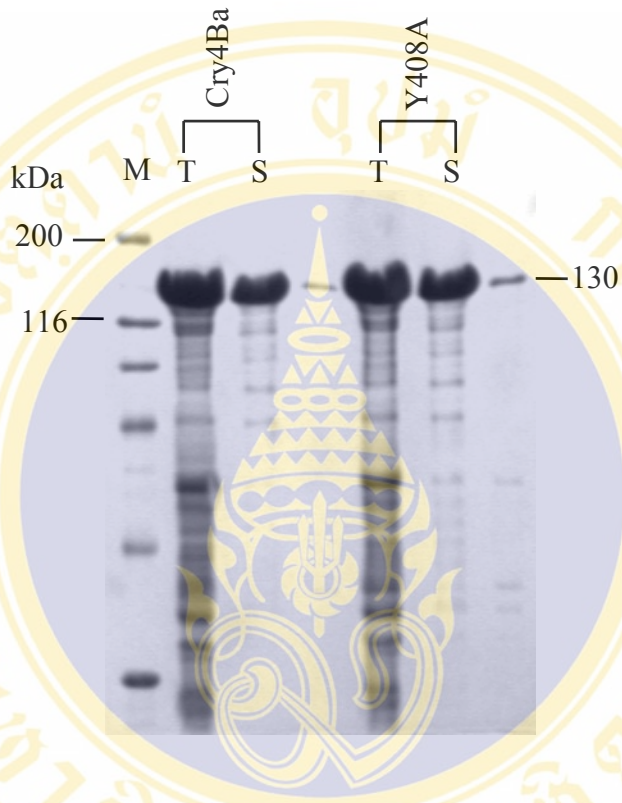

Figure 63: Solubility of Cry4Ba wild type and Y408A mutant inclusions

The figure shows Coomassie brilliant blue-stained 10% SDS-PAGE comparing the solubility of the wild type and the mutant inclusions in 50 mM Na_2CO_3 (pH 9.0). T and S represent total and solubilised fractions, respectively. M represents standard protein markers.

Copyright by Mahidol University

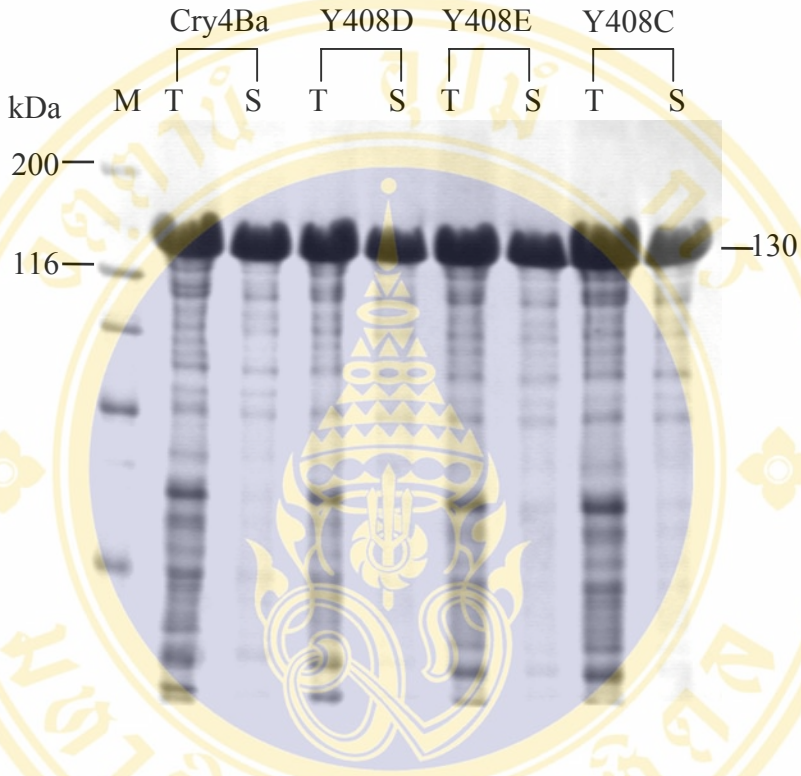

Figure 64: Solubility of the Cry4Ba wild type and its mutant (Y408D, Y408E and Y408C) inclusions

The figure shows Coomassie brilliant blue-stained 10% SDS-PAGE comparing the solubility of the wild type and its mutant inclusions in 50 mM Na_2CO_3 (pH 9.0). T and S represent total and solubilised fractions, respectively. M represents standard protein markers.

Copyright by Mahidol University

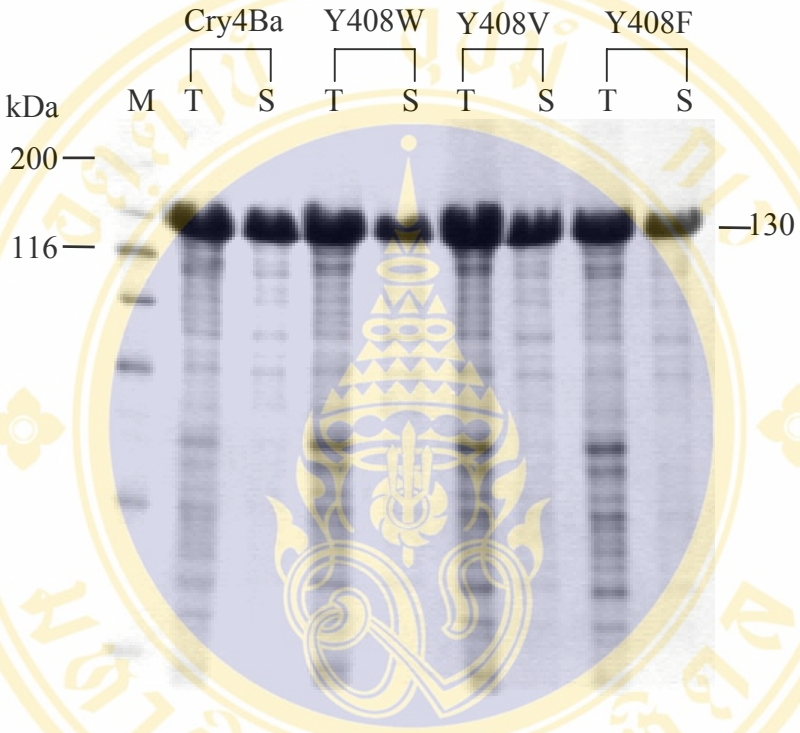

Figure 65: Solubility of the Cry4Ba wild type and its mutant (Y408W, Y408V and Y408F) inclusions

The figure shows Coomassie brilliant blue-stained 10% SDS-PAGE comparing the solubility of the wild type and its mutant inclusions in 50 mM Na_2CO_3 (pH 9.0). T and S represent total and solubilised fractions, respectively. M represents standard protein markers.

Copyright by Mahidol University

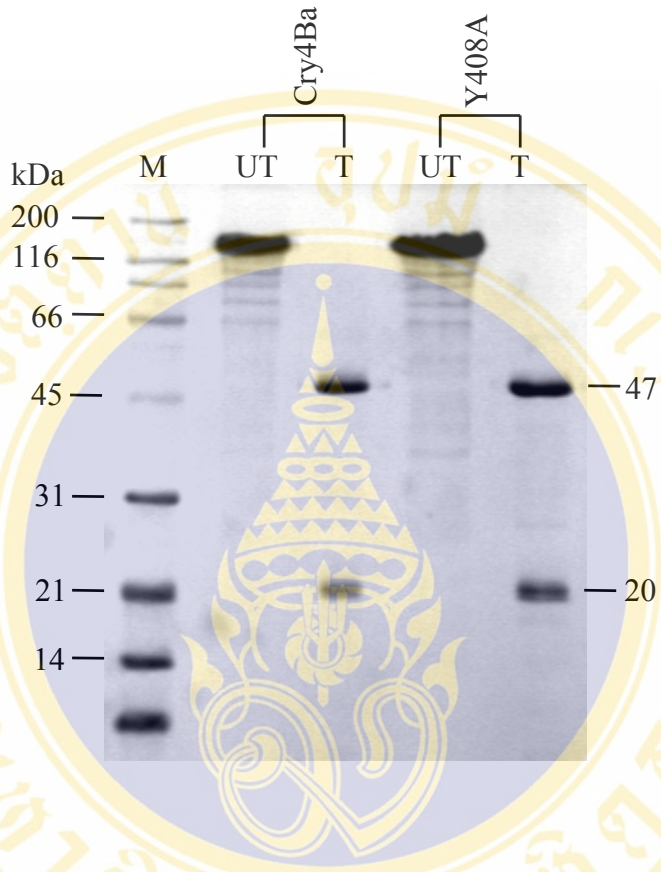

Figure 66: Proteolytic processing of Cry4Ba wild type and Y408A mutant protoxins

The figure shows Coomassie brilliant blue-stained 15% SDS-PAGE comparing trypsin digestion of the wild type and the mutant protoxins solubilised in 50 mM Na_2CO_3 (pH 9.0). UT and T represent untreated and treated protoxins with trypsin, respectively. M represents standard protein markers.

Copyright by Mahidol University

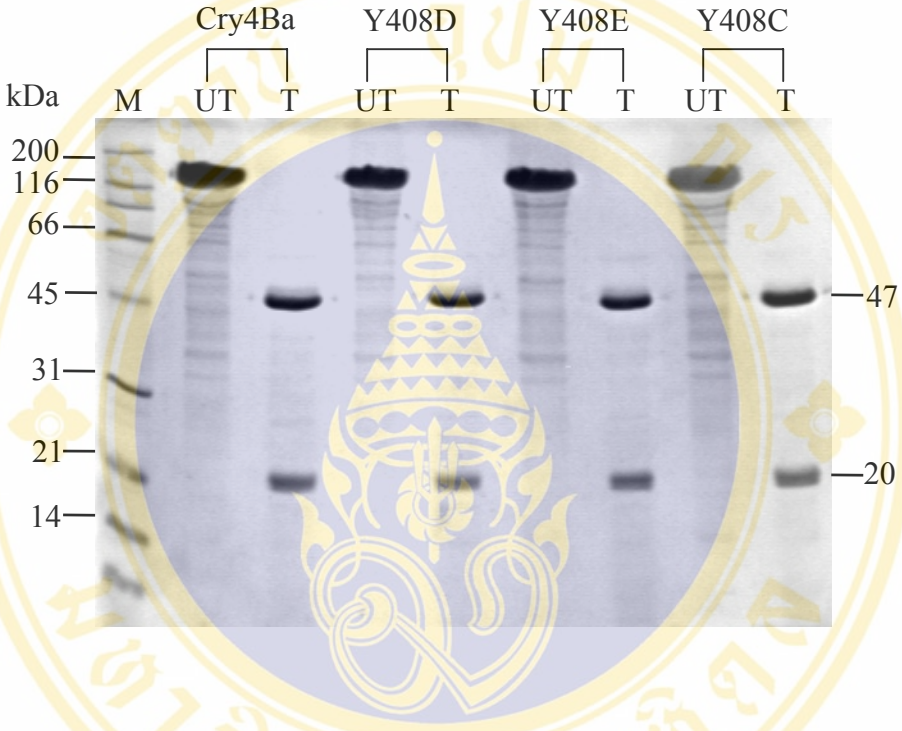

Figure 67: Proteolytic processing of the Cry4Ba wild type and its mutant (Y408D, Y408E and Y408C) protoxins

The figure shows Coomassie brilliant blue-stained 15% SDS-PAGE comparing trypsin digestion of the wild type and its mutant protoxins solubilised in 50 mM Na_2CO_3 (pH 9.0). UT and T represent untreated and treated protoxins with trypsin, respectively. M represents standard protein markers.

Copyright by Mahidol University

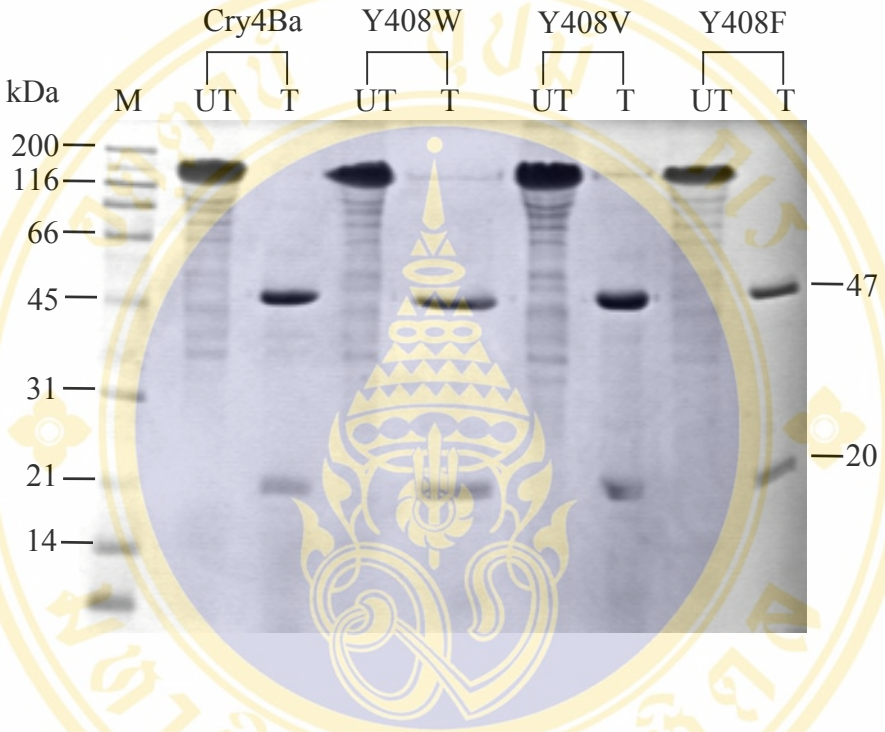

Figure 68: Proteolytic processing of the Cry4Ba wild type and its mutant (Y408W, Y408V and Y408F) protoxins

The figure shows Coomassie brilliant blue-stained 15% SDS-PAGE comparing trypsin digestion of the wild type and its mutant protoxins solubilised in 50 mM Na_2CO_3 (pH 9.0). UT and T represent untreated and treated protoxins with trypsin, respectively. M represents standard protein markers.

Copyright by Mahidol University

6.8 Binding activity of the Y408D mutant toxin

The Y408D mutant was selected to examine for its mutagenic effect on binding activity since this mutant clone showed a drastic loss in larvicidal activity (see Figure 59). *In vitro* binding assays were performed on *A. aegypti* gut sections based on the method of immunocytochemistry (Method 4.14). The mouse monoclonal antibody, 2F (1H2) that specifically recognises the Cry4Ba-domain III was used in the binding assay to confirm that the antibody could bind to the 65-kDa purified Cry4Ba wild-type toxin (see Figure 69, lane 3) and the 65-kDa purified Y408D mutant toxin (see Figure 69, lane 5) with the same sensitivity. Immunocytochemical staining revealed that the purified Y408D mutant toxin showed a reduction in signal intensity of the dark brown-colour products of 3,3´-diaminobenzidine substrate detected on the apical region of the posterior midgut epithelial cell sections when compared with that of the purified Cry4Ba wild-type toxin. However, no signal of the dark brown products was observed when no addition of toxin in the immunocytochemical reaction (Figures 70 and 71).

Copyright by Mahidol University

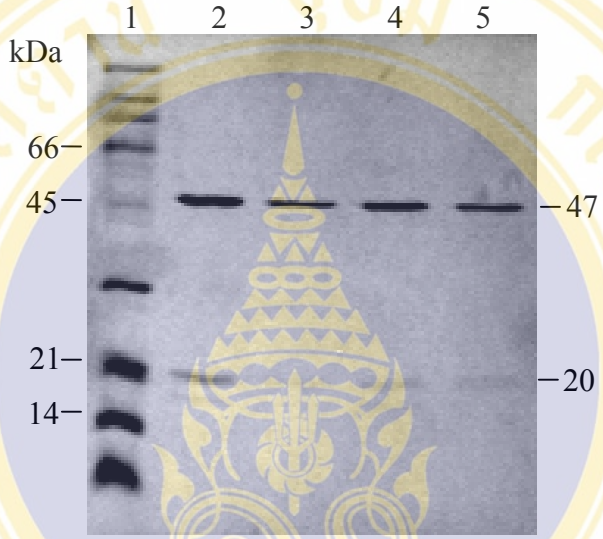

Figure 69: Purification of the activated Cry4Ba and its Y408D mutant toxins

The figure shows Coomassie brilliant blue-stained 15% SDS-PAGE of the 65-kDa FPLC purified Cry4Ba and its Y408D mutant toxins.

Lane 1: standard protein marker
Lanes 2 & 4: the activated Cry4Ba and Y408D mutant toxins before purification, respectively
Lanes 3 & 5: the activated Cry4Ba and Y408D mutant toxins after purification, respectively

Copyright by Mahidol University

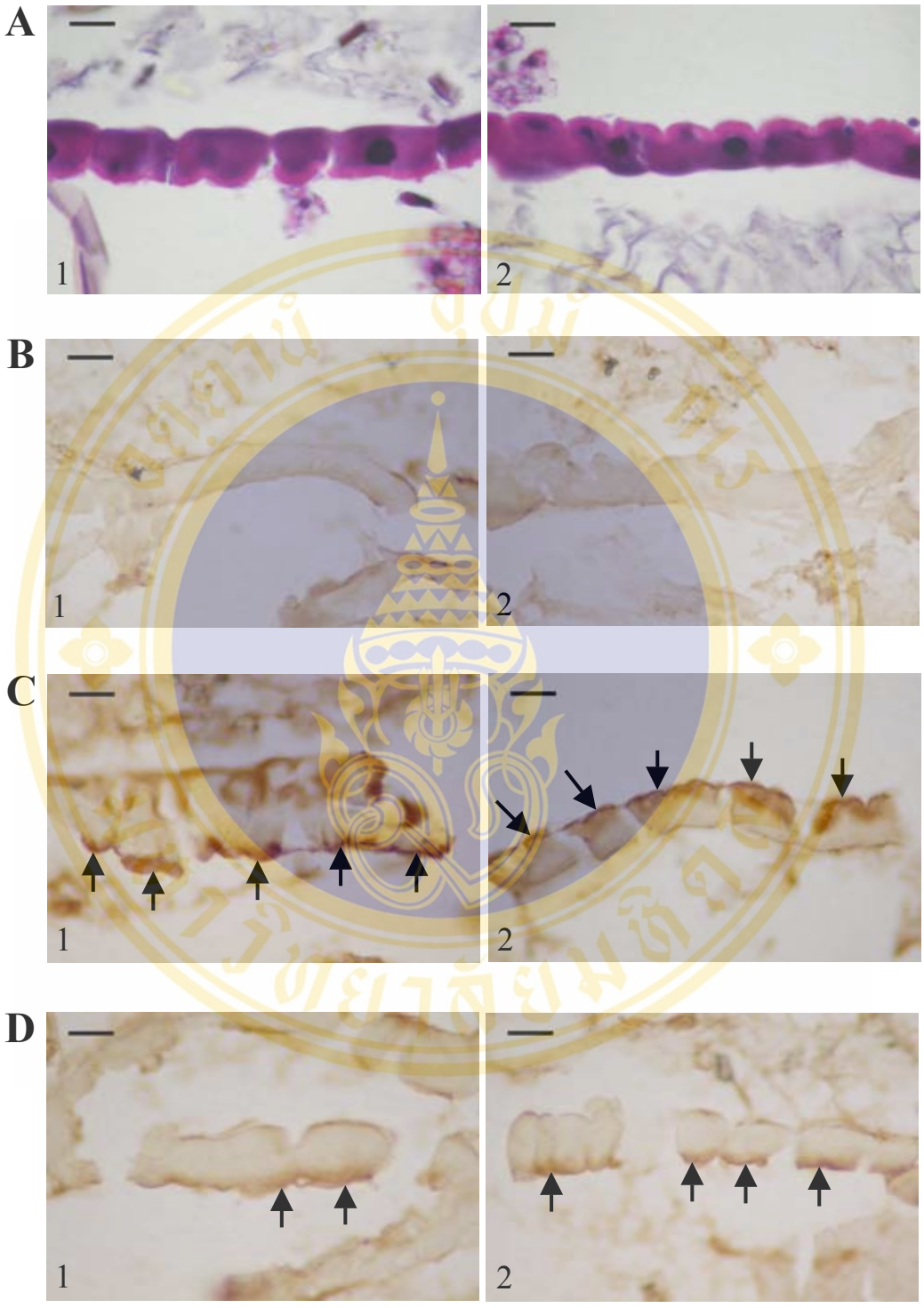

Figure 70: Immunocytochemical staining of the Y408D mutant toxin detected with undiluted monoclonal antibody

This figure shows the posterior midgut sections of *A. aegypti* mosquito larvae stained with hematoxylin & eosin dye (A, purple colour: apical microvilli), incubated with 50 mM Na_2CO_3 buffer, pH 9.0 (B), the 65-kDa Cry4Ba wild-type toxin (C) and the 65-kDa Y408D mutant toxin (D), and incubated with undiluted mouse-anti Cry4Ba-domain III monoclonal antibody (2F(1H2)), and 1:2,000 dilution of rabbit-anti mouse IgGs conjugated with biotin. Arrows indicate positive areas (dark brown colour). 1 & 2 represent selected duplicate samples. Scale bars, 50 μm.

Copyright by Mahidol University

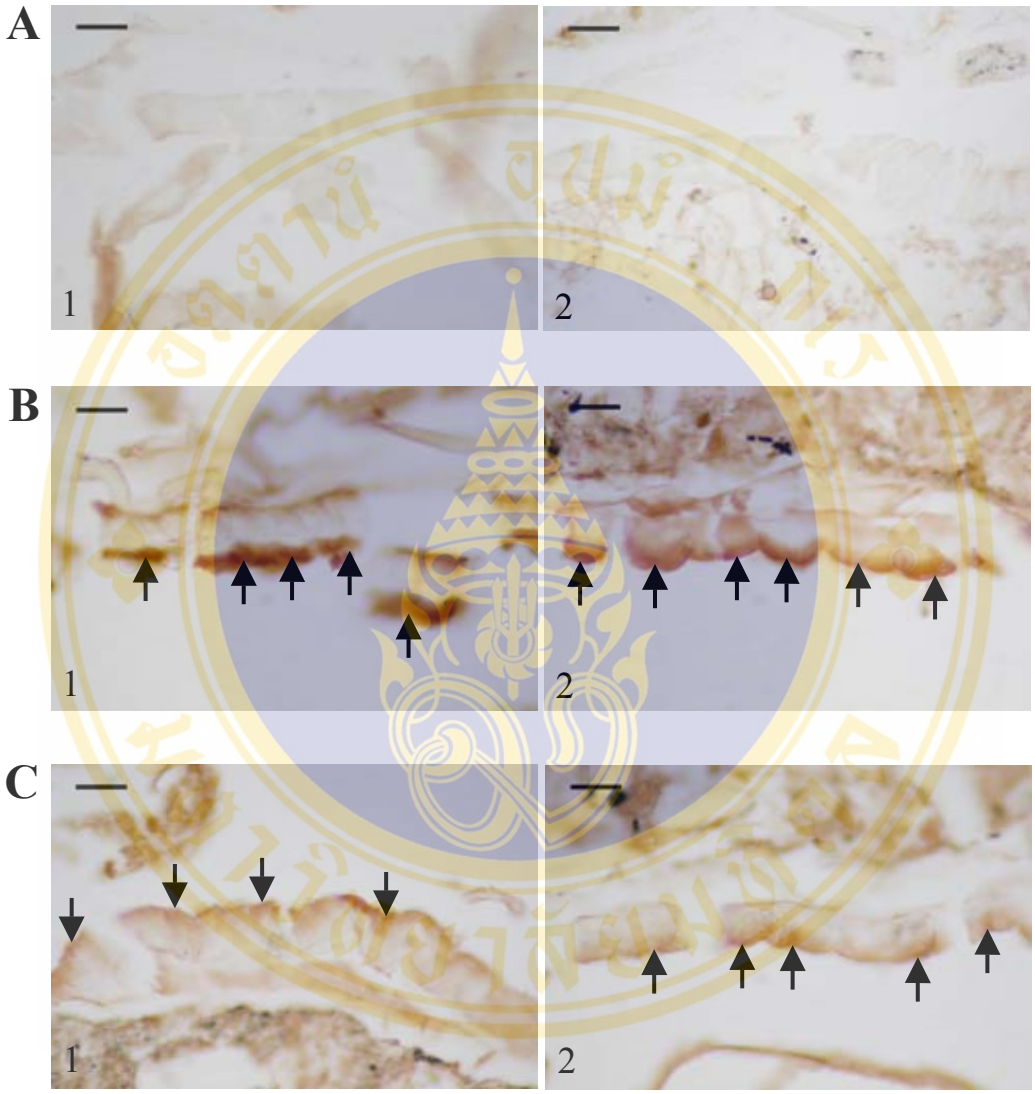

Figure 71: Immunocytochemical staining of the Y408D mutant toxin detected with 1:20 dilution of monoclonal antibody

This figure shows the posterior midgut sections of *A. aegypti* mosquito larvae incubated with 50 mM Na_2CO_3 buffer, pH 9.0 (A), the 65-kDa Cry4Ba wild-type toxin (B) and the 65-kDa Y408D mutant toxin (C), and incubated with 1:20 dilution of mouse-anti Cry4Ba-domain III monoclonal antibody (2F(1H2)), and 1:8,000 dilution of rabbit-anti mouse IgGs conjugated with biotin. Arrows indicate positive areas (dark brown colour). 1 & 2 represent selected duplicate samples. Scale bars, 50 μm.

Copyright by Mahidol University

CHAPTER VII
DISCUSSION

7.1 Involvement of β6-β7, β8-β9 and β10-β11 loop residues in toxicity

In this study, certain loop regions corresponding to surface-exposed domain II loops of the Cry4Ba toxin were explored in search of sites involved in larvicidal activity. All residues in the β6-β7 ($SSPS_{390}$) and the β10-β11 ($DYNS_{457}$) loops and selected residues in the β8-β9 loop (S_{410}, N_{411}, T_{413}, T_{415}, E_{417} and G_{418}) (Figures 3, 9 and 72) were changed individually to alanine. For the β8-β9 loop, only polar uncharged residues (i.e. S_{410}, N_{411}, T_{413} and T_{415}), a negatively charged residue (i.e. E_{417}) and G_{418} which is conserved among Cry3Aa, Cry1Aa and Cry4Ba (Figure 72) were selected for the study.

As shown in the results, all the 130-kDa mutant protoxins were highly expressed in *E. coli* with yields similar to the wild type. This suggests that the structural folding of the mutant protoxins might be similar to that of the wild type. In other word, these loop mutations did not affect the structural folding of the mutant molecules, as protein misfolding or protease sensitivity can be attributed to low levels of the protein expression in the bacterial cells (162).

The toxicity results suggest that P_{389} in the β6-β7 loop, S_{410} and E_{417} in the β8-β9 loop, and Y_{455} and N_{456} in the β10-β11 loop play a role in larvicidal activity of the Cry4Ba toxin. The results also indicate that the Cry4Ba activity needs more than one loop residues. Two double mutants, S410A/E417A and Y455A/N456A, were therefore constructed and revealed a more adverse effect on toxicity by reducing larvicidal activity to about 20% (Figure 32). This confirms that both S_{410} and E_{417} in the β8-β9 loop and both Y_{455} and N_{456} in the β10-β11 loop are needed for larvicidal activity of the Cry4Ba toxin. Further characterisation revealed that both double mutants were over expressed as protoxin inclusions at the wild type level (Figure 37) and showed the same solubility in carbonate buffer (pH 9.0) and trypsin digestion patterns as the wild type (Figures 38 and 39). These results suggest that the two double mutants were

Copyright by Mahidol University

expressed as structurally stable protoxins and the mutations did not cause protein misfolding. Thus, the reduced toxicity observed for these two double mutants is least likely to be caused by protoxin expression, solubilisation and proteolytic activation of the toxins.

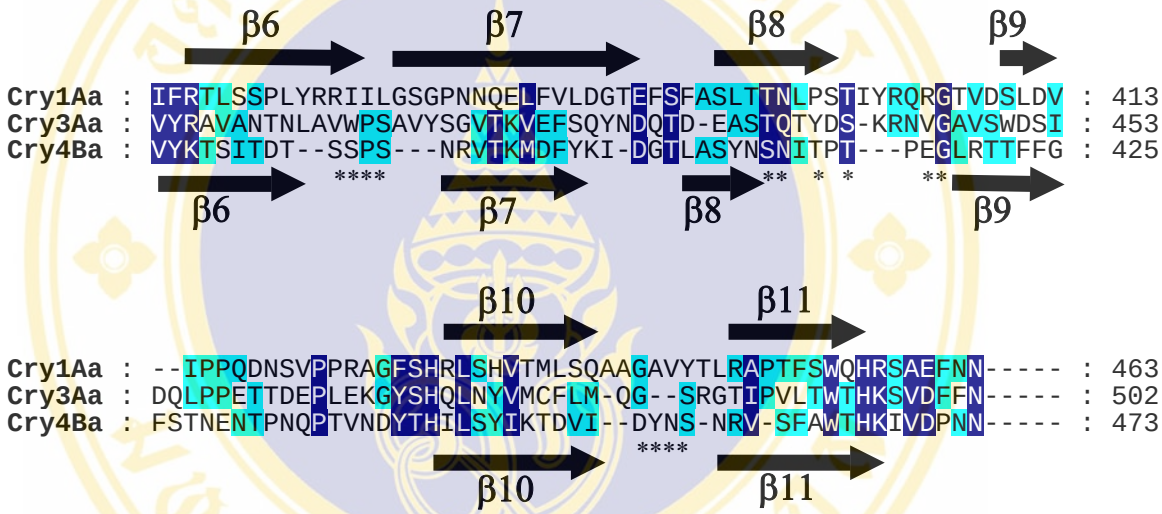

Figure 72: Sequence alignment of parts of different Cry toxin-domain II

The figure shows multiple sequence alignment of parts of the domain II of Cry4Ba with those of the crystal structures of Cry1Aa and Cry3Aa. The sequences were aligned using the program Clustal X. The degree of conservation among the three sequences is represented by background shading of the residues. The positions of secondary elements of Cry3Aa and Cry4Ba are illustrated over and under the alignments, respectively. Mutated residues are indicated by *.

Copyright by Mahidol University

Previously, Wu and Dean (17) showed that the double mutation of the β6-β7 loop residues (P412A/S413A) of the Cry3Aa toxin had no effect on toxicity to *Tenebrio moliter* larvae. Here, individual alanine substitutions of P_{389} and S_{390} which are relatively conserved in the β6-β7 loop of Cry4Ba (Figure 72) revealed that the P389A mutant, but not the S390A mutant, showed a loss in mosquito-larvicidal activity of about 30%. This proline residue might be needed for conformational stability of the β 6-β7 loop ($SSPS_{390}$) in Cry4Ba (Figure 73), but apparently not for the shorter β6-β7 loop (PS_{413}) of the Cry3Aa toxin. Conceivably, the P389A mutation might alter conformation of the β6-β7 loop in Cry4Ba, resulting in a decrease in toxin activity by likely interfering the receptor binding step. It was previously published for the Cry1Ca toxin that toxicity and binding to *A. aegypti* BBMVs required P_{377} in the predicted β6-β7 loop (113). Recently, Abdullah et al. (163) showed that the addition of the putative β6-β7 loop (NDY_{437}) of the closely related Cry4Aa mosquito-larvicidal protein between V_{393} and T_{394} in β7 of Cry4Ba caused the mutant toxin to lose toxicity against *Aedes* and *Anopheles* larvae.

As mentioned before, both S_{410} and E_{417} in the β8-β9 loop and both Y_{455} and N_{456} in the β10-β11 loop are required for larvicidal activity of the Cry4Ba toxin. Except for the β8-β9 loop, several studies have supported evidence for functional significance of the β10-β11 loop residues that are responsible for binding to specific receptors and, therefore, for toxicity to several insect larvae (19; 111; 113; 163). However, it is not obvious to conclude how these important loop residues (S_{410}, E_{417}, Y_{455} and N_{456}) contribute to Cry4Ba activity, but for Cry3Aa it was shown that alanine substitutions for N_{353} and D_{354} in the β2-β3 loop caused the loss of receptor binding and toxicity (17). Notwithstanding the lack of binding studies, E_{417} and N_{456} which are located at the apex of β8-β9 and β10-β11 loops, respectively (Figure 73) might be directly involved in Cry4Ba-receptor binding. It should be noted that the D454A mutation in the β10-β11 loop did not significantly affect Cry4Ba toxicity, apparently agreeing well with the findings of Abdullah et al. (163) which showed that substitutions of this aspartate residue with a short peptide (PAT, GAT or GAV) did not suppress *Aedes* larvicidal activity of this toxin, but rather significantly increased toxicity against *Culex* larvae.

Copyright by Mahidol University

The functional role of tyrosine in toxicity and binding to toxin receptors has been demonstrated for other Cry toxins (111; 164; 165) and proposed that its aromatic phenol ring might contribute to tight binding affinity to the receptors via hydrophobic interactions (164). Similar to E_{417} and N_{456}, Y_{455} which is found at the tip of the β10-β 11 loop (Figure 73) might also play a role in Cry4Ba-receptor binding. Since S_{410} is not located apically at the surface-exposed β8-β9 loop, this implies that this important residue might not directly contact with the receptor. However, the structural basis for this implication is not yet clear. As illustrated in Figure 74, a hydrogen bond is formed between the hydroxyl group of S_{410} in the β8-β9 loop and the peptide carbonyl group of R_{336} in the β2-β3 loop, therefore a disruption of this interaction with the S410A mutation might destabilise the structural integrity of the β8-β9 loop, resulting in a reduced Cry4Ba toxicity.

Copyright by Mahidol University

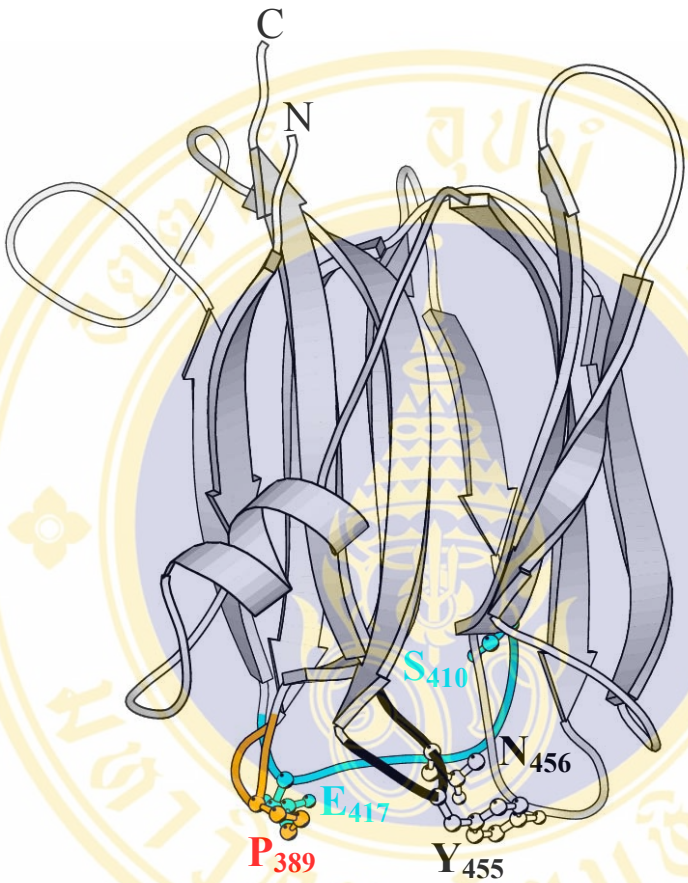

Figure 73: Domain II of the Cry4Ba toxin

The figure shows the Cry4Ba-domain II generated by MolScript v2.1.2 based on the crystal structure of Cry4Ba (10), illustrating residues in the three surface-exposed loops at molecular apex that are involved in Cry4Ba toxicity. The orange, cyan and white colours represent P_{389} in β6-β7 loop, S_{410} and E_{417} in β8-β9 loop, and Y_{455} and N_{456} in β10-β11 loop, respectively.

Copyright by Mahidol University

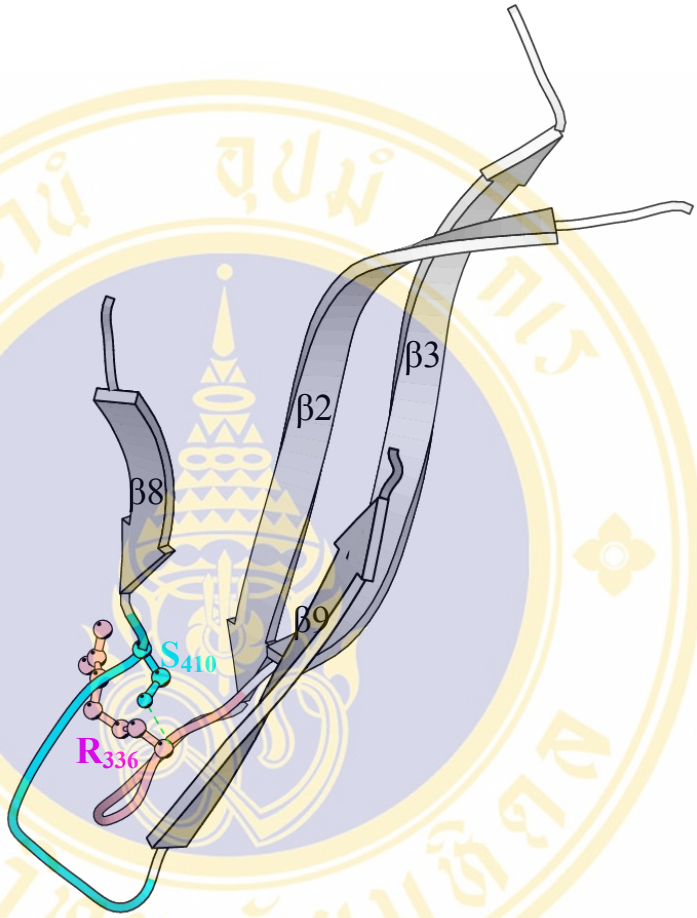

Figure 74: β2-β3 and β8-β9 hairpins in domain II of the Cry4Ba toxin

The figure shows a part of domain II of Cry4Ba generated by MolScript v2.1.2 based on the crystal structure of Cry4Ba (10), illustrating β2-β3 and β8-β9 hairpins. A hydrogen bond formed between the hydroxyl group of S_{410} in the β8-β9 loop and the peptide carbonyl group of R_{336} in the β2-β3 loop is indicated with a green-colour dash line.

Copyright by Mahidol University

7.2 Involvement in toxicity of residues stabilising β2-β3 and β4-β5 hairpins

Previously (21), Y_{332} and F_{364} that are located at the tip of β2-β3 and β4-β5 loops, respectively (Figures 9 and 40) were shown to play a critical role in larvicidal activity of Cry4Ba. Hydrogen bonding between T_{328} in β2 and T_{369} in β5 (Figure 40) were also shown to play a critical role in Cry4Ba activity possibly by stabilising structural integrity of these two critical β-hairpins. In this study, Y_{408} in β8 as shown to form the inter β-sheet hydrogen bonding with T_{328} in β2 (Figure 42) is also apparently involved in larvicidal activity of the Cry4Ba toxin. However, further mutagenic analysis suggested that this hydrogen bonding between Y_{408} and T_{328} is not the factor that is involved in Cry4Ba larvicidal activity, but rather aromatic interaction and/or hydrophobic interactions between Y_{408} with the other residues could possibly be involved in the toxicity, since the Y408F mutant still retained larvicidal activity at the wild type level and the Y408V mutant still retained larvicidal activity at about 50%. However, the Y408W mutant almost abolished Cry4Ba toxicity by showing about 9% larvicidal activity, indicating that such a bulky side chain of tryptophan could give rise to steric clashes, possibly interfering these critical interactions. Based on the structural detail of domain II, the F_{326} residue is the most possible aromatic residue in β2 that could interact with Y_{408} when compared with the other two aromatic residues, W_{320} and W_{327} (Figure 75). Therefore, it is possible that the aromatic side chain of the mutated F_{408} (Figure 75) and the hydrophobic side chain of the mutated V_{408} could retain interactions with F_{326} in β2 and these interactions might stabilise β2-β3 and β4-β 5 hairpins.

When the larvicidal inactive Y408D mutant was further investigated for receptor binding in comparison with the wild type toxin using immunocytochemical staining. It revealed that the Y408D toxin bound to *A. aegypti* larval midgut section at the apical microvilli of posterior epithelial cells with a signal lower than the wild type toxin. This result suggests that the Y_{408} in β8 is apparently involved in receptor binding step of Cry4Ba toxicity. As mentioned before, the aromatic side chain of Y_{408} could significantly interact with an aromatic side chain of nearby F_{326} in β2 (Figure 75), and hence this interaction seems to be important for stabilising the receptor-binding orientation of β2-β3 and β4-β5 hairpins.

Copyright by Mahidol University

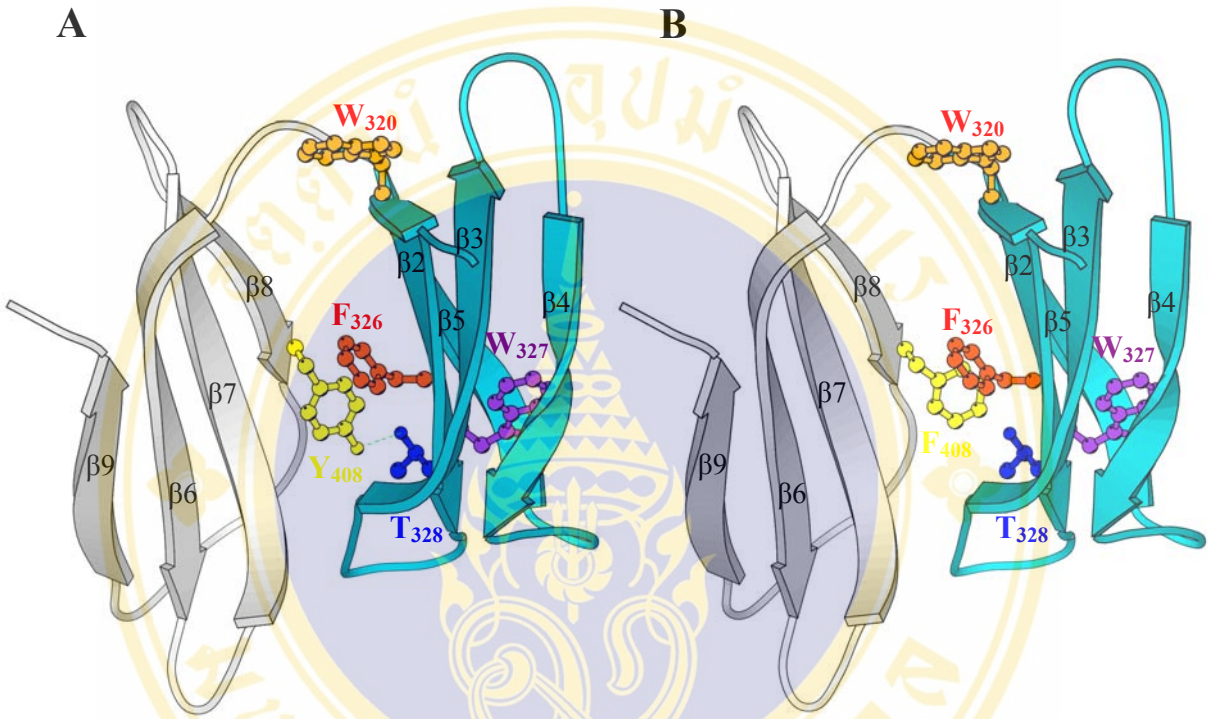

Figure 75: β-sheets 1 and 2 in domain II of the Cry4Ba toxin and its Y408F mutant

The figure shows a part of domain II of Cry4Ba (A) and its Y408F mutant (B) generated by MolScript v2.1.2 based on the crystal structure of Cry4Ba (10), illustrating β-sheets 1 and 2 as shaded with cyan and grey colours, respectively. An inter β-sheet hydrogen bond forming between Y_{408} in β8 and T_{328} in β2 (a green-colour dash line), an aromatic interaction and/or hydrophobic interactions between Y_{408} in β8 and F_{326} in β2 (A) and a putative aromatic interaction and/or hydrophobic interactions between F_{408} in β8 and F_{326} in β2 (B) are illustrated. The W_{320}, F_{326} and W_{327} are the three aromatic residues in β2.

Copyright by Mahidol University

Subunit-subunit hydrophobic interaction of the phenyl ring of F_{56} that is located in a loop directly connected to the active site of the rGSTM1-1 enzyme with a close hydrophobic pocket (at 15-20 Å away from the active site) was shown to be important for conformational stability of the active site, catalytic activity of the enzyme and binding ability to enzyme substrate (166). In similar experiment, F_{59} and W_{63}, the two residues in a surface loop at carbohydrate binding cleft of *B. licheniforinis* 1,3-1,4-glucanase that both have an aromatic side chain interacting with the core structure of the enzyme were shown to be important for enzyme activity, by contributing substrate binding and structural integrity of the loop (167). For the Cry2Aa toxin, hydrogen bonds between residues (T_{314} in β2 and S_{334}, N_{336} and S_{337} in β3 in domain II) that are packed behind the putative receptor binding loop with the loop residues were suggested to be involved in toxicity and receptor binding by directing the orientation of the putative receptor binding loop (9).

As was shown that the activated Cry4Ba toxin bound to the apical microvilli of epithelial cells in the posterior midguts of *A. aegypti* larval sections with a strong immunochemical signal (Figures 70 and 71). This finding is consistent with the previous observation of strong binding of Cry4Aa, Cry4Ba, Cry11Aa and Cyt1Aa on the apical microvilli of posterior midgut cells of *Anopheles gambiae* larvae (125). Recently, Cry4Aa was also found to bind to apical microvilli of posterior midgut cells of *Culex pipiens* larvae (126). In contrast, a less intense signal was also detected on microvilli of gastric caecae cells in the two previous studies (125; 126), and to a lesser intensity (125) or no binding signal (126) on microvilli of the anterior midgut cells. In addition, binding of the lepidopteran or coleopteran-specific toxins, Cry1Ab, Cry1Ac, Cry1Ba or Cry3Aa to apical midgut microvilli was shown to correlate well with the Cry toxicity (168), in contrast, the *in vitro* binding of these toxins to peritrophic membranes was shown without any correlation with toxicity (168; 169). This finding is consistent with the finding of Cry1Aa, Cry1Ab, Cry1Ac, Cry1Ba, Cry1Da and Cry1Ea binding *in vitro* to *Ostrinia nubilalis* midguts (170). In addition, adherance of Cry1Ab, Cry1Ac and Cry1Ba to the Malpighian tubules microvilli of *O. nubilalis in vitro* was indicated to be not relevant for *in vivo* toxicity (170). Taken together, as mentioned before (125), the binding of Cry toxins to apical microvilli of midgut cells is consistent with the involvement of specific receptor binding in toxicity.

Copyright by Mahidol University

CHAPTER VIII
CONCLUSIONS

8.1 For studying an involvement of β6-β7, β8-β9 and β10-β11 loop residues in toxicity, the desired loop mutants in domain II of the Cry4Ba toxin were constructed by using PCR-based mutagenesis: β6-β7 loop mutants (S387A, S388A, P389A and S390A), β8-β9 loop mutants (S410A, N411A, T413A, T415A, E417A and G418A), β 10-β11 loop mutants (D454A, Y455A, N456A and S457A) and two double mutants (S410A/E417A and Y455A/N456A).

8.2 All the 130-kDa loop mutant protoxins were highly expressed in *E. coli* JM109 cells with a yield similar to the Cry4Ba wild type under IPTG induction. In addition, *E. coli* cells expressing each mutant protoxin of P389A, S410A, E417A, Y455A or N456A showed reduced larvicidal activity to about 65% against *A. aegypti* mosquito larvae while the cells expressing S410A/E417A or Y455A/N456A exhibited a further reduction in toxicity to about 20%. However, the other mutants, i.e. S387A, S388A, S390A, N411A, T413A, T415A, G418A, D454A and S457A, showed the same larvicidal activity as the wild type at about 90%.

8.3 Both S410A/E417A and Y455A/N456A double mutant protoxins were produced as sedimentable inclusions which were soluble in 50 mM Na_2CO_3 (pH 9.0) and were digestable with trypsin at the ratio of 1:20 (enzyme:protein, w/w) at 37 °C, giving protease-resistant products of 47 and 20 kDa as similar to the wild type .

The results of this study suggest that P_{389} in the β6-β7 loop, S_{410} and E_{417} in the β 8-β9 loop, and Y_{455} and N_{456} in the β10-β11 loop are involved in larvicidal activity of the Cry4Ba toxin. In addition, the adverse effect on toxicity of both S410A/E417A and Y455A/N456A mutations was not caused by protoxin expression levels or solubilisation and proteolytic activation of the mutant inclusions.

Copyright by Mahidol University

8.4 For studying an involvement in toxicity of residues stabilising β2-β3 and β4-β5 hairpins, T319A and R323A mutants in β2 and Y408A, Y408V, Y408F, Y408W, Y408D, Y408E and Y408C mutants in β8 were also constructed via PCR-based mutagenesis.

8.5 Swiss-Pdb showed that T_{319} and R_{323} in β2 are involved in two side chain-side chain hydrogen bonding networks with other residues and Y_{408} in β8 could form an inter β-sheet hydrogen bond between β-sheets 1 and 2 with T_{328} in β2. When replaced with other amino acids including alanine, valine, phenylalanine, tryptophan, aspartate, glutamate and cysteine at position 408, no any side chain-side chain hydrogen bonding was found with T_{328} in β2. In addition, a putative aromatic interaction was found between the side-chains of Y_{408} and nearby F_{326} in β2.

8.6 Upon IPTG induction, all the mutants were highly expressed in *E. coli* cells as 130-kDa protoxins with a similar yield to the wild type. For toxicity assay, Y408A and Y408V mutants showed reduced larvicidal activity to about 40% while a drastic decrease in toxicity was observed for Y408W, Y408D, Y408E and Y408C mutants. However, T319A, R323A and Y408F mutations did not affect larvicidal activity.

8.7 All the Y408A, Y408V, Y408F, Y408W, Y408D, Y408E and Y408C mutant protoxins were found to be structurally stable upon solubilisation in carbonate buffer (pH 9.0) and trypsin digestion.

8.8 For further characterisation of receptor binding activity of the larvicidal inactive Y408D mutant, immunocytochemical staining revealed that the 65-kDa FPLC purified mutant toxin showed a reduced binding to *A. aegypti* larval midgut section when compared with the wild-type toxin.

The results of this studying aspect suggest that Y_{408} in β8 is involved in receptor binding step of larvicidal activity of the Cry4Ba toxin, reasonably directing the correct conformation of β2-β3 and β4-β5 hairpins in receptor binding, through aromatic

Copyright by Mahidol University

interaction and/or hydrophobic interactions (with an optimal van der Waals volume) with nearby F_{326} in β2.

Copyright by Mahidol University

REFERENCES

1. Federici BA, Park HW, Bideshi DK, Wirth MC, Johnson JJ. Recombinant bacteria for mosquito control. J Exp Biol 2003; 206:3877-3885.
2. Aronson AI, Beckman W, Dunn P. *Bacillus thuringiensis* and related insect pathogens. Microbiol Rev 1986; 50(1):1-24.
3. Hofte H, Whiteley HR. Insecticidal crystal proteins of *Bacillus thuringiensis*. Microbiol Rev 1989; 53(2):242-255.
4. Crickmore N, Zeigler DR, Feitelson J, Schnepf E, Van Rie J, Lereclus D, Baum J, Dean DH. Revision of the nomenclature for the *Bacillus thuringiensis* pesticidal crystal proteins. Microbiol Mol Biol Rev 1998; 62(3):807-813.
5. Knowles BH. Mechanism of action of *Bacillus thuringiensis* subsp. *israelensis* insecticidal δ-endotoxins. Adv Insect Physiol 1994; 24:275-308.
6. Li J, Carroll J, Ellar DJ. Crystal structure of insecticidal δ-endotoxin from *Bacillus thuringiensis* at 2.5 Å resolution. Nature 1991; 353:815-821.
7. Grochulski P, Masson L, Borisova S, Pusztai-Carey M, Schwartz JL, Brousseau R, Cygler M. *Bacillus thuringiensis* CryIAa insecticidal toxin: crystal structure and channel formation. J Mol Biol 1995; 254 (3):447-464.
8. Galitsky N, Cody V, Wojtczak A, Ghosh D, Luft JR, Pangborn W, English L. Structure of the insecticidal bacterial δ-endotoxin Cry3Bb1 of *Bacillus thuringiensis*. Acta Cryst 2001; D57:1101-1109.
9. Morse RJ, Yamamoto T, Stroud RM. Structure of Cry2Aa suggests an unexpected receptor binding epitope. Structure (Camb) 2001; 9 (5):409-417.
10. Boonserm P. Structure-function studies of the *Bacillus thuringiensis* subsp. *israelensis* mosquitocidal toxin [Ph.D. thesis]. University of Cambridge, UK, 2002.

Copyright by Mahidol University

11. Ahmad W, Ellar DJ. Directed mutagenesis of selected regions of a *Bacillus thuringiensis* entomocidal protein. FEMS Microbiol Lett 1990; 56(1-2):97-104.

12. Gazit E, Bach D, Kerr ID, Sansom MS, Chejanovsky N, Shai Y. The alpha-5 segment of the *Bacillus thuringiensis* delta-endotoxin: in vitro activity, ion channel formation and molecular modelling. Biochem J 1994; 304(Pt3):895-902.

13. Chen XJ, Curtiss A, Alcantara E, Dean DH. Mutations in domain I of *Bacillus thuringiensis* δ-endotoxin CryIAb reduce the irreversible binding of toxin to *Manduca sexta* brush border membrane vesicle. J Biol Chem 1995; 270:6412-6419.

14. Gazit E, Shai Y. The assembly and organization of α5 and α7 helices from the pore-forming domain of *Bacillus thuringiensis* delta endotoxin. J Biol Chem 1995; 270(6):2571-2578.

15. Schwartz JL, Juteau M, Grochulski P, Cygler M, Prefontaine G, Brousseau R, Masson L. Restriction of intramolecular movements within the Cry1Aa toxin molecular of *Bacillus thuringiensis* through disulfide bond engineering. FEBS Lett 1997; 410(2-3):397-402.

16. Gazit E, La Rocca P, Sansom MS, Shai Y. The structure and organization within the membrane of the helices composing the pore-forming domain of *Bacillus thuringiensis* delta-endotoxin are consistent with an umbrella-like structure of the pore. Proc Natl Acad Sci USA 1998; 95(21):12289-12294.

17. Wu SJ, Dean DH. Functional significance of loops in the receptor binding domain of *Bacillus thuringiensis* CryIIIA delta-endotoxin. J Mol Biol 1996; 255:628-640.

18. Lu H, Rajamohan F, Dean DH. Identification of amino acid residues of *Bacillus thuringiensis* delta-endotoxin CryIAa associated with membrane binding and toxicity to *Bombyx mori*. J Bacteriol 1994; 176:5554-5559.

Copyright by Mahidol University

19. Rajamohan F, Hussain SA, Cotrill JA, Gould F, Dean DH. Mutations at domain II, loop 3, of *Bacillus thuringiensis* CryIAa and CryIAb δ-endotoxins suggest loop 3 is involved in initial binding to lepidopteran midguts. J Biol Chem 1996; 271:25220-25226.

20. Kwak IS, Lu H, Dean DH. Exploration of receptor binding of *Bacillus thuringiensis* toxins. Mem Inst Oswaldo Cruz Rio J 1995; 90:75-79.

21. Barusrux S. Functional characterisation of two β-hairpins in the receptor-binding domain of the *Bacillus thuringiensis* Cry4B toxin [Ph.D. thesis]. Mahidol University, Thailand, 2003.

22. Chen XJ, Lee MK, Dean DH. Site-directed mutation in a highly conserved region of *Bacillus thuringiensis* δ-endotoxin affect inhibition of short circuit current across *Bombyx mori* midgut. Proc Natl Acad Sci USA 1993; 90(19):9041-9045.

23. Schwartz JL, Potvin L, Chen XJ, Brousseau R, Laprade R, Dean DH. Single-site mutations in the conserved alternating-arginine region affect ionic channels formed by CryIAa, a *Bacillus thuringiensis* toxin. Appl Environ Microbiol 1997; 63(10):3978-3984.

24. Lee MK, Young BA, Dean DH. Domain III exchanges of *Bacillus thuringiensis* CryIA toxins affect binding to different gypsy moth midgut receptors. Biochem Biophys Res Commun 1995; 216:306-312.

25. Lee MK, You TH, Gould FL, Dean DH. Identification of residues in domain III *Bacillus thuringiensis* Cry1Ac toxin that affect binding and toxicity. Appl Environ Microbiol 1999; 65:4513-4520.

26. de Maagd RA, Kwa MSG, van der Klei H, Yamamoto T, Schipper B, Vlak JM, Stiekema WJ, Bosch D. Domain III substitution in *Bacillus thuringiensis* delta-endotoxin Cry1Ab result in superior toxicity for *Spodoptera exigue* and altered membrane protein recognition. Appl Environ Microbiol 1996; 62:1537-1543.

Copyright by Mahidol University

27. de Maagd RA, Bakker PL, Masson L, Adang MJ, Sangadala S, Stiekema W, Bosch D. Domain III of the *Bacillus thuringiensis* delta-endotoxin Cry1Ac is involved in binding to *Manduca sexta* brush border membrane and to its purified aminopeptidase N. Mol Microbiol 1999; 31(2):463-471.

28. Burton SL, Ellar DJ, Li J, Derbyshire DJ. *N*-acetylgalactosamine on the putative insect receptor aminopeptidase N is recognized by a site on the domain III lectin-like fold of a *Bacillus thuringiensis* insecticidal toxin. J Mol Biol 1999; 287(5):1011-1022.

29. Jenkins JL, Lee MK, Valaitis AP, Curtiss A, Dean DH. Bivalent sequential binding model of a *Bacillus thuringiensis* toxin to gypsy moth aminopeptidase N receptor. J Biol Chem 2000; 275:14423-14431.

30. Aronson AI, Han ES, McGaughey W, Johnson D. The solubility of inclusion proteins from *Bacillus thuringiensis* is dependent upon protoxin composition and is a factor in toxicity to insects. Appl Environ Microbiol 1991; 57:981-986.

31. Du C, Martin PAW, Nickerson KW. Comparison of disulfide contents and solubility at alkaline pH of insecticidal and noninsecticidal *Bacillus thuringiensis* protein crystals. Appl Environ Microbiol 1994; 60:3847-3853.

32. McGaughey WH, Whalon ME. Managing insect resistance to *Bacillus thuringiensis* toxins. Science 1992; 258:1415-1455.

33. Bietlot H, Vishnubhatla I, Carey PR, Poszgay M, Kaplan H. Characterization of the cysteine residues and disulphide linkages in the protein crystal of *Bacillus thuringiensis*. Biochem J 1990; 267:309-315.

34. Choma CT, Kaplan H. *Bacillus thuringiensis* crystal protein: effect of chemical modification of the cysteine and lysine residues. J Invertebr Pathol 1992; 59:75-80.

35. Knowles BH, Dow JAT. The crystal δ-endotoxins of *Bacillus thuringiensis*: models for their mechanism of action on the insect gut. Bioassays 1993; 15:469-476.

Copyright by Mahidol University

36. Mohan M, Gujar GT. Characterization and comparison of midgut proteases of *Bacillus thuringiensis* susceptible and resistant diamondback moth (Plutellidae:Lepidoptera). J Invertebr Pathol 2003; 82:1-11.

37. Ogiwara K, Indrasith LS, Asano S, Hori H. Processing of δ-endotoxin from *Bacillus thuringiensis* subsp. *kurstaki* HD-1 and HD-73 by gut juices of various insect larvae. J Invertebr Pathol 1992; 60:121-126.

38. Yamagiwa M, Esaky M, Otake K, Inagaki M, Komano T, Amachi T, Sakai H. Activation process of dipteran-specific insecticidal protein produced by *Bacillus thuringiensis* subsp. *israelensis*. Appl Environ Microbiol 1999; 65:3464-3469.

39. Angsuthanasombat C, Crickmore N, Ellar DJ. Comparison of *Bacillus thuringiensis* subsp. *israelensis* CryIVA and CryIVB cloned toxins reveals synergism in vivo. FEMS Microbiol Lett 1992; 94:63-68.

40. Angsuthanasombat C, Crickmore N, Ellar DJ. Effect on toxicity of eliminating a cleavage site in a predicted interhelical loop in *Bacillus thuringiensis* CryIVB δ-endotoxin. FEMS Microbiol Lett 1993; 111:255-262.

41. Carroll J, Convents D, Van Damme J, Boets A, Van Rie J, Ellar DJ. Intramolecular proteolytic cleavage of *Bacillus thuringiensis* Cry3A δ-endotoxin may facilitate its coleopteran toxicity. J Invertebr Pathol 1997; 70:41-49.

42. Dai SM, Gill S. *In vitro* and *in vivo* proteolysis of the *Bacillus thuringiensis* subsp. *israelensis* CryIVD protein by *Culex quinquefasciatus* larval midgut proteases. Insect Biochem Mol Biol 1993; 23:273-283.

43. Park HW, Bideshi DK, Federici BA. Molecular genetic manipulation of truncated Cry1C protein synthesis in *Bacillus thuringiensis* to improve stability and yield. Appl Environ Microbiol 2000; 66:4449-4455.

44. Martens JW, Knoester M, Weijts F, Groffen SJ, Hu Z, Bosch D, Vlak JM. Characterization of baculovirus insecticides expressing tailored *Bacillus thuringiensis* Cry1A(b) crystal proteins. J Invertebr Pathol 1995; 66:249-257.

Copyright by Mahidol University

45. Strizhov N, Keller M, Koncz-Kalman Z, Regev A, Sneh B, Schell J, Koncz C, Zilberstein A, Konez-Kalman Z. Mapping of the entomocidal fragment of Spodoptera-specific *Bacillus thuringiensis* toxin Cry1C. Mol Gen Genet 1996; 253:11-19.

46. Kouskoura T, Tickner C, Crickmore N. Expression and crystallization of an N-terminally activated form of the *Bacillus thuringiensis* Cry1Ca toxin. Curr Microbiol 2001; 43:371-373.

47. Bravo A, Sanchez J, Kouskoura T, Crickmore N. N-terminal activation is an essential early step in the mechanism of action of the *Bacillus thuringiensis* Cry1Ac insecticidal toxin. J Biol Chem 2002; 277:23985-23987.

48. Convents D, Cherlet M, Van Damme J, Lasters I, Lauwereys M. Two structural domains as a general fold of the toxic fragment of the *Bacillus thuringiensis* δ-endotoxins. Eur J Biochem 1991; 195:631-635.

49. Audtho M, Valiatis AP, Alzate O, Dean DH. Production of chymotrypsin-resistance *Bacillus thuringiensis* Cry2Aa1 δ-endotoxin by protein engineering. Appl Environ Microbiol 1999; 65:4601-4605.

50. Zalunin IA, Revina LP, Kostina LI, Chestukhina GG, Stepanov VM. Limited proteolysis of *Bacillus thuringiensis* CryIG and CryIVB δ-endotoxins leads to formation of active fragments that do not coincide with the structural domains. J Protein Chem 1998; 17:463-471.

51. Choma CT, Surewicz WK, Carey PR, Pozsgay M, Raynor T, Kaplan H. Unusual proteolysis of the protoxin and toxin from *Bacillus thuringiensis*. Structural implications. Eur J Biochem 1990; 189:523-527.

52. Pang AS, Gringorten JL, Bai C. Activation and fragmentation of *Bacillus thuringiensis* δ-endotoxin by high concentrations of proteolytic enzymes. Can J Microbiol 1999; 45:816-825.

Copyright by Mahidol University

53. Miranda R, Zamudio FZ, Bravo A. Processing of Cry1Ab δ-endotoxin from *Bacillus thuringiensis* by *Manduca sexta* and *Spodoptera frugiperda* midgut proteases: role in protoxin activation and toxin inactivation. Insect Biochem Mol Biol 2001; 31:1155-1163.

54. Krittanai C, Lungchukiet P, Ruangwetdee S, Tuntitippawan T, Panyim S, Katzenmeier G, Angsuthanasombat C. Redesign of an interhelical loop of the *Bacillus thuringiensis* Cry4B delta-endotoxin for proteolytic cleavage. J Biochem Mol Biol 2001; 34:1-5.

55. Christeller JT, Laing WA, Markwick NP, Burgess EPJ. Midgut protease activities in 12 phytophagous lepidopteran larvae: dietary and protease inhibitor interactions. Insect Biochem Molec Biol 1992; 22:735-746.

56. Rymerson RT, Bodnaryk PR. Gut proteinase activity in insect pest of canola. Can Entomol 1995; 127:41-48.

57. Michaud D, Bermier-Vornais N, Overney S, Yelle S. Constitutive expression of digestive cysteine proteinase forms during development of the Colorado potato beetle, *Leptinotarsa decemlineata* Say (Coleoptera: Chrysomelidae). Insect Biochem Mol Biol 1995; 25:1041-1048.

58. Shao Z, Cui Y, Liu X, Yi H, Ji J, Yu Z. Processing of δ-endotoxin of *Bacillus thuringiensis* subsp. *kurstaki* HD-1 in *Heliothis armigera* midgut juice and the effects of protease inhibitors. J Invertebr Pathol 1998; 72:73-81.

59. Oppert B, Kramer KJ, Beeman RW, Johnson D, McGaughey WH. Proteinase-mediate insect resistance to *Bacillus thuringiensis* toxins. J Biol Chem 1997; 272:23473-23476.

60. Forcada C, Alcacer E, Garcera MD, Martinez R. Differences in the midgut proteolytic activity of two *Heliothis virescens* strains, one susceptible and one resistant to *Bacillus thuringiensis* toxins. Arch Insect Biochem Physiol 1996; 31:257-272.

Copyright by Mahidol University

61. Gomez I, Sanchez J, Miranda R, Bravo A, Soberon M. Cadherin-like receptor binding facilitates proteolytic cleavage of helix α-1 in domain I and oligomer pre-pore formation of *Bacillus thuringiensis* Cry1Ab toxin. FEBS Lett 2002; 513:242-246.

62. Rausell C, Garcia-Robles I, Sanchez J, Munoz-Garay C, Martinez-Ramirez AC, Real MD, Bravo A. Role of toxin activation on binding and pore formation activity of the *Bacillus thuringiensis* Cry3 toxins in membranes of *Leptinotarsa decemlineata* (Say). Biochim Biophys Acta 2004; 1660:99-105.

63. Rosenberger CM, Brumell JH, Finlay BB. Microbial pathogenesis: lipid rafts as pathogen portals. Curr Biol 2000; 10:823-825.

64. Cabiaux V, Wolff Ch, Ruysschaert JM. Interaction with a lipid membrane: a key step in bacterial toxins virulence. Int J Biol Macromol 1997; 21:285-298.

65. Abrami L, van der Goot FG. Plasma membrane microdomains act as concentration platforms to facilitate intoxication by aerolysin. J Cell Biol 1999; 147:175-184.

66. Valaitis AP, Jenkin JL, Lee MK, Dean DH, Garner KJ. Isolation and partial characterization of gypsy moth BTR-270, an anionic brush border membrane glycoconjugate that binds *Bacillus thuringiensis* Cry1A toxins with high affinity. Arch Insect Biochem Physiol 2001; 46:186-200.

67. Lee MK, You TH, Young BA, Cotrill JA, Valaitis AP, Dean DH. Aminopeptidase N purified from gypsy moth brush border membrane vesicles is a specific receptor for *Bacillus thuringiensis* CryIA(c) toxin. Appl Environ Microbiol 1996; 62:2845-2849.

68. Valaitis AP, Mazza A, Brousseau R, Masson L. Interaction analyses of *Bacillus thuringiensis* Cry1A toxins with two aminopeptidases from Gypsy Moth midgut brush border membranes. Insect Biochem Mol Biol 1997; 27:529-539.

Copyright by Mahidol University

69. Gomez I, Miranda-Rios J, Rudino-Pinera E, Oltean DI, Gill SS, Bravo A, Soberon M. Hydropathic complementarity determines interaction of epitope ^{869}HITDTNNK^{876} in *Manduca sexta* Bt-R_1 receptor with loop 2 of domain II of *Bacillus thuringiensis* Cry1A toxins. J Biol Chem 2002; 277:30137-30143.

70. Garczynski SF, Adang MJ. *Bacillus thuringiensis* CryIA(c) delta-endotoxin binding aminopeptidase N in the *Manduca sexta* midgut has glycosyl-phosphatidylinositol anchor. Insect Biochem Mol Biol 1995; 25:409-415.

71. Knight PJK, Crickmore N, Ellar DJ. The receptor for *Bacillus thuringiensis* CryIA(c) delta-endotoxin in the brush border membrane of the lepidopteran *Manduca sexta* is aminopeptidase N. Mol Microbiol 1994; 11:429-436.

72. Sangadala S, Walters FS, English LH, Adang MJ. A mixture of *Manduca sexta* aminopeptidases and phosphatase enhances *Bacillus thuringiensis* insecticidal CryIA(c) toxin binding and ^{86}Rb-K^+ efflux *in vitro*. J Biol Chem 1994; 269:10088-10092.

73. Denolf P, Hendrickx K, Van Damme J, Jansens S, Peferoen M, Degheele D, Van Rie J. Cloning and characterization of *M. sexta* and *P. xylostella* midgut aminopeptidase N enzymes related to *Bacillus thuringiensis* toxin-binding proteins. Eur J Biochem 1997; 248:748-761.

74. Luo K, Lu YJ, Adang MJ. A 106-kDa form of aminopeptidase is a receptor for *Bacillus thuringiensis* CryIC δ-endotoxin in the brush border membrane of *Manduca sexta*. Insect Biochem Mol Biol 1996; 26:783-791.

75. Masson L, Lu Y, Mazza A, Brousseau R, Adang MJ. The CryIA(c) receptor purified from *Manduca sexta* displays multiple specificities. J Biol Chem 1995; 270:20309-20315.

76. Jenkins JL, Lee MK, Sangadala S, Adang MJ, Dean DH. Binding of *Bacillus thuringiensis* Cry1Ac toxin to *Manduca sexta* aminopeptidase-N receptor is not directly related to toxicity. FEBS Lett 1999; 462:373-376.

Copyright by Mahidol University

77. Lee MK, Gould F, Dean DH. Mutations in domain III of *Bacillus thuringiensis* CryIAc toxin affect toxicity and receptor binding to *Manduca sexta* and *Heliothis virescens*, p. 41. In Abstracts of the 30th Annual Meeting of the Society for Invertebrate Pathology 1997.

78. Nagamatsu Y, Koike T, Sasaki K, Yoshimoto A, Furukawa Y. The cadherin-like protein is essential to specificity determination and cytotoxic action of the *Bacillus thuringiensis* insecticidal CryIAa toxin. FEBS Lett 1999; 460:385-390.

79. Jenkins JL, Dean DH. Binding specificity of *Bacillus thuringiensis* Cry1Aa for purified, native *Bombyx mori* aminopeptidase N and cadherin-like receptors. BMC Biochem 2001; 2:12-19.

80. Ikawa S, Tsuda Y, Fukada T, Sugimoto K, Himeno M. cDNA cloning of the Cry1Aa receptor variants from *Bombyx mori* and their expression in mammalian cells. Biosci Biotechnol Biochem 2000; 64:2682-2685.

81. Tsuda Y, Nakatani F, Hashimoto K, Ikawa S, Matsuura C, Fukada T, Sugimoto K, Himeno M. Cytotoxic activity of *Bacillus thuringiensis* Cry proteins on mammalian cells transfected with cadherin-like Cry receptor gene of *Bombyx mori*. Biochem J 2003; 369:697-703.

82. Yaoi K, Kadotani T, Kuwana H, Shinkawa A, Takahashi T, Iwahana H, Sato R. Aminopeptidase N from *Bombyx mori* as a candidate for the receptor of *Bacillus thuringiensis* Cry1Aa toxin. Eur J Biochem 1997; 246:652-657.

83. Yaio K, Nakanishi K, Kadotani T, Imamura M, Koizumi N, Iwahana H, Sato R. *Bacillus thuringiensis* Cry1Aa toxin-binding region of *Bombyx mori* aminopeptidase N. FEBS Letters 1999; 463:221-224.

84. Hua G, Tsukamoto K, Ikezawa H. Cloning and sequence analysis of the aminopeptidase N isozyme (APN2) from *Bombyx mori* midgut. Comp Biochem Physiol 1998; B121:213-222.

Copyright by Mahidol University

85. Luo K, Sangadala S, Masson L, Mazza A, Brousseau R, Adang MJ. The *Heliothis virescens* 170 kDa aminopeptidase functions as "receptor A" by mediating specific *Bacillus thuringiensis* CryIA δ-endotoxin binding and pore formation. Insect Biochem Mol Biol 1997; 27:735-743.

86. Gill S, Cowles E, Francis V. Identification, isolation and cloning of a *Bacillus thuringiensis* CryIA(a) toxin-binding protein from the midgut of the lepidopteran insect *Heliothis virescens*. J Biol Chem 1995; 270:27277-27282.

87. Oltean DI, Pullikuth AK, Lee HK, Gill SS. Partial purification and characterization of *Bacillus thuringiensis* Cry1A toxin receptor A from *Heliothis virescens* and cloning of the correspoding cDNA. Appl Environ Microbiol 1999; 65:4760-4766.

88. Agrawal N, Malhotra P, Bhatnagar R. Interaction of gene-cloned and insect cell-expressed aminopeptidase N of *Spodoptera litura* with insecticidal crystal protein Cry1C. Appl Environ Microbiol 2002; 68:4583-4592.

89. Sanchis V, Ellar DJ. Identification and partial purification of a *Bacillus thuringiensis* Cry1C δ-endotoxin binding protein from *Spodoptera littoralis* gut membranes. FEBS Lett 1993; 316:264-268.

90. Yamagiwa M, Kamauchi S, Okegawa T, Esaki M, Otake K, Amachi T, Komano T, Sakai H. Binding properties of *Bacillus thuringiensis* Cry4A toxin to the apical microvilli of larval midgut of *Culex pipiens*. Biosci Biotechnol Biochem 2001; 65:2419-2427.

91. Krieger IV, Revina LP, Kostina LI, Buzdin AA, Zalunin IA, Chestukhina GG, Stepanov VM. Membrane proteins of *Aedes aegypti* larvae bind toxins Cry4B and Cry11A of *Bacillus thuringiensis* ssp. *israelensis*. Biochemistry (Mosc) 1999; 64:1163-1168.

92. Schnepf E, Crickmore N, Van Rie J, Lereclus D, Baum J, Feitelson J, Zeigler DR, Dean DH. *Bacillus thuringiensis* and its pesticidal crystal proteins. Microbiol Mol Biol Rev 1998; 62:775-806.

Copyright by Mahidol University

93. Dorsch JA, Candas M, Griko NB, Maaty WSA, Midboe EG, Vadlamudi RK, Bulla Jr LA. Cry1A toxins of *Bacillus thuringiensis* bind specifically to a region adjacent to the membrane-proximal extracellular domain of Bt-R_1 in *Manduca sexta*: involvement of a cadherin in the entomopathogenicity of *Bacillus thuringiensis*. Insect Biochem Mol Biol 2002; 32:1025-1036.

94. Cooper MA, Carroll J, Travis ER, Williams DH, Ellar DJ. *Bacillus thuringiensis* Cry1Ac toxin interaction with *Manduca sexta* aminopeptidase N in a model membrane environment. Biochem J 1998; 333:677-683.

95. Schwartz JL, Lu YJ, Sohnlein P, Brousseau R, Laprade R, Masson L, Adang MJ. Ion channels formed in planar lipid bilayers by *Bacillus thuringiensis* toxins in the presence of *Manduca sexta* midgut receptors. FEBS Lett 1997; 412:270-276.

96. Sangadala S, Azadi P, Carlson R, Adang MJ. Carbohydrate analyses of *Manduca sexta* aminopeptidase N, co-purifying neutral lipids and their functional interactions with *Bacillus thuringiensis* Cry1Ac toxin. Insect Biochem Mol Biol 2001; 32:97-107.

97. Brand AH, Perrimon N. Targeted gene expression as a means of altering cell fate and generating dominant phenotypes. Development 1993; 118:401-415.

98. Phelps CB, Brand AH. Ectopic gene expression in *Drosophila* using the GAL4 system. Methods-A Companion Meth Enzymol 1998; 14:367-379.

99. Gill M, Ellar DJ. Transgenic *Drosophila* reveals a functional *in vivo* receptor for the *Bacillus thuringiensis* toxin Cry1Ac1. Insect Mol Biol 2002; 11(6):619-625.

100. Gomez I, Oltean DI, Gill SS, Bravo A, Soberon M. Mapping the epitope in cadherin-like receptors involved in *Bacillus thuringiensis* Cry1A toxin interaction using phage display. J Biol Chem 2001; 276:28906-28912.

Copyright by Mahidol University

101. Gomez I, Dean DH, Bravo A, Soberon M. Molecular basis for *Bacillus thuringiensis* Cry1Ab toxin specificity: two structural determinants in the *Manduca sexta* Bt-R_1 receptor interact with loops α-8 and 2 in domain II of Cry1Ab toxin. Biochem 2003; 42:10482-10489.

102. Ge AZ, Shivarova NI, Dean DH. Location of the *Bombyx mori* specificity domain on a *Bacillus thuringiensis* δ-endotoxin protein. Proc Natl Acad Sci USA 1989; 86:4037-4041.

103. Lee MK, Milne RE, Ge AZ, Dean DH. Location of *Bombyx mori* receptor binding region of a *Bacillus thuringiensis* delta-endotoxin. J Biol Chem 1992; 267:3115-3121.

104. Ge AZ, Rivers D, Milne R, Dean DH. Functional domains of *Bacillus thuringiensis* insecticidal crystal proteins: refinement of the *Heliothis virescens* and *Trichoplusia ni* specificity domains on CryIAc. J Biol Chem 1991; 266(27):17954-17958.

105. Schnepf HE, Tomczak K, Ortega JP, Whiteley HR. Specificity-determining regions of a lepidopteran-specific insecticidal protein produced by *Bacillus thuringiensis*. J Biol Chem 1990; 265:20923-20930.

106. Bosch D, Schipper B, van der Klei H, de Maagd RA, Stiekema W. Recombinant *Bacillus thuringiensis* crystal proteins with new properties: possibilities for resistance management. Bio/Technology 1994; 12:915-918.

107. Masson L, Mazza A, Gringorten L, Baines D, Aneliunas V, Brousseau R. Specificity domain localization of *Bacillus thuringiensis* insecticidal toxins is highly dependent on the bioassay system. Mol Microbiol 1994; 14:851-860.

108. de Maagd RA, Weemen-Hendriks M, Stiekema W, Bosch D. *Bacillus thuringiensis* delta-endotoxin Cry1C domain III can function as a specificity determinant for *Spodoptera exigue* in different, but not all, Cry1-Cry1C hybrids. Appl Environ Microbiol 2000; 66:1559-1563.

Copyright by Mahidol University

109. Rajamohan F, Alzate O, Cotrill J, Curtiss A, Dean DH. Protein engineering of *Bacillus thuringiensis* δ-endotoxin: mutations at domain II of CryIAb enhance receptor affinity and toxicity toward gypsy moth larvae. Proc Natl Acad Sci USA 1996; 93:14338-14343.

110. Rajamohan F, Cotrill JA, Gould F, Dean DH. Role of domain II, loop 2 residues of *Bacillus thuringiensis* CryIAb δ-endotoxin in reversible and irreversible binding to *Manduca sexta* and *Heliothis virescens*. J Biol Chem 1996; 271(5):2390-2396.

111. Smedley DP, Ellar DJ. Mutagenesis of three surface-exposed loops of a *Bacillus thuringiensis* insecticidal toxin reveals residues important for toxicity, receptor recognition and possibly membrane insertion. Microbiology 1996; 142:1617-1624.

112. Lee MK, Rajamohan F, Jenkins JL, Curtiss AS, Dean DH. Role of two arginine residues in domain II, loop 2 of Cry1Ab and Cry1Ac *Bacillus thuringiensis* δ-endotoxin in toxicity and binding to *Manduca sexta* and *Lymantria dispar* aminopeptidase N. Mol Microbiol 2000; 38(2):289-298.

113. Abdul-Rauf M, Ellar DJ. Mutations of loop 2 and loop 3 residues in domain II of *Bacillus thuringiensis* Cry1C delta-endotoxin affect insecticidal specificity and initial binding to *Spodoptera littoralis* and *Aedes aegypti* midgut membranes. Curr Microbiol 1999; 39:94-98.

114. Smith GP, Ellar DJ. Mutagenesis of two surface-exposed loops of the *Bacillus thuringiensis* CryIC delta-endotoxin affects insecticidal specificity. Biochem J 1994; 302(2):611-616.

115. Lee MK, Jenkins JL, You TH, Curtiss A, Son JJ, Adang MJ, Dean DH. Mutations at the arginine residues in α8 loop of *Bacillus thuringiensis* δ-endotoxin Cry1Ac affect toxicity and binding to *Manduca sexta* and *Lymantria dispar* aminopeptidase N. FEBS Lett 2001; 497:108-112.

Copyright by Mahidol University

116. Wright DJ, Iqbal M, Granero F, Ferre J. A change in a single midgut receptor in the diamondback moth (*Plutella xylostella*) is only in part responsible for field resistance to *Bacillus thuringiensis* subsp *kurstaki* and *Bacillus thuringiensis* subsp *aizawai*. Appl Environ Microbiol 1997; 63:1814-1819.

117. Iqbal M, Verkerk RHJ, Furlong MJ, Rahman SA, Wright DJ. Evidence for resistance to *Bacillus thuringiensis* (*Bt*) subsp *kurstaki* HD-1, *Bt* subsp *aizawai* and avamectin in field populations of *Plutella xylostella* from Malaysia. Pestic Sci 1996; 48:89-97.

118. Tabashnik BE, Liu YB, Malvar T, Heckel DG, Masson L, Ballester V, Granero F, Mensua JL, Ferre J. Global variation in the genetic and biochemical basis of diamondback moth resistance to *Bacillus thuringiensis*. Proc Natl Acad Sci USA 1997; 94:12780-12785.

119. Gahan LJ, Gould F, Heckel DG. Identification of a gene associated with Bt resistance in *Heliothis virescens*. Science 2001; 293:857-860.

120. Ferre J, Van Rie J. Biochemistry and genetics of insect resistance to *Bacillus thuringiensis*. Annu Rev Entomol 2002; 47:501-533.

121. Jurat-Fuentes JL, Gould FL, Adang MJ. Altered glycosylation of 63- and 68-kilodalton microvillar proteins in *Heliothis virescens* correlates with reduced Cry1 toxin binding, decreased pore formation, and increased resistance to *Bacillus thuringiensis* Cry1 toxins. Appl Environ Microbiol 2002; 68:5711-5717.

122. Zhuang Z, Linser PJ, Harvey WR. Antibody to H^+ V-ATPase subunit E colocalizes with portasomes in alkaline larval midgut of a freshwater mosquito (*Aedes aegypti* L.). J Exp Biol 1999; 202:2449-2460.

123. Volkmann A, Peters W. Investigation on the midgut caeca of mosquito larva. I. Fine structure. Tissue Cell 1989; 21:243-251.

124. Volkmann A, Peters W. Investigation on the midgut caeca of mosquito larva. II. Functional aspects. Tissue Cell 1989; 21:253-261.

125. Ravoahangimalala O, Charles J-F. In vitro binding of *Bacillus thuringiensis* var. *israelensis* individual toxins to midgut cells of *Anopheles gambiae* larvae (Diptera: Culicidae). FEBS Lett 1995; 362:111-115.

Copyright by Mahidol University

126. Yamagiwa M, Kamauchi S, Okegawa T, Esaki M, Otake K, Amachi T, Komano T, Sakai H. Binding properties of *Bacillus thuringiensis* Cry4A toxin to the apical microvilli of larval midgut of *Culex pipiens*. Biosci Biotechnol Biochem 2001; 65:2419-2427.

127. Escriche B, Tabashnik B, Finson N, Ferre J. Immunohistochemical detection of binding of CryIA crystal proteins of *Bacillus thuringiensis* in highly resistance strains of *Plutella xylostella* (L.) from Hawaii. Biochem Biophys Res Commun 1995; 212:388-395.

128. Flores H, Soberon X, Sanchez J, Bravo A. Isolated domain II and III from the *Bacillus thuringiensis* Cry1Ab δ-endotoxin binds to lepidopteran midgut membranes. FEBS Lett 1997; 414:313-318.

129. Kamauchi S, Yamagiwa M, Esaki M, Otake K, Sakai H. Binding properties of *Bacillus thuringiensis* Cry1C δ-endotoxin to the midgut epithelial membranes of *Culex pipiens*. Biosci Biotechnol Biochem 2003; 67:94-99.

130. Vie V, Vau Mau N, Pomarde P, Dance C, Schwartz JL, Laprade R, Frutos R, Rang C, Masson L, Heitz F, Le Grimellec C. Lipid-induced pore formation of the *Bacillus thuringiensis* Cry1Aa insecticidal toxin. J Membr Biol 2001; 180:195-203.

131. Aronson A, Geng C, Wu L. Aggregation of *Bacillus thuringiensis* Cry1A toxins upon binding to target insect larval midgut vesicles. Appl Environ Microbiol 1999; 65:2503-2507.

132. Tigue JN, Jacoby J, Ellar DJ. The alpha-helix 4 residue, Asn135, is involved in the oligomerization of Cry1Ac1 and Cry1Ab5 *Bacillus thuringiensis* toxins. Appl Environ Microbiol 2001; 67:5715-5720.

133. Rausell C, Munoz-Garay C, Miranda-CassoLuengo R, Gomez I, Rudino-Pinera E, Soberon M, Bravo A. Tryptophan spectroscopy studies and black lipid bilayer analysis indicate that the oligomeric structure of Cry1Ab toxin from *Bacillus thuringiensis* is the membrane-insertion intermediate. Biochem 2004; 43:166-174.

Copyright by Mahidol University

134. Raja SM, Rawat SS, Chattopadhyay A, Lala AK. Localization and enviroment of tryptophans in soluble and membrane-bound states of a pore-forming toxin from *Staphylococcus aureus*. Biophys J 1999; 76:1469-1479.

135. Hodgman TC, Ellar DJ. Models for the structure and function of *Bacillus thuringiensis* δ-endotoxins determined by compilational analysis. J DNA Seq Mapping 1990; 1:97-106.

136. Masson L, Tabashnik BE, Liu YB, Brousseau R, Schwartz JL. Helix 4 of the *Bacillus thuringiensis* Cry1Aa toxin lines the lumen of the ion channel. J Biol Chem 1999; 274:31996-32000.

137. Walter FS, Slatin SL, Kulesza CA, English LH. Ion-channel activity of N-terminal fragments from CryIA(c) delta-endotoxin. Biochem Biophys Res Commun 1993; 196:921-926.

138. Von Tersch MA, Slatin SL, Kulesza CA, English LH. Membrane-permeabilizing activities of *Bacillus thuringiensis* coleopteran-active CryIIIB2 and CryIIIB2 domain I peptide. Appl Environ Microbiol 1994; 60:3711-3717.

139. Wu D, Aronson AI. Localized mutagenesis defines regions of the *Bacillus thuringiensis* δ-endotoxin involved in toxicity and specificity. J Biol Chem 1992; 267:2311-2317.

140. Alzate O. Doctoral dissertation 1998, The Ohio State University.

141. Uawithaya P, Tuntitippawan T, Katzenmeier G, Panyim S, Angsuthanasombat C. Effects on larvicidal activity of single proline substitutions in α3 and α4 of the *Bacillus thuringiensis* CryIVB toxin. Biochem Mol Biol Int 1998; 44:825-832.

142. Vachon V, Prefontaine G, Coux F, Rang C, Marceau L, Masson L, Brousseau R, Frutos R, Schwartz JL, Laprade R. Role in helix 3 in pore formation by the *Bacillus thuringiensis* insecticidal toxin Cry1Aa. Biochem 2002; 41:6178-6184.

143. Aronson AI, Wu D, Zhang C. Mutagenesis of specificity and toxicity regions of a *Bacillus thuringiensis* protoxin gene. J Biol Chem 1995; 177:4059-4065.

Copyright by Mahidol University

144. Chandra A, Ghosh P, Mandaokar AD, Bera AK, Sharma RP, Das S, Kumar PA. Amino acid substitution in α-helix 7 of Cry1Ac δ-endotoxin of *Bacillus thuringiensis* leads to enhanced toxicity to *Helicoverpa armigera* Hubner. FEBS Lett 1999; 458:175-179.

145. Alcantara EP, Alzate O, Lee MK, Curtiss A, Dean DH. Role of α-helix seven of *Bacillus thuringiensis* Cry1Ab δ-endotoxin in membrane insertion, structural stability and ion channel activity. Biochem 2001; 40:2540-2547.

146. Wolfersberger MG, Chen XJ, Dean DH. Site-directed mutations in the third domain of *Bacillus thuringiensis* delta-endotoxin CryIAa affect its ability to increase the permeability of *Bombyx mori* midgut brush border membrane versicles. Appl Environ Microbiol 1996; 62:279-282.

147. Masson L, Tabashnik BE, Mazza A, Prefontaine G, Potvin L, Brousseau R, Schwartz JL. Mutagenic analysis of a conserved region of domain III in the Cry1Ac toxin of *Bacillus thuringiensis*. Appl Environ Microbiol 2002; 68:194-200.

148. Slatin SL, Abrams CK, English L. Delta-endotoxins form cation-selective channels in planar lipid bilayers. Biochem Biophys Res Commun 1990; 169:765-772.

149. Smedley D, Armstrong G, Ellar DJ. Channel activity caused by a *Bacillus thuringiensis* δ-endotoxin preparation depends on the method of activation. Mol Membr Biol 1997; 14:13-18.

150. Schwartz JL, Garneau L, Savaria D, Masson L, Brousseau R, Rousseau E. Lepidopteran-specific crystal toxins from *Bacillus thuringiensis* form cation- and anion-selective channels in planar lipid bilayers. J Membr Biol 1993; 132:53-62.

151. Peyronnet O, Nieman B, Genereux F, Vachon V, Laprade R, Schwartz JL. Estimation of the radius of the pores formed by the *Bacillus thuringiensis* Cry1C δ-endotoxin in planar lipid bilayers. Biochim Biophys Acta 2002; 1567:113-122.

Copyright by Mahidol University

152. Lorence A, Darszon A, Diaz C, Lievano A, Quintero R, Bravo A. δ-endotoxins induce cation channels in *Spodoptera frugiperda* brush border membranes in suspension and in planar lipid bilayers. FEBS Lett 1995; 360:217-222.

153. Peyronnet O, Vachon V, Schwartz JL, Laprade R. Ion channels induced in planar lipid bilayers by the *Bacillus thuringiensis* toxin Cry1Aa in the presence of gypsy moth (*Lymantria dispar*) brush border membrane. J Membr Biol 2001; 184:45-54.

154. Yanisch-Perron C, Vieira J, Messing J. Improved M13 phage cloning vectors and host strains: nucleotide sequences of the M13mp18 and pUC19 vectors. Gene 1985; 33:105-119.

155. Chungjatupornchai W, Hofte H, Seurinck J, Angsuthanasombat C, Vaeck M. Common features of *Bacillus thuringiensis* toxins specific for Diptera and Lepidoptera. Eur J Biochem 1988; 173:9-16.

156. Angsuthanasombat C, Chungjatupornchai W, Kertbundit S, Luxananil P, Settasatian C, Wilairat P, Panyim S. Cloning and expression of 130-kDa mosquito-larvicidal δ-endotoxin gene of *Bacillus thuringiensis* var. *israelensis* in *Escherichai coli*. Mol Gen Genet 1987; 208:384-389.

157. Del Sal G, Manfioletti G, Schneider C. A one-tube plasmid DNA mini preparation suitable for sequencing. Nucl Acids Res 1988; 16:9878.

158. Birnboim HC, Doly J. A rapid alkaline extraction procedure for screening recombinant plasmid DNA. Nucl Acids Res 1979; 7:1513-1523.

159. Sambrook J, Maniatis T, Fritsch EF. Molecular cloning: a laboratory manual. New York: Cold spring Harbor laboratory, 1989.

160. Angsuthanasombat C. Mechanism of action of *Bacillus thuringiensis* subsp. *israelensis* mosquito-larvicidal δ-endotoxins [PhD Thesis in Biochemistry]. University of Cambridge, UK, 1993.

161. Bradford MM. A rapid and sensitive method for the quantitation of microgram quantities of protein utilizing the principle of protein-dye binding. Anal Biochem 1976; 72:248-254.

Copyright by Mahidol University

162. Almond BD, Dean DH. Structural stability of *Bacillus thuringiensis* δ-endotoxin homolog-scanning mutants determined by susceptibility to protease. Appl Environ Microbiol 1993; 59:2442-2448.

163. Abdullah MAF, Alzate O, Mohammad M, McNall RJ, Adang MJ, Dean DH. Introduction of *Culex* toxicity into *Bacillus thuringiensis* Cry4Ba by protein engineering. Appl Environ Microbiol 2003; 69:5343-5353.

164. Wu SJ, Koller N, Miller DL, Bauer LS, Dean DH. Enhanced toxicity of *Bacillus thuringiensis* Cry3A δ-endotoxin in coleopterans by mutagenesis in a receptor binding loop. FEBS Lett 2000; 473:227-232.

165. Cummings CE, Ellar DJ. Chemical modification of *Bacillus thuringiensis* activated δ-endotoxin and its effect on toxicity and binding to *Manduca sexta* midgut membranes. Microbiology 1994; 140:2737-2747.

166. Hornby JAT, Codreanu SG, Armstrong RN, Dirr HW. Molecular recognition at the dimer interface of a class mu glutathione transferase: role of a hydrophobic interaction motif in dimer stability and protein function. Biochemistry 2002; 41:14238-14247.

167. Pons J, Querol E, Planas A. Mutational analysis of the major loop of *Bacillus* 1,3-1,4-β-D-glucan 4-glucanohydrolases. J Biol Chem 1997; 272:13006-13012.

168. Bravo A, Jansens S, Peferoen M. Immunocytochemical localization of *Bacillus thuringiensis* insecticidal crystal proteins in intoxicated insects. J Invertebr Pathol 1992; 60:237-246.

169. Bravo A, Hendrickx K, Jansen S, Peferoen M. Immunocytochemical analysis of specific binding of *Bacillus thuringiensis* insecticidal crystal proteins to lepidopteran and coleopteran midgut membranes. J Invertebr Pathol 1992; 60:247-253.

Copyright by Mahidol University

170. Denolf P, Jansens S, Peferoen M, Degheele D, Van Rie J. Two different *Bacillus thuringiensis* delta-endotoxin receptors in the midgut brush border membrane of the European corn borer, *Ostrinia nubilalis* (Hü bner) (Lepidoptera: Pyralidae). Appl Environ Microbiol 1993; 59:1828-1837.

Copyright by Mahidol University

APPENDIX

Copyright by Mahidol University

APPENDIX

The complete nucleotide sequence of the cloned *cry4Ba* gene encoding the 130-kDa crystal protein (155). Capital letters represent deduced amino acid sequence. The bolded amino acids represent the mutated amino acids. The oligonucleotide primers for automated DNA sequencing are underlined.

```
  1  atg aat tca ggc tat ccg tta gcg aat gac tta caa ggg tca atg
      M   N   S   G   Y   P   L   A   N   D   L   Q   G   S   M
 46  aaa aac acg aac tat aaa gat tgg cta gcc atg tgt gaa aat aac
      K   N   T   N   Y   K   D   W   L   A   M   C   E   N   N
 91  caa cag tat ggc gtt aat cca gct gcg att aat tct tct tca gtt
      Q   Q   Y   G   V   N   P   A   A   I   N   S   S   S   V
136  agt acc gct tta aaa gta gct gga gct atc ctt aaa ttt gta aac
      S   T   A   L   K   V   A   G   A   I   L   K   F   V   N
181  cca cct gca ggt act gtc tta acc gta ctt agc gcg gtg ctt cct
      P   P   A   G   T   V   L   T   V   L   S   A   V   L   P
226  att ctt tgg ccg act aat act cca acg cct gaa aga gtt tgg aat
      I   L   W   P   T   N   T   P   T   P   E   R   V   W   N
271  gat ttc atg acc aat aca ggg aat ctt att gat caa act gta aca
      D   F   M   T   N   T   G   N   L   I   D   Q   T   V   T
316  gct tat gta cga aca gat gca aat gca aaa atg acg gtt gtg aaa
      A   Y   V   R   T   D   A   N   A   K   M   T   V   V   K
361  gat tat tta gat caa tat aca act aaa ttt aac act tgg aaa aga
      D   Y   L   D   Q   Y   T   T   K   F   N   T   W   K   R
406  gag cct aat aac cag tcc tat aga aca gca gta ata act caa ttt
      E   P   N   N   Q   S   Y   R   T   A   V   I   T   Q   F
451  aac tta acc agt gcc aaa ctt cga gag acc gca gtt tat ttt agc
      N   L   T   S   A   K   L   R   E   T   A   V   Y   F   S
496  aac tta gta ggt tat gaa tta ttg tta tta cca ata tac gca caa
      N   L   V   G   Y   E   L   L   L   L   P   I   Y   A   Q
541  gta gca aat ttc aat tta ctt tta ata aga gat ggc ctc ata aat
      V   A   N   F   N   L   L   L   I   R   D   G   L   I   N
586  gca caa gaa tgg tct tta gca cgt agt gct ggt gac caa cta tat
      A   Q   E   W   S   L   A   R   S   A   G   D   Q   L   Y
631  aac act atg gtg cag tac act aaa gaa tat att gca cat agc att
      N   T   M   V   Q   Y   T   K   E   Y   I   A   H   S   I
676  aca tgg tat aat aaa ggt tta gat gta ctt aga aat aaa tct aat
      T   W   Y   N   K   G   L   D   V   L   R   N   K   S   N
721  gga caa tgg att acg ttt aat gat tat aaa aga gag atg act att
      G   Q   W   I   T   F   N   D   Y   K   R   E   M   T   I
766  caa gta tta gat ata ctc gct ctt ttt gcc agt tat gat cca cgt
      Q   V   L   D   I   L   A   L   F   A   S   Y   D   P   R
811  cga tac cct gcg gac aaa ata gat aat acg aaa cta tca aaa aca
      R   Y   P   A   D   K   I   D   N   T   K   L   S   K   T
856  gaa ttt aca aga gag att tat aca gct tta gta gaa tct cct tct
      E   F   T   R   E   I   Y   T   A   L   V   E   S   P   S
```

Copyright by Mahidol University

```
 901  agt aaa tct ata gca gca ctg gag gca gca ctt aca cga gat gtt
       S   K   S   I   A   A   L   E   A   A   L   T   R   D   V
 946  cat tta ttc act tgg cta aag aga gta gat ttc tgg acc aat act
       H   L   F   T   W   L   K   R   V   D   F   W   T   N   T
 991  ata tat caa gat tta aga ttt tta tct gcc aat aaa att ggg ttt
       I   Y   Q   D   L   R   F   L   S   A   N   K   I   G   F
1036  tca tat aca aat tct tct gca atg caa gaa agt gga att tat gga
       S   Y   T   N   S   S   A   M   Q   E   S   G   I   Y   G
1081  agt tct ggt ttt ggt tca aat ctt act cat caa att caa ctt aat
       S   S   G   F   G   S   N   L   T   H   Q   I   Q   L   N
1126  tct aat gtt tat aaa act tct atc aca gat act agc tcc ccc tct
       S   N   V   Y   K   T   S   I   T   D   T   S   S   P   S
1171  aat cga gtt aca aaa atg gat ttc tac aaa att gat ggt act ctt
       N   R   V   T   K   M   D   F   Y   K   I   D   G   T   L
1216  gcc tct tat aat tca aat ata aca cca act cct gaa ggt tta agg
       A   S   Y   N   S   N   I   T   P   T   P   E   G   L   R
1261  acc aca ttt ttt gga ttt tca aca aat gag aac aca cct aat caa
       T   T   F   F   G   F   S   T   N   E   N   T   P   N   Q
1306  cca act gta aat gat tat acg cat att tta agc tat ata aaa act
       P   T   V   N   D   Y   T   H   I   L   S   Y   I   K   T
1351  gat gtt ata gat tat aac agt aac agg gtt tca ttt gct tgg aca
       D   V   I   D   Y   N   S   N   R   V   S   F   A   W   T
1396  cat aag att gtt gac cct aat aat caa ata tac aca gat gct atc
       H   K   I   V   D   P   N   N   Q   I   Y   T   D   A   I
1441  aca caa gtt ccg gcc gta aaa tct aac ttc ttg aat gca aca gct
       T   Q   V   P   A   V   K   S   N   F   L   N   A   T   A
1486  aaa gta atc aag gga cct ggt cat aca ggg ggg gat cta gtt gct
       K   V   I   K   G   P   G   H   T   G   G   D   L   V   A
1531  ctt aca agc aat ggt act cta tca ggc aga atg gag att caa tgt
       L   T   S   N   G   T   L   S   G   R   M   E   I   Q   C
1576  aaa aca agt att ttt aat gat cct aca aga agt tac gga tta cgc
       K   T   S   I   F   N   D   P   T   R   S   Y   G   L   R
1621  ata cgt tat gct gca aat agt cca att gta ttg aat gta tca tat
       I   R   Y   A   A   N   S   P   I   V   L   N   V   S   Y
1666  gta tta caa gga gtt tct aga gga aca acg att agt aca gaa tct
       V   L   Q   G   V   S   R   G   T   T   I   S   T   E   S
1711  acg ttt tca aga cct aat aat ata ata cct aca gat tta aaa tat
       T   F   S   R   P   N   N   I   I   P   T   D   L   K   Y
1756  gaa gag ttt aga tac aaa gat cct ttt gat gca att gta ccg atg
       E   E   F   R   Y   K   D   P   F   D   A   I   V   P   M
1801  aga tta tct tct aat caa ctg ata act ata gct att caa cca tta
       R   L   S   S   N   Q   L   I   T   I   A   I   Q   P   L
1846  aac atg act tca aat aat caa gtg att att gac aga atc gaa att
       N   M   T   S   N   N   Q   V   I   I   D   R   I   E   I
1891  att cca atc act caa tct gta tta gat gag aca gag aac caa aat
       I   P   I   T   Q   S   V   L   D   E   T   E   N   Q   N
1936  tta gaa tca gaa cga gaa gtt gtg aat gca ctg ttt aca aat gac
       L   E   S   E   R   E   V   V   N   A   L   F   T   N   D
1981  gcg aaa gat gca tta aac att gga acg aca gat tat gac ata gat
       A   K   D   A   L   N   I   G   T   T   D   Y   D   I   D
2026  caa gcc gca aat ctt gtg gaa tgt att tct gaa gaa tta tat cca
       Q   A   A   N   L   V   E   C   I   S   E   E   L   Y   P
2071  aaa gaa aaa atg ctg tta tta gat gaa gtt aaa aat gcg aaa caa
       K   E   K   M   L   L   L   D   E   V   K   N   A   K   Q
2116  ctt agt caa tct cga aat gta ctt caa aac ggg gat ttt gaa tcg
       L   S   Q   S   R   N   V   L   Q   N   G   D   F   E   S
2161  gct acg ctt ggt tgg aca aca agt gat aat atc aca att caa gaa
       A   T   L   G   W   T   T   S   D   N   I   T   I   Q   E
```

Copyright by Mahidol University

```
2206  gat gat cct att ttt aaa ggg cat tac ctt cat atg tct ggg gcg
       D   D   P   I   F   K   G   H   Y   L   H   M   S   G   A
2251  aga gac att gat ggt acg ata ttt ccg acc tat ata ttc caa aaa
       R   D   I   D   G   T   I   F   P   T   Y   I   F   Q   K
2296  att gat gaa tca aaa tta aaa ccg tat aca cgt tac cta gta agg
       I   D   E   S   K   L   K   P   Y   T   R   Y   L   V   R
2341  gga ttt gta gga agt agt aaa gat gta gaa cta gtg gtt tca cgc
       G   F   V   G   S   S   K   D   V   E   L   V   V   S   R
2386  tat ggg gaa gaa att gat gcc atc atg aat gtt cca gct gat tta
       Y   G   E   E   I   D   A   I   M   N   V   P   A   D   L
2431  aac tat ctg tat cct tct acc ttt gat tgt gaa ggg tct aat cgt
       N   Y   L   Y   P   S   T   F   D   C   E   G   S   N   R
2476  tgt gag acg tcc gct gtg ccg gct aac att ggg aac act tct gat
       C   E   T   S   A   V   P   A   N   I   G   N   T   S   D
2521  atg ttg tat tca tgc caa tat gat aca ggg aaa aag cat gtc gta
       M   L   Y   S   C   Q   Y   D   T   G   K   K   H   V   V
2566  tgt cag gat tcc cat caa ttt agt ttc act att gat aca ggg gca
       C   Q   D   S   H   Q   F   S   F   T   I   D   T   G   A
2611  tta gat aca aat gaa aat ata ggg gtt tgg gtc atg ttt aaa ata
       L   D   T   N   E   N   I   G   V   W   V   M   F   K   I
2656  tct tct cca gat gga tac gca tca tta gat aat tta gaa gta att
       S   S   P   D   G   Y   A   S   L   D   N   L   E   V   I
2701  gaa gaa ggg cca ata gat ggg gaa gca ctg tca cgc gtg aaa cac
       E   E   G   P   I   D   G   E   A   L   S   R   V   K   H
2746  atg gag aag aaa tgg aac gat caa atg gaa gca aaa cgt tcg gaa
       M   E   K   K   W   N   D   Q   M   E   A   K   R   S   E
2791  aca caa caa gca tat gat gta gcg aaa caa gcc att gat gct tta
       T   Q   Q   A   Y   D   V   A   K   Q   A   I   D   A   L
2836  ttc aca aat gta caa gat gag gct tta cag ttt gat acg aca ctc
       F   T   N   V   Q   D   E   A   L   Q   F   D   T   T   L
2881  gct caa att cag tac gct gag tat ttg gta caa tcg att cca tat
       A   Q   I   Q   Y   A   E   Y   L   V   Q   S   I   P   Y
2926  gtg tac aat gat tgg ttg tca gat gtt cca ggt atg aat tat gat
       V   Y   N   D   W   L   S   D   V   P   G   M   N   Y   D
2971  atc tat gta gag ttg gat gca cga gtg gca caa gcg cgt tat ttg
       I   Y   V   E   L   D   A   R   V   A   Q   A   R   Y   L
3016  tat gat aca aga aat att att aaa aat ggt gat ttt aca caa ggg
       Y   D   T   R   N   I   I   K   N   G   D   F   T   Q   G
3061  gta atg ggg tgg cat gta act gga aat gca gac gta caa caa ata
       V   M   G   W   H   V   T   G   N   A   D   V   Q   Q   I
3106  gat ggt gtt tct gta ttg gtt cta tct aat tgg agt gct ggc gta
       D   G   V   S   V   L   V   L   S   N   W   S   A   G   V
3151  tct caa aat gtc cat ctc caa cat aat cat ggg tat gtc tta cgt
       S   Q   N   V   H   L   Q   H   N   H   G   Y   V   L   R
3196  gtt att gcc aaa aaa gaa gga cct gga aat ggg tat gtc acg ctt
       V   I   A   K   K   E   G   P   G   N   G   Y   V   T   L
3241  atg gat tgt gag gag aat caa gaa aaa ttg acg ttt acg tct tgt
       M   D   C   E   E   N   Q   E   K   L   T   F   T   S   C
3286  gaa gaa gga tat att acg aag aca gta gat gta ttc cca gat aca
       E   E   G   Y   I   T   K   T   V   D   V   F   P   D   T
3331  gat cgt gta cga att gag ata ggc gaa acc gaa ggt tcg ttt tat
       D   R   V   R   I   E   I   G   E   T   E   G   S   F   Y
3376  atc gaa agc att gaa tta att tgc atg aac gag tga 3411
       I   E   S   I   E   L   I   C   M   N   E   *
```

Copyright by Mahidol University

ELSEVIER
FEMS Microbiology Letters xxx (2004) xxx–xxx
FEMS MICROBIOLOGY Letters
www.fems-microbiology.org

Targeted mutagenesis of loop residues in the receptor-binding domain of the *Bacillus thuringiensis* Cry4Ba toxin affects larvicidal activity

Tipparat Tuntitippawan, Panadda Boonserm, Gerd Katzenmeier, Chanan Angsuthanasombat *

Laboratory of Molecular Biophysics and Structural Biochemistry, Institute of Molecular Biology and Genetics, Mahidol University, Salaya Campus, Nakornpathom 73170, Thailand

Received 27 June 2004; received in revised form 26 September 2004; accepted 15 November 2004

First published online

Edited by T.H. Birkbeck

Abstract

Loop residues in domain II of *Bacillus thuringiensis* Cry δ-endotoxins have been demonstrated to be involved in insecticidal specificity. In this study, selected residues in loops β6–β7 ($S_{387}SPS_{390}$), β8–β9 (S_{410}, N_{411}, T_{413}, T_{415}, E_{417} and G_{418}) and β10–β11 ($D_{454}YNS_{457}$) in domain II of the Cry4Ba mosquito-larvicidal protein were changed individually to alanine by PCR-based directed mutagenesis. All mutant toxins were expressed in *Escherichia coli* JM109 cells as 130-kDa protoxins at levels comparable to the wild type. Only *E. coli* cells that express the P389A, S410A, E417A, Y455A or N456A mutants exhibited a loss in toxicity against *Aedes aegypti* mosquito larvae of approximately 30% when compared to the wild type. In addition, *E. coli* cells expressing double mutants, S410A/E417A or Y455A/N456A, at wild-type levels revealed a significantly higher loss in larvicidal activity of approximately 70%. Similar to the wild-type protoxin, both double mutant toxins were structurally stable upon solubilisation and trypsin activation in carbonate buffer, pH 9.0. These results indicate that S_{410} and E_{417} in the β8–β9 loop, and Y_{455} and N_{456} in the β10–β11 loop are involved in larvicidal activity of the Cry4Ba toxin.
© 2004 Published by Elsevier B.V. on behalf of the Federation of European Microbiological Societies.

Keywords: *Bacillus thuringiensis*; δ-Endotoxin; Loop residue; Mosquito-larvicidal activity; Site-directed mutagenesis

1. Introduction

Biological insecticides have become a preferred choice over chemical agents because they possess higher specificity and lower rates of resistance development. A number of products based on *Bacillus thuringiensis* (*Bt*) δ-endotoxins have been widely used as efficient and safe bacterial insecticides [1]. During sporulation, *Bt* produces insecticidal proteins in the form of cytoplasmic inclusions, which are specifically toxic to several orders of insect larvae including Diptera (mosquitoes and flies), Lepidoptera (butterflies and moths), Coleoptera (beetles), and Hymenoptera (wasps and bees) [2]. The *Bt*δ-endotoxins can be classified into two families, Cry (crystal) and Cyt (cytolytic) toxins, based on their deduced amino acid sequence identity [3]. Four major insecticidal proteins produced by *Bt* subsp. *israelensis* (Bti) have been classified as Cry4Aa, Cry4Ba, Cry11Aa and Cyt1Aa which are highly active against mosquito larvae

* Corresponding author. Tel.: +662 800 3624x1237; fax: 662 441 9906.
E-mail address: stcas@mahidol.ac.th (C. Angsuthanasombat).

0378-1097/$22.00 © 2004 Published by Elsevier B.V. on behalf of the Federation of European Microbiological Societies.
doi:10.1016/j.femsle.2004.11.026

UNCORRECTED PROOF
Copyright by Mahidol University

[2,3]. Up to now, no resistance towards *Bti* toxins has been detected in field populations of mosquito larvae despite extensive use during the past two decades [1].

The *Bt* δ-endotoxins are present in the native crystalline inclusions as insoluble inactive protoxins. After ingestion by susceptible insect larvae, the toxin inclusions are exposed to the larval midgut lumen that is highly alkaline in a number of dipteran and lepidopteran insects (for reviews, see [2]). The solubilised protoxins are then processed by larval midgut proteases to yield the toxic fragments. For several Cry toxins, it has been shown that the activated toxins bind to specific receptors in the luminal plasma membranes of midgut epithelial cells of the target insect larvae [4]. Subsequently, the toxins insert into the membranes to form ion-leakage pores. These leakage pores cause the target midgut cells to swell and lyse by colloid-osmotic lysis [5], resulting in extensive damage to the midgut and eventually larval death. However, the precise molecular basis of *Bt* toxin function is still not completely elucidated.

The previously solved tertiary structures of different Cry toxins, butterfly and moth-specific Cry1Aa [6], mosquito and moth-specific Cry2Aa [7], beetle-specific Cry3Aa [8], rootworm and beetle-specific Cry3Bb [9] and mosquito-specific Cry4Ba [10], suggest that the active toxins are globular molecules of three distinct domains with a high degree of overall structural similarity. Domain I, which is composed of seven α-helices, has been shown to play a critical role in membrane insertion and lytic pore formation [11,12]. Domain II consists of three anti-parallel β-sheets, each terminating in surface-exposed loops which are the most variable part of the five Cry toxin structures. This domain has been demonstrated to participate in receptor recognition and hence determines insect specificity [13,14]. Domain III is a β-sandwich comprising two anti-parallel β-sheets. The role of this C-terminal domain is still unclear, although it has been implicated in structural integrity of toxin molecules [8], membrane permeabilisation [15] or receptor binding and specificity determination [16,17].

Site-directed mutagenesis approaches have been used by several research groups to investigate the role in toxicity of the domain II surface-exposed loops of some Cry toxins. Alanine replacements of residues in the β10–β11 loop of Cry3Aa showed an increase in larvicidal activity against *Tenebrio molitor*, while substitutions in the β6–β7 loop did not affect the toxin activity [18]. Deletion or alanine substitutions of residues 365–371 in the β6–β7 loop of Cry1Aa abolished nearly all larvicidal activity against *Bombyx mori* [19], and deletion of residues $A_{440}AGA_{443}$ in the β10–β11 loop also resulted in greatly reduced toxicity to *B. mori* and *Manduca sexta* [14]. In addition, some residues in the β6–β7 loop and the β10–β11 loop of Cry1Ab, Cry1Ac and Cry1Ca were demonstrated to be important for toxicity and receptor-binding interaction [13,20,21].

Based on its crystal structure, the dipteran-specific Cry4Ba toxin contains six surface-exposed loops (β1–α8, β2–β3, β4–β5, β6–β7, β8–β9 and β10–β11 loops) at the molecular apex of domain II [10]. In this study, we have started to investigate a possible involvement of β6–β7, β8–β9 and β10–β11 loop residues in toxicity by constructing a number of alanine Cry4Ba mutants. Our results suggest that P_{389} in the β6–β7 loop, S_{410} and E_{417} in the β8–β9 loop, and Y_{455} and N_{456} in the β10–β11 loop are involved in mosquito-larvicidal activity of the Cry4Ba toxin.

2. Materials and methods

2.1. Constructions of loop-mutant plasmids

All loop-mutant plasmids were generated by PCR-based site-directed mutagenesis using high fidelity *Pfu* DNA polymerase following the procedure of the QuickChange™ Mutagenesis Kit (Stratagene). The recombinant pMU388 plasmid encoding the 130-kDa Cry4Ba toxin, which had been cloned from *Bti* into the pUC12 vector [22], was used as a template for alanine substitutions of β6–β7, β8–β9 and β10–β11 loop residues, while the S410A and N456A mutant plasmids were used as templates for constructions of the S410A/E417A and Y455A/N456A double mutants, respectively. Fifteen pairs of complementary mutagenic oligonucleotide primers (Table 1) designed according to the published *cry4Ba* gene sequence [22] were purchased from Proligo Inc. (Singapore). Selected clones with the required mutations were first identified by restriction endonuclease digestion of the plasmids and then verified by DNA sequencing, using a BigDye™ Terminator Cycle Sequencing Kit (Perkin–Elmer).

2.2. Toxin expression and inclusion purification

The wild-type Cry4Ba and its loop mutant toxins were expressed in the *E. coli* strain JM109 under control of the *lacZ* promoter. Cells were grown in a Luria–Bertani medium containing 100 $\mu g\,ml^{-1}$ ampicillin until OD_{600} reached 0.3–0.5. Expression was induced with isopropyl-β-D-thiogalactopyranoside (IPTG) at a final concentration of 0.1 mM for 4 h. Protein expression was analysed by sodium dodecyl sulfate-(10% w/v) polyacrylamide gel electrophoresis (SDS–PAGE).

E. coli cells expressing each mutant as cytoplasmic inclusion bodies were harvested by centrifugation, resuspended in distilled water, and disrupted in a French Pressure Cell at 10,000 psi. The crude lysates were centrifuged at 5000*g* for 20 min and the pellets obtained were washed three times in cold distilled water and suspended by sonication. Protein concentra-

Copyright by Mahidol University

Table 1
Complementary primers for substituting a code residue with different amino acids

Primer	Sequence[a]	Restriction site
S387A-f:	5′-CACAGATACT**GC**CTCCCC**T** TC**G**AATCGAGTTAC-3′	*Bst*BI
S387A-r:	5′-CTCGATT**C**GAA**G**GGGGAG**GC**AGTATCTGTGATAG-3′	
S388A-f:	5′-GATACTAGC**G**CCCC**T** TC**G**AATCGAGTTAC-3′	*Bst*BI
S388A-r:	5′-CTCGATT**C**GA **A**GGGG**C**GCTAGTATCTGTG-3′	
P389A-f:	5′-CACAGATAC**G** AGCTCC**G**CCTCTAATCGAG-3′	*Sac*I
P389A-r:	5′-CGATTAGAGG**C**G**GAGCTC**GTATCTGTGATAG-3′	
S390A-f:	5′-GCTCCCCC**G**CTAATA**G**G GTTAC**C**AAAATGGATTTC-3′	*Bst*EII
S390A-r:	5′-CCATTTT**G**GTAAC **C**C**T**ATTAG**C**GGGGGAGCTAG-3′	
S410A-f:	5′-GATGGTAC**C**CTTGCCTCTTATAAT**G**CAAATATAACACC-3′	*Kpn*I
S410A-r:	5′-GTTATATTTG**C**ATTATAAGAGGCAAG**G**GTACCATCAATTTTG-3′	
N411A-f:	5′-GATGGTAC**C** CTTGCCTCTTATAATTCA**GC**TATAACACC-3′	*Kpn*I
N411A-r:	5′-GGTGTTATA**GC**TGAATTATAAGAGGCAAG **G**GTACCATCAATTTTG-3′	
T413A-f:	5′-CTTATAATTC**G** AATATA**G**CACCAACTCC-3′	*Bst*BI
T413A-r:	5-GAGTTGGTG**C**TATATT**C**GAATTATAAGAG-3′	
T415A-f:	5′-CTTATAATTC**G**AATATAACACCA**G**CTCCTGAAGG-3′	*Bst*BI
T415A-r:	5′-CTTCAGGAG**C**TGGTGTTATATT **C**GAATTATAAGAG-3′	
E417A-f:	5′-CAACTCCTG**C**AGGTTTAAGGACCAC-3′	*Pst*I
E417A-r:	5′-GTCCTTAAACCT**G**CAGGAGTTGGTG-3′	
G418A-f:	5′-CAACTCCTGAAG**C**TTTAAGGACCAC-3′	*Hin*dIII
G418A-r:	5′-GTCCTTAAA**G**CTTCAGGAGTTGGTG-3′	
D454A-f:	5′-CTGATGT**G**AT**C**G**CG**TATAACAGTAACAG-3′	*Sau*3AI
D454A-r:	5′-CTGTTATA**CG**C**G** AT**C**ACATCAGTTTTTATATAG-3′	
Y455A-f:	5′-GATGTTAT**C**GAT**GCG**AACAGTAACAG-3′	*Cla*I
Y455A-r:	5′-GTTACTGTT**CGC**ATC GATAACATCAG-3′	
N456A-f:	5′-GATGTTAT**C** GATTAT**GC**CAGTAACAGG-3′	*Cla*I
N456A-r:	5′-CTGTTACTG**GC**ATAATC**G**ATAACATCAG-3′	
S457A-f:	5′-GATGTTAT**C**GATTATAAC**GC**TAACAGGGTTTC-3′	*Cla*I
S457A-r:	5′-CCCTGTTA**GC**GTTATAATC**G**ATAACATCAG-3′	
Y455A/N456A-f:	5′-GATGTTAT**A**GAT**GCG**GCCAGTAACAGGG-3′	
Y455A/N456A-r:	5′-CCCTGTTACTGGC**CGC**ATC**T**ATAACATC-3′	

[a] Recognition sites introduced for restriction enzyme analysis are underlined. Bold letters indicate mutated nucleotide residues; f and r represent forward and reversed primers, respectively.

tions of the partially purified inclusions were determined by using the Bradford-based protein microassay (Bio-Rad), with bovine serum albumin fraction V (Sigma) as a standard.

2.3. Inclusion solubilisation and trypsin treatment

Protoxin inclusions (1 mg ml^{-1}) were solubilised in carbonate buffer (50 mM Na_2CO_3/$NaHCO_3$, pH 9.0) at 37 °C for 1 h as previously described [23]. After centrifugation at 12,000*g* for 10 min, the supernatants were analysed by SDS–PAGE in comparison with the inclusion suspension. To test the stability of the mutant toxins, the solubilised protoxins were incubated with tolylsulfonyl phenylalanyl chloromethyl ketone (TPCK)-treated trypsin at a ratio of 1:20 (w/w) enzyme/toxin in carbonate buffer, pH 9.0 for 16 h and the digestion pattern was analysed by 15% SDS–PAGE.

2.4. Mosquito-larvicidal activity assays

Bioassays were performed as previously described [24], using 2-day old *A. aegypti* mosquito-larvae reared from eggs that were supplied by the mosquito-rearing facility of the Institute of Molecular Biology and Genetics, Mahidol University, Nakornpathom, Thailand. About 500 larvae were reared in a container ($22 \times 30 \times 10$ cm) with approximately 3 l of distilled water supplemented with a small amount of rat diet pellets. Both the rearing and the bioassays were done at room temperature (25 °C). The assays were carried out in 1 ml of *E. coli* suspension (10^8 cells suspended in distilled water) in a 48-well microtitre plate (11.3 mm well diameter, Costar) with 10 larvae per well and a total of 100 larvae for *E. coli* cells expressing each type of the Cry4Ba toxin. *E. coli* cells containing the pUC12 vector were used as a negative control. Mortality was recorded

UNCORRECTED PROOF
Copyright by Mahidol University

after a 24-h incubation period. The student's *t*-test [25] was employed to compare the means for determining the significant difference between larvicidal activity of each mutant and that of the wild-type.

3. Results and discussion

In the present study, we initially explored certain loop regions corresponding to surface-exposed domain II loops of the Cry4Ba mosquito-larvicidal protein in search of sites involved in toxicity. All residues in the β6–β7 loop ($S_{387}SPS_{390}$) and the β10–β11 loop ($D_{454}YNS_{457}$) and some residues in the β8–β9 loop (S_{410}, N_{411}, T_{413}, T_{415}, E_{417} and G_{418}) in domain II (see Fig. 1) were changed individually to alanine via PCR-based site-directed mutagenesis. It should be noted that only polar, uncharged residues (S_{410}, N_{411}, T_{413} and T_{415}), one negatively charged residue (E_{417}) and G_{418}, which is conserved among Cry3Aa, Cry1Aa and Cry4Ba (see Fig. 1(a)), were selected to analyse the β8–β9 loop.

All 130-kDa mutant protoxins were highly expressed in *E. coli* JM109 cells as sedimentable inclusion bodies upon IPTG induction, with yields similar to the wild-type Cry4Ba toxin (see Fig. 2). This indicates that these loop mutations did not affect the folding of the mutant molecules, as protein misfolding can result in low levels of expression and protease sensitivity [26]. When *E. coli* cells expressing each mutant protoxin were examined for their relative toxicity against *A. aegypti* mosquito-lar-

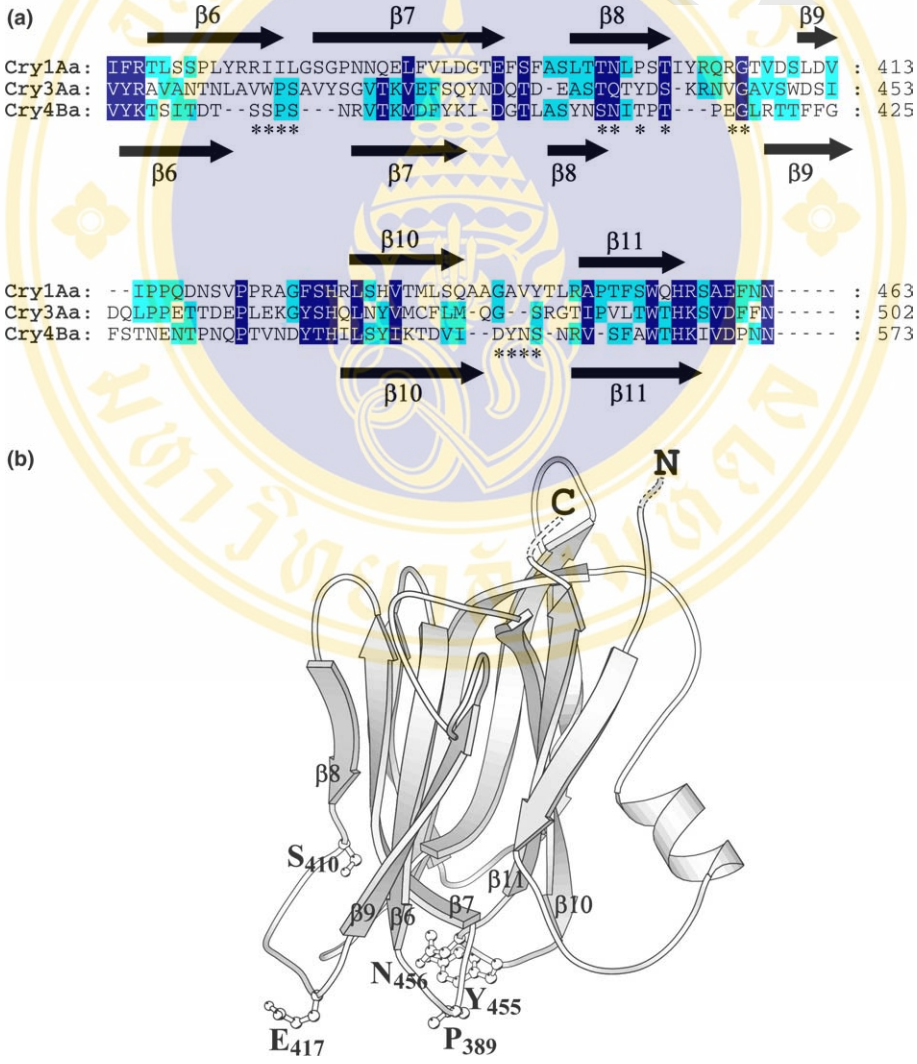

Fig. 1. (a) Multiple sequence alignment of parts of the domain II of Cry4Ba with the corresponding parts in Cry1Aa and Cry3Aa determined by X-ray crystallography. The sequences were aligned using the program Clustal X. The degree of conservation among the three sequences is represented by background shading of the residues. The positions of secondary structure elements of Cry3Aa and Cry4Ba are illustrated over and under the alignments, respectively. Mutated residues are indicated by ∗. (b) Ribbon representation of the three-sheet assembly of domain II of the Cry4Ba crystal structure [10], as viewed from the exterior of the domain. Critical residues, P_{389} in the β6–β7 loop, S_{410} and E_{417} in the β8–β9 loop, and Y_{455} and N_{456} in the β10–β11 loop, are shown in ball-and-stick representation.

Copyright by Mahidol University

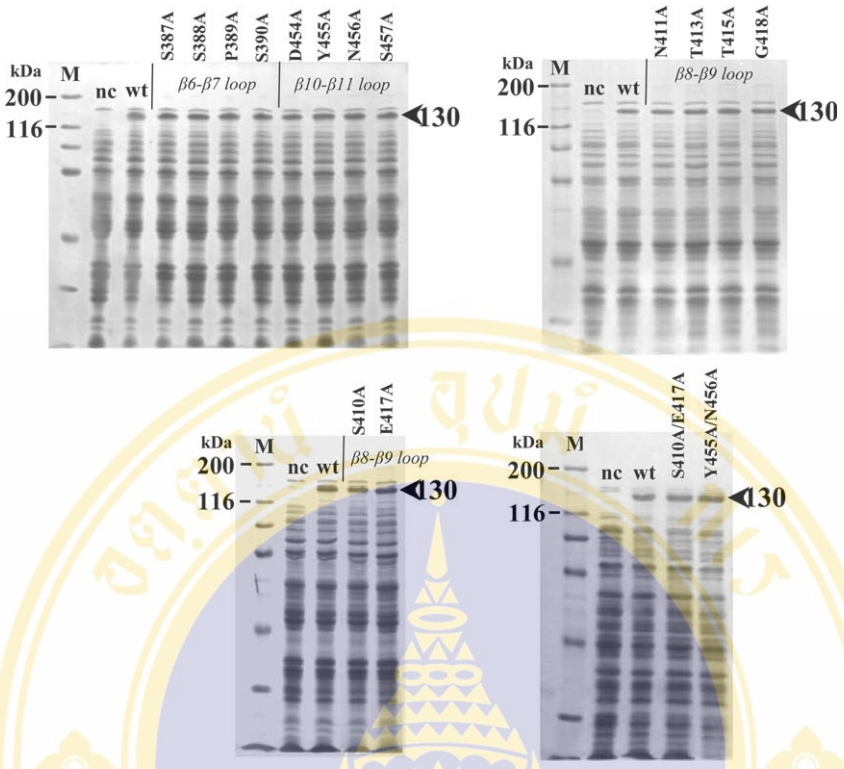

Fig. 2. SDS–PAGE (Coomassie brilliant blue-stained 10% gel) analysis of lysates extracted from *E. coli* (10^7 cells) harbouring the Cry4Ba wild-type protein (wt), its mutant plasmids-S387A, S388A, P389A, S390A, D454A, Y455A, N456A, S457A, N411A, T413A, T415A, G418A, S410A, E417A, S410A/E417A and Y455A/N456A or the pUC12 vector (nc, a negative control). (M) represents the molecular mass standards.

vae, the mortality data recorded after 24-h incubation revealed that the P389A, S410A, E417A, Y455A and N456A mutants exhibited reduced larvicidal activity (approximately 65% of the control value). On the other hand, the nine other mutants (S387A, S388A, S390A, N411A, T413A, T415A, G418A, D454A and S457A) still retained larvicidal activity at approximately 90%, similar to the wild-type toxin (see Fig. 3). These results suggest that P_{389} in the β6–β7 loop, S_{410} and E_{417} in the β8–β9 loop, and Y_{455} and N_{456} in the β10–β11 loop play a role in Cry4Ba toxicity.

To confirm the involvement in toxicity of S_{410} and E_{417} in the β8–β9 loop, and Y_{455} and N_{456} in the β10–β11 loop, two double mutants, S410A/E417A and Y455A/N456A, were further constructed. SDS–PAGE analysis of these double mutants showed that they both

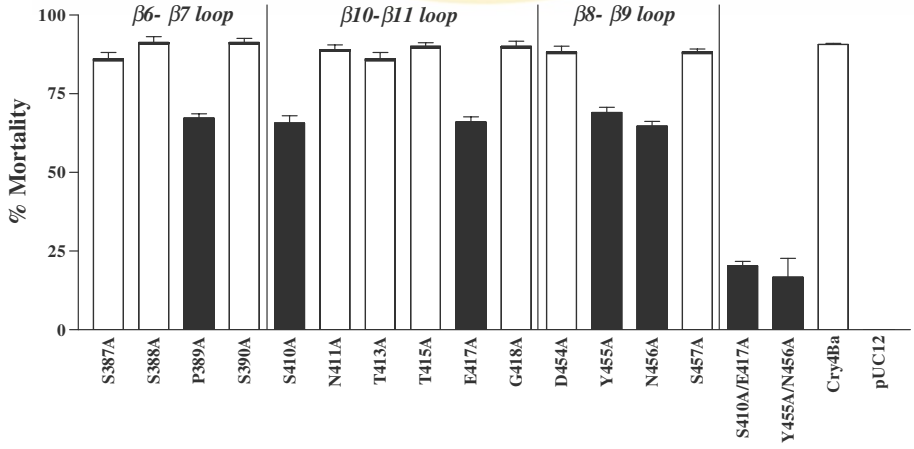

Fig. 3. Mosquito-larvicidal activities of *E. coli* cells expressing the Cry4Ba wild-type protein or its mutant toxins (S387A, S388A, P389A, S390A, S410A, N411A, T413A, T415A, E417A, G418A, D454A, Y455A, N456A, S457A, S410A/E417A and Y455A/N456A) against *A. aegypti* larvae. *E. coli* cells containing the pUC12 vector were used as a negative control. Error bars indicate standard errors of the mean from three independent experiments. Shaded boxes represent the larvicidal activity of the mutants that are significantly different (p-values < 0.01) from that of the wild-type.

Copyright by Mahidol University

expressed the 130-kDa protoxin at wild-type levels (see Fig. 2). Interestingly, the S410A/E417A and Y455A/N456A mutations revealed a more adverse effect on toxicity by reduction of mosquito-larvicidal activity to about 20% (see Fig. 3), indicating that both S_{410} and E_{417} in the β8–β9 loop and both Y_{455} and N_{456} in the β10–β11 loop are required for the Cry4Ba toxin activity.

Experiments were further carried out to assess the solubility of the double mutant inclusions in comparison with that of the wild-type protein. As assessed by SDS–PAGE (Fig. 4(a)), partially purified inclusions of both double mutants were found to be soluble in carbonate buffer, pH 9.0, similar to that of the wild-type inclusion under similar conditions. As previously demonstrated, the 130-kDa Cry4Ba toxin was cleaved by trypsin into ≈47- and ≈20-kDa fragments, in addition to the removal of the C-terminal half of the protoxin [27]. The 130-kDa solubilised mutant protoxins were also examined for their proteolytic stability by digestion with trypsin and both were found to produce trypsin-resistant fragments of ≈47 and ≈20 kDa similar to those obtained with the wild-type protoxin (see Fig. 4(b)), indicating that the mutants were expressed as structurally stable protoxins and that the mutations did not cause misfolding of the proteins. Therefore, the reduced toxicity observed for these double mutants is unlikely to be caused by solubilisation and proteolytic activation steps.

Previously, Wu and Dean [18] demonstrated that double mutation of the β6–β7 loop residues (P412A/S413A) of the coleopteran-specific Cry3Aa toxin had no effect on toxicity to beetle larvae (*Tenebrio molitor*). Here, single alanine substitutions of the two relatively conserved residues, P_{389} and S_{390} (see Fig. 1(a)), in the β6–β7 loop of Cry4Ba revealed that the P389A mutant, but not the S390A mutant, showed a reduction in mosquito-larvicidal activity of approximately 30% as mentioned earlier. This proline residue might be needed for conformational stability of the β6–β7 loop ($S_{387}SPS_{390}$) in Cry4Ba, but apparently not for the shorter β6–β7 loop ($P_{412}S_{413}$) of Cry3Aa. Conceivably, the P389A mutation might alter conformation of the β6–β7 loop in Cry4Ba leading to a decrease in toxin lethality, possibly disrupting the receptor-binding interaction. As was previously reported for the Cry1Ca toxin, P_{377} in the predicted β6–β7 loop was shown to be important for toxicity and initial binding to *A. aegypti* brush border membrane vesicles [21]. In addition, Abdullah et al. [28] have recently shown that insertion of residues of the putative β6–β7 loop ($N_{435}DY_{437}$) of the closely related Cry4Aa mosquito-larvicidal protein in between V_{393} and T_{394} located within β7 of Cry4Ba caused the mutant toxin to lose toxicity against *Aedes* and *Anopheles* larvae.

As was clearly demonstrated, both S_{410} and E_{417} in the β8–β9 loop, and both Y_{455} and N_{456} in the β10–β11 loop play a role in toxicity of the Cry4Ba toxin against *Aedes* larvae. Although the involvement of the β8–β9 loop residues in toxicity was first reported here, numerous studies have previously provided evidence for functional significance of the β10–β11 loop residues that are responsible for binding to specific receptors and, thus, for toxicity to several insect larvae [13,14,21,28]. However, it is not clear how these critical loop residues (S_{410}, E_{417}, Y_{455} and N_{456}) contribute to Cry4Ba toxicity. For Cry3Aa it was demonstrated that alanine substitutions for N_{353} and D_{354} in the β2–β3 loop caused the loss of receptor binding and larvicidal activity [29]. Notwithstanding the lack of binding studies, E_{417} and N_{456} which are located at molecular apexes in β8–β9 and β10–β11 loops, respectively (see Fig. 1(b)), may indeed be involved in Cry4Ba-receptor binding. It should be noted that the D454A mutation in the β10–β11 loop did not significantly affect Cry4Ba toxicity, apparently agreeing with the results of Abdullah et al. [28] which showed that the replacements of this aspartate residue

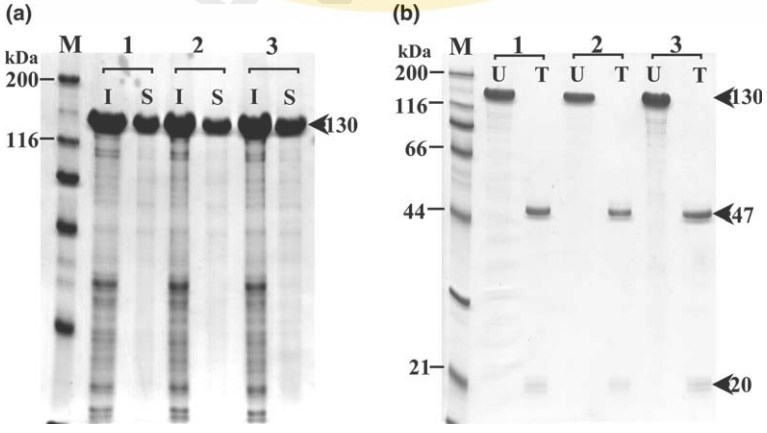

Fig. 4. SDS–PAGE (Coomassie brilliant blue-stained 10% gel) analysis of (a) the partially purified 130-kDa Cry4Ba protoxin inclusions extracted from *E. coli* cells expressing the wild-type protein (lane 1) or its mutants-S410A/E417A and Y455A/N456A (lanes 2 and 3, respectively), and solubilised in carbonate buffer, pH 9.0. (I) and (S) represent the total fractions and an equivalent volume of the supernatants after centrifugation, respectively. (M) represents the molecular mass standards. (b) SDS–PAGE analysis of proteolytic processing of solubilised protoxins from (a). (U) and (T) represent the 130-kDa protoxins and their trypsin-treated products, respectively.

Copyright by Mahidol University

with a short peptide stretch (PAT, GAT or GAV) did not suppress *Aedes* larvicidal activity of this toxin, but rather significantly increased toxicity against *Culex* larvae. The functional role of tyrosine in toxicity and affinity binding to toxin receptors has been previously highlighted for other insecticidal Cry proteins [13,29] and it was proposed that its aromatic phenol ring could contribute to tight binding affinity to the receptors via hydrophobic interaction [29]. Similar to E_{417} and N_{456}, Y_{455} which is located at the tip of the β10–β11 loop (see Fig. 1(b)) might also play a role in Cry4Ba-receptor binding. Since S_{410} is not apically exposed from the β8–β9 loop (see Fig. 1(b)), this implies that this critical residue may not be the contact interface with the receptor, albeit the structural basis for this possibility is not yet clear. As illustrated in Fig. 5, there is a hydrogen bond formed between the hydroxyl group of S_{410} in the β8–β9 loop and the peptide carbonyl group of R_{336} in the β2–β3 loop, hence a disruption of this bonding by the S410A mutation may interfere with the structural integrity of the β8–β9 loop, and thus causes a reduction in Cry4Ba toxicity.

In conclusion, we have provided evidence that P_{389} in the β6–β7 loop, S_{410} and E_{417} in the β8–β9 loop, and Y_{455} and N_{456} in the β10–β11 loop within domain II are involved in Cry4Ba toxicity. It remains to be tested whether these critical loop residues are involved in receptor binding. In addition, our present results do not exclude the possibility that other loop regions within this receptor-binding domain are also responsible for the mosquito-larvicidal activity of the Cry4Ba toxin.

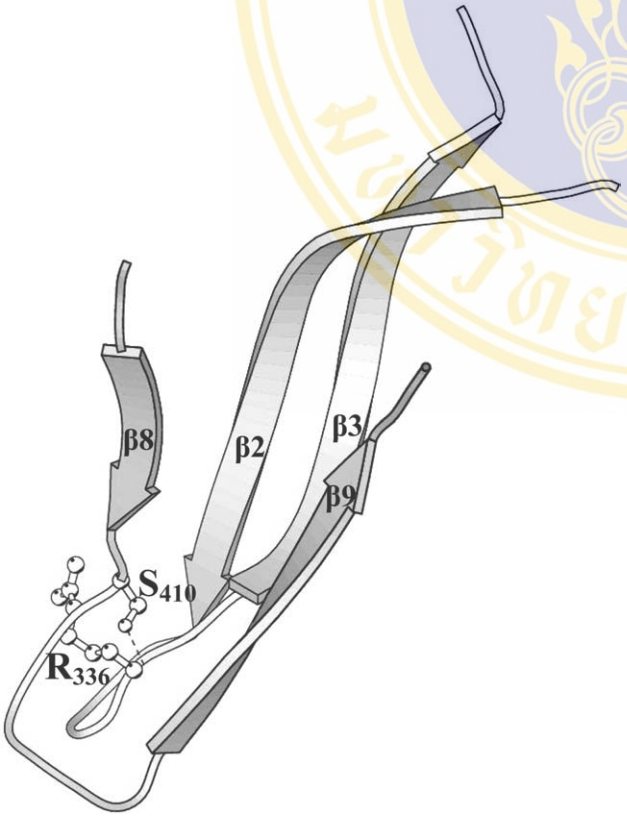

Fig. 5. Ribbon representation of the β2–β3 and β8–β9 hairpins in domain II of the Cry4Ba crystal structure showing a hydrogen bond, as illustrated by a dashed line, formed between the hydroxyl group of S_{410} in the β8–β9 loop and the peptide carbonyl group of R_{336} in the β2–β3 loop.

Acknowledgements

We are grateful to Prof. Sakol Panyim and Dr. Kusol Pootanakit for helpful comments. We also thank Ms. Somsri Sakdee and Ms. Chaweewan Shimwai for technical assistance. This work was supported in part by the National Center for Genetic Engineering and Biotechnology, the National Science and Technology Development Agency of Thailand. A Ph.D. scholarship of the Ministry of Science and Technology to T.T. is gratefully acknowledged.

References

[1] Federici, B.A., Park, H.W., Bideshi, D.K., Wirth, M.C. and Johnson, J.J. (2003) Recombinant bacteria for mosquito control. J. Exp. Biol. 206, 3877–3885.
[2] Schnepf, E., Crickmore, N., Van Rie, J., Lereclus, D., Baum, J., Feitelson, J., Zeigler, D.R. and Dean, D.H. (1998) *Bacillus thuringiensis* and its pesticidal crystal proteins. Microbiol. Mol. Biol. Rev. 62, 775–806.
[3] Crickmore, N., Zeigler, D.R., Feitelson, J., Schnepf, E., Van Rie, J., Lereclus, D., Baum, J. and Dean, D.H. (1998) Revision of the nomemclature for the *Bacillus thuringiensis* pesticidal crystal proteins. Microbiol. Mol. Biol. Rev. 62, 807–813.
[4] Whalon, M.E. and Wingerd, B.A. (2003) *Bt*: mode of action and use. Arch. Insect. Biochem. Physiol. 54, 200–211.
[5] Knowles, B.H. and Ellar, D.J. (1987) Colloid-osmotic lysis is a general feature of the mechanism of action of *Bacillus thuringiensis* δ-endotoxin with different insect specificity. Biochem. Biophys. Acta 924, 509–518.
[6] Grochulski, P., Masson, L., Borisova, S., Pusztai-Carey, M., Schwartz, J.L., Brousseau, R. and Cygler, M. (1995) *Bacillus thuringiensis* CryIAa insecticidal toxin: crystal structure and channel formation. J. Mol. Biol. 254, 447–464.
[7] Morse, R.J., Yamamoto, T. and Stroud, R.M. (2001) Structure of Cry2Aa suggests an unexpected receptor binding epitope. Structure 9, 409–417.
[8] Li, J., Carroll, J. and Ellar, D.J. (1991) Crystal structure of insecticidal δ-endotoxin from *Bacillus thuringiensis* at 2.5 Å resolution. Nature 353, 815–821.
[9] Galitsky, N., Cody, V., Wojtczak, A., Ghosh, D., Luft, J.R., Pangborn, W. and English, L. (2001) Structure of the insecticidal bacterial δ-endotoxin Cry3Bb1 of *Bacillus thuringiensis*. Acta Cryst. D 57, 1101–1109.
[10] Boonserm, P. (2002) In Structure-function studies of the *Bacillus thuringiensis* subsp. *israelensis* mosquitocidal toxin. Ph.D. thesis, University of Cambridge, UK.
[11] Gazit, E., La Rocca, P., Sansom, M.S. and Shai, Y. (1998) The structure and organization within the membrane of the helices composing the pore-forming domain of *Bacillus thuringiensis* delta-endotoxin are consistent with an umbrella-like structure of the pore. Proc. Natl. Acad. Sci. USA 95, 12289–12294.

Copyright by Mahidol University

[12] Masson, L., Tabashnik, B.E., Liu, Y.B., Brousseau, R. and Schwartz, J.L. (1999) Helix 4 of the *Bacillus thuringiensis* Cry1Aa toxin lines the lumen of the ion channel. J. Biol. Chem. 274, 31996–32000.
[13] Smedley, D.P. and Ellar, D.J. (1996) Mutagenesis of three surface-exposed loops of a *Bacillus thuringiensis* insecticidal toxin reveals residues important for toxicity, receptor recognition and possibly membrane insertion. Microbiology 142, 1617–1624.
[14] Rajamohan, F., Hussain, S.A., Cotrill, J.A., Gould, F. and Dean, D.H. (1996) Mutations at domain II, loop 3, of *Bacillus thuringiensis* CryIAa and CryIAb δ-endotoxins suggest loop 3 is involved in initial binding to lepidopteran midgets. J. Biol. Chem. 271, 25220–25226.
[15] Masson, L., Tabashnik, B.E., Mazza, A., Préfontaine, G., Potvin, L., Brousseau, R. and Schwartz, J.L. (2002) Mutagenic analysis of a conserved region of domain III in the Cry1Ac toxin of *Bacillus thuringiensis*. Appl. Environ. Microbiol. 68, 194–200.
[16] Burton, S.L., Ellar, D.J., Li, J. and Derbyshire, D.J. (1999) *N*-acetylgalactosamine on the putative insect receptor aminopeptidase N is recognized by a site on the domain III lectin-like fold of a *Bacillus thuringiensis* insecticidal toxin. J. Mol. Biol. 287, 1011–1022.
[17] Jenkin, J.L., Lee, M.K., Valaitis, A.P., Curtiss, A. and Dean, D.H. (2000) Bivalent sequential binding model of a *Bacillus thuringiensis* toxin to gypsy moth aminopeptidase N receptor. J. Biol. Chem. 275, 14423–14431.
[18] Wu, S.J. and Dean, D.H. (1996) Functional significance of loops in the receptor binding domain of *Bacillus thuringiensis* CryIIIA delta-endotoxin. J. Mol. Biol. 255, 628–640.
[19] Lu, H., Rajamohan, F. and Dean, D.H. (1994) Identification of amino acid residues of *Bacillus thuringiensis* delta-endotoxin CryIAa associated with membrane binding and toxicity to *Bombyx mori*. J. Bacteriol. 176, 5554–5559.
[20] Lee, M.K., Rajamohan, F., Jenkins, J.L., Curtiss, A.S. and Dean, D.H. (2000) Role of two arginine residues in domain II, loop 2 of Cry1Ab and Cry1Ac *Bacillus thuringiensis* δ-endotoxin in toxicity and binding to *Manduca sexta* and *Lymantria dispar* aminopeptidase N. Mol. Microbiol. 38, 289–298.
[21] Abdul-Rauf, M. and Ellar, D.J. (1999) Mutations of loop 2 and loop 3 residues in domain II of *Bacillus thuringiensis* Cry1C delta-endotoxin affect insecticidal specificity and initial binding to *Spodoptera littoralis* and *Aedes aegypti* midgut membranes. Curr. Microbiol. 39, 94–98.
[22] Angsuthanasombat, C., Chungjatupornchai, W., Kertbundit, S., Luxananil, P., Settasatian, C., Wilairat, P. and Panyim, S. (1987) Cloning and expression of 130-kDa mosquito-larvicidal δ-endotoxin gene of *Bacillus thuringiensis* var. *israelensis* in *Escherichia coli*. Mol. Gen. Genet. 208, 384–389.
[23] Angsuthanasombat, C., Crickmore, N. and Ellar, D.J. (1993) Effects on toxicity of eliminating a cleavage site in a predicted interhelical loop in *Bacillus thuringiensis* CryIVB δ-endotoxin. FEMS Microbiol. Lett. 111, 255–262.
[24] Uawithya, P., Tuntitippawan, T., Katzenmeier, G., Panyim, S. and Angsuthanasombat, C. (1998) Effects on larvicidal activity of single proline substitutions in alpha 3 or alpha 4 of the *Bacillus thuringiensis* Cry4B toxin. Biochem. Mol. Biol. Int. 44, 825–832.
[25] Glover, T., and Mitchell, K. (2002) Testing the difference between two means of independent samples. In: Glover, T., Mitchell, K. (Eds.), An introduction to biostatistics international edition, McGraw-Hill Higher Education.
[26] Almond, B.D. and Dean, D.H. (1993) Structural stability of *Bacillus thuringiensis* δ-endotoxin homolog-scanning mutants determined by susceptibility to protease. Appl. Environ. Microbiol. 59, 2442–2448.
[27] Angsuthanasombat, C., Crickmore, N. and Ellar, D.J. (1991) Cytotoxicity of a cloned *Bacillus thuringiensis* subsp. *israelensis* CryIVB toxin to an *Aedes aegypti* cell line. FEMS Microbiol. Lett. 83, 273–276.
[28] Abdullah, M.A.F., Alzate, O., Mohammad, M., McNall, R.J., Adang, M.J. and Dean, D.H. (2003) Introduction of *Culex* toxicity into *Bacillus thuringiensis* Cry4Ba by protein engineering. Appl. Environ. Microbiol. 69, 5343–5353.
[29] Wu, S.J., Koller, N., Miller, D.L., Bauer, L.S. and Dean, D.H. (2000) Enhanced toxicity of *Bacillus thuringiensis* Cry3A δ-endotoxin in coleopterans by mutagenesis in a receptor binding loop. FEBS Lett. 473, 227–232.

UNCORRECTED PROOF
Copyright by Mahidol University

BIOGRAPHY

NAME	Miss Tipparat Tuntitippawan
DATE OF BIRTH	21 April 1973
PLACE OF BIRTH	Saraburi, Thailand
INSTITUTES ATTENDED	Chulalongkorn University, 1991-1994: Bachelor of Science (Medical Technology) Mahidol University, 1995-1998: Master of Science (Molecular Genetics and Genetic Engineering) Mahidol University, 2002-2004: Doctor of Philosophy (Molecular Genetics and Genetic Engineering)
RESEARCH GRANT	PhD scholarship of Ministry of Science and Technology
HOME ADDRESS	22 Soi 1, Judsan Rd., T. Pakpriew, A. Muang, Saraburi

Copyright by Mahidol University